Lysosome Morphology, Exocytosis and Immunity

Abbie Louise Neilson

Submitted in accordance with the requirements for the degree of
Doctor of Philosophy

The University of Leeds

Faculty of Medicine and Health
School of Medicine

April, 2013

The candidate confirms that the work submitted is her own and that appropriate credit has been given where reference has been made to the work of others.

Good research is not learned in books, but at the bench,

like the crafts in the middle ages.

Christian de Duve

The Joy of Discovery, Nature; 2010

Acknowledgements

I wish to thank my supervisor Graham Cook for his expert guidance, unwavering support and most of all, for granting me creative freedom throughout my PhD and inspiring curiosity in science. I express enormous gratitude to my wonderful co-supervisors Jacquie Bond, Josie Meade and Erica Wilson for their excellent training and reassurance, and for their superb humour. I am grateful to all members of the Cook group, past and present, for patiently answering all my questions over the years. I thank Emma Black for performing blood separations, Adam Davison and Liz Straszynski for flow cytometry training, and Kate Passam from Nikon Instruments UK for her invaluable advice and support on the confocal microscope. I thank Laura Wetherill for tips on thesis writing, stress management and the occasional much-needed gin. I also wish to thank my dear friends Nici Reece and Laura Trinick for their boundless energy, encouragement and friendship throughout my final year. My deepest thanks go to my parents, Pauline and Graham, for their unconditional support throughout my entire education. Lastly, words cannot fully express my eternal gratitude to Christopher, for his exceptional culinary skills, for giving me a sense of perspective, for enduring the low points with ceaseless optimism and for inspiring hard work and dedication.

Abstract

Many types of immune cells rely on secretory lysosomes to execute their function. These specialised organelles perform the catabolic function of conventional lysosomes and possess the added capacity to undergo regulated exocytosis. In particular, the cytotoxic function of natural killer (NK) cells depends on the rapid, polarised secretion of secretory lysosomes, known as lytic granules, for the targeted destruction of malignant and virally infected cells. Dysregulation of the biogenesis and exocytosis of secretory lysosomes is the cause of several severe immunological diseases such as Chédiak-Higashi syndrome (CHS). In CHS, mutations in the LYST gene result in enlarged secretory lysosomes that cannot undergo exocytosis. However, the mechanisms underlying LYST function remain elusive. Here, characterisation of the giant lysosome phenotype of *beige* cells reveals altered phosphoinositide metabolism and increased autophagy, indicating a potential role for LYST in regulating these pathways. Furthermore, RNA interference of LYST recapitulated the giant lysosome phenotype, suggesting a strategy for analysis of the pathways in which LYST functions. Pharmacological inhibition of the phosphoinositide kinase PIKfyve induces a giant vesicle phenotype resembling that in *beige* cells. However, on further analysis PIKfyve inhibition was shown to induce giant endosomes as opposed to the giant lysosomes found in *beige* cells. Despite these differences, PIKfyve inhibition, like LYST mutations, reduced NK cell granule exocytosis at a late stage in the pathway. Thus, LYST and PIKfyve act upon different intracellular compartments but inhibit the formation and exocytosis of NK cell granules. These results extend our knowledge of the exocytosis of secretory lysosomes within the immune system and suggest future strategies to define the pathways by which lysosomal biogenesis and exocytosis is regulated.

Table of Contents

List of Figures

List of Tables

Abbreviations

14-3-3τ	Tyrosine 3-monooxygenase/tryptophan 5-monooxygenase activation protein, theta polypeptide
7-AAD	7-amino-actinomycin D
α	Alpha
A-SMase	Acid sphingomyelinase
AKAP550	A kinase anchor protein 550
ALFY	Autophagy-linked FYVE protein
AP-1	Adaptor protein 1
AP-2	Adaptor protein 2
AP-3	Adaptor protein 3
AP-4	Adaptor protein 4
AP-5	Adaptor protein 5
AP3B1	Adaptor-related protein complex 3, beta 1 subunit
APS	Ammonium persulphate
ARM	Armadillo
ArPIKfyve	Associated regulator of PIKfyve
B	Beta
BEACH	Beige and Chédiak-Higashi syndrome
BSA	Bovine serum albumin
C_{12}FDG	5-dodecanoylaminofluorescein di-*β*-D-galactopyranoside
$CaCl_2$	Calcium chloride
CD-MPR	Cation-dependent mannose-6-phosphate receptor
CD107a	Cluster of differentiation 107a
CD11a	Cluster of differentiation 11a
CD28	Cluster of differentiation 28
CD63	Cluster of differentiation 63

CDC42	Cell division control protein 42
cDNA	Complementary deoxyribonucleic acid
CENPJ	Centromere protein J
CHS	Chédiak-Higashi syndrome
CI-MPR	Cation-independent mannose 6-phosphate receptor
CK2β	Casein kinase II beta
CO_2	Carbon dioxide
ConA	Concanavalin A
cSMAC	Central supramolecular activation cluster
Ct	Cycle threshold
CTL	Cytotoxic T lymphocyte
DAG	1,2-Diacylglycerol
DAPI	4',6-Diamidino-2-phenylindole
dH_20	Deionised water
ddH_20	Double distilled water
DMSO	Dimethyl sulphoxide
DNA	Deoxyribonucleic acid
dATP	Deoxyadenosine triphosphate
dCTP	Deoxycytidine triphosphate
dGDP	Deoxyguanosine triphosphate
dNTP	Deoxyribonucleoside triphosphate
dTTP	Deoxythymidine triphosphate
EDTA	Ethylenediaminetetracetic acid
EEA1	Early endosome antigen 1
EGF	Epidermal growth factor
EGTA	Ethylene glycol-bis(2-aminoethylether)-*N,N,N',N'*-tetraacetic acid
ELISA	Enzyme-linked immunosorbent assay
F-actin	Filamentous actin
FACS	Fluorescence-activated cell sorting

FAN	Factor associated with neutral sphingomyelinase activity
FCS	Foetal calf serum
FHL	Familial hemophagocytic lymphohistiocytosis
FHL-3	Familial hemophagocytic lymphohistiocytosis type 3
FHL-4	Familial hemophagocytic lymphohistiocytosis type 4
FHL-5	Familial hemophagocytic lymphohistiocytosis type 5
FITC	Fluorescein isothiocyanate
FSC	Forward scatter
FSP1	Fibroblast-specific protein 1
FYVE	Fab 1, YOTB, Vac 1 and EEA1
GAPDH	Glyceraldehyde 3-phosphate dehydrogenase
GFP	Green fluorescent protein
GLUT4	Glucose transporter type 4
GTP	Guanosine-5'-triphosphate
Gy	Gray, unit of radiation
HCL	Hydrochloric acid
HEAT	Huntingtin, elongation factor 3, protein phosphatase 2A and target of rapamycin kinase 1
HEPES	4-(2-hydroxyethyl)-1-piperazineethanesulfonic acid
HOPS	Homotypic fusion and vacuole protein sorting
Hprt1	Hypoxanthine phosphoribosyltransferase 1
HPS	Hermansky-Pudlak syndrome
HPS-2	Hermansky-Pudlak syndrome type 2
HRS	Hepatocyte growth factor-regulated tyrosine kinase substrate
hVps34	Human vacuolar protein sorting 34
I	Ionomycin
IFNγ	Interferon gamma
IL-15	Interleukin 15
IL-2	Interleukin 2

ILVs	Intraluminal vesicles
$Ins(1,4,5)P_3$	Inositol 1,4,5-trisphosphate
IU	International unit
K_2EDTA	Potassium ethylenediaminetetraacetic acid
kDa	Kilodaltons
LAMP1	Lysosome-associated membrane protein 1
LAMP2	Lysosome-associated membrane protein 2
LDCV	Large dense core vesicle
LIMP2	Lysosome integral membrane protein 2
LRBA	Lipopolysaccharide-responsive vesicle trafficking, beach and anchor containing
LvsA	Large volume sphere A
LvsB	Large volume sphere B
LYST	Lysosomal trafficking regulator
M	Molar
mg	Milligram
$MgCl_2$	Magnesium chloride
MHC	Major histocompatability complex
mL	Millilitre
mm	Millimetre
mM	Millimolar
MPR	Mannose-6-phosphate receptor
MTOC	Microtubule organising centre
Munc13-4	Unc-13 homolog 4
Munc18-2	Unc-13 homolog 2
MVB	Multivesicular body
N-SMase	Neutral sphingomyelinase
NaCl	Sodium chloride
ng	Nanograms
NH_4Cl	Ammonium chloride

NK	Natural killer
nM	Nanomolar
PBMCs	Peripheral blood mononuclear cells
PBS	Phosphate buffered saline
PE	Phycoerythrin
pH	-log10 concentration of hydrogen ions
PH	Pleckstrin homology
PHD	Plant homeodomain
PI3K	Phosphoinositide 3-kinase
PIKfyve	Phosphoinositide kinase for 5 position containing a FYVE finger domain
PIP5Kβ	Phosphatidylinositol 4-phoshate 5-kinase beta
PIPES	Piperazine-N,N′-bis(2-ethanesulfonic acid)
PIs	Phosphoinositides
PKA	Protein kinase A
PKC	Protein kinase C
PKCβ	Protein kinase C, beta isoform
PLC	Phospholipase C
PLCγ1	Phospholipase C gamma 1
PLCγ2	Phospholipase C gamma 2
PLK2	Polo-like kinase 2
PLK4	Polo-like kinase 4
PMA	Phorbol 12-myristate 13-acetate
Pmol	Picomol
PS	Phosphatidylserine
pSMAC	Peripheral supramolecular activation cluster
PtdIns	Phosphatidylinositol
PtdIns(3)P	Phosphatidylinositol 3-phosphate
PtdIns(3,4,5)P_3	Phosphatidylinositol 3,4,5-trisphosphate
PtdIns(3,5)P_2	Phosphatidylinositol 3,5-bisphosphate

PtdIns(4)P	Phosphatidylinositol 4-phosphate
PtdIns(4,5)P_2	Phosphatidylinositol 4,5-bisphosphate
Q	Glutamine
qRT-PCR	Quantitative real-time polymerase chain reaction
R	Arginine
Rab27a	Ras-related protein Rab-27A
Rab5	Ras-related protein Rab-5
RNA	Ribonucleic acid
RNAi	Ribonucleic acid interference
ROI	Region of interest
RPMI	Roswell Park Memorial Institute
S100-A4	S100 calcium binding protein A4
S1P	Shingosine-1-phosphate
SA-*β*-Gal	Senescence-associated *β*-Galactosidase
SD	Standard deviation
SDS	Sodium dodecyl sulphate
siRNA	Small-interfering ribonucleic acid
Slp1	Synaptotagmin-like protein 1
Slp2a	Synaptotagmin-like protein 2a
SM	Sphingomyelin
SMAC	Supramolecular activation cluster
SMase	Sphingomyelinase
SNAP23	Synaptosomal-associated protein of 23 kilodaltons
SNAP25	Synaptosomal-associated protein of 25 kilodaltons
SNARE	Soluble *N*-ethylmaleimide sensitive factor attachment protein
SV40	Simian vacuolating virus 40
SV40T	Simian vacuolating virus 40 T antigen
TEMED	Tetramethylethylenediamine
TFEB	Transcription factor EB

TGN	*Trans*-Golgi network
TNF	Tumour necrosis factor
TNFα	Tumour necrosis factor alpha
V	Volts
V-ATPase	Vacuolar type H^+-adenosine triphosphatase
VAMP7	Vesicle-associated membrane protein 7
v/v	Volume per volume
w/v	Weight per volume
WASp	Wiscott-Aldrich syndrome protein
WD	Tryptophan-aspartic acid
WIDL	Tryptophan, isoleucine, aspartic acid, leucine
Wnt	Wingless and Int
X-gal	5-bromo-4-chloro-3-indolyl-*β*-D-galactopyranoside
YAC	Yeast artificial chromosome
YM	YM201636
YOTB	SPBc2 prophage-derived uncharacterized protein YotB
γ	Gamma
U	Enzyme unit
µg	Microgram
µL	Microlitre
µm	Micrometre
µM	Micromolar

Chapter 1
Introduction

1.1 Conventional and Secretory Lysosomes

Lysosomes are dynamic membrane-bound organelles found in all eukaryotic cells. Characterised by an acidified lumen containing many soluble lysosomal hydrolases, the lysosome is the primary degradative compartment of the cell. The term lysosome - meaning ‘digestive body’ - was coined by Christian de Duve in 1955 who serendipitously discovered the organelle through subcellular fractionation whilst investigating the hydrolase glucose-6-phosphatase (Duve et al., 1955). The lysosome participates in a wide variety of cellular functions aside from bulk degradation, including pathogen defence, autophagy, antigen processing, cell signalling, initiation of apoptosis and plasma membrane repair (Saftig and Klumperman, 2009). Lysosomes are abundant throughout the cytoplasm but cluster proximal to the nucleus in the region of the microtubule organising centre (MTOC), where they traffic to and from endosomal compartments along microtubules (Matteoni and Kreis, 1987). An acidified environment is an absolute requirement for the function of lysosomal hydrolases and luminal pH is maintained at a range of 4.5–5.0, primarily via the action of a proton-translocating vacuolar type H+ ATPase (V-ATPase) (Beyenbach and Wieczorek, 2006). Lysosomal hydrolases engage in the catabolism of macromolecules into their monomeric constituents that are then translocated into the cytosol by members of a second class of proteins – the integral lysosomal membrane proteins. The translocated monomers can then be recycled. The lysosomal membrane also contains a set of highly glycosylated proteins, the most abundant of these are the lysosome-associated membrane protein 1 (LAMP1), LAMP2 and lysosomal integral membrane protein type 2 (LIMP2); these molecules are commonly used as markers for distinguishing lysosomes from their endosomal counterparts.

Specialised secretory cells contain secretory vesicles that fuse with the plasma membrane to release their contents in response to external stimuli, whilst maintaining a separate lysosomal compartment. However, in a few cell types these two functions are merged together into one organelle: a fully functioning degradative compartment with similar pH, morphology and protein composition to lysosomes, but modified with additional machinery to enable them to participate in regulated exocytosis. These bifunctional organelles – termed secretory lysosomes – are a type of lysosome-related organelle found primarily in haematopoietic cells, but also in melanocytes. Examples of such secretory lysosomes include the major histocompatability complex (MHC) class II compartments of antigen presenting cells, the lytic granules of cytotoxic T lymphocytes (CTLs) and natural killer (NK) cells, basophil granules and platelet dense granules. They are generally distinguishable from conventional lysosomes by the presence of specialised proteins required for their function and for their secretory capacity, although conventional lysosomes are also capable of plasma membrane fusion in a Ca^{2+}-dependent manner during plasma membrane repair (Reddy et al., 2001).

Several genetic diseases have been described which selectively impair secretory lysosome function (Clark and Griffiths, 2003), demonstrating that these organelles are equipped with specialised machinery to enable secretory function. Studying these diseases has helped to identify vital components of the secretory machinery, but their exact functions are not fully understood and many proteins are yet to be discovered or characterised. The secretory lysosomes of the immune system in particular have been characterised in detail, not least because of the readily recognisable disease phenotypes, such as susceptibility to infection. Hence, investigating the fundamental pathways that underlie the biogenesis and exocytosis of secretory lysosomes is important for understanding the mechanisms that govern immune responses.

1.1.1 Targeting of Newly Synthesised Lysosomal Proteins to Lysosomes

The majority of newly synthesised luminal lysosomal hydrolases and some lysosomal membrane proteins are routed through the 'direct' pathway from the *trans*-Golgi network (TGN) to the endosome, and subsequently to lysosomes. Others adopt an alternative 'indirect' pathway of constitutive secretion to the cell surface, subsequent internalisation, followed by delivery to lysosomes through the endocytic pathway (Bonifacino and Traub, 2003). The majority of lysosomal hydrolases are modified in the *cis*-Golgi by the addition of mannose-6-phosphate, and following binding to the mannose-6-phosphate receptor (MPR) at the TGN, are packaged into clathrin-coated intermediates for endosomal delivery (Waguri et al., 2003). Two mannose-6-phosphate receptors exist: a 46 kDa protein and a 300 kDa protein. Both bind mannose-6-phosphate independent of divalent cations, but the small receptor binds with greater affinity in the presence of cations. Thus, they are named cation-independent (CI)- and cation-dependent (CD)-MPR accordingly (Kornfeld and Mellman, 1989). Upon arrival at the late endosome, hydrolases dissociate from MPRs at the low pH and continue onwards to lysosomes, leaving MPRs free to recycle back to the TGN. Mechanisms of endosome-to-TGN retrograde transport will not be discussed here in detail but are reviewed in Bonifacino and Rojas (2006). MPR is distributed between the Golgi, plasma membrane, early endosomes and late endosomes, yet steady-state localisation of the majority of MPR differs according to cell type (Griffiths et al., 1990, Geuze et al., 1988, Waguri et al., 2003).

Newly synthesised lysosomal membrane proteins on the other hand, are not modified with mannose-6-phosphate in the Golgi and instead rely on their C-terminal sorting motifs for trafficking to lysosomes, either directly or indirectly via the plasma membrane. Two well-studied sorting motifs are the tyrosine-based (YXXØ; where Ø is a bulky hydrophobic amino acid), and dileucine-based ([E/D]XXXL[L/I]) motifs. These serve as binding domains for subunits of the heterotrimeric adaptor protein (AP) complexes AP-1, -2, -3 and -4 which mediate protein incorporation into transport vesicles at different post-

Golgi compartments (Braulke and Bonifacino, 2009). For many years it was presumed there were four AP complexes, mediating the bidirectional trafficking of membrane proteins between early endocytic compartments. However, proteins facilitating trafficking out of late endosomes and lysosomes are less well-characterised. Recently, a fifth complex was identified, AP-5, that is a likely candidate for mediating budding from the late endosome and its depletion significantly disrupts endocytic trafficking (Hirst et al., 2011). The lack of knowledge regarding mechanisms involved in the trafficking of late endocytic compartments, coupled with this recent discovery, tells us that there is still much to learn about the complex and dynamic processes that govern the endosomal and lysosomal systems.

1.1.2 Endosome Maturation

Endocytosed plasma membrane proteins, such as receptors (with or without their bound ligands), reach the early endosome where they dissociate from any bound ligand due to mildly acidic lumenal pH. Early endosomes function to sort endocytosed material either for degradation or recycling back to the plasma membrane. Morphologically, they are described as having two distinct regions: a vacuolar part and a tubular part. The latter is commonly referred to as the tubular sorting endosome and is comprised of branching tubules that emanate from the vacuolar part (Figure 1.1, Tooze and Hollinshead, 1991). Internalised molecules can recycle to the plasma membrane directly from the early endosome, or via a distinct subpopulation of vesicles; recycling endosomes. Recycling endosomes are typically localised to the MTOC where they can form a point of intersection for both the endocytic and exocytic pathways (Ménager et al., 2007). The association of early endosome-specific proteins such as Ras-related protein 5 (Rab5) and human vacuolar protein sorting 34 (hVps34) are essential for preserving the identity and function of the organelle. The type III phosphatidylinositol 3-kinase, hVps34, converts phosphatidylinositol (PtdIns) to phosphatidyl-inositol 3-phosphate (PtdIns[3]P) (Schu et al., 1993). PtdIns(3)P is central to the recruitment of a number of effector proteins to the early endosomal membrane.

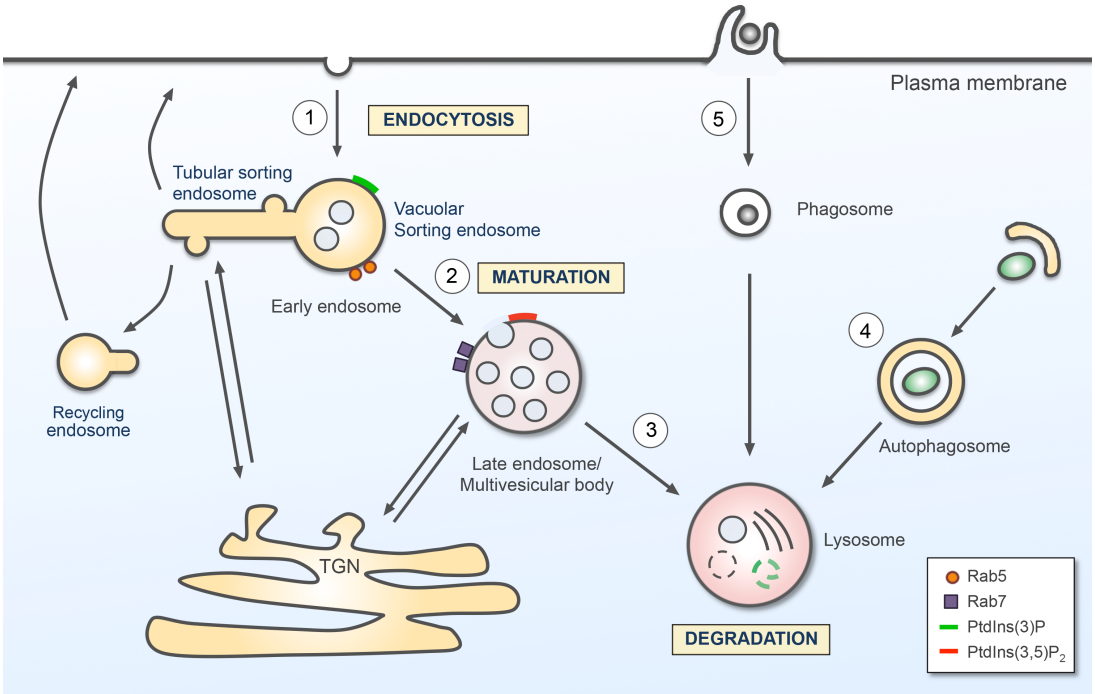

Figure 1.1. The endocytic pathway and delivery to lysosomes

A basic schematic representation of the endosome maturation pathway and delivery of cargo to lysosomes. Endocytosed plasma membrane proteins are delivered to the early endosome where they are sorted for further trafficking (*1*). Proteins destined for recycling enter the tubular sorting endosome to be recycled back to the plasma membrane directly or via recycling endosomes, or to the *trans*-Golgi network (TGN). Proteins destined for degradation are retained in the vacuolar sorting endosome for delivery to lysosomes. Proposed mechanisms for endosome maturation include gradual acidification (indicated by the transition from orange through to pink), loss of Rab5 in exchange for Rab7, conversion of PtdIns(3)P to PtdIns(3,5)P_2 and intraluminal vesicle (ILV) formation (*2*). Late endosome-lysosome fusion permits the degradation of the delivered molecules (*3*). Autophagosomes (*4*), formed from double membranes that engulf portions of the cytoplasm and organelles, fuse with lysosomes for degradation and nutrient recycling during starvation. Similarly, engulfed pathogens contained within phagosomes (*5*) are degraded by the lysosome. Newly synthesised lysosome-resident proteins are delivered from the TGN to early and late endosomes for subsequent transit to lysosomes, or via the plasma membrane (not shown) for subsequent re-internalisation and endocytic delivery.

One such protein is early endosomal antigen 1 (EEA1) that binds PtdIns(3)P through its FYVE (Fab 1, YOTB, Vac 1 and EEA1) domain (Gillooly et al., 2003) and is important for various endosomal trafficking and fusion events (Johnson et al., 2006, Roth, 2004).

Early endosomes undergo a multitude of changes that eventually lead to their maturation into late endosomes. The exact modifications and mechanisms vary according to cell type but include acidification, vesiculation, conversion of PtdIns(3)P to PtdIns(3,5)P_2, protein exchange, change in morphology and the acquisition of newly synthesised lysosomal hydrolases and membrane proteins (Figure 1.1; Huotari and Helenius, 2011). The inward budding of the endosomal membrane at discrete domains internalises ubiquitinated membrane-bound cargo into intraluminal vesicles (ILVs) ensuring their degradation upon delivery to the lysosomal lumen. The mechanisms mediating the transition from early- to late-endosomes are highly debated and several models have been proposed. One possibility is that early endosomes undergo protein remodelling; losing endosomal markers Rab5 and EEA1 in exchange for late endosomal markers such as Rab7. Evidence for such a transition comes from studies of *Caenorhabditis elegans* whereby early endosomes undergo a Rab5-to-Rab7 ‘switch’ that mediates their maturation to late endosomes (Poteryaev et al., 2010). An alternative model is that early and late endosomes exist as discrete entities with material passed between the organelles via transport carrier vesicles (Vonderheit and Helenius, 2005). Mesaki and colleagues, however, report the detachment of the entire tubular endosome from the vacuolar endosome, triggering the acidification and maturation of the remaining vacuolar part (Mesaki et al., 2011). It is conceivable that both direct maturation and exchange of content between organelles occurs. Carrier vesicles may be utilised for transporting cargo from early endosomes that requires rapid transit to late endosomes for the degradation pathway, for example viruses (Vonderheit and Helenius, 2005), whilst the early endosome undergoes a relatively slower and complex maturation process. Regardless of the mechanisms of formation, late endosomes become refractory to fusion with early endosomes, yet continue to receive newly synthesised lysosomal

hydrolases and membrane proteins from the TGN, such as LAMP1 and CD63 (Ihrke et al., 2004).

Late endosomes are often referred to as multivesicular bodies (MVBs) because of their numerous ILVs. ILV formation begins with early endosomes and continues during endosome maturation (Futter et al., 1996). ILV formation is mainly co-ordinated by four ESCRT complexes (endosomal sorting complexes required for transport); ESCRT-0, -I, -II and –III, together with a number of accessory proteins (Hurley, 2010). The role of ESCRTs is to sort ubiquitinated membrane proteins into discrete domains of the endosome limiting membrane and generate inward budding vesicles. Phosphoinositides (PIs) are critical for MVB-dependent cargo sorting as several ESCRT proteins are recruited to endosomes by PtdIns(3)P, and to a lesser extent by PtdIns(3,5)P_2 (Hurley, 2010). Similar to the Rab 'switch', the conversion of PtdIns(3)P to PtdIns(3,5)P_2 is important for endosome maturation and is coordinated by the action of specific kinases and phosphatases. PtdIns(3,5)P_2 is central to endosomal homeostasis as depletion of PtdIns(3,5)P_2 causes the gross swelling of early and/or late endosomes (Ikonomov et al., 2006, Jefferies et al., 2008, Osborne et al., 2008). The role of PtdIns(3,5)P_2 is discussed in more detail in section 1.1.4.

1.1.3 Delivery of Cargo to Lysosomes

Several models have been proposed for the delivery of endocytosed cargo from late endosomes to lysosomes. These include vesicular transport, late endosome-lysosome maturation and fusion of the two organelles (Luzio et al., 2007). Based on substantial evidence provided by studies utilising time-lapse microscopy that describe late endosome-lysosome fusion in live cells, this is currently the most widely accepted mechanism for content delivery to lysosomes (Futter et al., 1996, Bright et al., 1997, Mullock et al., 1998, Bright et al., 2005).

Time-lapse confocal microscopy of normal rat kidney fibroblasts revealed that fusion can be transient, whereby late endosomes and lysosomes engage in temporary fusion, exchanging luminal content before separating in a process termed 'kiss-and-run'. Or it can be direct, producing a single 'hybrid' organelle (Bright et al., 2005). In the same study, content mixing also

occurred via tubular extensions that emanated from either organelle. Following the complete fusion of a late endosome and lysosome and the bulk degradation of macromolecules, it is proposed that retrieval of late-endosomal proteins and membrane from the hybrid organelle permit the reformation of a fully condensed and acidified lysosome (Bright et al., 1997, Mullock et al., 1998). Evidence supporting this comes from studies which observe the budding and detachment of vesicles away from the hybrid organelle shortly after formation (Bright et al., 2005).

Fusion between closely proximal late endosomes and lysosomes requires tethering, likely mediated by the mammalian homotypic fusion and vacuole protein sorting (HOPS) complex, and transmembrane soluble *N*-ethylmaleimide sensitive factor attachment protein receptors (SNAREs) together with Ca^{2+} (Pryor and Luzio, 2009). SNARE proteins from opposing membranes form a trans-SNARE complex composed of a four-helix bundle; three of which contain a glutamine (Q) residue and one an arginine (R) residue. They are therefore referred to as Q-SNARES and R-SNARES respectively (Pryor and Luzio, 2009).

Lysosomes also receive material for degradation from the autophagic and phagocytic pathways by fusing with autophagosomes and phagosomes respectively (Figure 1.1). Autophagosomes are organelles that form during periods of nutrient starvation when a double membrane envelops and sequesters a portion of the cytoplasm which may contain whole organelles (Mizushima and Komatsu, 2011). The subsequent fusion with lysosomes to form a hybrid organelle, called the autolysosome, permits the degradation and recycling of sequestered material and the release of nutrients back into the cytoplasm. Autophagosome-lysosome fusion is dependent on the acidic pH of the lysosome, as raising lysosomal pH (for example, with chloroquine) prevents the formation of autolysosomes, resulting in the build-up of autophagosomal structures in the cytoplasm (Kawai et al., 2007). Similarly, the fusion of lysosomes with phagosomes containing engulfed extracellular pathogens is essential for the protection against microorganisms (Huynh et al., 2007).

1.1.4 PtdIns(3,5)P_2 in the Endolysosomal System

PtdIns(3,5)P_2 is generated by the phosphatidylinositol 3-phosphate 5-kinase PIKfyve (Phosphoinositide kinase for 5-position containing a FYVE finger domain) which catalyses the phosphorylation of PtdIns(3)P on the 5-position of the inositol ring (Sbrissa et al., 1999). PtdIns(3,5)P_2 is essential for endomembrane homeostasis as depletion of PtdIns(3,5)P_2 causes extensive vacuolation of the cytoplasm (Jefferies et al., 2008). Inhibition of PIKfyve activity, either through expression of kinase-dead mutants, RNA interference (RNAi) or pharmacological inhibition, causes the initial enlargement of early endosomes, followed by the appearance of grossly enlarged early endosomes, large endosomes or both (Rutherford et al., 2006, Jefferies et al., 2008, Osborne et al., 2008). The origin of the affected vesicles and the extent of enlargement varied according to different studies, likely due to the method of PIKfyve depletion (dominant negative, RNAi or pharmacological inhibition) and the cell type being investigated. PIKfyve is located both in the cytoplasm and on vesicle membranes, targeted to PtdIns(3)P-rich membranes via its FYVE domain. It forms a tetrameric complex with its scaffolding regulator ArPikfyve and the PtdIns(3,5)P_2 phosphatase Sac3 (Sbrissa et al., 2008). This complex, known as PAS (for PIKfyve, ArPikfyve and Sac3), enables the rapid turnover of PtdIns(3,5)P_2 at sites of synthesis (Figure 1.2, Sbrissa et al., 2008).

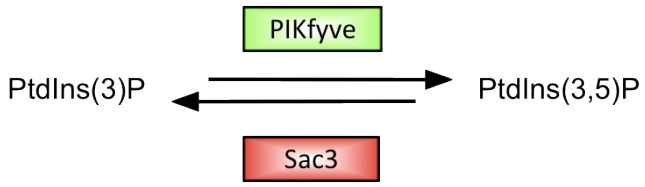

Figure 1.2. Phosphoinositide conversion by the kinase PIKfyve and the phosphatase Sac3

A role for PIKfyve and PtdIns(3,5)P_2 in the morphogenesis and function of late endosomes comes from studies in human embryonic kidney cells overexpressing dominant-negative kinase-deficient PIKfyve, which display enlarged late endosomes containing a reduced number or ILVs (Ikonomov et al., 2003a). However, the mechanisms underlying this function of PIKfyve are unclear. Initially, the expression of kinase-deficient PIKfyve results in the formation of EEA1-positive large endosomes. At later time points this is followed by the appearance of large perinuclearly clustered vesicles positive for CI-MPR that are described as late endosomes (Ikonomov et al., 2001, Ikonomov et al., 2003a). Similarly, both early- and late-endosomal enlargement occurs during PIKfyve silencing (Rutherford et al., 2006). Several studies have also demonstrated a role for PIKfyve in endosomes-to-TGN retrograde protein trafficking (Rutherford et al., 2006, de Lartigue et al., 2009), although the reports concerning trafficking of CI-MPR to the TGN are conflicting. Pharmacological inhibition of PIKfyve does not significantly affect CI-MPR trafficking (Jefferies et al., 2008) whereas trafficking of CI-MPR to the TGN is delayed upon silencing of PIKfyve (Rutherford et al., 2006). These discrepancies are likely attributed to the differences in cell types used and the duration of suppressed PIKfyve activity, with longer suppression achieved by PIKfyve silencing. Furthermore, the exact localisation of PIKfyve remains elusive, as the abundance of PIKfyve in many cell types is too low for robust detection by antibodies. Overexpressed wild-type PIKfyve was found to localise to late endosomes in COS cells, but to early endosomes in HeLa cells (Shisheva et al., 2001). It is suggested that PIKfyve cycles between membranes depending on their PtdIns(3)P/PtdIns(3,5)P_2 content and that the rate of conversion differs between cell types, resulting in the variable localisation of PIKfyve (Shisheva, 2008). Nonetheless, these studies support a role for PIKfyve-mediated PtdIns(3,5)P_2 synthesis in regulating endosome fusion/fission events and in maintaining correct endosomal trafficking.

In addition to endocytic trafficking, PIKfyve also functions in glucose transport and regulated exocytosis (Ikonomov et al., 2002b, Osborne et al., 2008). Insulin-induced translocation of the glucose transporter type 4 (GLUT4) to the cell surface is reduced upon expression of a kinase-deficient

PIKfyve mutant in adipocytes (Ikonomov et al., 2002b, Ikonomov et al., 2007). Although the mechanism by which this occurs is undefined, these studies suggest PIKfyve positively regulates the insulin-stimulated translocation of GLUT4 storage vesicles to the plasma membrane. Conversely, nicotine-stimulated exocytosis of large dense core vesicles (LDCV) is upregulated in neurosecretory cells during pharmacological inhibition of PIKfyve, suggesting that PIKfyve negatively regulates the exocytosis of these vesicles (Osborne et al., 2008). The generation of PtdIns(3)P on LDCV membranes is considered a priming factor for plasma membrane fusion (Osborne et al., 2008). Upon nicotine stimulation of PC12 cells, PIKfyve was recruited to a subpopulation of LDCVs where it is proposed to prevent the over-secretion of a pool of primed granules through the depletion of PtdIns(3)P (by conversion to PtdIns[3,5]P_2; Osborne et al., 2008). It is likely that the function of PIKfyve with regards to vesicle exocytosis varies according to cell type, the secretory organelle and the mechanism of organelle biogenesis. Nonetheless, the relocation of PIKfyve to secretory vesicles from the cytoplasm upon extracellular stimuli appears important for its function. Further work examining the effect of PIKfyve on exocytosis in other cell types is required before the extent of PIKfyve-mediated secretory regulation becomes clear.

PIKfyve was recently shown to be responsible for the synthesis of the total intracellular pool of PtdIns(3,5)P_2 (Zolov et al., 2012). It is also the major source of PtdIns(5)P synthesis through the phosphorylation of PtdIns (Ikonomov et al., 2011). Currently no other kinases are known to contribute to the synthesis of these two lipids. The disrupted endosomal morphology observed during PIKfyve activity suppression is mediated solely through the loss of PtdIns(3,5)P_2, as micro-injection of PtdIns(3,5)P_2, but not PtdIns(5)P, into vacuolated cells reversed the phenotype (Ikonomov et al., 2002a). The functional importance of cellular PtdIns(5)P is less well documented than for PtdIns(3,5)P_2. PIKfyve is vital in early embryonic development as conventional mouse knockout causes early embryonic lethality (Ikonomov et al., 2011). Mutations in PIKfyve are associated with Francois-Neetens corneal fleck dystrophy, an autosomal dominant syndrome characterised by numerous white flecks throughout the stroma and the presence of enlarged

vesicles within keratinocytes (Li et al., 2005). The disease is non-progressive and relatively asymptomatic, resulting from predominantly frame-shift or nonsense mutations within the *PIKFYVE* gene which are predicted to be protein-truncating (Li et al., 2005). Interestingly, although complete knockout of Pikfyve is lethal in mice, a single functional *Pikfyve* allele in heterozygotes is sufficient to support normal development into adulthood and mice lack the pathology of corneal fleck dystrophy (Ikonomov et al., 2011).

Mutations in the other PAS complex genes, *Arpikfyve* and *Sac3*, produce more severe phenotypes. ArPIKfyve functions as a scaffold for PIKfyve and is essential for PIKfyve-mediated PtdIns(3,5)P_2 production (Sbrissa et al., 2008). *Arpikfyve*-null mice die within two days after birth and exhibit severe neurodegeneration (Zhang et al., 2007b). The function of the phosphatase Sac3 is opposite to that of PIKfyve and reduces PtdIns(3,5)P_2 levels (Sbrissa et al., 2008). Interestingly, loss of Sac3 results in an unexpected loss of stead-state PtdIns(3,5)P_2, rather than an increase. Similar to *Arpikfyve*-null mice, '*pale tremor*' *Sac3*-null mice exhibit neurodegeneration as well as diluted pigmentation and die within the first six weeks of life (Chow et al., 2007). Furthermore, mutations in human Sac3 are associated with a form of the peripheral nerve disorder Charcot-Marie-Tooth disease type 4. The reason for reduced PtdIns(3,5)P_2 in the absence of Sac3 is as yet undetermined, but these findings emphasise the functional requirement of a full PAS complex for PIKfyve-mediated PtdIns(3,5)P_2 production, and that loss of either ArPIKfyve and Sac3 result in neuropathy associated with decreased PtdIns(3,5)P_2.

Despite extensive investigation, the exact roles of PtdIns(3,5)P_2 and PIKfyve in the endolysosomal system remain unclear. The lack of PtdIns(3,5)P_2-specific probes and the pleiotropic functions of PIKfyve make it difficult to draw definitive conclusions regarding the mechanistic link between PIKfyve suppression and endosomal morphology/trafficking.

1.1.5 Secretory Lysosomes

Only a few cell types rely on secretory lysosomes to carry out their specific effector functions (Table 1.1). These can be distinct organelles that coexist with conventional lysosomes, as in melanocytes (Raposo et al., 2001), or the sole degradation compartment, as in NK cells and CTLs (Burkhardt et al., 1990, Peters et al., 1991). The effector function of NK cells and CTLs requires the exocytosis of their secretory lysosomes (termed lytic granules in these cells) to release cytolytic proteins that initiate apoptosis in recipient cells (de Saint Basile et al., 2010). Lytic granules and the molecular machinery required for their secretion will be discussed in detail in Section 1.3. Much of our insight into the biogenesis, regulation and secretion of secretory lysosomes has been gained from the study of genetic diseases in humans and mammals. Many of theses diseases have similar clinical phenotypes, such as hypopigmentation and immunodeficiency, owing to the defective function of immune cells and melanocytes.

Hermansky-Pudlak syndrome (HPS) is an autosomal recessive disease with eight causative genes identified in humans (Wei, 2006). It is characterised by hypopigmentation, immunodeficiency and bleeding diathesis due to abnormal synthesis and/or vesicular trafficking of melanosomes, lytic granules and platelet dense granules, respectively, indicating that the affected proteins are common to all secretory lysosomes. Mutations in the *AP3B1* gene encoding the β3A subunit of AP-3 are the cause of HPS type 2 (HPS-2) and result in the miss-sorting of lysosomal and secretory lysosomal proteins such as LAMP1 and LAMP2 (Dell'Angelica et al., 1999). HPS-2 patients also suffer immunodeficiency as a result of defective NK cell and CTL cytotoxicity (Clark et al., 2003). Chédiak-Higashi syndrome (CHS) is a similar disorder characterised by hypopigmentation, immunodeficiency and neurologic dysfunction that arise from mutations in the lysosomal trafficking regulator (*LYST)* gene (previously known as CHS1, Perou et al., 1996).

Cell Type	Cell-Specific Secretory Lysosome	Specific Content	Function	Reference
NK cell	Lytic granule	Granzymes, perforin	Cell-mediated cytotoxicity	de Saint Basile et al., 2010
CTL	Lytic granule	Granzymes, perforin	Cell-mediated cytotoxicity	de Saint Basile et al., 2010
Platelet	Platelet dense granule	Aggregation factors	Clotting	McNicol and Israels, 1999
Mast cell	Mast cell granule	Histamine, serotonin	Inflammation	Marone et al., 1997
Basophil	Basophil cell granule	Histamine, serotonin	Inflammation	Marone et al., 1997
Neutrophil	Azurophil granule	Chemoattractants	Inflammation, phagocytosis	Kjeldsen et al., 1998
Macrophage	MHC class II compartment	MHC class II	Antigen presentation Phagocytosis	Harding, 1995
Dendritic cell	MHC class II compartment	MHC class II	Antigen presentation	Harding, 1995
B cell	MHC class II compartment	MHC class II	Antigen presentation	Harding, 1995
Osteoclast		Acid hydrolases	Bone remodelling	Stenbeck, 2002
Melanocyte	Melanosome	Melanin	Skin pigmentation	Raposo et al., 2001

Table 1.1. Cells containing secretory lysosomes and their function

This table provides examples of well-studied secretory lysosomes, but is not an exhaustive list. Secretory lysosomal content differs depending on cell type and function. The major protein constituents of each secretory lysosome type, their associated functions and relevant references are shown. Melanosomes are the pigment granules of melanocytes that are the site of synthesis and storage of melanin. They translocate to the cell periphery via microtubule-based transport where they pass from melanocyte dendrites to keratinocytes in a poorly understood mechanism.

Osteoclasts mediate bone remodelling through exocytosis of their secretory lysosomes (there is no specific term for these organelles in osteoclasts) and the released lysosomal hydrolases degrade the bone. Platelet dense granules (also known as delta granules or dense bodies) contain factors which mediate platelet aggregation and the formation of the haemostatic plug. Stimulation of basophils and mast cells causes the release of histamine and serotonin from secretory lysosomes that initiate an inflammatory response. MHC class II compartments are found within the professional antigen presenting cells B cells, macrophages and dendritic cells and contain proteins important for antigen processing and binding of the resulting peptides with MHC class II molecules. Natural killer (NK) cells and cytotoxic T lymphocytes (CTLs) exocytose their lytic granules to release cytolytic proteins that initiate apoptosis in recipient cells. Adapted from Blott and Griffiths, 2002.

The exact function of LYST is unknown, but it is thought to regulate protein and vesicular trafficking to and from lysosomes and secretory lysosomes, as these organelles are grossly enlarged in CHS patients cells (Burkhardt et al., 1993). The role of LYST in lysosome and secretory lysosome morphology will be reviewed in detail in Section 1.2.

Patients with Griscelli syndrome type 2 exhibit a similar clinical presentation to CHS patients, presenting with hypopigmentation of the skin, immunodeficiency and neurologic dysfunction (Ménasché et al., 2000). Autosomal recessive mutations in *RAB27A* encoding a member of the Rab family of small GTPases involved in membrane trafficking are the cause of Griscelli syndrome type 2. Through the recruitment of different effector proteins in each cell type, Rab27a (Ras-related protein Rab-27A) mediates the transfer of melanosomes from microtubules to the plasma membrane in melanocytes (Hume et al., 2001) and the docking of lytic granules to the plasma membrane in CTLs and NK cells (Neeft et al., 2005). The inability of lytic granules to dock at the plasma membrane means they are not secreted and the cells lack cytotoxic function (Neeft et al., 2005).

Defects in lysosomal pathways that arise through single gene mutations, are the cause of many rare and severe human genetic diseases. CHS, HPS-2 and Griscelli syndrome type 2 all share a common clinical phenotype of albinism and immunodeficiency, arising from the selective dysfunction of

cells with secretory lysosomes, suggesting common mechanisms for biogenesis and function shared by these organelles. Dissecting the molecular mechanisms underlying these conditions has revealed many novel proteins and continues to provide invaluable insight into the processes behind cellular function. Uncovering cell-specific mechanisms in lysosome and secretory lysosome biogenesis/homeostasis is essential to further our understanding of this complex process and to help fill the gaps in our current knowledge.

1.2 The LYST Protein

1.2.1 Chédiak-Higashi Syndrome

CHS was first described over 70 years ago and is named after the Cuban serologist Alejandro Moisés Chédiak and the Japanese paediatrician Otokata Higashi. CHS is a rare childhood autosomal recessive disorder characterised by partial oculocutaneous albinism, bleeding diathesis, immunodeficiency and neurologic dysfunction which present within the first decade of life. The hallmark of this disease at the cellular level is a remarkable clustering of abnormally large lysosomes proximal to the nucleus (Abe et al., 1982, Burkhardt et al., 1993). Although the ‘giant’ lysosomes are present in all cells, the clinical symptoms arise from the impaired exocytosis of cells with secretory lysosomes, such as melanocytes, platelets, CTLs and NK cells (Baetz et al., 1995, Targan and Oseas, 1983). The condition is often fatal in early childhood, usually as a result of recurrent or severe infections or from hemophagocytic lymphohistiocytosis; a widespread infiltration of lymphocytes and histiocytes into major organs, often referred to as the ‘accelerated phase’ of the disease (Shiflett et al., 2002). Central to the patho-physiology of hemophagocytic lymphohistiocytosis is the defective cytotoxicity of NK and CTLs (Targan and Oseas, 1983, Baetz et al., 1995, Barrat et al., 1999). This failure of cytotoxicity results in the persistence of the pathogen, with sustained but abortive attempts at clearance resulting in prolonged activation and proliferation of CTLs and the sustained secretion of cytokines, thus culminating in the massive infiltration of macrophages and dendritic cells into tissues (Jordan et al., 2004). Treatment consists of

prophylactic antibiotics and bone marrow transplantation to alleviate the immunological defects (Eapen et al., 2007). Despite this, patients who receive bone marrow transplantation and live past adolescence later develop neurologic dysfunction (Tardieu et al., 2005). Approximately 10% of all sufferers exhibit a milder form of CHS and survive to adulthood without bone marrow transplantation. Nonetheless, these patients also develop neurologic symptoms. Neurologic degeneration is not thought to occur from lymphocyte infiltration into the central nervous system, but instead from defective LYST function in neurons and glial cells (Tardieu et al., 2005). CHS can often be confused with HPS-2 and Griscelli syndrome type 2 given the similar initial clinical presentations of hypopigmentation and immunologic dysfunction. Distinction can be made easily with a peripheral blood smear that reveals giant granules in polymorphonuclear leukocytes in CHS.

1.2.2 Identification of the *LYST*/*beige* Gene and Protein Characteristics

LYST is located on chromosome 1 and the murine homologue *beige* is located on chromosome 13 (Barrat et al., 1996, Justice et al., 1990). *LYST* is one of the largest genes in the human genome; containing 55 exons with a corresponding protein of 3801 amino acids and a predicted molecular weight of 429 kDa. Human and mouse LYST share 85% amino acid identity and the *beige* mouse has long been studied as a model of CHS because of the similar cellular and pathological characteristics: hypopigmentation, bleeding and immune cell dysfunction together with the presence of giant lysosomes (Burkhardt et al., 1993). Perou and colleagues observed that fusion of wild-type fibroblasts with *beige* fibroblasts complemented the lysosomal defect, but complementation was not observed between *beige* and CHS fibroblasts, confirming that the defects originated from orthologous genes (Perou and Kaplan, 1993a). The 5’ and 3’ ends of the *beige* sequence were independently cloned by two groups in 1996 using positional cloning techniques and *in vitro* yeast artificial chromosome (YAC) complementation (Barbosa et al., 1996, Perou et al., 1996). The full length human *LYST* gene was soon afterwards identified by Nagle and colleagues, confirming that the

two sequences previously identified belonged to the same gene (Nagle et al., 1996).

LYST is predicted to be cytosolic based on the absence of identifiable transmembrane domains. LYST belongs to the BEACH (for beige and CHS) family of proteins, which in mammals includes FAN (factor associated with neutral sphingomyelinase), neurobeachin, LRBA (lipopolysaccharide-responsive vesicle trafficking, beach and anchor-containing) and ALFY (autophagy-linked FYVE protein). All of which carry BEACH and WD40 domains in their C-terminals (Figure 1.3). Although the function of the BEACH domain is unknown, it is highly conserved across several species and contains the amino acid sequence WIDL (tryptophan, isoleucine, aspartic acid, leucine), in addition to other conserved amino acids (Figure 1.3). BEACH proteins with known function are implicated in vesicle trafficking, membrane dynamics, autophagy and receptor signalling (Kwak et al., 1999, Wang et al., 2000, Montfort et al., 2010, Filimonenko et al., 2010). The WD40 domain of LYST contains seven tandem WD40 repeats (Nagle et al., 1996). WD40 repeats are short (typically 40 amino acids) sequences that form β-sheets, often ending with tryptophan and aspartic acid (WD). Tandem repeats fold into multi-bladed β-propeller structures that are thought to mediate protein-protein interactions (Li and Roberts, 2001). LYST also contains a perilipin domain (potentially lipid binding) and a series of hydrophobic helices which resemble ARM (armadillo) and HEAT (Huntingtin, Elongation factor 3, protein phosphatase 2A and TOR1) motifs (Figure 1.3, Nagle et al., 1996). ARM and HEAT motifs are also thought to mediate protein-protein interactions and are found in proteins with a diverse array of functions, including some involved in vesicular trafficking (Andrade et al., 2001).

Crystal structure analyses of the BEACH domain from neurobeachin and LRBA have revealed the presence of a novel pleckstrin homology (PH) domain; the sequence of which is weakly conserved among many BEACH proteins, including LYST (Figure 1.3, Jogl et al., 2002, Gebauer et al., 2004). PH domains can be phospholipid binding (important in recruiting proteins to membranes; Haubert et al., 2007), or protein binding (Yao et al., 1994).

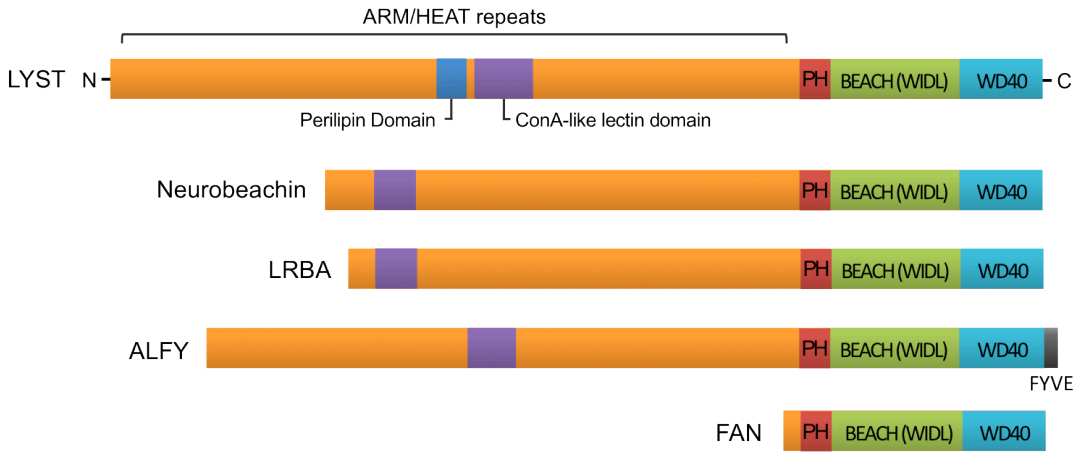

Figure 1.3. Domain organisation of LYST and mammalian BEACH proteins

All members of the BEACH family contain a BEACH domain of unknown function and a varying number of WD40 repeats, thought to mediate protein-protein interactions. The perilipin domain of LYST is potentially lipid-binding and the concanavalin A (conA)-like lectin domain identified in several BEACH family members may mediate oligosaccharide binding. The pleckstrin homology (PH) domain closely associated with the BEACH domain is thought to function as single unit in Neurobeachin, LRBA and FAN. ALFY is the only mammalian BEACH protein that contains the PtdIns(3)P-binding domain FYVE.

Structural analysis and protein binding assays demonstrate a strong interaction between the PH and BEACH domains. Mutating the PH domain reduces the BEACH-dependent signalling activity of FAN (Jogl et al., 2002), suggesting that the PH domain is required for BEACH domain function. Although structural analysis for LYST is not available, the strong interactions demonstrated between the PH and BEACH domains of FAN, LRBA and neurobeachin suggest a similar interaction might occur in LYST.

Recently, a concanavalin A-like lectin domain was identified in LYST that is also present in other BEACH family members (Figure 1.3, Burgess et al., 2009). The authors propose that the domain may mediate oligosaccharide binding and trafficking of vesicle fusion machinery components, due to the significant similarity of the domain with the concanavalin A-like lectin domain of clostridial neurotoxins which carry out a similar function (Burgess et al., 2009). In support of this hypothesis, LYST has been found to interact with

hepatocyte growth factor-regulated tyrosine kinase substrate (HRS), a protein which binds and inhibits SNAP25 (synaptosomal-associated protein of 25 kDa), a component of the SNARE fusion complex required for synaptic vesicle exocytosis (Tchernev et al., 2002). Furthermore, evidence that the concanavalin A-like lectin domain is important for LYST function is demonstrated by the finding that mutations in this domain are associated with CHS (Karim et al., 2002).

While mutations spanning the entire human LYST gene are reported, the clinical phenotype of CHS varies according to the mutation. Karim and colleagues found that severe early-onset disease was associated with truncating mutations predicted to abolish expression of the full-length peptide, whereas missense mutations that likely encode proteins with partial function, gave rise to a milder disease phenotype with a delayed onset and survival to adulthood (Karim et al., 2002). Although several *beige* mutant alleles have been identified, the two most frequently studied are $Lyst^{bg}$ and $Lyst^{bg\text{-}J}$. The $Lyst^{bg}$ allele arose from the radiation-induced retrotransposition of a LINE1 element into the *Lyst* gene and is predicted to encode a truncated protein product missing 1442 amino acids from the C-terminus that contains the BEACH and WD domains (Perou et al., 1997b). The $Lyst^{bg\text{-}J}$ allele carries a three base pair deletion resulting in the loss of isoleucine at position 3741, predicted to disrupt the seventh WD40 repeat of the encoded protein (Trantow et al., 2009).

LYST/*beige* is the only gene to be associated with CHS and identification of several functional protein domains has not provided an explanation as to the function of this large and highly conserved protein. The following section will discuss the effect of LYST deficiency at the cellular level and discuss recent work surrounding its proposed function.

1.2.3 Cellular Defects of CHS and LYST Function

The abnormal enlargement and clustering of lysosomes and lysosome-related organelles is a hallmark of CHS. Although the abnormal morphology occurs in all cells, the clinical manifestations of the disease are associated with the defective biogenesis and/or secretion of lysosome-related

organelles (Ward et al., 2000, Ward et al., 2002, Kaplan et al., 2008). Unfortunately, the large size of the LYST gene and protein render it difficult to study as a whole by many conventional molecular approaches, impeding the gain of useful functional information. Furthermore, the low expression level of LYST and lack of a specific working antibody have made determining the cellular localisation difficult.

Although lysosomes are enlarged and fewer in number in CHS/*beige* cells, the total volume of acidic compartments per cell is the same as in wild type cells (Burkhardt et al., 1993). Therefore, the reduced lysosome number is attributed to either increased heterotypic lysosome fusion or reduced fission, rather than reduced biosynthesis. Initial studies suggested that the giant organelles form as a result of aberrant heterotypic lysosome fusion (White and Clawson, 1980, Willingham et al., 1981, Perou and Kaplan, 1993b). Studies of CTLs from CHS patients indicated that lytic granule biogenesis is normal, but as the granules mature, they grow in size and become less numerous (Stinchcombe et al., 2000). It is difficult to distinguish from these studies whether vesicle enlargement is due to increased fusion or reduced fission, as vesicle fission events were not examined. Compelling evidence that lysosomal enlargement in CHS/*beige* cells is the result of reduced fission rates comes from a study in which overexpression of murine Lyst in fibroblasts results in the presence of very small lysosomes located near the cell periphery (Perou et al., 1997a). The lysosomes were smaller in size than those observed in cells with normal Lyst protein levels, strongly supporting the hypothesis that Lyst positively regulates lysosome fission. This was recently substantiated by Durchfort and colleagues, who, using live-cell time-lapse microscopy, found a decreased rate of lysosome fission in *beige* macrophages, while the rate of fusion remained unchanged (Durchfort et al., 2012). This is the only study to date which specifically examines fission events in Lyst-deficient cells. Studies in other cell types examining fission in such detail are required before a definitive conclusion can be drawn about the role of LYST in vesicle fusion/fission.

The hypothesis that LYST is required for the exocytosis of secretory lysosomes comes from studies that observed defective function of cells

containing secretory lysosomes, in particular NK cells and CTLs (Targan and Oseas, 1983, Baetz et al., 1995). NK cells were normal in number, but lacked the ability to kill target cells because of a failure to exocytose their lytic granules. For exocytosis to occur, granules must migrate along microtubules to the MTOC, which polarises toward the target contact zone, known as the immunological synapse (Orange, 2008). It was previously thought that the granules failed to mobilise to the synapse because of a microtubule defect. Perou and Kaplan demonstrated that enlarged *beige* macrophages were able to migrate to and from the cell periphery in response to phorbol esters and acidifying agents, albeit slower than their wild type counterparts (Perou and Kaplan, 1993b). Their data indicated that microtubule-based motility was intact in the absence of Lyst. However, the authors noted that very large lysosomes were immobile, suggesting that the large size may hinder the vesicle's migration through the filamentous meshwork of the cytoplasm. This did not seem to be the case for lytic granules of CHS CTLs, as granules polarised normally at the immunological synapse (Baetz et al., 1995, Barrat et al., 1999, Stinchcombe et al., 2000). Thus, it seems possible that LYST is required for secretory lysosome docking or fusion at the plasma membrane.

LYST is proposed to coordinate vesicle and/or protein trafficking to secretory lysosomes (Introne et al., 1999). Zhang and colleagues found that absence of LYST resulted in the abnormal appearance of endoplasmic reticulum-resident proteins in lysosomal membranes (Zhang et al., 2007a). Although this may indicate inappropriate trafficking of proteins to lysosomes, it may also suggest that LYST is required for the removal of proteins from the lysosome following vesicle fusion events, for example, after formation of a hybrid organelle. It is conceivable that the inappropriate presence of non-lysosomal proteins in secretory lysosome membranes could interfere with their capacity to fuse with the plasma membrane during exocytosis, however, this has not been directly assessed. Defective transport from the TGN or early endosomes to late multivesicular endosomes was observed in CHS B-cells that resulted in reduced levels of MHC class II molecules and LAMP proteins in late endosomes (Faigle et al., 1998). However, the trafficking of lytic granule proteins in CTLs from CHS patients was intact, as

granzymes, perforin and the lysosomal hydrolase cathepsin D were all targeted normally to lytic granules (Baetz et al., 1995, Stinchcombe et al., 2000). It is possible that the function of LYST differs according to cell type. The range of cellular defects described in the literature and seemingly conflicting reports certainly seem to suggest this is the case.

The BEACH domain sequence is highly conserved, yet the diverse range of functions of other BEACH-containing proteins has not helped identify a common function for the domain (Table 1.2). *Dictyostelium* large volume sphere B (LvsB) is required for the maturation and secretion of a lysosome-derived compartment (referred to as the postlysosome) while LvsA regulates the size of the contractile vacuole and is required for daughter cell separation during cytokinesis (Charette and Cosson, 2007, Kwak et al., 1999).

ALFY is not implicated in lysosome homeostasis, instead it is required for autophagic clearance of aggregate proteins (Filimonenko et al., 2010). It appears to recruit and scaffold a multiprotein complex required for the formation of autophagosomes around the protein aggregates (Filimonenko et al., 2010). Neurobeachin is a member of the AKAP (A kinase anchor protein) family of proteins that bind protein kinase A (PKA). It is selectively expressed in neurons and endocrine cells and associates with neuronal tubulovesicular endomembranes (Wang et al., 2000). A study using neurons from heterozygous neurobeachin knockout mice suggest neurobeachin is required for the direct targeting of neurotransmitter receptors to the cell surface for synaptic transmission (Nair et al., 2013).

LRBA (previously referred to as CDC4L) has a wide tissue distribution similar to LYST (Wang et al., 2001). When macrophages are stimulated with lipopolysaccharide, cytosolic LRBA becomes associated with lysosomes as well as the plasma membrane (Wang et al., 2000). The authors of the study propose a ‘two-signal’ model for the function of LRBA in vesicle trafficking. In this model, they suggest that LRBA binds to PKA after lipopolysaccharide stimulation (the first signal), enabling its association with vesicles through its BEACH domain.

Organism	Protein	Function	Reference
Mammals	FAN	TNF-induced N-SMase activation and generation of ceramide, TNF-induced CDC42-dependent cytoskeletal remodelling and filipodia formation, lysosome homeostasis	Montfort et al., 2010
	Neurobeachin	Protein Kinase A anchor protein involved in neuronal synaptic vesicle secretion	Wang et al., 2000,
	LRBA	Protein Kinase A anchor protein involved polarized vesicle secretion, autophagy	Wang et al., 2001 Lopez-Herrera et al., 2012
	ALFY	Elimination of aggregated proteins by autophagy	Filimonenko et al., 2010
Drosophila melanogaster	AKAP550	Protein Kinase A anchor protein involved in vesicular release in polarized cells	Han et al., 1997
	Mauve	Maturation of autophagosomes during nutrient deprivation	Rahman et al., 2012
Caenorhabditis elegans	SEL-2	Protein Kinase A anchor protein involved in endosomal trafficking	de Souza et al., 2007
Dictyostelium discoideum	LvsA	Regulation of the contractile vacuole and separation of daughter cells during cytokinesis	Kwak et al., 1999
	LvsB	Maturation and secretion of postlysosomes	Charette and Cosson, 2007

Table 1.2. Specific functions of known BEACH family members

Several characterised BEACH proteins and their cellular functions are listed, together with relevant references. FAN, Factor associated with N-sphingomyelinase; LRBA, Lipopolysaccharide-responsive and beige-like anchor protein; ALFY, autophagy-linked FYVE-protein; AKAP550, A kinase anchor protein 550; LvsA, large volume sphere A; LvsB, large volume sphere B; N-SMase, neutral sphingomyelinase; CDC42, cell division control protein 42.

This is supported by the finding that a green fluorescent protein (GFP)-fusion peptide carrying only the C-terminal portion of LRBA (containing the BEACH/WD40 domain) localised to vesicular structures in response to lipopolysaccharide; this was proposed to tether vesicles to microtubules for transport to the plasma membrane. A second signal that triggers the interaction of LRBA with proteins at the plasma membrane is proposed to result in vesicle fusion, thus providing a mechanism for polarised secretion in neuronal cells (Wang et al., 2001). A similar mechanism for LYST-mediated exocytosis of secretory lysosomes is plausible. Like LRBA, LYST is reported to be cytosolic in macrophages (Perou et al., 1997a), yet is capable of associating with punctate structures that partially align along microtubules (Faigle et al., 1998). In immune cells such as CTLs and NK cells, LYST may associate with secretory lysosomes upon target cell interaction. Although LYST is not required for granule movement (granules polarise to the plasma membrane independently of LYST in response to target ligation; Barrat et al., 1999, Clark and Griffiths, 2003), its association may be important for mediating granule docking or fusion events upon arrival at the plasma membrane. For example, LYST might interact with plasma membrane proteins at the immunological synapse, perhaps through its WD40 domains, and mediate the recruitment of fusion machinery components, such as SNAREs, to the granule membrane.

The PH domain of BEACH proteins is not thought to be phospholipid binding, based on the crystal structure of Neurobeachin that indicates that the two phospholipid binding pockets of the domain are otherwise occupied; one by an α-helix and the other by residues of the BEACH domain (Jogl et al., 2002). Gebauer and colleagues later showed that the PH domains of LRBA, neurobeachin and FAN did not bind any of the phospholipids tested in a lipid binding assay (Gebauer et al., 2004). FAN is the smallest protein belonging to the BEACH family and an adaptor protein important for mediating downstream responses to tumour necrosis factor (TNF). It binds to TNF receptor and activates neutral sphingomyelinase (N-SMase) to generate the lipid signalling molecule ceramide and is thought to be important for mediating inflammatory cellular reactions in response to TNF (Adam-Klages et al., 1996). FAN is also required for TNF-induced actin

reorganisation (Haubert et al., 2007). Haubert and colleagues showed that the PH domain of FAN binds to PtdIns(4,5)P_2, targeting FAN to the plasma membrane where it promotes CDC42 (cell division control protein 42) activation to induce cytoskeletal reorganisation (Haubert et al., 2007). Expression of a GFP-FAN mutant lacking the PH domain abolished membrane localisation, whereas deletion of the BEACH or WD domains had no effect on membrane localisation. PtdIns(4,5)P_2 was not included in the lipid overlay assay performed by Gebauer and colleagues (2004), thus, it is possible that neurobeachin, LRBA and indeed LYST, may also bind PtdIns(4,5)P_2 at the plasma membrane and this may be important for their function. It is interesting to note that PtdIns(4,5)P_2 is mislocalised in *beige* fibroblasts; Ward and colleagues reported a nuclear PtdIns(4,5)P_2 staining pattern in wild type fibroblasts that was absent in *beige* fibroblasts (Ward et al., 2000). Plasma membrane PtdIns(4,5)P_2 is required for regulated exocytosis of synaptic vesicles (Koch and Holt, 2012), mast cell granules (Hammond et al., 2006) and NK lytic granules (Capuano et al., 2012), however, the effect of PtdIns(4,5)P_2 mislocalisation on secretory lysosome exocytosis in CHS/*beige* cells has not been examined.

Lysosomal enlargement in CHS cells has been linked to altered protein kinase C (PKC) levels. PKC activity is down-regulated in *beige* polymorphonuclear leukocytes, NK cells and fibroblasts (Ito et al., 1989, Ito et al., 1988b, Tanabe et al., 1998, Tanabe et al., 2000). The down-regulation is attributed to enhanced proteolysis of PKC by calpain. Calpain is a cysteine protease that cleaves PKC into an inactive form (Nishizuka 1986). Addition of calpain inhibitors such as E-64-d have been shown to correct the lowered PKC activity and to correct other cellular defects of CHS/*beige*, such as the giant lysosomes in fibroblasts and the defective NK cell-mediated killing of target cells (Ito et al., 1989, Tanabe et al., 2000 Tanabe et al., 2009). The link between LYST and PKC activity is difficult to determine given that an association between PKC and LYST has not been established. Ceramide levels are increased in *beige* cells (Tanabe et al., 2000). Tanabe and colleagues demonstrated that ceramide promotes calpain mediated proteolysis of PKC, and suggest that increased ceramide in *beige* fibroblasts is responsible for PKC down-regulation (Tanabe et al., 1998, Tanabe et al.,

2000). Furthermore, addition of exogenous C_2-ceramide promotes lysosomal enlargement in normal fibroblasts, that is reversed upon treatment with E-64-d (Tanabe et al., 2000). Ceramide is generated by SMase-mediated hydrolysis of sphingomyelin (SM) and functions as a signalling lipid with important roles in cell proliferation and induction of apoptosis (Montfort et al., 2010). Activity of both acid-SMase (A-SMase) and N-SMase is enhanced in *beige* cells and stimulation with phorbol ester induces further ceramide production (Tanabe et al., 2000, Cui et al., 2001). Exactly why LYST deficient cells have elevated SMase activity is unknown, as is the mechanism by which ceramide mediates down-regulation of PKC in CHS/*beige* cells. It is interesting to note that deficiency of FAN results in reduced N-SMase activity (Adam-Klages et al., 1996), while deficiency of LYST appears to be linked to enhanced SMase activity, suggesting opposing functions of these two proteins regarding ceramide generation. Although SMase has not been identified as a binding partner of LYST, it is possible that LYST regulates ceramide levels by binding SMase under specific conditions, such as stimulated exocytosis. This may be important for controlling membrane fluidity and raft formation during vesicle exocytosis. It remains to be determined if reduced levels of PKC is an immediate biochemical defect resulting from loss of LYST, or whether the effects on PKC represent a more downstream effect.

1.2.4 LYST-Interacting Proteins

Twenty-four LYST-binding proteins were identified in a yeast two-hybrid screen (Tchernev et al., 2002). Three of these interactions were confirmed using *in vitro* binding assays: casein kinase IIβ (CK2β), HRS and tyrosine 3-monooxygenase/tryptophan 5-monooxygenase activation protein, theta polypeptide (14-3-3τ). The binding of LYST to HRS is of particular interest because HRS has been shown to bind and inhibit SNAP25, a component of the SNARE fusion machinery. Overexpression of HRS inhibits Ca^{2+}-dependent exocytosis of dense-core secretory vesicles in PC12 cells (Kwong et al., 2000). Thus, binding of LYST to HRS may release inhibition of SNAP25 and enable exocytosis of secretory lysosomes. Interestingly, several proteins identified as LYST-binding partners by Tchernev and

colleagues are implicated in cell cycle regulation and mitosis. CK2β forms the two regulatory subunits of the CK2 heterodimer that is required for progression through G1 and G2/M cell cycle checkpoints (Hanna et al., 1995). 14-3-3τ promotes proliferation by permitting cell cycle progression through degradation of p21 (Wang et al., 2010). Two other LYST binding proteins, centromere protein J (CENPJ) and centrobin are required for normal spindle formation during mitosis (Wang et al., 2010, Jeffery et al., 2010, Zou et al., 2005, McIntyre et al., 2012). These findings are compatible with the possibility that LYST functions in cellular pathways other than those governing secretory lysosome biogenesis and exocytosis.

Despite the prominent cellular defects associated with CHS and extensive investigation into the underlying biochemical defects, the molecular pathways governing LYST-mediated regulation of secretory lysosomes remain unknown. One reason for this is that LYST presents a technical challenge to investigators attributed to its large size. The majority of studies concerning LYST function have primarily addressed lysosomal enlargement - the most striking cellular defect of CHS/*beige*. On the basis of its large size and the diverse roles of potential binding partners, LYST is likely to have multiple functions and these may have been overlooked in previous studies. Moreover, one aspect of the CHS/*beige* phenotype has not been addressed: the effect of mislocalised PtdIns(4,5)P_2. In addition, other BEACH family members ALFY, LRBA and mauve are implicated in the autophagic pathway (Filimonenko et al., 2010, Lopez-Herrera et al., 2012, Rahman et al., 2012), yet investigation of the autophagic pathway in CHS/*beige* is limited to a single study (Zhang et al., 2010). Although the authors report similar levels of autophagy in *beige* and control fibroblasts, the effect of LYST depletion on the autophagic pathway cannot be concluded from one study alone, and requires further investigation. Closer examination of the CHS/*beige* phenotype, beyond the enlarged lysosomes, could identify important pathways of LYST function and the regulation of secretory lysosomes.

1.3 Natural Killer Cells

NK cells are lymphocytes of the innate immune system that form a first line of defence against pathogens. Their main function is the clearance of tumour cells and virus-infected cells by a mechanism known as cell-mediated cytotoxicity (de Saint Basile et al., 2010). Unlike CTLs, NK cells do not require prior sensitisation and provide host protection during the period when the adaptive immune response is developing (Kiessling et al., 1975). NK cell cytotoxicity involves the stimulated secretion of cytolytic effector molecules towards the recipient cell following direct contact and the ligation of specific NK cell receptors. The effector molecules are housed within specialised secretory lysosomes – the lytic granules – that function as degradative organelles but with the added capacity to engage in regulated exocytosis in response to extracellular stimuli (de Saint Basile et al., 2010).

1.3.1 Natural Killer Cell Function

NK cells express an array of germline encoded receptors that detect alterations in host cell surface molecules. The receptors fall into one of two groups: activating receptors that stimulate a cytolytic response, or inhibitory receptors that prevent a cytolytic response. Inhibitory receptors recognise MHC class I molecules on the surface of healthy cells, while ligands for activating receptors are upregulated in stressed, infected or malignant cells (Scott et al., 2008). Unstressed ‘healthy’ cells escape death by NK cells based on their expression of MHC class I, while cells with down-regulated MHC class I expression (such as during certain viral infections or malignancy) concomitantly expressing stress-induced ligands fail to initiate inhibitory signals and result in NK cell activation. An effector response is mounted based on the overriding signal received from many receptor molecules (Vivier et al., 2011).

NK cells contain numerous lytic granules that are packaged with cytotoxic effector proteins that initiate apoptosis in the target cell. Upon NK cell activation, the granules traffic to the immunological synapse with the target cell where they fuse with the plasma membrane. This results in the release of granule contents into the synaptic cleft and the externalisation of granule-

resident proteins such as LAMPs on the plasma membrane, in a process known as degranulation (Stinchcombe and Griffiths, 2007, Alter et al., 2004). The major effector proteins are granzymes and perforin. Granzymes (A, B, H, K and M in humans) are serine proteases that initiate target apoptosis primarily via the activation of the caspase cascade (Bots and Medema, 2006). Perforin is a pore-forming protein that oligomerises into transmembrane channels within the target cell membrane and facilitates the cytosolic delivery of granzymes by several proposed mechanisms (Lopez et al., 2012). A second essential function of NK cells is the secretion of immunomodulatory chemokines and cytokines, such as tumour necrosis factor alpha (TNFα) and interferon gamma (IFNγ). These recruit and activate inflammatory cells and other immune cells, coordinating both innate and adaptive immune responses (Vivier et al., 2011). Cytokines are contained within conventional secretory vesicles and are secreted in a pathway distinct from that of perforin and granzymes (Reefman et al., 2010).

The induction of an NK cell effector response requires a tight association with the target cell. Tight association ensures that the delivery of perforin and granzymes is spatially restricted to the intended cell, thus limiting inadvertent lysis of bystander cells. The formation of the immunological synapse and subsequent degranulation event follow several discrete stages.

1.3.2 Formation of the Immunological Synapse

Despite differences in target cell recognition, the mechanism by which NK cells and CTLs destroy target cells is similar and much of what we assume of the mechanisms governing NK cytotoxicity was first derived from the study of CTLs.

Once activated, the NK cell must develop a firm adhesion with the target and this is achieved via the integrin family of adhesion molecules (Bryceson et al., 2006). Studies of the mature synapse in CTLs reveal that receptors and adhesion molecules are organised into distinct clusters at the contact zone called supramolecular activation clusters (SMAC), comprised of a central SMAC (cSMAC) and a peripheral SMAC (pSMAC) (Stinchcombe and Griffiths, 2007). A similar receptor organisation is proposed for NK cells and is thought to be important for robust signalling (Giurisato et al., 2007). Also

critical to synapse maturation is the accumulation of filamentous actin (F-actin), which is dependent on CDC42 and Wiscott-Aldrich syndrome protein (WASp) that promote F-actin branching (Orange et al., 2002). Similarly, the enrichment of certain lipids into organised membrane domains (lipid rafts) is found at the synapse (Capuano et al., 2012) and may be important for co-ordinated signalling. The formation of a mature synapse in the initial stage of an effector response not only ensures tight contact with target cells, but serves as a platform for signalling and exocytic events during the effector stage of NK function.

1.3.3 Mechanisms of Granule Exocytosis

The delivery of granules to the immunological synapse involves several stages: the polarisation of granules to the immunological synapse, docking of granules at the plasma membrane and priming of the granules to facilitate fusion (reviewed in Orange, 2008). Granule polarisation requires both the minus-ended movement of granules along microtubules towards the MTOC and polarisation of the MTOC to the synapse. The kinetics of granule migration and the associated motor proteins have only recently been identified. Dynein is an essential motor protein required for movement of lytic granules towards the MTOC. Overexpression of dynein mutants results in peripheral granules that fail to converge after target conjugation (Mentlik et al., 2010). It was previously assumed that granule convergence occurred simultaneously with MTOC reorientation (Orange, 2008), however, Mentlik and colleagues argue that granule convergence is a prerequisite for MTOC polarisation (Mentlik et al., 2010). In their study, they observed that upon NK cell activation, granules rapidly clustered at the MTOC, and that a gradual reorientation of the MTOC to the synapse followed. Using antibodies directed against the activating receptor CD28 or integrin CD11a in the NK cell-like YTS cell line, they further demonstrated that activation can initiate granule convergence without MTOC polarisation or cytotoxicity. They propose that rapid granule clustering following NK cell activation serves to assemble the granules ready for delivery whilst a mature synapse is formed and a robust activation signal generated (Mentlik et al., 2010). This would ensure that granules are delivered in synchrony to the immunological

synapse following MTOC polarisation, thus guaranteeing a precise lethal hit to the recipient.

MTOC polarisation serves only to bring the granules into proximity with the immunological synapse. Further steps are required to deliver the granules to the plasma membrane. The importance of F-actin accumulation at the synapse for cytotoxicity is well recognised and agents that block actin polymerisation also block degranulation (Orange et al., 2002). However, the dense cortical actin also poses a barrier to lytic granule access to the plasma membrane. The current model proposes that clearance of a large (1-4 μm) but discrete region of actin within the cSMAC occurs to provide unobstructed access to the membrane prior to degranulation (Orange, 2008). This model is challenged by studies which demonstrate the actin motor protein myosin IIA is required for granule delivery to the plasma membrane (Sanborn et al., 2009). These apparently conflicting observations were recently clarified in study that exploited microscopy techniques with improved resolution to those previously employed. In the study, the authors report a region at the synapse where actin is hypodense, but not fully cleared from the plasma membrane (Rak et al., 2011). Within this region they observed that granules at the synapse were in close association with the actin network and secreted through minimal clearances that were just large enough to accommodate the organelle (Rak et al., 2011). This scenario would facilitate myosin IIA-mediated delivery of granules along actin filaments to the site of fusion. Docking of the granule at the plasma membrane might then trigger clearance of the remaining actin in the vicinity of the granule, permitting fusion and release. It is likely that granule membrane-associated proteins might trigger actin reorganisation to mediate this clearance.

A number of proteins are recruited to the granule prior to degranulation that mediate the terminal stages of exocytosis. These enable docking of the granules at the plasma membrane, priming to regulate secretion, and fusion of the two membranes to release granule contents into the synaptic cleft. Many of the proteins characterised share a common function in CTLs and NK cells but the mechanisms proposed remain mostly hypothetical. Two

essential molecules of the granule exocytosis machinery are Rab27a (mutated in Griscelli syndrome type 2, as described in Section 1.1.5) and unc-13 homolog 4 (Munc13-4). Rab27a associates with granule membranes and facilitates their docking at the plasma membrane, while Munc13-4 is implicated in a SNARE-mediated priming step that renders granules competent to fuse with the plasma membrane (Neeft et al., 2005, Ménager et al., 2007, Feldmann et al., 2003). Furthermore, a direct interaction between Munc13-4 and Rab27a is required for cytotoxicity (Ménager et al., 2007). Interestingly, it has been shown in CTLs that many components of the granule fusion machinery are not associated with perforin and granzyme-containing vesicles until just prior to exocytosis, indicating that additional granule maturation steps are required to deliver the fusion machinery to the granule. In the study by Ménager and colleagues, Munc13-4 was found to be localised to Rab11-positive recycling endosomes and mediated the association of recycling endosomes with Rab27-positive late endosomes, which fused together to form an ‘exocytic vesicle’ carrying secretory machinery components. Upon target recognition, the exocytic vesicles simultaneously polarised to the immunological synapse together with perforin-containing lytic granules, where they fused together immediately before secretion (Figure 1.4, Ménager et al., 2007). This fusion step confers Munc13-4 and Rab27a to the membranes of lytic granules, rendering them competent to dock and fuse with the plasma membrane (Ménager et al., 2007). Munc13-4 and Rab27a were also found to independently but simultaneously polarise to the synapse with perforin in NK cells, however, the endocytic localisations of Rab27a and Munc13-4 were not investigated (Wood et al., 2009). Together, these findings support the notion that heterotypic fusion of endocytic vesicles contributes to lytic granule maturation. In their study in NK cells, Reefman and colleagues observe a partial colocalisation of perforin with Rab11 (Reefman et al., 2010). Although disrupting the recycling endosome did not significantly impair perforin secretion, it did retard granule reformation or the filling of immature granules with perforin.

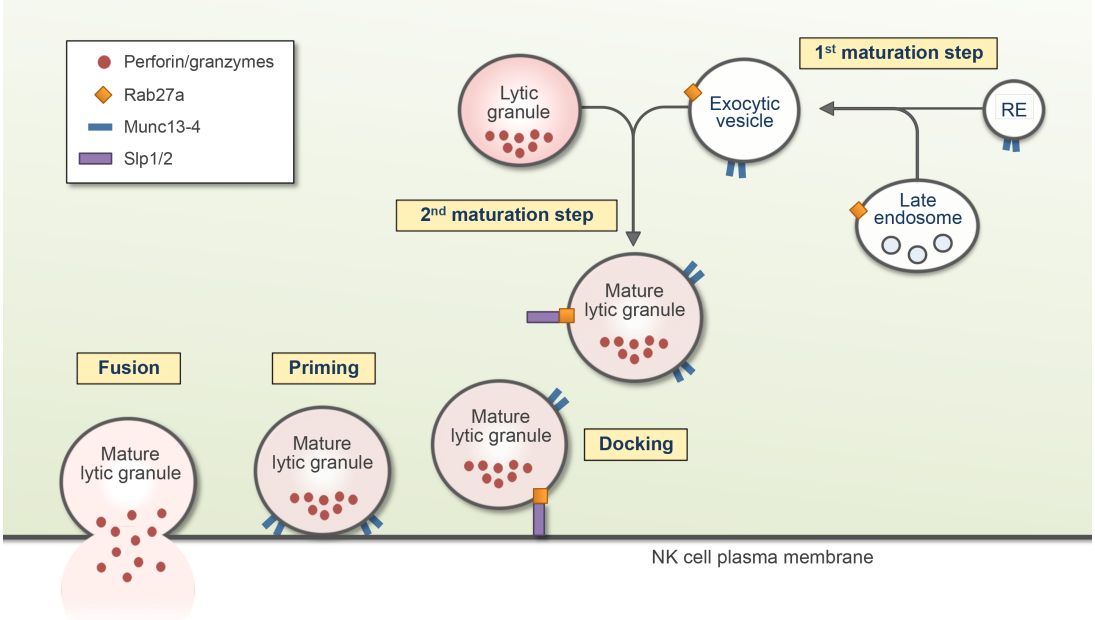

Figure 1.4. Proposed lytic granule maturation steps and associated proteins

Munc13-4 located on recycling endosomes mediates the association of recycling endosomes with Rab27-positive late endosomes, which fuse together to form an 'exocytic vesicle' (*1st maturation step*). Upon target conjugation, the exocytic vesicles simultaneously polarise to the immunological synapse together with perforin-containing lytic granules, where they fuse together to form a mature lytic granule (*2nd maturation step*). This confers exocytic machinery components to the membranes of lytic granules, including Munc13-4 and Rab27a. Rab27a recruits its effector proteins synaptotagmin-like protein 2a (Slp2a, and possibly Slp1) to the granule which tethers granules to the plasma membrane through their C2 domains (*docking*). Munc13-4 engages with plasma membrane proteins in a post-docking step that promotes assembly of the SNARE complex (*priming*). In the final stage in the granule exocytosis pathway, fusion of the two membranes permits the release of perforin and granzymes into the synaptic cleft.

These findings suggest that interaction between recycling endosome proteins and the lytic granule is important for a mature secretory granule. In this study, the authors relied on phorbol ester stimulation to induce NK cell lytic granule exocytosis (Reefman et al., 2010). The combination of phorbol ester and ionomycin evokes a mass degranulation event which bypasses receptor activation and many of the sequential steps of exocytosis induced by target conjugation (Alter et al., 2004). Thus, the exact functional

significance of the recycling endosome on target-induced lytic granule maturation and secretion in NK cells remains to be determined.

Two proteins, synaptotagmin-like protein 1 (Slp1) and Slp2a, have recently been identified as effectors of Rab27a in CTLs and NK cells (Holt et al., 2008, Ménasché et al., 2008). In CTLs, Slp2a is recruited to Rab27a-positive vesicles but remains distinct from perforin-containing vesicles. Upon conjugation, it partially colocalises with perforin-containing granules and is carried to the synapse where it associates with the plasma membrane via its C2 domain (Ménasché et al., 2008). This recruitment of Slp2a to lytic granules appears to mediate docking at the plasma membrane via a Rab27a/Slp2a complex that is important for cytotoxicity. However, Slp2a depletion does not impair lytic granule secretion, suggesting that additional Rab27a effectors can compensate for the loss of Slp2a. Slp1 has been suggested as a candidate effector, as depletion of both Slp2a and Slp1 impair CTL cytotoxicity (Holt et al., 2008).

The final step in lytic granule exocytosis requires fusion with the plasma membrane and is mediated by SNAREs. The SNARE proteins vesicle-associated membrane protein 7 (VAMP7), syntaxin 11 and synaptosomal-associated protein of 23 kDa (SNAP23) appear to be the main proteins mediating lytic granule fusion in NK cells (Bryceson et al., 2007, Marcet-Palacios et al., 2008). Syntaxin 11 and its accessory protein unc-13 homolog 2 (Munc18-2) are both essential for NK granule secretion, as mutations in either of these two proteins result in immunodeficiency (discussed in Section 1.3.4; Bryceson et al., 2007, Cote et al., 2009). Once the lytic vesicles are docked at the plasma membrane, Munc13-4 is thought to exert its priming function by triggering syntaxin 11 to adopt an open conformation which could facilitate binding to SNAP23 and promote SNARE complex formation (de Saint Basile et al., 2010), although this has not been formally demonstrated. Formation of a stable SNARE complex drives the fusion of the two membranes and granule contents are released into the synaptic cleft where they are taken up by the recipient cell, initiating apoptosis.

The multiple stages of NK lytic granule maturation and exocytosis provide several points at which degranulation can be regulated. Such tight regulation

likely serves to prevent the inappropriate elimination of normal healthy cells. The functions of many proteins implicated in lytic granule biogenesis and secretion were identified through studying primary immunodeficiency diseases arising from single gene mutations, such as CHS, resulting in defective cytotoxicity.

1.3.4 Lessons from Genetic Diseases

CHS, HPS-2 and Griscelli syndrome type 2 are similar disorders exhibiting impaired secretion of both melanosomes and lytic granules, resulting in the clinical symptoms of hypopigmentation and immunodeficiency. Individuals with HPS-2 have enlarged lytic granules that are unable to migrate along microtubules and therefore do not reach the immunological synapse (Clark et al., 2003). HPS-2 patients lack activity of the adaptor protein AP-3. This adaptor appears to be required for the correct sorting of an unidentified protein to the lytic granule, that mediates the attachment of granules to microtubules and their transport in response to target conjugation (Figure 1.5, Clark et al., 2003).

As described previously (Section 1.2.1), the accelerated phase of CHS results in a systemic inflammatory syndrome, hemophagocytic lymphohistiocytosis, resulting from defective NK cell and CTL cytotoxicity. Diseases caused by mutations in several components of the lytic granule exocytic machinery also result in inherited forms of hemophagocytic lymphohistiocytosis, such as familial hemophagocytic lymphohistiocytosis (FHL) and Griscelli syndrome type 2. Similar to CHS, Griscelli syndrome type 2 is characterised by immunodeficiency and hypo-pigmentation, resulting from mutations in the *RAB27A* gene (Ménasché et al., 2000). Studies from CTLs derived from Griscelli syndrome type 2 patients show granules polarise to the immunological synapse but are unable to dock at the plasma membrane (Stinchcombe et al., 2001). This is likely due to a failure to recruit the docking protein Slp2a, as Slp2a remains cytoplasmic in CTLs from Griscelli syndrome patients and is thus unable to mediate granule docking at the plasma membrane (Figure 1.5, Ménasché et al., 2008).

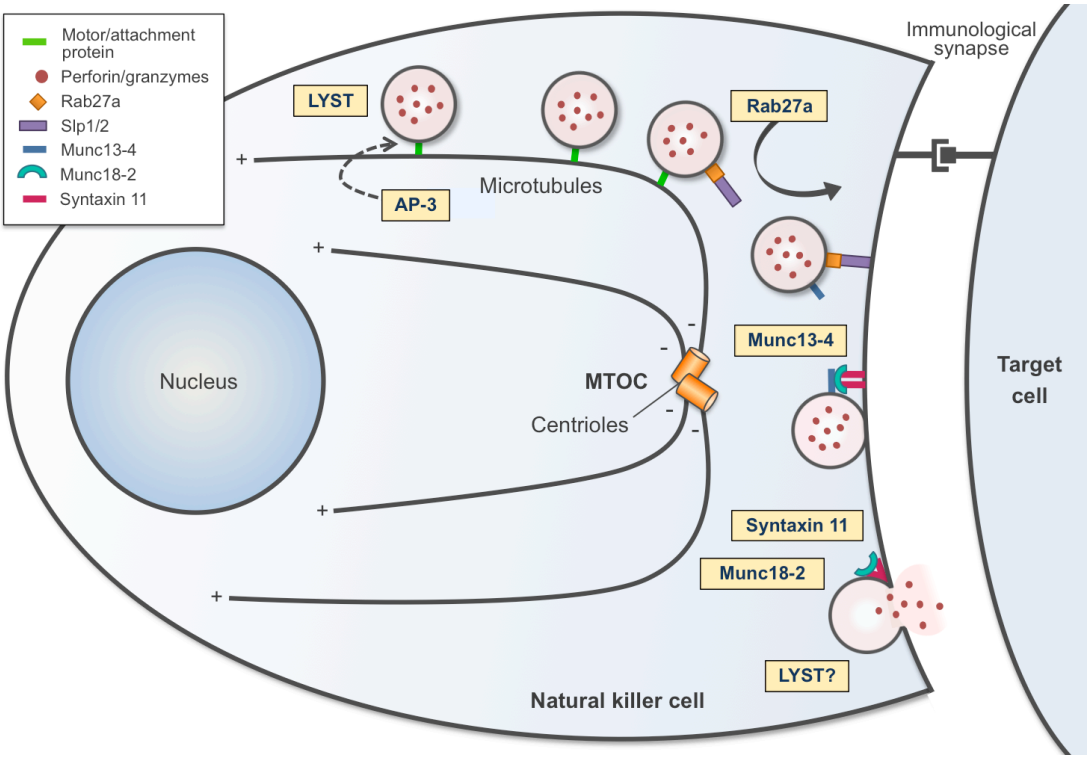

Figure 1.5. Functions of proteins that are defective in diseases affecting lytic granules

Mutations in AP-3 or LYST result in defective granule biogenesis and cause Hermansky-Pudlak syndrome and Chédiak-Higashi syndrome, respectively. AP-3 sorts a protein to the granule which allows attachment or minus-ended movement along microtubules to the microtubule organising centre (MTOC), following target conjugation. Granule docking at the membrane is mediated by Rab27a and synaptotagmin-like proteins Slp1/Slp2. Rab27a is mutated in patients with Griscelli syndrome type 2. Docked granules interact with the plasma membrane SNARE syntaxin 11 and its accessory protein Munc18-2 at the plasma membrane. Priming by Munc13-4 is proposed to change syntaxin 11 from a closed to an open conformation. The formation of a SNARE complex (not shown) composed of syntaxin 11, VAMP7 and SNAP23 triggers membrane fusion and the release of granule contents. Mutations in Munc13-4, syntaxin 11 and Munc18-2 inhibit granule fusion and cause familial hemophagocytic lymphohistiocytosis type 3 (FHL-3), FHL-4 and FHL-5, respectively. LYST may also be required to mediate fusion at the plasma membrane.

Interestingly, the addition of the cytokine interleukin-2 (IL-2) to Rab27a-deficient NK cells partially restores cytotoxicity (Plebani et al., 2000), suggesting there may be other as yet uncharacterised proteins which can substitute for Rab27a to mediate granule docking at the plasma membrane.

FHL type-3 (FHL-3), -4 (FHL-4) and -5 (FHL-5) are caused by mutations in the genes encoding the granule fusion machinery components Munc13-4, syntaxin 11 and Munc18-2, respectively (Figure 1.5, Feldmann et al., 2003, Bryceson et al., 2007, Cote et al., 2009). In the absence of Munc13-4, granules are observed docked at the plasma membrane but are not secreted, resulting in defective cytotoxicity (Feldmann et al., 2003). It is from these observations that Munc13-4 is implicated in priming granules for membrane fusion.

Similar to Munc13-4-deficiency, NK cells deficient in the SNARE protein syntaxin 11 polarised normally at the synapse but failed to fuse with the plasma membrane (Bryceson et al., 2007). However, activation with IL-2 prior to exposure to targets stimulated degranulation in FHL-4 cells, partially restoring cytotoxicity, indicating that syntaxin 11-deficiency can be compensated by other proteins induced by cytokine activation (Bryceson et al., 2007). Mutations in Munc18-2 were only recently identified as a new genetic form of FHL, FHL-5, and led to the discovery of Munc18-2 as a regulator of syntaxin 11 (Cote et al., 2009).

Despite recent advances in our knowledge of the complex mechanisms involving lytic granule biogenesis and exocytosis, there is still much to learn. The role of LYST, for example, in lytic granule biogenesis and secretion remains elusive and despite their critical role in many intracellular trafficking events, the contribution of PIs to NK granule exocytosis is largely unexplored. Moreover, the heterotypic fusion events co-ordinating the maturation of lytic granules into secretion-competent vesicles are not well established in NK cells. Lytic granules share common features with other secretory lysosomes, the majority of which are found in cells of the immune system. The impact of defective secretory lysosome exocytosis is evident from the severity of diseases involving such organelles, which is not just limited to immunological dysfunction, but neurologic dysfunction also. A

better understanding of these organelles is required if we are to fully comprehend the mechanisms which govern our immune system.

1.4 Aims

Many questions still remain unanswered regarding the mechanisms that govern the biogenesis and exocytosis of secretory lysosomes. CHS is a lethal disorder that affects the function of cells with secretory lysosomes and arises from mutations in the LYST gene. The role of LYST is poorly understood despite its identification 16 years ago, and the technical challenge that such a large gene and protein presents has hindered the elucidation of the pathway(s) in which it functions. Furthermore, several aspects of the CHS/beige phenotype remain relatively unexplored. To this end, the specific aims of the study are:

- To investigate the contribution of both PtdIns(4,5)P_2 and autophagy to the cellular defect of CHS and to identify proteins downstream of LYST that may also function in exocytosis of secretory lysosomes.
- To model the CHS/*beige* phenotype using RNA interference and explore the function of LYST.
- To examine the contribution of PIKfyve to the biogenesis and exocytosis of NK cell lytic granules.

Chapter 2
Materials and Methods

2.1 Culture of Mammalian Cell Lines

The cell lines used in this study were obtained from laboratory collections. Cell lines and their respective culture media are listed in Table 2.1.

2.1.1 Cell Line Maintenance

All cell lines were maintained at 37 °C and 5% CO_2 in a humidified incubator and passaged every 3-4 days using standard aseptic techniques. Foetal calf serum (FCS; Sigma-Aldrich, USA) was heat inactivated at 56 °C for 30 minutes before use. During routine passage, adherent cells were washed with phosphate buffered saline (PBS) and detached with trypsin (0.25% w/v trypsin and 0.2 % w/v ethylenediaminetetraacetic acid [EDTA] in PBS) for 2-5 minutes at 37 ^{o}C. Cells were then washed in culture media, centrifuged for 5 minutes at 300 x *g* and the pellets resuspended in fresh culture medium.

2.1.2 Storage and Recovery

For long term storage, with the exception of human NK cells, cells harvested by trypsin were pelleted by centrifugation at 300 x *g* for 5 minutes and resuspended in cell-specific complete medium (Table 2.1) containing 10% v/v dimethyl sulphoxide (DMSO; Sigma-Aldrich, USA). Cells were then frozen at -80 ^{o}C for 2 days before being transferred to liquid nitrogen.

For recovery, cells were thawed rapidly in a 37 ^{o}C water bath, diluted with complete culture medium, centrifuged at 300 x *g* for 5 minutes and the pellet resuspended in complete culture medium. Cells were transferred to tissue culture flasks and allowed to recover for at least 5 days before use.

Cell Line	Origin	Type	Culture Medium
NK-92MI	Derived from the human natural killer cell line (NK-92), stably expressing human IL-2 from the retroviral MFG-hIL-2-IL-2 vector (Tam et al., 1999)	Suspension	RPMI 1640 supplemented with 1% L-glutamine and 10% FCS
K562	Human erythromyeloblastoid leukemia	Suspension	
3T3-J2	Swiss mouse embryonic fibroblasts	Adherent	DMEM supplemented with 1% L-glutamine and 10% FCS

Table 2.1. Cell lines used in this study, their origin and complete culture medium

Roswell Park Memorial Institute (RPMI) 1640 and Dulbecco's Modified Eagle Medium (DMEM) were obtained from Sigma-Aldrich, USA.

2.2 Human NK Cells

Human NK cells were isolated from peripheral blood using Ficoll density gradient separation, followed by magnetic-activated cell sorting (MACS). Ethical approval was granted by the Leeds East Research Ethics Committee; reference number 06/Q1206/106, for the use of human blood samples. Peripheral blood samples were obtained from consenting healthy volunteers and obtained by venepuncture and collected into sterile potassium ethylenediaminetetraacetic acid (K_2EDTA)-coated vacuum tubes (BD Biosciences, USA).

2.2.1 Isolation of Peripheral Blood Mononuclear Cells

Peripheral blood mononuclear cells (PBMCs) were isolated from peripheral blood by density gradient separation. Whole blood was diluted with an equal volume of sterile PBS, layered over Lymphoprep™ (Axis-Shield,UK) and centrifuged at 800 x *g* for 20 minutes, with the brake disabled. PBMCs were collected from the blood plasma/Lymphoprep™ interface and washed with PBS. Cells were counted using a haemocytometer and resuspended in cold MACS buffer (0.5% w/v bovine serum albumin [BSA] and 2 mM sodium EDTA in PBS).

2.2.2 Isolation of NK Cells

Isolation of untouched NK cells from PBMCs was achieved using NK Cell Isolation Kit II (Miltenyi Biotech, Germany) according to the manufacturer's protocol. Briefly, PBMCs were labelled using a cocktail of biotin-conjugated monoclonal antibodies against the non-NK cell fraction. Magnetically labelled anti-biotin antibodies were added and the cells passed through a 40 µm cell strainer (Thermo Fisher Scientific, USA). Cells were passed through a MACS® cell separation column, which was placed within the magnetic field of a MACS® separator stand (both Miltenyi Biotech, Germany). Magnetically labelled non-NK cells were retained in the column. The eluted fraction, containing the unlabelled NK cells, was washed with PBS before centrifugation at 200 x *g* for 10 minutes. Isolated NK cells were assessed by flow cytometry using anti-CD3 and anti-CD56 antibodies (Table 2.5) and the purity of the $CD56^+CD3^-$ fraction (corresponding to NK cells) was found to be > 90%.

2.2.3 NK Cell Maintenance

Cells were maintained in culture medium (DMEM, 10% AB serum, 2 mM L-glutamine, 50 µg/mL penicillin, 50 µg/mL streptomycin) containing 50 U/mL recombinant human IL-2 (Miltenyi Biotech, Germany) for 6-10 days before use.

2.2.4 NK Cell Stimulation

For target cell stimulation, primary NK or NK-92 cells were co-incubated with K562 cells (NK:target ratio of 1:1), in a 96-well plate at 37 ^oC for 1 hour. NK-92 cells were chemically stimulated with 50 ng/mL phorbol 12-myristate 13-acetate (PMA) in combination with 500 ng/mL ionomycin and incubated for 30 minutes at 37 ^oC.

2.3 Murine Fibroblasts

Dermal fibroblast cultures were established from ear explants and animal work was performed under licence and following local ethical review.

2.3.1 Mice

Female Fox Chase SCID® (CB17/Icr-*Prkdc*^{scid}/IcrIcoCrl; Strain Code 236) and Fox Chase SCID® Beige (CB17.Cg-*Prkdc*^{scid}*Lyst*^{bg}/Crl; Strain Code 250) mice (4-11 weeks old) were purchased from Charles River Laboratories International, USA. Mice were culled on arrival by cervical dislocation in accordance with Schedule 1 Code of Practice, UK Animals Scientific Procedures Act 1986.

2.3.2 Establishment of Fibroblast Cultures

Ears were surgically excised from mice and washed in PBS several times. The epidermis was removed mechanically by scraping across the dermal explants using a scalpel and the skin washed in PBS. The skin was cut into small squares (2-3 mm), placed in wells of a 6-well tissue culture plate and sandwiched with sterile 22 mm glass coverslips. Complete growth medium (DMEM plus 10% FCS, 1% L-glutamine, 10 nM HEPES, 10 mM of each non-essential amino acid [glycine, L-alanine, L-asparagine, L-aspartic acid, L-glutamic acid, L-proline, L-serine], 50 IU/mL penicillin, 50 µg/mL streptomycin, 1 mM sodium pyruvate) was added and the explants incubated in a humidified incubator at 37 ^{o}C, 5% CO_2. Medium was changed every 3-4 days until confluency was attained, then cells were routinely passaged according to Section 2.1.1.

2.3.3 Fibroblast Purity and Maintenance

The expression of fibroblast-specific protein 1 (FSP1) was used to determine the purity of fibroblast cultures and was assessed by immunofluorescence microscopy (Section 2.8) after the 3rd passage. Frozen stocks were then prepared and fresh or thawed cells were used until the 12th passage then discarded. Phase contrast images were acquired with an Olympus CKX41 inverted light microscope (Olympus Corporation, Japan).

2.4 SV40T Transfection

The plasmid pBSV-early containing DNA encoding simian vacuolating virus 40 T antigen (SV40T) was a kind gift from Professor GE Blair (University of Leeds, UK. At the 5th passage, *beige* cells were seeded into wells of a 6-well

plate at a density of 2.5 x 10^5 cells per well, 24 hours prior to transfection. Plasmid DNA (2 µg) diluted in 200 µL Opti-MEM® I medium (Life Technologies, USA), was mixed with 4 µL Lipofectamine™ 2000 transfection reagent (Life Technologies, USA) diluted in 200 µL Opti-MEM® I and incubated for 20 minutes at room temperature. The mixture was added to *beige* cells containing 2 mL of fresh culture medium and the cells incubated at 37 °C. The expression of SV40T was assessed 27 days later by immunofluorescence microscopy using the anti-SV40T mouse monoclonal antibody PAb419 (Section 2.8).

2.5 YM201636 Treatment

6-amino-N-[3-[4-(4-morpholinyl)pyrido[3',2':4,5]furo[3,2-d]pyrimidin-2-yl]phenyl]-3-pyridinecarboxamide (YM201636; CAS number 371942-69-7) is a potent small molecule inhibitor of mammalian PIKfyve and was purchased from Merck KGaA, Germany. YM201636 was solubilised in DMSO and cells were treated with either YM201636 or DMSO alone (control) at the concentration and time specified.

2.6 Gene Silencing Using Small Inhibitory RNA (siRNA)

Small inhibitory RNA (siRNA) molecules against murine LYST were purchased from Life Technologies, UK (siLyst 1-4) and Thermo Fisher Scientific, USA (siLyst 5-8). A negative control sequence with no known sequence homology to mouse genes (siControl) was purchased from Life Technologies, UK (sequences are listed in Table 2.2). 3T3-J2 cells were seeded in 12-well plates at a density of 2 x 10^4 cells per well in 1 mL complete culture medium, 24 hours prior to transfection. Cells were transfected with either siLyst 1-8 or siControl, at the specified concentration. For each well, the desired concentration of siRNA was prepared in 100 µL (final volume) Opti-MEM® I medium (Life Technologies, USA). This was added to a solution containing 2 µL Lipofectamine™ RNAiMAX transfection reagent (Life Technologies, USA) and 98 µL Opti-MEM® I and incubated for 20 minutes at room temperature. The transfection mixture was added to cells, giving a final volume of 1.2 mL/well. All transfections were performed

alongside a mock control, in the absence of siRNA. Cells were incubated for 24-96 hours before use. For cells requiring immunofluorescence microscopy analysis, cells were seeded onto coverslips prior to transfection.

Cell Line	Origin	
siLyst 1	Sense:	CCUUUUUCGAAAAAUCAGGtt
	Antisense:	CCUGAUUUUUCGAAAAAGGtt
siLyst 2	Sense:	GGAAAGAAGAAGAAGAGGAtt
	Antisense:	UCCUCUUCUUCUUCUUCCCtg
siLyst 3	Sense:	GGAUUUAGUGUUUCUCUUGtt
	Antisense:	CAAGAGAAACACUAAAUCCtt
siLyst 4	Sense:	CGAGGAUUUCUGUUACUUAtt
	Antisense:	UAAGUAACAGAAAUCCUCGtc
siLyst 5	Sense:	GCAUUAGCACUGCGGGUUA
	Antisense:	UAACCCGCAGUGCUAAUGC
siLyst 6	Sense:	CCGAGAAGUUUGUAGAUCA
	Antisense:	UGAUCUACAAACUUCUCGG
siLyst 7	Sense:	CAGAAUGGAGAGCGGGUUA
	Antisense:	UAACCCGCUCUCCAUUCUG
siLyst 8	Sense:	GAAGAUUGCUAGCGCAUAU
	Antisense:	AUAUGCGCUAGCAAUCUUC

Table 2.2. Sequences of siRNA used in this study

2.7 Quantification of Vesiculated Phenotype

For vesiculation analysis, phase contrast images were acquired with an Olympus CKX41 inverted light microscope using a 20X objective and analysed using ImageJ public domain software version 1.46r (http://rsb.info.nih.gov/ij/; National Institutes of Health, USA) as described in Sections 2.8.3, 2.11 and 2.18. Images were converted to 8-bit greyscale and the threshold pixel brightness was set to the same value for all images using the 'threshold' function. Threshold pixels were converted to binary and a region of interest was drawn around each cell. Particles with an area greater than 2 μm^2 and a circularity value greater that 0.65 were counted for each

cell using the 'analyse particle' function. Cells were deemed positive for a vesiculated phenotype if they contained at least four or more vesicles with an area greater than 2 μm^2.

2.8 Immunofluorescence

Indirect immunofluorescence was used to assess the subcellular localisation of various proteins. All antibody incubations were performed in a humidified chamber at room temperature, unless otherwise stated. For specific information regarding the antibodies used for immunofluorescence, see Table 2.3.

2.8.1 Indirect Immunofluorescence

For immunofluorescence analysis of *beige*, *SCID* or 3T3-J2 fibroblasts, cells were seeded directly onto sterile coverslips in 12-well plates. 3T3-J2 cells were either transfected with siRNA (Section 2.6), or treated with YM201636 (Section 2.5) for the times specified. NK-92 cells were resuspended in growth medium supplemented with either 1 μM YM201636 or an equivalent volume of DMSO for 90 minutes. NK-92 cells were then seeded onto microscope slides coated with poly-L-lysine (Sigma-Aldrich, USA) and allowed to adhere for a further 30 minutes (2 hours total YM201636 incubation time). All cells were washed with PBS, fixed with 4% w/v paraformaldehyde in PBS for 20 minutes and permeabilised with 0.1% v/v Triton X-100 (Sigma-Aldrich, USA) in PBS for 15 minutes. Cells were washed with PBS, blocked with 1% w/v BSA in PBS for 30 minutes then the solution discarded. Primary antibodies were prepared in PBS containing 0.1% Triton X-100 and 1% BSA and the cells incubated with 200 μL/coverslip for 1 hour. Cells were washed three times with PBS and incubated with 200 μL/coverslip of the appropriate AlexaFluor-conjugated secondary antibody (prepared in PBS containing 0.1% Triton X-100 and 1% BSA) for 1 hour. For cells requiring staining of F-actin, 50 nM Texas Red®-X Phalloidin (Life Technologies, USA) was included in the secondary antibody incubation step. Cells were washed once with PBS, stained with 0.5 μg/mL 4',6-diamidino-2-phenylindole (DAPI) for 10 minutes, then washed three times in PBS before mounting with Vectashield® mounting medium (Vector

Laboratories, USA). Cells were stored at 4 ^{o}C prior to imaging with a confocal microscope. (Section 2.9)

2.8.2 Immunofluorescence Analysis of NK-92-K562 Conjugates

K562 cells (1.5 x 10^6) were washed and resuspended in 1 mL medium containing 5 µM Cell Trace Far Red DDAO-SE (Life Technologies, UK) and incubated for 90 minutes at 37 ^{o}C. NK-92 cells (3 x 10^6) were washed and resuspended in 1 mL medium containing 235 nM Hoechst and incubated for 30 minutes at 37 ^{o}C. K562 and NK cells were then washed three times in PBS and resuspended in medium containing either 1 µM YM201636 or an equivalent volume of DMSO for 20 minutes. NK and K562 cells were mixed together (NK-92:K562 ratio of 2:1) and centrifuged gently for 5 minutes at 20 x *g* to encourage conjugate formation. Conjugates were incubated at 37 ^{o}C for 10 minutes, then gently resuspended. Volumes of 100 µL were pipetted onto poly-L-lysine-coated microscope slides within a circle drawn in hydrophobic ink (Pap Pen, Sigma Aldrich, USA). Cells were allowed to adhere for 15 minutes at room temperature in a humidified chamber. Slides were gently dipped in PBS to remove non-adherent cells, fixed with 4% w/v paraformaldehyde in PBS for 20 minutes and permeabilised with 0.1% v/v Triton X-100 in PBS for 15 minutes. Cells were washed by gentle immersion in PBS containing 1% BSA and 0.1% saponin (Sigma-Aldrich, USA; PBS/S) three times, then blocked with PBS/S for 30 minutes. Primary antibodies were prepared in PBS/S and incubated with cells for 1 hour. Cells were washed by gentle immersion three times in PBS/S, then incubated with the appropriate Alexa Fluor-conjugated secondary antibody prepared in PBS/S for 1 hour. Cells were washed by gentle immersion twice in PBS, then once in water before coverslips were mounted onto the cells using Vectashield®. Cells were stored at 4 ^{o}C prior to imaging with a confocal microscope (Section 2.9).

2.8.3 Plasma Membrane PtdIns(4,5)P_2

SCID and *beige* fibroblasts were seeded into wells of an 8-well chamber slide (Merck KGaA, Germany) at a density of 1 x 10^4 cells per well and allowed to adhere overnight at 37 ^{o}C. Cells were washed with PBS and fixed with 4% w/v methanol-free formaldehyde (Thermo Fisher Scientific, USA)

and 0.2% v/v electron microscopy grade gluteraldehyde (VWR International, USA) in PBS for 15 minutes at room temperature. Cells were then rinsed three times with PBS containing 50 mM ammonium chloride (NH_4Cl), to remove unreacted aldehydes. Slides were then placed on a metal plate in a deep ice bath and chilled for a minimum of 5 minutes. All subsequent steps were performed on ice and solutions were pre-chilled. Cells were blocked and permeabilised for 45 minutes with staining buffer (20 mM piperazine-N,N′-bis[2-ethanesulfonic acid] [PIPES] pH 6.8, 137 mM NaCl and 2.7 mM KCl) containing 5% v/v goat serum (Sigma-Aldrich, USA), 0.5% w/v saponin and 50 nM NH_4Cl. Anti-PtdIns(4,5)P_2 antibody (Table 2.3) was applied in staining buffer containing 5% goat serum and 0.1% saponin for 1 hour. Cells were washed twice with staining buffer and incubated for 1 hour with an appropriate Alexa Fluor-conjugated secondary antibody prepared in PtdIns(4,5)P_2-staining buffer containing 5% goat serum and 0.1% saponin. Slides were washed four times with 50 nM NH_4Cl, then post-fixed with 2% formaldehyde in PBS for 10 minutes. Cells were allowed to adjust to room temperature and washed three times with 50 mM NH_4Cl before staining with 0.5 µg/mL DAPI for 10 minutes. Cells were rinsed twice with 50 mM NH_4Cl and once with dH_20 before mounting with coverslips using Vectashield®.

To determine the plasma membrane/cytoplasmic ratio of PtdIns(4,5)P_2, the fluorescence intensities of regions of interest (ROI) both over the plasma membrane and in the adjacent cytoplasmic area (close to the plasma membrane) were determined using ImageJ software version 1.46r. 35 ROI pairs from a total of 18 different cells were averaged and the background fluorescence (determined from ROIs in control areas without cells) was subtracted from all other values.

Immunogen	Host [Clone]	Working Dilution		Manufacturer
		IF	WB	
β-Actin	Mouse	-	1:10,000	Sigma-Aldrich, USA
CI-MPR	Rabbit	1:200	-	Abcam, UK
EEA1	Rabbit	1:200	1:1000	Cell Signalling Technology, USA
FSP1	Rabbit	1:500	-	Abcam, UK
GAPDH	Mouse [6C5]	-	1:2000	Life Technologies, USA
LAMP1	Rat [G2a]	1:500	1:1000	BD Biosciences, USA
LAMP1	Mouse [1D4B]	1:500	1:1000	Abcam, UK
LC3B	Rabbit	1:200	1:1000	Cell Signalling Technology, USA
PIP5K3 (PIKfyve)	Rabbit	1:300	-	Novus Biologicals, USA
PLCγ1	Rabbit	1:200	1:1000	Cell Signalling Technology, USA
PLCγ2	Rabbit	-	1:500	Cell Signalling Technology, USA
PtdIns(4,5)P_2	Mouse [2C11]	1:100	-	Abcam, UK
PRKCB (PKCβ)	Rabbit	-	1:1000	Proteintech Group, USA
SV40T	Mouse [Pab419]	1:1	-	Eric Blair, University of Leeds, UK

Table 2.3. Primary antibodies for immunofluorescence and Western blotting

IF, Immunofluorescence; WB, Western blotting

Immunogen	Conjugate	Host [Clone]	Working Dilution	Manufacturer
Mouse IgG	Alexa Flour 488	Goat	1:500	Life Technologies, USA
Mouse IgG	Alexa Flour 594	Goat	1:500	Life Technologies, USA
Rabbit IgG	Alexa Flour 488	Goat	1:500	Life Technologies, USA
Rabbit IgG	Alexa Flour 594	Goat	1:500	Life Technologies, USA
Rabbit IgG	Alexa Flour 405	Goat	1:500	Life Technologies, USA
Rat IgG	Alexa Flour 488	Donkey	1:500	Life Technologies, USA
Rat IgG	Alexa Flour 594	Donkey	1:500	Life Technologies, USA
Rabbit IgG	Horseradish peroxidase	Goat	1:10,000	Sigma-Aldrich, USA
Mouse IgG	Horseradish peroxidase	Sheep	1:10,000	Sigma-Aldrich, USA

Table 2.4. Secondary antibodies for immunofluorescence and Western blotting

2.8.4 LysoTracker Staining

Acidified organelles were visualized using LysoTracker® Red DND-99 (Life Technologies, USA). Culture media was aspirated from *beige* and *SCID* fibroblasts (seeded onto sterile coverslips the previous day) and replaced with 0.5 mL medium containing 100 nM LysoTracker®. Cells were incubated at 37 ^{o}C for 1 hour, then washed once with PBS. Cells were then stained with 0.5 µg/mL DAPI for 10 minutes, washed three times in PBS and mounted onto microscope slides using Vectashield® (Vector Laboratories, USA). Slides were stored at 4 ^{o}C prior to imaging with a confocal microscope (Section 2.9).

2.9 Confocal Microscopy

Images of immunofluorescently labelled cells were acquired using a Nikon A1R confocal microscope with Plan Apo VC objectives (40X, numerical aperture 1.3 or 60X oil immersion, numerical aperture 1.4) using NIS Elements software version 4.00.07 (all Nikon Instruments, UK). Images were analysed using ImageJ software, version 1.46r and figures were created using Adobe® Photoshop CS6 (Adobe systems, USA). Where appropriate, and as indicated in the figure legends, increased image brightness was achieved in Photoshop CS6 using the 'brightness/contrast' function

2.10 Live-Cell Time-Lapse Microscopy

3T3-J2 cells were seeded at a density of 6 x 10^4 in 35 mm glass bottom dishes (MatTek, USA) and immediately transfected with 50 nM siLyst 2 or siControl siRNA according to Section 2.6. The medium was replaced after six hours with phenol red-free CO_2-independent medium (Life Technologies, USA) supplemented with 10% FCS and 2 mM L-glutamine. The cells were then placed in a BioStation IM-Q microscope with a 37 ^oC humidified chamber (Nikon Instruments, UK). Phase contrast images were acquired at several points with a 20X objective every 60 seconds.

2.11 LC3B Puncta Quantification

Beige and *SCID* fibroblasts or siRNA-transfected 3T3-J2 cells (Section 2.6), seeded onto sterile coverslips, were washed in PBS. Cells were treated with 10 μM (*beige* and *SCID*) or 25 μM (3T3-J2) chloroquine (Cambridge Bioscience, UK) or an equivalent volume of DMSO. After 24 hours, the presence of LC3B puncta was determined by immunofluorescence and confocal microscopy using an anti-LC3B antibody, according to Sections 2.8 and 2.9. The number and size of puncta per cell were determined from confocal images using ImageJ software version 1.46r. Images were split into red, green and blue channels and the green channel (corresponding to LC3B fluorescence) was converted to 8-bit greyscale. The fluorescence intensity threshold was set using the 'threshold' function (constant for all

image analysis) and the threshold pixels converted to binary format. A region of interest was drawn around each cell and particles greater than 0.2 μm^2 were counted for each cell using the 'analyse particle' function.

2.12 Lipid-Overlay Assay

To test the binding specificity of anti-PtdIns(4,5)P_2 antibody (Table 2.3), a lipid overlay assay was performed using a PIP Strip™ membrane (Life Technologies, USA). Each strip contains 100 pmol of 15 different phospholipids spotted onto a nitrocellulose membrane. The membrane was blocked in TBS/T (10 mM Tris-HCL pH 8.0, 150 mM NaCl, 0.1% v/v Tween 20) containing 3% fatty acid-free BSA (Sigma-Aldrich, USA) for 1 hour at room temperature with gentle agitation. The membrane was then incubated with 0.5 µg/mL anti-PtdIns(4,5)P_2 antibody prepared in TBS/T containing 3% fatty acid-free BSA for 1 hour at room temperature. The membrane was washed with TBS/T three times using gentle agitation for 10 minutes each. The membrane was then incubated with a horseradish peroxidase-conjugated sheep anti-mouse IgG secondary antibody (Table 2.3) diluted 1:5000 in TBS/T containing 3% fatty acid-free BSA, for 1 hour at room temperature. The membrane was then washed with TBS/T three times for 10 minutes each with gentle agitation and the bound protein was detected using Amersham enhanced chemiluminescence reagent (GE Healthcare, UK). The membrane was transferred to a light proof cassette and developed using CL-XPosure film (Thermo-Fisher Scientific, USA) and an automated Konica SRX 101A X-ray developer (Konica, UK). The densities of the spots were analysed using Quantity One software (Bio-Rad Laboratories, USA) and the area of the membrane containing no lipid (blank) was used for background correction.

2.13 Degranulation Assay

LAMP1 (also known as CD107a) surface expression was used to measure NK cell degranulation following chemical- or target cell-stimulation and assessed by flow cytometry. Primary NK or NK-92 cells were treated with YM301636 or DMSO (in triplicate) at the concentrations specified and incubated at 37 ^{o}C for 20 minutes, prior to the degranulation assay. Cells were stimulated with K562 cells or PMA/ionomycin according to Section 2.2.4. Cells were then stained with anti-LAMP1-FITC monoclonal antibody (1:100) or isotype-FITC (Table 2.5), together with GolgiSTOP™ (1:1000 v/v; BD Biosciences, USA) and incubated at 37 ^{o}C for a further 2 hours. Cells were subsequently stained with anti-CD56-PE antibody (1:200) or isotype (Table 2.5) for 15 minutes at room temperature to distinguish NK cells from K562 cells. Cells were pelleted at 300 x *g* for 3 minutes, washed twice with ice-cold FACS buffer (PBS containing 0.5% BSA, and 0.05% sodium azide) and resuspended in cold FACS buffer before being analysed by an LSR II flow cytometer running FACSDiva™ software, version 6.2 (both BD Biosciences, USA). Forward and side scatter parameters were used to gate for single cells, eliminating dead cells and debris from the analysis. A minimum of 1 x 10^4 cell events were recorded per sample. NK-92 cells stained with FITC-isotype control were used to set the threshold between bright and dim FITC fluorescence. Cells with FITC fluorescence above this threshold were deemed to be positive for surface LAMP1 and therefore to have undergone degranulation. This population of cells was expressed as a percentage of the total number of cells. Unstimulated and untreated cells were analysed for basal LAMP1 surface expression and single stained controls were included to allow for compensation. The degranulation response was expressed relative to the degranulation induced in the absence of YM201636.

Immunogen	Fluoro-chrome	Host [Clone]	Manufacturer
CD3	FITC	Mouse [UCHT1]	BD Biosciences, USA
CD56	PE	Mouse [AF127H3]	Miltenyi Biotech, Germany
LAMP1 (CD107a)	FITC	Mouse [H4A3]	BD Biosciences, USA
Mouse IgG1 (Isotype)	PE	[IS5-21F5]	Miltenyi Biotech, Germany
Mouse IgG1 (Isotype)	FITC	[MOPC-21]	BD Biosciences, USA

Table 2.5. Antibodies and isotype controls used for flow cytometry

2.14 Enzyme-Linked Immunosorbent Assay (ELISA)

To quantify IFNγ secreted from NK-92 cells in response to target cell stimulation, a sandwich ELISA was performed. NK-92 cells were plated into wells of a 96 well plate at a density of 1 x 10^5. YM201636 or DMSO (vehicle) was added for 20 minutes at 37 ^oC at the concentrations specified. Cells were then co-incubated with K562 target cells as outlined in Section 2.2.4 for 4 hours at 37 ^oC. Cells were pelleted at 300 x *g* for 3 minutes, the supernatants collected and either used immediately or stored at -20 ^oC. ELISA plates were prepared by coating MaxiSorp™ 96 well plates (Thermo Fisher Scientific, USA) with mouse monoclonal anti-IFNγ antibody (BD Biosciences, USA) at 4 µg/mL in coating buffer (0.1 M $NaHCO_3$, pH 8.2) overnight. Plates were washed three times with PBS containing 0.05% v/v Tween-20 (PBS/T) and blocked with PBS containing 10% FCS for 1 hour at room temperature. Plates were washed three times with PBS/T, and undiluted supernatants were added to plates in triplicate wells for 2 hours at room temperature. Supernatants from unstimulated NK and K562 cells were plated to measure background IFNγ secretion. Fresh media was used as a background control. Serial dilutions of recombinant IFNγ (BD Biosciences, USA) were plated alongside samples and used to prepare a standard curve. Plates were washed six times with PBS/T and mouse monoclonal anti-IFNγ

detection antibody (BD Biosciences, USA) was added at 2 µg/mL in PBS containing 10% FCS for 1 hour at room temperature. Plates were then washed six times with PBS/T and incubated with ExtrAvidin®-alkaline phosphatase (Sigma-Aldrich, USA; 1:5000 in PBS/T) for 1 hour at room temperature. Plates were washed three times with PBS/T then three times with double distilled water (ddH_2O) before adding SIGMA*FAST*™ substrate solution (1 mg/mL p-Nitrophenyl phosphate, 0.2 M Tris buffer, 5 mM magnesium chloride; Sigma-Aldrich, USA). The absorbance at 405 nm was measured using a plate reader (Multiskan EX, Thermo-Fisher Scientific, USA) after 30 minutes. The background absorbance generated by the medium was subtracted from all other sample values and the amount of basal IFNγ secreted from resting untreated cells was deducted from all other samples.

2.15 Assessment of Cell Viability

The translocation of phosphatidylserine (PS) from the inner- to the outer-leaflet of the plasma membrane during early apoptosis allows the binding of fluorochrome-labelled Annexin V protein. Counterstaining with propidium iodide allows the discrimination of late apoptotic and necrotic cells from cells in early apoptosis. Approximately 1 x 10^5 YM201636-treated NK-92 cells or siRNA-transfected 3T3-J2 cells were washed twice in PBS and resuspended in 100 µL of Annexin V binding buffer (10 µM HEPES pH 7.4, 0.14 M NaCl, 2.5 mM $CaCl_2$; BD Biosciences, USA). Cells were stained with 5 µL of FITC-Annexin V and propidium iodide (both BD Biosciences, USA) for 3T3-J2, or propidium iodide only for NK-92 and incubated at room temperature for 15 minutes. Cells were washed and pelleted, the supernatant removed and the pellet resuspended in 400 µL of Annexin V binding buffer before analysing on an LSR II flow cytometer with FACSDiva™ software version 6.2 (both BD Biosciences, USA). Single stain controls were included to allow for compensation.

2.16 Gamma (*γ*)-Radiation to Induce Senescence

To generate a senescent population of 3T3-J2 cells, 2 x 10^4 cells were plated in wells of a 12-well plate and allowed to adhere overnight. The next day, in parallel to siRNA-transfections, cells were subjected to 80 Gray *γ*-radiation for 60 minutes and incubated for 24 hours at 37 ^oC, before use.

2.17 Senescence-Associated *β*-Galactosidase Activity

Senescence-associated β-Galactosidase (SA-*β*-Gal) activity was determined by measuring the activity of *β*-galactosidase at pH 6.0 in fixed (colourimetric assay) or live cells (flow cytometric- assay).

2.17.1 X-Gal Colourimetric Assay

5-bromo-4-chloro-3-indolyl-*β*-D-galactopyranoside (X-gal) was cleaved by SA-*β*-Gal to yield an insoluble blue product that was readily detectable by phase contrast microscopy. 3T3-J2 cells, seeded into 12-well plates, were transfected according to Section 2.6 or irradiated according to Section 2.16 and incubated for 48 hours. Cells were stained with the Senescence *β*-Galactosidase Staining Kit (Cell signalling Technology, USA) according the manufacturer's instructions. Briefly, cells were washed with PBS, fixed with 1X fixative solution (2% v/v formaldehyde and 0.2% v/v gluteraldehyde in PBS) for 15 minutes at room temperature and washed twice with PBS. Cells were stained with 500 µL X-Gal staining solution (2.45 µM X-Gal in N,N-dimethyformamide, 5 nM potassium ferrocyanide, 5 nM potassium ferricyanide, 40 mM citric acid/sodium phosphate (pH 6.0), 150 mM sodium chloride, 2 mM magnesium chloride; pH 5.9-6.1). The blue colour was evident 2-4 hours after staining and phase contrast images were acquired after 12-16 hours (when colour was maximal) using an Olympus CKX41 inverted light microscope.

2.17.2 C_{12}FDG Flow Cytometric Assay

5-dodecanoylaminofluorescein di-beta-D-galactopyranoside (C_{12}FDG, Sigma-Aldrich, USA) is a non-fluorescent membrane-permeable substrate of *β*-galactosidase, which after hydrolysis of the galactosyl residues becomes

fluorescent and is sequestered intracellularly. 3T3-J2 cells transfected in triplicate according to Section 2.6 or irradiated according to Section 2.16, were washed with PBS after 48 hours and pre-treated with 100 nM bafilomycin A1 (BioViotica, Germany) in culture medium, for one hour at 37 ^{o}C in a humidified 5% CO_2 incubator to raise the lysosomal pH to 6.0. C_{12}FDG was then added to the culture medium at a final concentration of 33 µM and cells incubated for two hours at 37 ^{o}C. After washing three times with PBS, the cells were harvested using trypsin, centrifuged at 300 x *g* for 10 minutes at 4 ^{o}C and resuspended in cold FACS buffer (0.5% BSA and 0.05% sodium azide in PBS). Cells were analysed immediately using an LSR II flow cytometer with FACSDiva™ software, version 6.2. Forward and side scatter parameters were used to gate for single cells, eliminating dead cells and debris from the analysis. A minimum of 1 x 10^4 cell events were recorded per sample. Untreated 3T3-J2 cells stained with C_{12}FDG were used to set the threshold between bright and dim C_{12}FDG fluorescence. Cells with fluorescence above this threshold were deemed to be positive for C_{12}FDG (and therefore positive for SA-*β*-Gal activity) and were expressed as a percentage of the total number of cells. Unstained controls were included for each sample analysed and used to determine the amount of autofluorescence emitted.

2.18 Cell Size Analysis

For analysis of cell size using confocal images, 3T3-J2 cells were transfected with siRNA and stained with 50 nM Texas Red®-X Phalloidin after 48 hours (Sections 2.6 and 2.8.1). Using phalloidin staining to delineate the cells, cell areas were determined from maximum intensity projections of confocal z-stacks using ImageJ analysis software (version 1.46r).

The low-angle forward scatter of light that occurs when a cell passes through a laser beam is roughly proportional to the diameter of the cell, therefore the forward scatter parameter of a flow cytometer was used to determine the number of enlarged cells in siRNA-transfected or irradiated 3T3-J2 cells. 3T3-J2 cells transfected with siRNA or irradiated according to Sections 2.6 and 2.16 were harvested using trypsin after 48 hours, washed in PBS and

pelleted. Cell pellets were resuspended in cold FACS buffer (PBS containing 0.5% BSA and 0.05% sodium azide) at a density of 1 x 10^6 cells/mL before being analysed by an LSR II flow cytometer with FACSDiva™ software version 6.2. Forward and side scatter parameters were used to gate for single cells, eliminating dead cells and debris from the analysis, and at least 1 x 10^4 cell events were recorded per sample. Untreated 3T3-J2 cells were used to set the threshold between high and low forward scatter. Cells with forward scatter above this threshold were deemed to be enlarged and the number of enlarged cells were expressed as a percentage of the total number of cells. The number of enlarged cells in a mock-transfected siRNA population was deducted from the number of enlarged cells in the siLyst and siControl populations.

2.19 Quantification of Aberrant Nuclei

3T3-J2 cells transfected with siRNA or irradiated according to Sections 2.6 and 2.16, were imaged with an Olympus CKX41 inverted light microscope using a 20X objective. Phase contrast images were used to score cells that displayed an abnormal nuclear morphology or number, and the number of aberrant cells were expressed as a percentage of the total number of cells counted.

2.20 Quantification of Protein Expression by Western Blotting

Protein expression was quantified by Western blotting of proteins extracted from cell lysates and separated by gel electrophoresis. Buffer recipes and the chemicals used for Western blotting are listed in Table 2.6 and Table 2.7.

2.20.1 Preparation of Cell Lysates

Cells cultured in 10 mm dishes were detached with trypsin, washed twice in PBS and lysed on ice for 20 minutes with 300 µL RIPA buffer. Protease inhibitor cocktail (Sigma-Aldrich, USA) was added to the lysis buffer to prevent protein degradation. The lysate was centrifuged at 13,000 x *g* (5

minutes, 4 ^{o}C) and the soluble fraction was either used immediately or stored at -20 ^{o}C. The protein concentration of lysates was determined using the Pierce Coomassie Plus Protein Assay (Thermo Fisher Scientific, USA), following the manufacturer's microplate protocol. Briefly, 300 µL of coomassie blue was added to 10 µL of lysate diluted 1:10 in PBS (in triplicate) and incubated at room temperature for 10 minutes. A series of protein standards (0 - 2000 µg/mL) were prepared using BSA and used to generate a standard curve. The absorbance was measured at 620 nm using a plate reader (Multiskan EX, Thermo-Fisher Scientific, USA) and the average absorbance of RIPA buffer (diluted 1:10 in PBS) was subtracted from all samples and standards.

2.20.2 Sodium Dodecyl Sulphate-Polyacrylamide Gel Electrophoresis (SDS-PAGE)

For all proteins, with the exception of EEA1 and LAMP1, the following method was applied. According to cell size, an 8% or 10% sodium dodecyl sulphate-polyacrylamide gel electrophoresis (SDS-PAGE) resolving gel with a 5% stacking gel (Table 2.6) was prepared, loaded into an XCell S*ure*Lock™ gel electrophoresis tank (Bio-Rad Laboratories, USA) and immersed in 1 x SDS-PAGE buffer (Table 2.6). Cell lysates were mixed with an equal volume of 2X Laemmli buffer (Table 2.6) supplemented with 5% β-mercaptoethanol, heated for 5 minutes at 95 ^{o}C and then cooled on ice for 2 minutes. Protein samples (20 µL at 1 µg/µL) were loaded into wells of the SDS-PAGE gel alongside a well containing 10 µL Precision Plus Protein™ Dual Colour Standard marker (Bio-Rad Laboratories, USA). A potential difference of 100-120 V was applied across the gel for approximately 2 hours.

For electrophoretic separation of EEA1 and LAMP1, pre-cast 3-8% Tris acetate gels (Life Technologies, USA) were used. 4X NuPAGE® LDS Sample Buffer (10 µL, Life Technologies, USA) was added to a sample lysate (26 µL at 0.77 µg/µL protein), together with 10X NuPAGE® Sample Reducing Agent containing 500 mM dithiothreitol (Life Technologies, USA). Samples were heated at 70 ^{o}C for 10 minutes then cooled on ice for 2 minutes. Gels were assembled into an XCell S*ure*Lock™ gel electrophoresis tank and immersed in 1X NuPAGE® Tris-Acetate SDS Running Buffer

containing 0.25% v/v NuPAGE® Antioxidant (both Life Technologies, USA). Samples were loaded alongside 10 µL HiMark™ Pre-Stained High Molecular Weight protein standard (Life Technologies, USA) and subjected to a potential difference of 150V for 1 hour.

Proteins were then transferred from the gel to polyvinylidene (PVDF) membranes by wet transfer (Section 2.20.3).

2.20.3 Western Blotting

Western blotting was performed by sandwiching the gel between a sheet of PVDF membrane and two pieces of Whatman™ 3MM Chr paper (both GE Healthcare, USA) that had been pre-soaked in transfer buffer (Table 2.6) for 10 minutes. The proteins were transferred using an XCell S*ure*Lock™ Mini-Cell fitted with an XCell II™ Blot Module (Life Technologies, USA). For membranes containing EEA1 and LAMP1, the tank was filled with 1X NuPage® Transfer Buffer containing 0.1% NuPAGE® Antioxidant (both Life Technologies, USA) and 10% v/v methanol. A potential difference of 20 V was applied to the system overnight at 4 ^{o}C. For all other membranes, the tank was filled with transfer buffer (Table 2.6) containing 20% methanol before transfer overnight as previously described.

2.20.4 Probing

Following the transfer of proteins to PVDF, membranes were blocked for 1 hour at 4 ^{o}C in 1X Tris-buffered saline, 0.1% v/v Tween-20 (TBS/T; Table 2.6) plus 10% w/v Marvel dried milk powder. The block was replaced with fresh TBS/T containing 1% dried milk powder, to which the primary antibody was added at the relevant dilution (Table 2.3). The membrane was incubated in the presence of primary antibody for 1 hour at room temperature or overnight at 4 ^{o}C, with continuous rocking. Membranes were washed in TBS/T (3 X 5 minutes) with continuous agitation. The secondary antibody was added at the relevant dilution (Table 2.4) in 5% dried milk powder for 1 hour at room temperature or overnight at 4 ^{o}C, with continuous rocking. Membranes were washed in TBS/T (3 X 5 minutes) with continuous agitation. The membrane was rinsed in dH_20 and protein detected using Amersham enhanced chemiluminescence reagent (GE Healthcare, UK).

Membranes were transferred to a light proof cassette and developed using CL-XPosure film (Thermo-Fisher Scientific, USA) and an automated Konica SRX 101A X-ray developer (Konica, UK). The expression of β-actin or glyceraldehyde 3-phosphate dehydrogenase (GAPDH; Table 2.3) was assessed to confirm equal loading of protein samples.

Buffer or Gel	Contents
RIPA buffer	10 mM Tris-HCL pH 8, 1 mM EDTA, 0.5 mM EGTA, 140 mM NaCl, 1% Triton X-100, 0.1% sodium deoxycholate, 0.1% v/v SDS, dH_20
8% resolving gel	8% v/v Acrylamide*, 0.375 M Tris-HCL pH 8.8, 0.1% SDS, 0.6% v/v ammomium persulphate (APS), 0.1% v/v TEMED, dH_20
10% resolving gel	10% Acrylamide*, 0.375 M Tris-HCL pH 8.8, 0.1% SDS, 0.6% APS, 0.1% TEMED, dH_20
5% stacking gel	5% Acrylamide*, 0.126 M Tris-HCL pH 6.8, 0.1% SDS, 0.6% APS, 0.1% TEMED, dH_20
10X SDS-PAGE buffer	0.25 M Tris base, 0.19 M glycine, 1% SDS, dH_20
2X Laemmli buffer	4% SDS, 20% glycerol, 0.02% w/v bromophenol blue, 0.125 M Tris-HCL
10X Transfer buffer	0.25 M Tris base, 0.19 M glycine, dH_20, pH 8.3
10X TBS buffer	0.25 M Tris base, 1.34 M sodium chloride, 54 mM potassium chloride, ddH_20, pH 7.4

Table 2.6. Buffers and gels used for quantification of protein expression by Western blotting

*Acrylamide, N,N'-methylene- bis-acrylamide 37.5:1

Reagent	Manufacturer
Acrylamide*	National Diagnostics, UK
Bromophenol blue	Sigma-Aldrich, USA
Gycerol	Sigma-Aldrich, USA
Glycine	Sigma-Aldrich, USA
Potassium chloride	VWR International, USA
SDS	Sigma-Aldrich, USA
Sodium chloride	Sigma-Aldrich, USA
Sodium deoxycholate	Sigma-Aldrich, USA
TEMED	National Diagnostics, UK
Tris base	Sigma-Aldrich, USA
Tris-HCL	Sigma-Aldrich, USA
Tween-20	Sigma-Aldrich, USA

Table 2.7. Chemicals used for preparation of buffers for Western blotting

*Acrylamide, N,N'-methylene-bis-acrylamide 37.5:1

2.20.5 Densitometry Analysis of Western Blots

ImageJ software (version 1.46r) was used to analyse the density of protein bands on scanned Western blotting film. Rectangular marquees were drawn around bands to be compared. Densitometry values were generated using the 'analyse gel' and 'plot lane' functions and the background subtracted from each value.

2.21 Quantitative Real-Time Polymerase Chain Reaction (qRT-PCR)

For gene expression analysis, quantitative real-time polymerase chain reaction (qRT-PCR) was performed to determine the level of mRNA following siRNA-mediated silencing according to the following procedure.

2.21.1 RNA Extraction

Roughly 1 x 10^6 cells per treatment were lysed for RNA extraction. Cells were detached with trypsin, washed in PBS and pelleted by centrifugation. Total RNA was extracted using GeneElute™ Mammalian Total RNA Miniprep Kit (Sigma-Aldrich, USA) according to the manufacturer's instructions. All centrifugation steps were performed at 13,000 x *g* in a benchtop microcentrifuge. Briefly, cells were lysed with the supplied guanidine thiocyanate lysis solution containing β-mercaptoethanol and the lysate passed through a filtration column to remove cellular debris. An equal volume of 70% ethanol was added and the lysate/ethanol mixture passed through a binding column. RNA bound to the column was washed three times with the provided wash solutions and then centrifuged for 1 minute to remove residual traces of ethanol. Finally, the RNA was eluted in distilled water and immediately treated as described in Section 2.21.2.

2.21.2 RNA Treatment and Quantitation

Extracted RNA was treated to remove contaminating genomic DNA using DNA-*free*™ kit according to the manufacturer's instructions (Life Technologies, USA). Briefly, 10X DNase buffer (100 mM Tris at pH 7.5, 25mM $MgCl_2$, 5 mM $CaCl_2$) and 2 U of DNase I per 50µL of RNA was added to samples, followed by incubation at 37 ^oC for 20-30 minutes. DNase I was inactivated and removed by the addition of DNase inactivation reagent for 2 minutes at room temperature. Samples were centrifuged at 10,000 x *g* for 2 minutes, and the pellet discarded. RNase activity was inhibited to preserve the integrity of purified RNA by the addition of RNasin (Promega Corporation, USA) at 1 U/µL of RNA solution. The quantity of RNA was estimated using a spectrophotometer, measuring the absorbance at 260 nm. RNA purity was estimated from the ratio of absorbance at A_{260nm}/A_{280nm}, and a value of 1.8-2.1 was considered pure. RNA was used immediately for complementary DNA (cDNA) synthesis or stored at -80 ^oC.

2.21.3 Complementary DNA (cDNA) Synthesis

The synthesis of cDNA from extracted RNA was carried out in a reaction consisting of 1 µL random hexamers (50 µM; Life Technologies, USA), 2 µg

RNA, 1 µL deoxyribonucleos§ide triphosphate (dNTP) mix (10 mM each of dATP, dCTP, dGTP and dTTP) and sterile nuclease-free water to a final volume of 13 µL. The mixture was heated at 65 ^{o}C for 5 minutes and quickly chilled on ice to prevent secondary structure formation. A 4 µL aliquot of 5X First-Strand Buffer (250mM Tris-HCL, pH 8.3; 3.75 M KCl; 15mM $MgCl_2$), together with 2 µL of 100 mM 1,4-Dithiothreitol (both Life Technologies, USA), was added to the sample and incubated for a further 2 minutes at 25 ^{o}C. Finally, 1µL (200 U) of SuperScript II reverse transcriptase (Life Technologies, USA) was added, giving a final volume of 20 µL. The sample was incubated at 25 ^{o}C for 10 minutes, followed by 50 minutes at 42 ^{o}C. Reverse transcriptase was inactivated by heating at 70 ^{o}C for 15 minutes and the resulting cDNA was stored at -20 ^{o}C. A mock reaction (where reverse transcriptase was omitted) was performed and included in qRT-PCR reactions to assess for genomic DNA contamination. Samples of cDNA were stored at -80 °C.

2.21.4 qRT-PCR

Inventoried TaqMan® Gene Expression Assays (Table 2.8) were purchased from Life Technologies, USA. Reactions were performed in MicroAmp® Optical 96-well reaction plates (Life Technologies, USA). Each 20 µL reaction contained: 1X TaqMan® Gene Expression Master Mix, 1X TaqMan® Gene Expression Assay Mix, 20 ng of sample cDNA and deionised nuclease-free water,to a final volume of 20 µL. Negative controls included in each reaction plate consisted of a mock reverse transcription (‘no amplification control’, Section 2.21.3) to control for genomic DNA contamination, and a ‘no template control’ whereby cDNA was substituted with nuclease-free water, to assess for contamination of the reagents. Each sample was run in triplicate and the reaction was performed using a 7500 Real-Time PCR thermal cycler running 7500 software version 2.0.3 (both Life Technologies, USA). The comparative cycle threshold (C_T) method was used to determine mRNA expression. The C_T values and baseline were automatically determined by the software for each transcript and were normalised to the expression level of the endogenous control, Hprt1 (mean

target gene C_T - mean Hprt1 C_T). The expression of the target gene relative to the non-silencing control was calculated by the value of $2^{-\text{delta CT}}$.

Gene	Accession Number of mRNA	Catalogue Number
Lyst	NM_010748.2	Mm00465000_m1
Tcf7l1	NM_001079822.1, NM_009332.2	Mm01188711_m1
Tcf7l2	NM_001142918.1, NM_001142919.1, NM_001142920.1, NM_001142921.1, NM_001142922.1, NM_001142923.1, NM_001142924.1, NM_009333.3	Mm00501505_m1
Hprt1	NM_013556.2	Mm00446968_m1

Table 2.8. TaqMan® gene expression primers used for qRT-PCR

All primers spanned an exon junction. Lyst, lysosomal trafficking regulator; Tcf7l1, transcription factor 7-like 1 [T-cell specific, HMG-box]; Tcf7l2, transcription factor 7-like 2 [T-cell specific, HMG-box]; Hprt1, hypoxanthine phosphoribosyltransferase 1.

2.22 Statistical Analysis

Statistical analyses were performed using Prism 6 software (GraphPad Software, USA). Data pertaining to the relative mRNA level in response to siRNA-mediated silencing were analysed using a one sample t-test against a hypothetical mean of 100. All other data illustrating the difference between two groups were analysed using a two-tailed student's t-test and are presented as the mean with error bars corresponding to the standard deviation (SD). The level of significance was set at $P < 0.05$ and exact P values are reported where appropriate.

Chapter 3
Characterisation of the *beige* Phenotype

3.1 Introduction

The perturbed homeostasis of the endolysosomal system in CHS patients and *beige* mice has been studied in depth for almost three decades and considerable work has been devoted to pinpointing the underlying mechanisms. Despite this, the function of the highly conserved LYST remains to be determined, and is largely due to the technical challenge of manipulating a gene and protein of such large size. It is clear that LYST plays a fundamental role in the formation and exocytosis of secretory lysosomes, as the clinical manifestations of CHS all arise from the defective exocytosis of these organelles. Although several binding partners for LYST have been identified, no pathways have yet been established for LYST-dependent secretory lysosomes biogenesis or exocytosis.

Despite the autophagic and lysosomal pathways converging at the point of the autolysosome, few studies have explored the autophagic pathway in CHS. Similarly, phosphoinositide metabolism plays a pivotal role in membrane and vesicle trafficking, yet remains relatively unexplored in CHS. The first evidence to signal that such a pathway might be disrupted was presented by Ward et al., 2003, who reported a mislocalisation of PtdIns(4,5)P_2 in both CHS and *beige* cells. Here, using the *beige* mouse model, The contribution of both PtdIns(4,5)P_2 and autophagy to the cellular defect of CHS has been investigated; the central aim being to identify proteins downstream of LYST that may also function in exocytosis.

3.2 Establishment of *beige* Fibroblast Cultures

To study the CHS/*beige* phenotype, dermal fibroblasts from mice homozygous for the *beige* mutation (CB17.Cg-Prkdc^{scid}Lyst^{bg}) and from control SCID mice (CB17.Cg-Prkdc^{scid}) were obtained from ears using a skin

explant culture system. In this system, dermal and epidermal fibroblasts and keratinocytes were allowed to migrate out from the edges of skin explants placed in plastic culture dishes (Figure 3.1A). The high growth rate of fibroblasts compared to keratinocytes was exploited to obtain cultures highly enriched in fibroblasts. Expression of fibroblast-specific protein 1 (FSP1, also known as S100-A4) is widely used to identify fibroblasts (Strutz et al., 1995) and was used to assess the purity of the explant cultures. Substantial cytoplasmic expression of FSP1 was found in all cells from explant cultures after three passages, as determined by immunofluorescence microscopy (Figure 3.1B). Compared to SCID control fibroblasts, *beige* cells had greatly enlarged vesicles that were clustered proximal to the nucleus (Figure 3.1C). This feature is typical of CHS/*beige* fibroblasts and is well documented elsewhere (Burkhardt et al., 1993, Abe et al., 1982, Perou et al., 1997a). However, there was considerable variation in the morphology of *beige* vesicles. Enlarged vesicles were either non-refractive and of a granular appearance (Figure 3.1C, panel *ii*) or refractive and vacuole-like (Figure 3.1C, panel *iii*). Many cells contained one or two grossly enlarged vesicles with heterogeneous content (Figure 3.1C, panel *iv, arrowhead*).

Primary fibroblasts undergo a limited number of divisions before entering the non-replicative state of senescence (Hayflick, 1965). Expression of viral oncogenes such as Simian virus 40 large T antigen (SV40T) can significantly extend the replicative capacity of mammalian cells *in vitro* (Ali and DeCaprio, 2001, Ozer et al., 1996). A plasmid vector carrying SV40T was transfected into *beige* fibroblasts, in an attempt to prolong their replicative lifespan for continuous study. Following transfection of *beige* with SV40T, the cells became rapidly proliferative, whereas the growth rate of mock transfected cells or cells transfected with empty vector remained unchanged (data not shown). Immunofluorescent labelling of cells with anti-SV40T antibody showed high expression of SV40T within nuclei of all cells, 27 days post-transfection (Figure 3.2A). However, the morphology of the SV40T-transfected cells changed and cells no longer displayed the enlarged vesicle phenotype typical of *beige* when examined by light microscopy. Vesicles became smaller in size and less numerous after transfection (Figure 3.2B), and *beige* cells were indistinguishable from *SCID* cells.

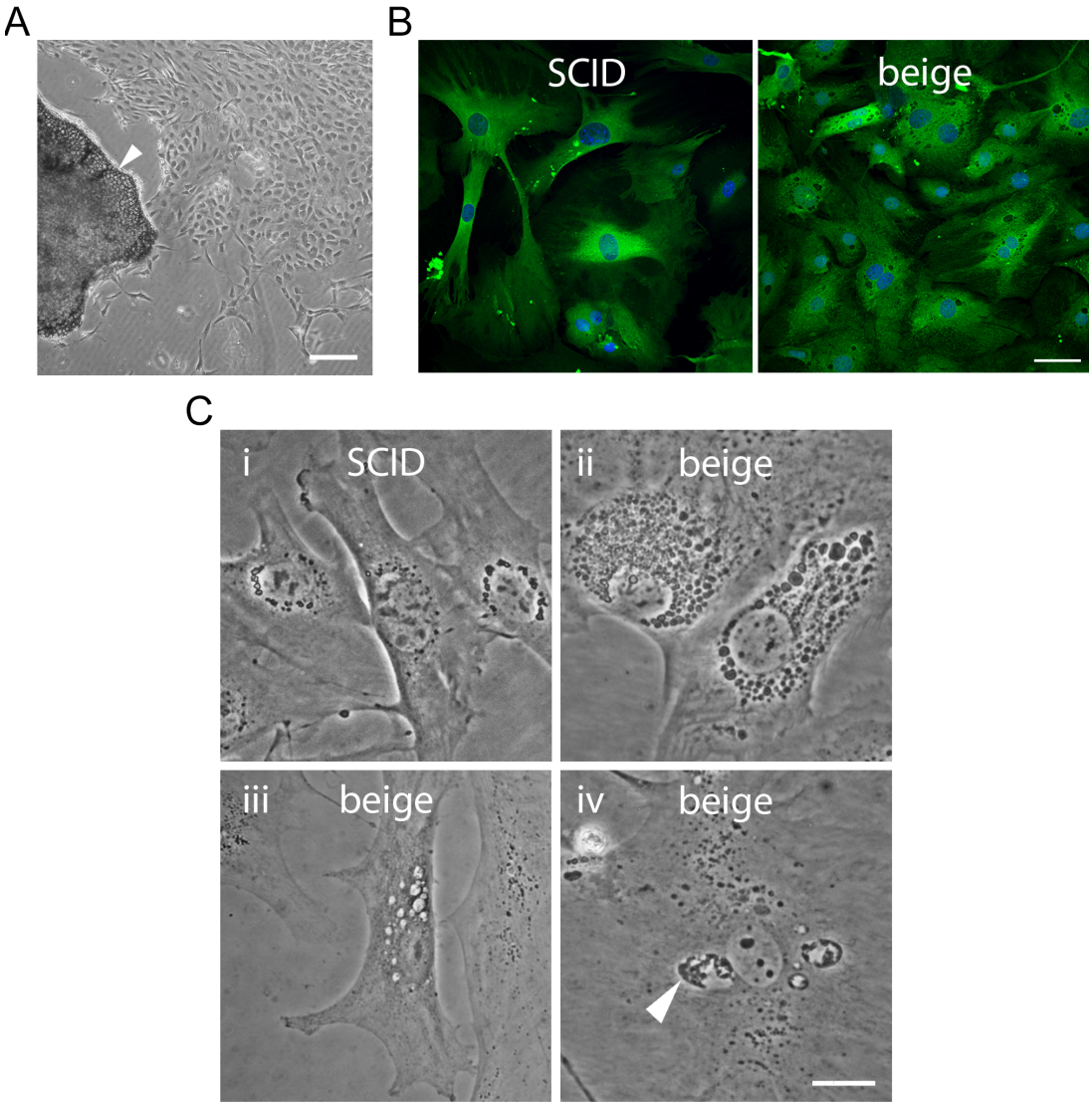

Figure 3.1. Characterisation of *beige* and *SCID* fibroblasts

A) Phase contrast image of cell outgrowth from mouse ear skin explant after 22 days. Cells attach to the culture vessel and migrate outwards from edges of the explant (*arrow*). B) Confocal sections of *SCID* and *beige* cells immunofluorescently labelled with the fibroblast specific anti-FSP1 antibody (*green*) and counterstained with DAPI (*blue*) to visualise nuclei. C) Light micrographs of *SCID* (*i*) and *beige* (*ii-iv*) cells. *Beige* cells displayed large vesicles clustered proximal to the nucleus, but the morphology of the vesicles varied considerably (*ii-iv)*. *Arrowhead* in *iv* depicts a grossly enlarged vesicle with heterogeneous content. Scale bar: *A*, 500 µm; *B*, 50 µm; *C,* 20 µm

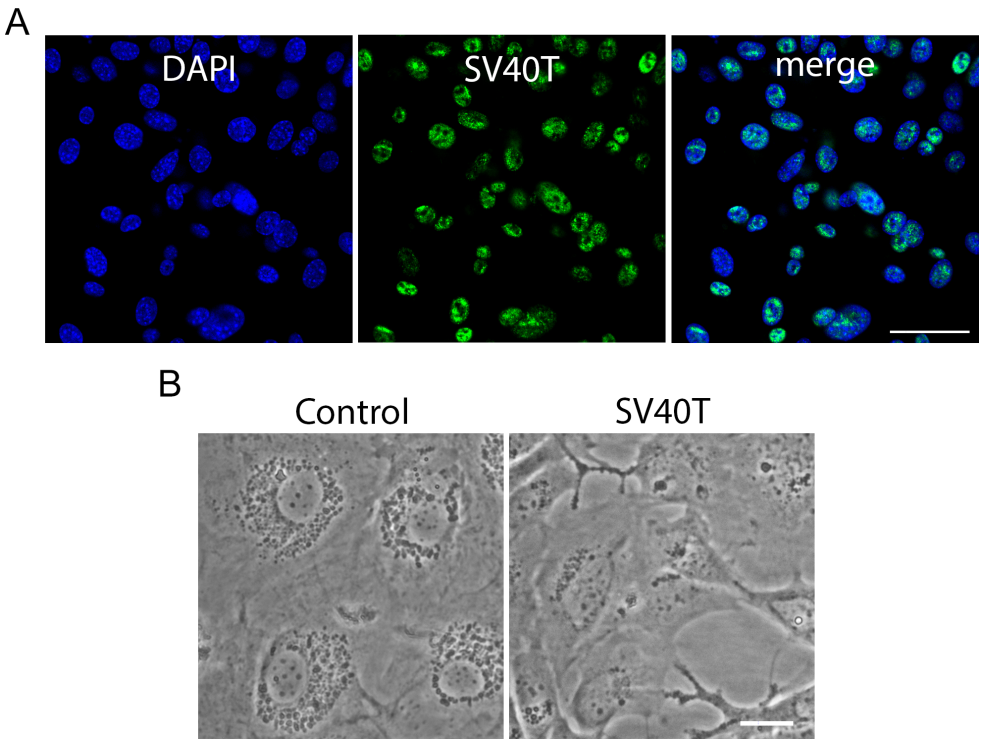

Figure 3.2. Immortalisation of *beige* fibroblasts with SV40T

Beige fibroblasts transfected with pBSV3-early plasmid containing SV40T DNA were examined 27 days post-transfection. A) SV40T expression was detected using anti-SV40T antibody (*green*) and found within nuclei counterstained with DAPI (*blue*). Images are single confocal sections. B) Phase contrast images of *beige* cells transfected with empty vector (*control*) or SV40T, 27 days-post transfection. Scale bar: *A*, 50 µm; *B*, 20 µm.

A similar loss of phenotype is observed in *beige-j* fibroblasts maintained in long-term culture (Gow et al., 1993). *beige-j* fibroblasts cultured for more than 70 passages were indistinguishable from control fibroblasts based on vesicle size and this was concurrent with a decreased doubling time of *beige-j* fibroblasts (Gow et al., 1993). Lysosomal biogenesis is apparently normal in CHS cells, only becoming aberrant as the organelle matures, as is the case for mast cell and CTL secretory lysosomes (Chi and Lagunoff, 1975, Stinchcombe et al., 2000). I postulated that the increased proliferation rate of SV40T-transformed *beige* cells reduces the number of vesicle fusion events that can occur between divisions, therefore thwarting the formation of large vesicles. For this reason, SV40T-expressing cells were rejected in favour of primary *beige* cells that were used throughout this study.

3.3 The Enlarged Vesicles of *beige* Fibroblasts are Lysosomes

To determine the identity of the enlarged *beige* organelles, fibroblasts were immunofluorescently labelled with specific endocytic markers and examined by confocal microscopy. EEA1 is present exclusively in early endosomes (Mu et al., 1995) and CI-MPR is present in both early and late endosomes, but excluded from mature lysosomes (Griffiths et al., 1990). Labelling with antibodies against EEA1 and CI-MPR revealed a similar size and distribution pattern of these structures in *beige* and *SCID* fibroblasts (Figure 3.3A and C). Conversely, LAMP1 is present in lysosomal membranes but absent from the early endosome (Lewis et al., 1985). *SCID* cells displayed small LAMP1-positive structures dispersed throughout the cytoplasm (Figure 3.3D). In stark contrast however, a dramatic increase in the size of LAMP1-positive structures was seen in *beige*, with the majority of large vesicles remaining clustered in the perinuclear region. The fluorescence intensity of *beige* cells labelled with anti-LAMP1 antibody was notably higher than in *SCID* cells (Figure 3.3D), raising the possibility that this protein is overexpressed in *beige* cells. Western blot analysis was carried out to test this. Equivalent amounts of *SCID* and *beige* lysates were analysed by SDS-PAGE and Western blot using the same anti-LAMP1 antibody as for the immunofluorescence studies. Results confirmed an elevated level of LAMP1 protein in beige lysates (1.77 fold, Figure 3.3E), while the abundance of the 180 kDa band detected with anti-EEA1 antibody was unaltered between *beige* and *SCID* lysates (Figure 3.3B). Furthermore, LAMP1 in the *beige* lysate was of a lower molecular weight than that detected in *SCID* lysate (Figure 3.3E), which may be due to differential *N*- and *O*-glycosylation.

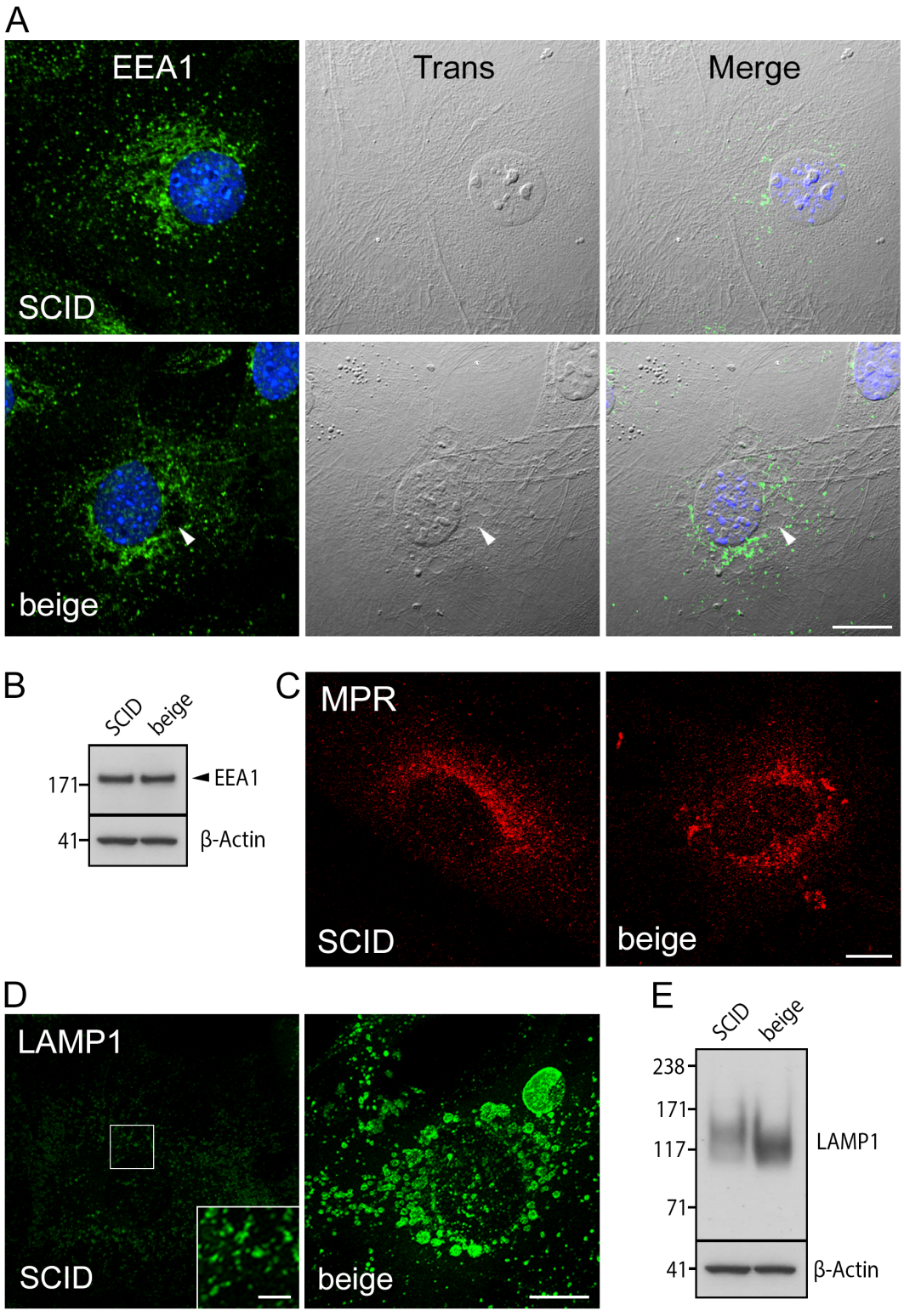

Figure 3.3. The enlarged vesicles of *beige* cells are lysosomes

A) SCID and *beige* fibroblasts were immunofluorescently labelled with anti-EEA1 antibody (*green*) and counterstained with DAPI (*blue*) to visualise the nucleus. Enlarged vesicles were visualised in transillumination (*trans*) and are demarcated by the *arrowhead*. Contrast was increased equally across all transillumination

images to aid visualisation. B) SDS-PAGE and western blot analysis of lysates probed with anti-EEA1 and anti-β-actin antibodies. C) *SCID* and *beige* fibroblasts immunofluorescently labelled with anti-CI-MPR antibody (*red*). D) *SCID* and *beige* fibroblasts labelled with anti-LAMP1 antibody (*green*). The brightness of the indicated region within the *SCID* image (*inset*) has been increased to aid visualisation. E) LAMP1 protein level in *SCID* and *beige* lysates from SDS-PAGE and western blot analysis using anti-LAMP1 antibody. Fold change in LAMP1 protein was calculated from the relative band densities: 1.77 ± 0.39. Fluorescence images are maximum intensity projections of confocal z-stacks. Western blots are representative of two independent experiments. Molecular masses indicated are in kDa. Scale bar = 10 μm; inset, *D* = 5 μm.

As the enlarged organelles contained LAMP1 but not EEA1 or MPR, it was concluded that these vesicles were of lysosomal origin, consistent with current literature (Burkhardt et al., 1993, Abe et al., 1982, Perou et al., 1997a).

The acidified lumen of mature lysosomes is required for the proper function of lysosomal hydrolases. CHS/*beige* lysosomes are acidified and accumulate LysoTracker (Mohlig et al., 2007), an acidotropic dye which is used to label late endosomes and lysosomes (Huynh et al., 2007). LysoTracker accumulated in small punctate structures throughout the cytoplasm in *SCID* fibroblasts, and this pattern was consistent across all cells (Figure 3.4A). Despite considerable cell-to-cell variation in the LysoTracker staining pattern of *beige* fibroblasts (Figure 3.4B and C), large positively-stained vesicles clustered proximal to the nucleus were present in the majority of cells (Figure 3.4B). Interestingly, a number of cells with large vesicles that did not accumulate LysoTracker were observed. These negatively-stained vesicles were made visible by a ring of smaller positively-stained organelles surrounding it (Figure 3.4C, *bottom arrowhead*). Grossly enlarged vesicles distant from the nucleus were occasionally observed and LysoTracker accumulation within these structures was irregular, appearing as dark, negatively-stained areas interspersed with brightly fluorescent regions (Figure 3.4C, *top arrowhead*).

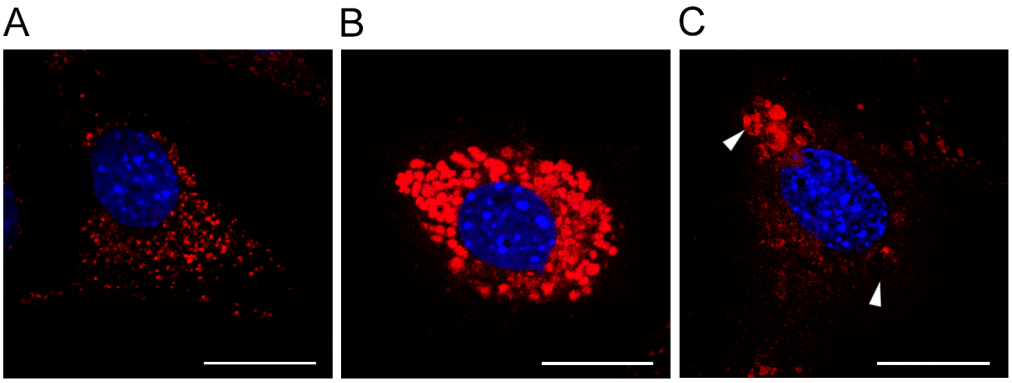

Figure 3.4. The enlarged vesicles of *beige* have varying LysoTracker accumulation

Beige and *SCID* fibroblasts were stained with 100 nM LysoTracker (*red*) to label acidified organelles. A) *SCID* fibroblast with punctate cytoplasmic distribution of LysoTracker. B and C) *Beige* fibroblasts displaying different LysoTracker staining patterns. Enlarged vesicles lacking LysoTracker (*bottom arrowhead, C*) or with heterogeneous LysoTracker accumulation (*top arrowhead, C*) were observed. Cells were counterstained with DAPI to visualise the nucleus (*blue*). Images are single optical sections. Scale bar = 20 μm.

In conclusion, fibroblasts from the *beige* mouse exhibit the enlarged lysosomal phenotype of CHS and were used in further study of Lyst.

3.4 Enhanced Constitutive Autophagy in *beige* Fibroblasts

Autophagosomes are double membrane organelles which form around and selectively engulf portions of the cytoplasm containing organelles and proteins (Mizushima and Komatsu, 2011). As they mature, autophagosomes fuse heterotypically with lysosomes and form autolysosomes, whereby the contents are degraded and recycled. The enlarged vesicles of *beige* were found to be of lysosomal origin due to the presence of LAMP1. However, several large vesicles did not fully accumulate LysoTracker. A possible reason for this is that some lysosomes are not properly acidified, or they may in fact be autolysosomes. Since other BEACH family members are implicated in the autophagic pathway (Simonsen et al., 2004, Lopez-Herrera et al., 2012, Rahman et al., 2012), I assessed the contribution of autophagy to the large vesicle phenotype of *beige* fibroblasts. For this, an antibody

against the beta isoform of LC3, a well-known marker of autophagosomes, was employed to detect autophagosomes using fluorescence microscopy. LC3 is cleaved at the carboxy terminus immediately after synthesis to produce the cytosolic form, LC3-I. Upon induction of autophagy, this becomes lipidated with phosphatidylethanolamine to form LC3-II, which associates with autophagic membranes (Kabeya et al., 2000). Figure 3.5A shows the localisation of anti-LC3B antibody in *beige* fibroblasts under normal conditions. LC3B is visible as discrete puncta distributed throughout the cytoplasm in both *SCID* and *beige* cells. Many puncta were in close proximity to LAMP1-positive lysosomes and the location of LAMP1 and LC3B frequently overlapped, suggesting autophagosome formation. Importantly, anti-LC3B antibody did not label the very large lysosomes (Figure 3.5A, *left arrowhead*). Although discrete LC3B puncta were seen adjacent to the large lysosomes (Figure 3.5A, *right arrowhead*), LC3B fluorescence was predominantly absent from large vesicle membranes and did not form the ring-like patterns typical of membrane-association. This suggests that the large LAMP1-positive vesicles are not autophagosomes. Despite this finding, it does not rule out the possibility that increased autophagy might contribute to the increased size of *beige* lysosomes. To examine this, the number of LC3B puncta from immunofluorescent images was quantified under basal conditions and conditions where normal autophagic degradation is inhibited. Chloroquine raises lysosomal pH and inhibits fusion of autophagosomes with lysosomes through an unknown mechanism (Kawai et al., 2007). Thus, chloroquine inhibits autophagosome clearance and causes their accumulation within the cytoplasm. There was no difference in the size of LC3B puncta between *beige* and *SCID* fibroblasts (Figure 3.5B). Upon the addition of chloroquine, a modest increase in average puncta size was seen in *beige* cells but not in *SCID* (Figure 3.5B). *Beige* fibroblasts contained a higher average number of LC3 puncta per cell than *SCID* fibroblasts in the control treatment and further induction of puncta occurred upon addition of chloroquine (Figure 3.5B). The large variation between experimental replicates is likely attributed to differences in constitutive autophagy during cell propagation. Indeed, the confluency of the culture can affect basal autophagy levels, as reported by Wu et al., 2006.

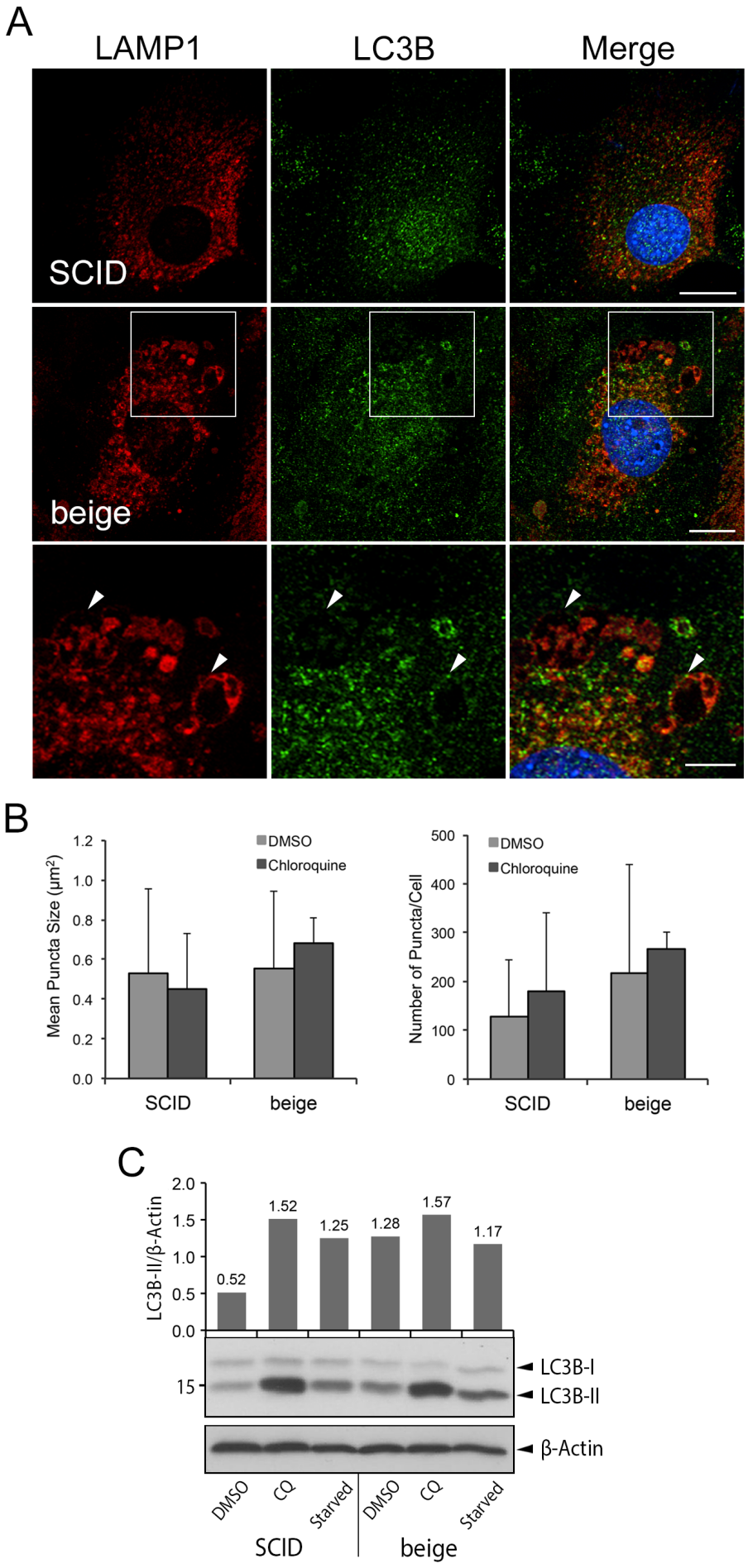
A
LAMP1
LC3B
Merge
SCID
beige
B
Mean Puncta Size (μm²)
DMSO
Chloroquine
SCID
beige
Number of Puncta/Cell
C
LC3B-II/β-Actin
0.52
1.52
1.25
1.28
1.57
1.17
LC3B-I
LC3B-II
β-Actin
DMSO
CQ
Starved
SCID
beige

Figure 3.5. LC3B-associated puncta formation and LC3B processing in *beige* and *SCID* fibroblasts

A) LC3B-positive puncta in *beige* and *SCID* fibroblasts. Cells immunofluorescently labelled with anti-LC3B (*green*) and anti-LAMP1 (*red*) antibodies were counterstained with DAPI (*blue).* An overlay of the three fluorescent channels is shown (*merge*). Images in the bottom panel are magnifications of the demarcated areas in the middle panel. Scale bar: *top* and *middle panels*, 20 μm; *bottom panel*, 10 μm. B) The mean puncta size (*left panel*) and mean number of puncta per cell (*right panel*) were quantified from immunofluorescent images of cells treated with 10 μM chloroquine or DMSO for 24 hours, using ImageJ software. Mean values and SD are given (n = 2). C) Western blot analysis of LC3B-I and LC3B-II levels in *Beige* and *SCID* fibroblasts treated with 10 μM chloroquine, DMSO or serum starved for 24 hours. β-actin was used as a loading control. The ratio of LC3B-II to β-actin was calculated from the relative densities of the two bands using ImageJ software.

Therefore, an alternative quantitative method employing a widely used immunoblotting technique (Proikas-Cezanne et al., 2007) was performed and the ratio of LC3B-II/β-actin calculated. As shown in Figure 3.5C, the abundance of the LC3B-I larger, but faster-migrating LC3B-II was greater in control-treated *beige* cells compared to *SCID* cells, with LC3B-II/β-actin ratios of 1.28 and 0.52, respectively. The addition of chloroquine induced further production of LC3B-II in both cell types, but was more pronounced in *SCID* cells. Interestingly, serum starvation, an autophagy stimulus, induced LC3B-II production in *SCID* cells but no such induction occurred in *beige* cells (Figure 3.5C). These results suggest *beige* fibroblasts have a higher level of constitutive autophagy. From these data alone it is unclear whether the increased number of LCB-II-associated autophagosomes are contributing to the enlarged lysosomal phenotype of *beige*.

3.5 Altered Abundance of Lipid-Binding Proteins in *beige*

PtdIns(4,5)P_2 is a phosphoinositide that is enriched in subdomains of the inner leaflet of membrane bilayers. Ward and colleagues reported an altered localisation of PtdIns(4,5)P_2 in CHS and *beige* fibroblasts, describing a

dramatic reduction in nuclear PtdIns(4,5)P_2 that was restored in LYST-complemented *beige* cells (Ward et al., 2003). Reduced nuclear PtdIns(4,5)P_2 might therefore coincide with an increase PtdIns(4,5)P_2 in an alternative subcellular compartment. I postulated that altered plasma membrane-associated PtdIns(4,5)P_2, or atypical lysosome-associated PtdIns(4,5)P_2 might disrupt PtdIns(4,5)P_2-dependent signalling pathways or normal lysosome homeostasis, respectively. To test this, cells were immunofluorescently labelled using a monoclonal antibody against PtdIns(4,5)P_2 (2C11). Cells were immunofluorescently labelled with 2C11 antibody under conditions optimal for plasma membrane preservation, and the amount of PtdIns(4,5)P_2 located at the plasma membrane was evaluated by confocal microscopy. PtdIns(4,5)P_2 antibody labelling was generally diffuse but with some concentrated at plasma membrane in both *SCID* and *beige* cells (Figure 3.6A). Large areas of PtdIns(4,5)P_2 staining appeared to coincide with LAMP1 in *beige* cells. However, this was due to autofluorescence emitted from some large lysosomes, and was detected across all channels. Dot blot analysis revealed the antibody also bound to PtdIns(3)P, PtdIns(4)P and phosphatidylinositol 3,4,5-trisphosphate (PtdIns(3,4,5)P_3) as reported by others (Thomas et al., 1999, Ward et al., 2003), as well as phosphatidylethanolamine and PtdIns(5)P (Figure 3.6B). Although the antibody bound to PtdIns(4,5)P_2 with the highest affinity, binding to other PI species may contribute to the widespread labelling of anti-PtdIns(4,5)P_2 antibody in these cells. Nonetheless, mean fluorescence intensities of defined regions from the plasma membrane and adjacent cytoplasm were used to calculate plasma membrane/cytoplasmic ratio of PtdIns(4,5)P_2 and this was found to be higher in *beige* than in *SCID* fibroblasts (1.43 versus 1.1, Figure 3.6C). Given the lack of absolute specificity of the antibody for PtdIns(4,5)P_2, it cannot be concluded whether the increase in fluorescence at the plasma membrane in *beige* fibroblasts is due to increased levels of PtdIns(4,5)P_2 or other PI species.

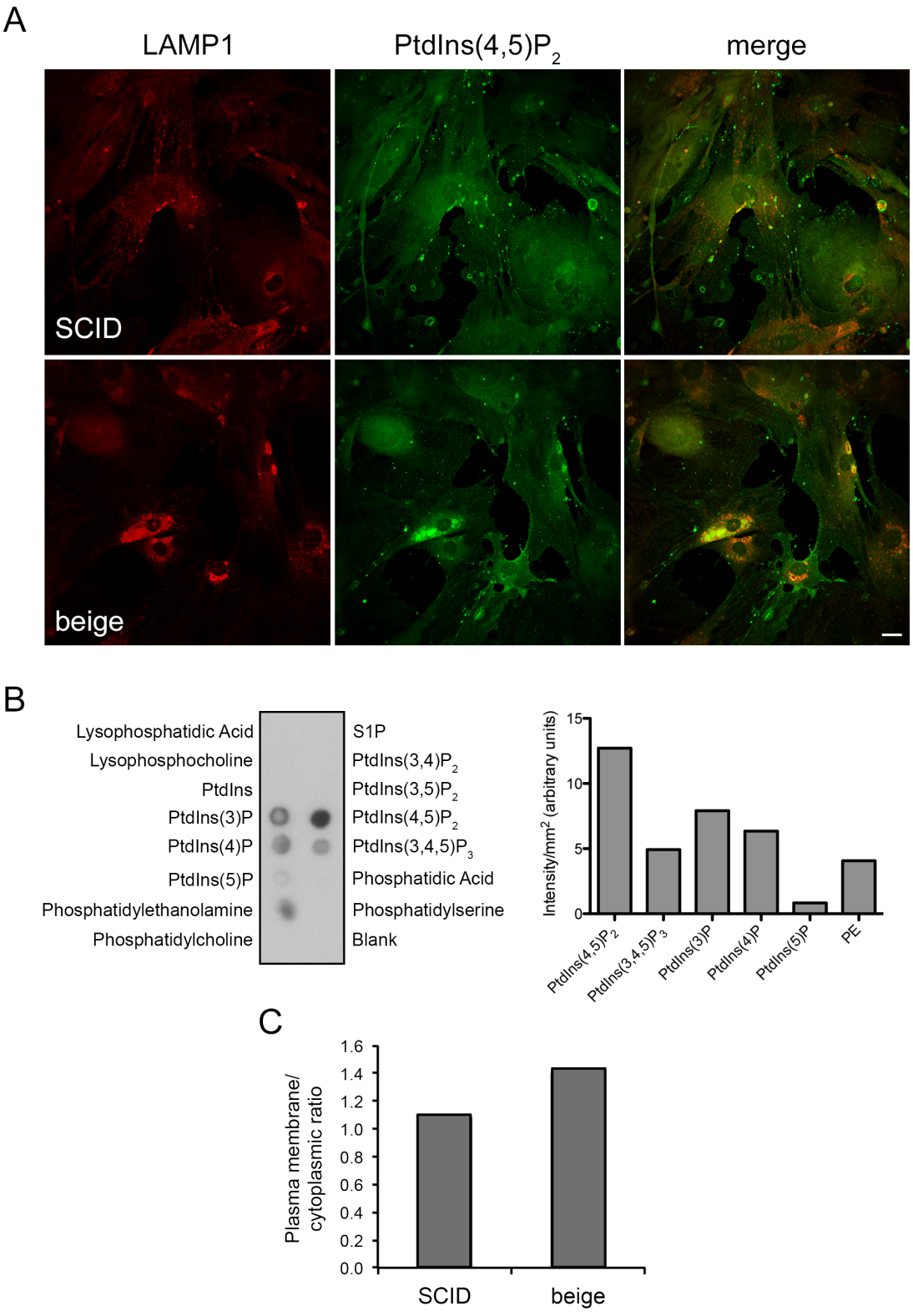

Figure 3.6. PtdIns(4,5)P_2 localisation in *beige* fibroblasts

A) Immunofluorescent analysis of *SCID* and *beige* fibroblasts labelled with anti-PtdIns(4,5)P_2 (*green*) and anti-LAMP1 (*red*) antibodies. An overlay of the two colours is shown (merge) and the yellow colour indicates areas where both fluorescent signals are present. Images are maximum intensity projections of

confocal z-stacks. B) The binding specificity of anti-PtdIns(4,5)P_2 antibody was assessed using a lipid-overlay assay (*left*). Densities of the spots were analysed and the 'Blank' used for background correction (*right*). C) The fluorescence intensities of ROIs at the plasma membrane and adjacent cytoplasm were used to calculate the plasma membrane/cytoplasmic ratio of PtdIns(4,5)P_2, found to be elevated in *beige* cells. The ratios from at least 35 ROI pairs from 18 cells were averaged. S1P, Sphingosine-1-phosphate; PE, Phosphatidylethanol-amine. Scale bar = 20 μm.

Attention was turned instead to the abundance of a PtdIns(4,5)P_2-hydrolysing protein, PLC, at the plasma membrane. Hydrolysis of PtdIns(4,5)P_2 by PLC generates 1,2-diacylglycerol (DAG) and inositol 1,4,5-trisphosphate (Ins[1,4,5]P_3), both of which are necessary for regulated exocytosis in professional secretory cells.

The abundance of two isoenzymes of the PLCγ subfamily, PLCγ1 and PLCγ2, was examined by Western blot in *beige* and *SCID* fibroblast whole cell lysates (Figure 3.7A). Surprisingly, *beige* fibroblasts displayed a moderate reduction in the level of both PLCγ1 and PLCγ2 proteins. Fold change in protein level was calculated from the relative band densities and found to be 0.59 ± 0.04 for PLCγ1 and 0.44 ± 0.15 for PLCγ2 (Figure 3.7A). The extra bands detected with PLCγ2 antibody are likely to be degradation products. Reduced levels of PLCγ1 was echoed in reduced immuno-fluorescence in *beige* fibroblasts labelled with anti-PLCγ1 antibody (Figure 3.7B). Successful immunolabelling of cells with PLCγ2 was not achieved. The serine/threonine kinase PKC is a downstream effector in the PtdIns(4,5)P_2 signalling pathway, activated by DAG and Ca^{2+} to modulate regulated exocytosis (Morgan et al., 2005). Ito and colleagues (1989) reported a down-regulation of PKC in *beige* NK cells that was later linked with the formation of giant lysosomes in *beige* fibroblasts (Tanabe et al., 2000). Western blot analysis with antibody against the beta isoform of PKC (PKCβ) revealed a modest reduction in PKCβ in *beige* fibroblasts, with a 0.67 ± 0.21 fold reduction compared to *SCID* fibroblasts (Figure 3.7C). Taken together, these results suggest a perturbation of the PLCγ-dependent signalling pathway might occur in *beige* cells.

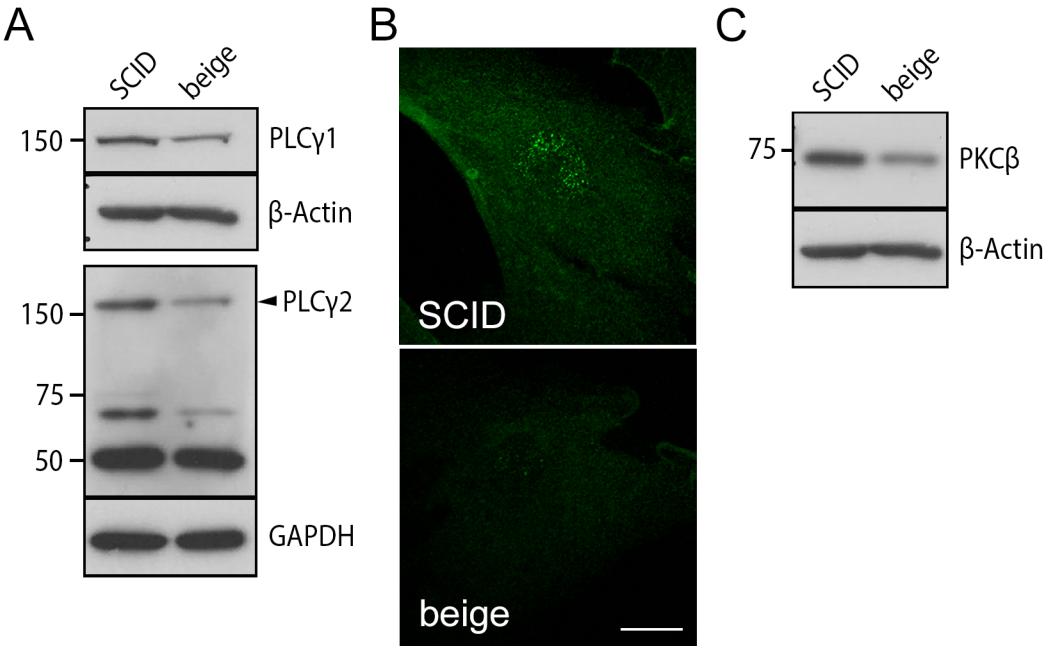

Figure 3.7. Abundance of PLCγ and PKCβ in *beige* fibroblasts

A) Western blot analysis of *SCID* and *beige* lysates probed with anti-PLCγ1 and anti-PLCγ2 antibodies, showing reduced levels of both PLCγ1 and PLCγ2 protein in *beige* cells. β-actin and GAPDH were used as loading controls. B) Confocal images of *SCID* and *beige* fibroblasts immunofluorescently labelled with anti-PLCγ1 antibody, showing reduced PLCγ1 staining in *beige* cells. C) Western blots analysis of *SCID* and *beige* lysates probed with anti-PKCβ antibody. β-actin was included as a loading control. Western blots are representative of two independent experiments. Molecular masses indicated are in kDa. Fold change in protein level was calculated from the relative band densities: PLCγ, 0.59 ± 0.04; PLCγ2, 0.44 ± 0.15; PKCβ, 0.67 ± 0.21. Scale bar = 20 μm.

3.6 Discussion

The giant vesicle phenotype of CHS/*beige* is well documented but poorly characterised. In agreement with previously published findings (Burkhardt et al., 1993, Abe et al., 1982, Perou et al., 1997a), I find that the enlarged vesicles are lysosomes and not early or late endosomes. However, two aspects of the phenotype described here differ from those reported in the literature by Burkhardt et al., 1993. Firstly, considerable cell-to-cell variation occurred in the morphology and acidification of enlarged lysosomes, and secondly, exceptionally large organelles (>4 μm in diameter) in C57BL/6J-

bg^{J} *beige* cells were reported to be relatively rare but were common in the cells analysed here.

The basis of the differences in vesicle phenotype between this study and the previous reports is not known. One possibility is that the phenotype varies according to the *beige* mutant allele. Karim and colleagues reported that truncating mutations in LYST were associated with severe early-onset disease, whereas missense mutations were associated with a milder disease with delayed onset (Karim et al., 2002). The *Lyst*$^{bg\text{-}J}$ mutation studied by Burkhardt and colleagues is predicted to disrupt one of the WD40 repeats of LYST (Trantow et al., 2009). This domain is believed to mediate protein-protein interactions (Li and Roberts, 2001) and while some interactions may be abolished by this mutation, the large size of the LYST protein suggests that other LYST functions may be retained. In contrast, the mice used here carry the *Lyst*^{bg} allele, which arose from the retrotransposition of a LINE1 element and is predicted to encode a truncated protein product missing 1442 amino acids from the C-terminal that encodes the BEACH and WD40 domains (Perou et al., 1997b). BEACH domains are essential to the function of other BEACH domain-containing proteins, such as LvsA and FAN, as deletion of the domain abrogates their function (Wu et al., 2004, Adam-Klages et al., 1996). Furthermore, expression of truncated *beige* constructs lacking the BEACH and WD40 domains resulted in a dominant-negative effect and induced the *beige* phenotype in wild type cells (Ward et al., 2003). Differences in the vesicle phenotype of fibroblasts carrying the *Lyst*$^{bg\text{-}J}$ and *Lyst*^{bg} alleles are not reported elsewhere. However, differences in their respective encoded proteins, in particular the truncation caused by the *Lyst*^{bg} allele used here, may account for the differences between the results presented here and those documented in previous reports.

The *beige* and control fibroblasts used in the present study had the same genetic background (CB17.Cg-Prkdc^{scid}). Although unlikely, it cannot be ruled out that the differences in vesicle morphology seen here are the result of an interaction between the *beige* and *SCID* mutations. More likely is the influence of the CB17 genetic background. The effect of genetic background

on the physiology of *beige* mice is demonstrated by work showing that high susceptibility to pneumonitis only occurs when the *beige* alleles are in the SB/Le background (Lane and Murphy, 1972). Furthermore, studies from the irises of *beige* mice revealed expression changes dependent on the genetic background (Trantow et al., 2009, Trantow et al., 2010). However, neither of these studies analysed the vesicle phenotype. Furthermore, the vesicle phenotype of the primary cells used in the present study may be more susceptible to the effects of different passage and culture conditions than the cell lines routinely used elsewhere (Burkhardt et al., 1993, Mohlig et al., 2007, Huynh et al., 2004, Wilson et al., 2008).

The LAMP proteins are highly glycosylated proteins resident in the lysosomal membrane (Kornfeld and Mellman, 1989). Western blot analysis and immunofluorescence microscopy showed a greater level of LAMP1 in *beige* compared to *SCID* fibroblasts and that the *beige* LAMP1 molecules were faster migrating, suggestive of reduced glycosylation (Figure 3.3E). It has been suggested previously that fusion between lysosomes and phagosomes in macrophages requires clustering of the organelles at the MTOC that is mediated by LAMP proteins (Huynh et al., 2007). The increased LAMP1 in *beige* cells could promote the clustering of vesicles at the MTOC, increasing the likelihood of fusion events between closely proximal vesicles and thus give rise to the grossly enlarged lysosomes documented here. Increased LAMP1 expression in *beige* or CHS is not reported elsewhere and the basis of the differential expression and glycosylation of LAMP1 in *beige* cells found here is unknown. LAMP glycosylation affords protection from lysosomal luminal proteases and deglycosylation of LAMP1 results in its rapid degradation (Kundra and Kornfeld, 1999). However, the reduced glycosylation of LAMP1 in *beige* was associated with increased LAMP1 expression (Figure 3.3D and E). LYST deficiency perturbs protein trafficking between the endoplasmic reticulum and lysosomes (Zhang et al., 2007a), therefore defective trafficking of glycosylation machinery may affect LAMP1 glycosylation in *beige* fibroblasts.

The data provided here suggest that constitutive autophagy is enhanced in the absence of functional Lyst, revealed by an increase in LC3B-II in *beige*

cells that correlated with increased LC3B puncta formation (Figure 3.5). Increased LC3B-II levels can arise from either enhanced autophagosome synthesis or reduced degradation. The increased constitutive autophagy in *beige* cells appears to be the results of increased autophagosome synthesis, as blocking degradation using chloroquine resulted in further accumulation of LC3B-II and autophagic puncta. Interestingly, amino acid withdrawal did not induce further LC3B-II production, and the level of LC3B-II was comparable in *beige* and control cell lysates with this treatment. Zhang and colleagues also reported similar levels of LC3-II in *beige-j* and control fibroblast lysates under starvation conditions. However, they detected no LC3-II under basal conditions in either *beige-j* or control cell lysates (Zhang et al., 2010). Experimental conditions such as confluence are known to affect constitutive autophagy (Kimura et al., 2009). Therefore, differences in cell confluency levels may account for the inability of Zhang and colleagues to detect basal LC3-II.

There are two likely explanations for the enhanced constitutive autophagy in *beige* fibroblasts. Either Lyst signals in the autophagic pathway or autophagy is secondary to perturbed membrane and vesicle trafficking in *beige* cells. On the basis that other BEACH family members, such as ALFY, LRBA and mauve, are implicated in the autophagic pathway (Filimonenko et al., 2010, Lopez-Herrera et al., 2012, Rahman et al., 2012), there is a compelling argument for a novel autophagic function of Lyst. ALFY is a 400 kDa protein that shares PH, BEACH and WD40 domains with LYST and is involved in the autophagic degradation of aggregated proteins (Simonsen et al., 2004, Filimonenko et al., 2010, Deretic, 2010). ALFY translocates out of the nucleus and is recruited to membranes containing PtdIns(3)P through its FYVE domain, where it functions as a scaffold adapter to link ubiquitinated cargo with nascent autophagosomes (Simonsen et al., 2004, Filimonenko et al., 2010). Silencing of ALFY with siRNA reduced the clearance of aggregated proteins, whereas overexpression of the C-terminal of ALFY containing the WD40 and FYVE domains enhanced aggregate clearance (Filimonenko et al., 2010). Interestingly, ALFY is reported to only participate in selective autophagic clearance of aggregated proteins, as siRNA-mediated silencing of ALFY had little effect on the starvation response.

The link between the autophagic pathway and LYST was also recently shown in *Drosophila*; cells from flies carrying mutations in *mauve*, an orthologue of LYST, have enlarged lysosomes and these flies exhibit increased susceptibility to infections (Rahman et al., 2012). *Mauve* mutants possessed a significantly greater number of enlarged autophagosomal structures than wild type cells during serum-starvation (Rahman et al., 2012). The underlying mechanism remains to be elucidated, however, it was proposed that mauve acts to restrict homotypic fusion of autophagosomes, allowing their proper maturation. The enhanced autophagy in *beige* cells suggests that Lyst may be involved in negatively regulating autophagy under basal conditions, but unlike mauve, it does not appear to function in autophagy that is induced by external stimuli such as nutrient deprivation.

A PKA phosphorylation site has recently been discovered in LC3 that regulates its involvement in autophagy. An LC3 mutant incapable of being phosphorylated by PKA had greater LCB-II and enhanced autophagic puncta formation under basal conditions (Cherra et al., 2010). The similarly enhanced LC3B-II and autophagic puncta observed in *beige* fibroblasts suggests that LC3 modification might be dysregulated in the absence of LYST, possibly in a PKA-dependent manner. Proteins belonging to the AKAP family bind and scaffold PKA to its substrates at discrete cellular locations (Newlon et al., 1999). Several AKAP family members (Neurobeachin, LRBA and its *Drosophila* orthologue AKAP550) contain either a defined or putative AKAP domain (Wang et al., 2000, Wang et al., 2001, Han et al., 1997). Of these three proteins, only LRBA is implicated in autophagy. LRBA-deficient cells accumulate autophagosomes but the mechanism underlying this is unknown (Lopez-Herrera et al., 2012). No such AKAP domain has been identified in LYST, though a PKA interaction mediated by its WD40 domain is possible. LYST could negatively regulate autophagy under basal conditions by promoting PKA-dependent phosphorylation of LC3, thus inhibiting autophagosome formation. However, we might expect further enhancement of LC3-II formation in response to autophagy inducers such as starvation, similar to reports by Cherra and colleagues who found LC3-II increased in response to rapamycin when a PKA inhibitor is also present (Cherra et al., 2010). However no further

increase in LC3B-II above basal levels was observed in *beige* fibroblasts during amino acid-starvation.

The data presented here suggest that autophagy is enhanced in the absence of functional Lyst. Whether this is a direct result of the *beige* mutation, or occurs secondary to the perturbed membrane and vesicle trafficking in *beige* cells is not known and the exact role of *beige* in autophagic flux remains uncertain. Although LC3B did not appear to contribute to membrane staining of large *beige* vesicles as assessed by immunofluorescence and confocal microscopy, it remains to be determined whether the increased level of constitutive autophagy contributes to enlargement of *beige* lysosomes.

PtdIns(4,5)P_2 is primarily located at the plasma membrane (Watt et al., 2002, Hammond et al., 2009), where it is an intermediate in the DAG and Ins(1,4,5)P_3 signalling pathway. Ward and colleagues reported an intense punctate nuclear localisation of PtdIns(4,5)P_2 in normal fibroblasts that was absent in the majority of *CHS* and *beige* counterparts analysed, but total cellular PtdIns(4,5)P_2 level remained unchanged (Ward et al., 2003). They postulated that reduced nuclear PtdIns(4,5)P_2 would coincide with an increase in the lipid at an alternative subcellular compartment. This study aimed to establish whether *beige* cells have altered plasma membrane-associated PtdIns(4,5)P_2 or atypical lysosome-associated PtdIns(4,5)P_2, which might disrupt PtdIns(4,5)P_2-dependent signalling pathways or normal lysosome homeostasis, respectively. Using the same monoclonal antibody as Ward and colleagues (2003) together with a staining methodology optimized for preservation of the plasma membrane (Hammond et al., 2009), the level of plasma membrane-associated PtdIns(4,5)P_2 appeared modestly elevated in *beige* fibroblasts compared to *SCID* controls. However, analysis of the specificity of this antibody revealed cross-reactivity with other lipids, making interpretation of the cellular staining difficult. Furthermore, strong autofluorescence from LAMP1-positive lysosomes in *beige* cells made assessing the presence of PtdIns(4,5)P_2 at the lysosome problematic. Therefore, attention was turned instead to the PtdIns(4,5)P_2-binding protein PLC.

I report for the first time that *beige* fibroblasts have decreased abundance of PLCγ as well as PKCβ, both of which are key players in the same lipid-signalling pathway. The modest elevation of PtdIns(4,5)P_2 at the plasma membrane could be attributed to the reduced abundance of PLCγ1 and PLCγ2, as PtdIns(4,5)P_2 is a substrate for these enzymes. Hydrolysis of PtdIns(4,5)P_2 by PLCγ yields two second messenger lipids, Ins(1,4,5)P_3 and DAG (Carpenter and Ji, 1999). Ins(1,4,5)P_3 is released into the cytosol and binds Ins(1,4,5)P_3 receptors in the endoplasmic reticulum, triggering the release of Ca^{2+}. DAG remains inserted in the lipid bilayer of the plasma membrane and facilitates the activation and translocation of PKC from the cytosol to the plasma membrane (Morgan et al., 2005). A well-characterized phenotype of CHS/*beige* is the defective exocytosis of cells containing secretory lysosomes, such as NK cells, CTLs and platelets (Roder and Duwe, 1979, Jessen et al., 2011, Stinchcombe et al., 2000, Shiraishi et al., 2002a). PLC molecules and their products, Ins(1,4,5)P_3 and DAG, have indispensable roles in stimulated exocytosis (Caraux et al., 2006, Hammond et al., 2006) and perturbation of this signaling pathway would undoubtedly affect the regulated secretion of secretory lysosomes. Shiraishi and colleagues noted that platelets from CHS cattle had defective collagen-induced Ca^{2+} signalling and reduced exocytosis that they attributed to reduced PLCγ-dependent production of Ins(1,4,5)P_3, explaining the bleeding tendency of CHS cattle (Shiraishi et al., 2002a, Shiraishi et al., 2002b). However, the abundance of PLCγ was not investigated. It will be of interest to evaluate the abundance of PLC isoenzymes in CHS/*beige* cells whose primary secretory function is blocked, such as CTLs and NK cells.

PKC is central to the degranulation of NK cells (Ito et al., 1988a) and down-regulated PKC activity in CHS/*beige* NK cells is thought to underlie the secretion defect (Ito et al., 1989, Tanabe et al., 1998). The down-regulation is attributed to enhanced proteolysis of PKC by calpain, as addition of calpain inhibitors such as E-64-d correct the lowered PKC activity. E-64-d also corrects other cellular defects of CHS/*beige*, such as giant lysosome formation in fibroblasts (Tanabe et al., 2000) and the defective NK cell-mediated killing of target cells (Ito et al., 1989, Tanabe et al., 2009). Exactly why PKC proteolysis occurs in CHS/*beige* is not fully understood. PKC is

regulated by its phosphorylation status and Tanabe and colleagues suggest that the elevated ceramide level in CHS/*beige* cells stimulates autophosphorylation of PKCβ, rendering it susceptible to calpain proteolysis (Tanabe et al., 1998, Tanabe et al., 2000). An alternative explanation is that LYST scaffolds a protein complex involved in PKC phosphorylation. PKCβ is one of many substrates for phosphorylation by CK2β (Tominaga et al., 1991). CK2β was identified as a LYST binding partner in a yeast-2-hybrid binding assay (Tchernev et al., 2002) and subsequently confirmed to bind the LYST WD40 domain in a GST pull-down assay (Trantow, 2009). LYST might bring CK2β into contact with PKC and when absent, the normal phosphorylation status of PKC would be altered, rendering it susceptible to autophosphorylation and proteolysis. Alternatively, decreased activation and recruitment of PKC to the plasma membrane as a result of lowered PLCγ-mediated Ca^{2+} and DAG production, may result in PKC degradation.

PI metabolism has also been linked to autophagy. A recent study by Decuypere and colleagues demonstrated that a Ins(1,4,5)P_3-mediated Ca^{2+} release was critical for starvation-induced autophagy, because in its absence, starvation-induced LC3-puncta and LC3-II formation were abolished (Decuypere et al., 2011). Low Ins(1,4,5)P_3 production as a result of decreased PLCγ activity may in part explain why a starvation-induced increase in LC3B-II formation and LC3B puncta above the basal level was not observed in *beige* fibroblasts. Analysis of Ins(1,4,5)P_3 levels and Ins(1,4,5)P_3-mediated signalling in *beige* cells would confirm this.

The link between Lyst*,* mislocalised PtdIns(4,5)P_2 and reduced PLCγ isoenzymes is unclear. Mounting evidence from studies of the BEACH and WD40 domains using expression constructs (Ward et al., 2003) and LYST homologues (Han et al., 1997, Wang et al., 2000) suggest LYST serves a scaffold for other protein interactions. LYST might be targeted to the plasma membrane through binding of its PH domain to PtdIns(4,5)P_2 in a similar manner to FAN (Haubert et al., 2007), or through its HEAT and Armadillo-like domains, that have recently been confirmed to be PtdIns(4,5)P_2-binding modules using affinity-capture techniques (Catimel et al., 2008). Membrane targeting might serve to recruit and scaffold protein complexes such as

those involving PLCγ1 or PKCβ, at specific sites at the plasma membrane such as PtdIns(4,5)P_2-rich lipid rafts. In the absence of a LYST scaffold, these proteins may become vulnerable to degradation, thus restricting unwarranted downstream signalling elsewhere. The present study documents for the first time that *beige* fibroblasts have decreased abundance of PLCγ and PKCβ, both of which are key players in the same signalling pathway that is fundamental to the later stages of secretory lysosome exocytosis, that is, the fusion with the plasma membrane. Examining the abundance of these proteins and the PIs with which they interact in CHS/*beige* cells with secretory lysosomes might shed some light on the mechanism behind their defective exocytosis.

The data presented in this chapter suggest that Lyst may have roles in autophagy and lipid signalling. However, the mechanisms by which this might occur in *beige* cells is speculative, as information on the functional activity of Lyst is lacking. Any attempt to understand the functional role of Lyst will require a more detailed analysis of the pathways in which Lyst participates. In the next chapter, RNA interference was exploited to attempt to reveal these pathways in more detail.

Chapter 4
Modelling the *beige* Phenotype Using RNA Interference

4.1 Introduction

The use of post-transcriptional gene silencing via RNA interference has revolutionised the study of mammalian gene function. However, to date, RNA interference has not been reported in the study of LYST. It is therefore of great interest to examine the effect of *Lyst* silencing as this might yield further information on the role of LYST and aid in the characterisation of proteins in the same functional pathway. Synthetic small interfering (si) RNAs are duplexes of 21-23 nucleotides in length that induce post-transcriptional gene silencing in mammalian cells by an endogenous mechanism known as RNA interference (Elbashir et al., 2001). The duplexes are incorporated into the multiprotein RNA-induced silencing complex (RISC) which is targeted to the mRNA, directing its cleavage (Meister and Tuschl, 2004). The cleaved mRNA is then degraded, silencing the expression of the target gene.

4.2 Reduction of *Lyst* Expression Causes Accumulation of Enlarged Cytoplasmic Vesicles

Four siRNA sequences targeted to different and unique regions within the mouse *Lyst* mRNA sequence were purchased together with a non-targeting sequence with no known sequence similarity to mouse genes, to be used as a negative control. The sequences are herein referred to as *siLyst* 1-4 and *siControl*, respectively. To achieve maximal transfection efficiency with minimal cell death, preliminary experiments were carried out to determine the optimal conditions for liposome-mediated transfection of 3T3-J2 fibroblasts using Lipofectamine™ RNAiMAX transfection reagent (data not shown). In the absence of an antibody to detect Lyst protein level, qRT-PCR was performed to quantify the expression of *Lyst* mRNA transcripts and the cells were monitored for the appearance of an enlarged vesicle phenotype.

siRNAs were transfected individually into 3T3-J2 cells at a concentration of 50 nM and after 72 hours, total RNA was isolated from cell lysates and reverse transcription was used to generate cDNA. The cDNA was then PCR-amplified with primers spanning a *Lyst* exon boundary to eliminate amplification of pre-mRNAs. Three out of the four *siLyst* sequences significantly reduced expression of *Lyst* transcripts compared with the control (Figure 4.1A). The greatest silencing was observed in *siLyst* 2-transfected cells with *Lyst* mRNA reduced by 69% relative to the control, compared to 39.2%, 43.4% and 34.1% reduction in cells transfected with *siLyst* 1, -3, and -4 respectively. Increasing the concentration of *siLyst* 1, -2 or -3 to 100 nM did not achieve further silencing and caused only modest further reduction of *Lyst* mRNA with *siLyst* 4. A mock transfection in which siRNA was omitted, had no effect on *Lyst* mRNA expression (data not shown). Transfection efficiency was estimated using a fluorescein-labelled double-stranded RNA oligomer (BLOCK-iT™), which was transfected into 3T3-J2 under identical conditions to *Lyst* siRNA, and the fluorescence quantified by flow cytometry. The percentage of fluorescent cells was 76.3 ± 6.9% (n = 3 independent experiments), 72 hours post-transfection with 50 nM BLOCK-iT™ (data not shown).

Examination of 3T3-J2 by phase contrast microscopy 72 hours post-transfection, revealed distinct morphological differences between cells transfected with 50 nM *siLyst* 2 and *siControl* (Figure 4.1B). *siLyst* 2-transfected cells contained numerous large refractive cytoplasmic vesicles that were not found in *siControl*- or mock-transfected cells. The vesicles were clustered around the nucleus and excluded from peripheral extensions. In the *siLyst* 4-transfected culture, cells appeared less confluent than the control culture (Figure 4.1B). However, enlarged vesicles were not observed in cells transfected with either *siLyst* 1, -3, -4 or *siControl*.

As transfection with *siLyst* 2 stimulated the greatest reduction in mRNA and appearance of an enlarged vesicular phenotype, *siLyst* 2 was selected for further optimisation. The concentration of *siLyst* 2 was titrated (range 1 -

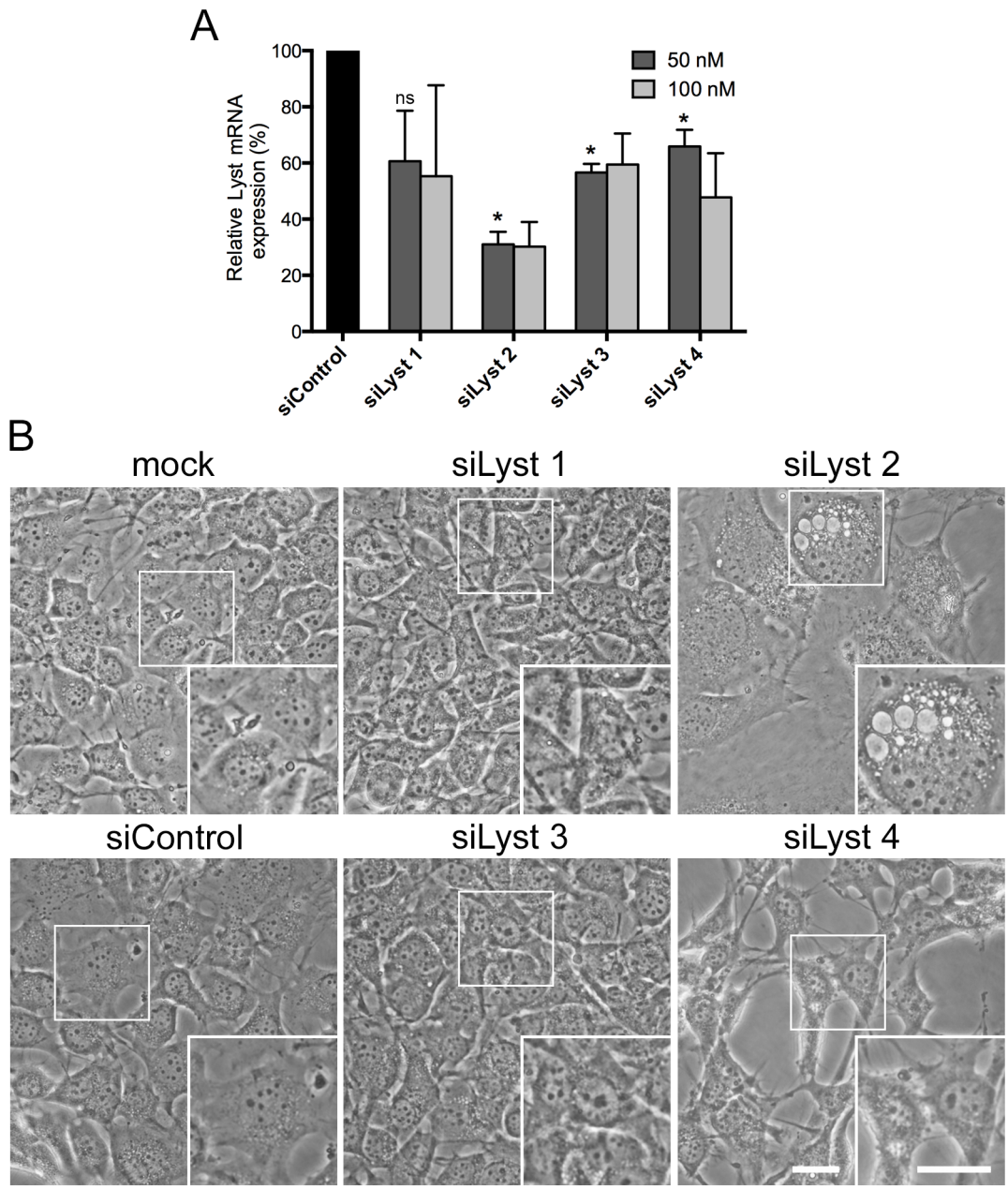

Figure 4.1. siRNA-mediated silencing of *Lyst* expression causes accumulation of large cytoplasmic vesicles in 3T3-J2 fibroblasts

A) Real-time qRT-PCR measurements of the relative levels of *Lyst* mRNA in 3T3-J2 fibroblasts transfected with 50 or 100 nM individual *Lyst* siRNA sequences (*siLyst*) or 50 or 100 nM non-targeting sequence (*siControl*), 72 hours post-transfection. Values are expressed as a percentage of the *Lyst* mRNA level in cells transfected with *siControl* and represent the means and SDs of three independent experiments. * = P<0.01; ns, not significant. B) Phase contrast images of 3T3-J2 fibroblasts transfected with 50 nM of individual siRNA sequences, 72 hours post-transfection. Scale bars = 20μm.

100 nM) and *Lyst* mRNA expression quantified 72 hours post-transfection. At the lowest concentration (1 nM), *Lyst* mRNA was reduced to 30.6 ± 6.9% of the *siControl*-transfected cells (Figure 4.2A). To determine the extent of vesiculation triggered by *siLyst* 2, phase contrast images were used to calculate the percentage of cells displaying an enlarged vesicle phenotype. Cells that contained four or more large vesicles (>2 μm^2) were considered to be positive for the phenotype. Despite relatively similar levels of *Lyst* mRNA expression in cells transfected with 1nM and 50 nM *siLyst* 2, a three-fold greater percentage of cells carried the phenotype when treated with 50 nM (Figure 4.2B) Transfection with 1 nM and 25 nM induced a vesicle phenotype in 15.5% and 18.9% respectively, while 47.3% were vesiculated after transfection with 50 nM. These results indicate that 50 nM of *siLyst* 2 is sufficient to induce a vesiculated phenotype in half the cell population after 72 hours.

The duration of siRNA-mediated gene silencing and the corresponding phenotypic effects can vary significantly depending on the stability of the siRNA-mRNA complex and the half-life of the remaining protein. As the half-life of Lyst is unknown, the effect of *Lyst* silencing was examined over several time points. Relative *Lyst* mRNA expression in cultures 24-96 hours after transfection and corresponding phase contrast images are shown in Figure 4.2C and Figure 4.2D, respectively. The reduction in *Lyst* mRNA expression was maximal at the earliest time point measured (24 hours after transfection, Figure 4.2C). Although large cytoplasmic vesicles were present in cells at this time point, large vesicles were also observed in *siControl* cells (Figure 4.2D). This was attributed to the introduction of siRNA into cells, as no vesiculation was observed in the mock-transfected culture (data not shown). The abundance of vesiculated cells in the *siControl* population decreased after 24 hours. The exhibition of vesiculated cells increased at 48 hours (58.3%) and was maximal at 72 hours (68.3%, Figure 4.2E). No further increase in the number of vesiculated cells occurred at 96 hours. This may be due to a greater presence of Lyst protein, as *Lyst* mRNA transcripts were more abundant at 96 hours than at earlier time points.

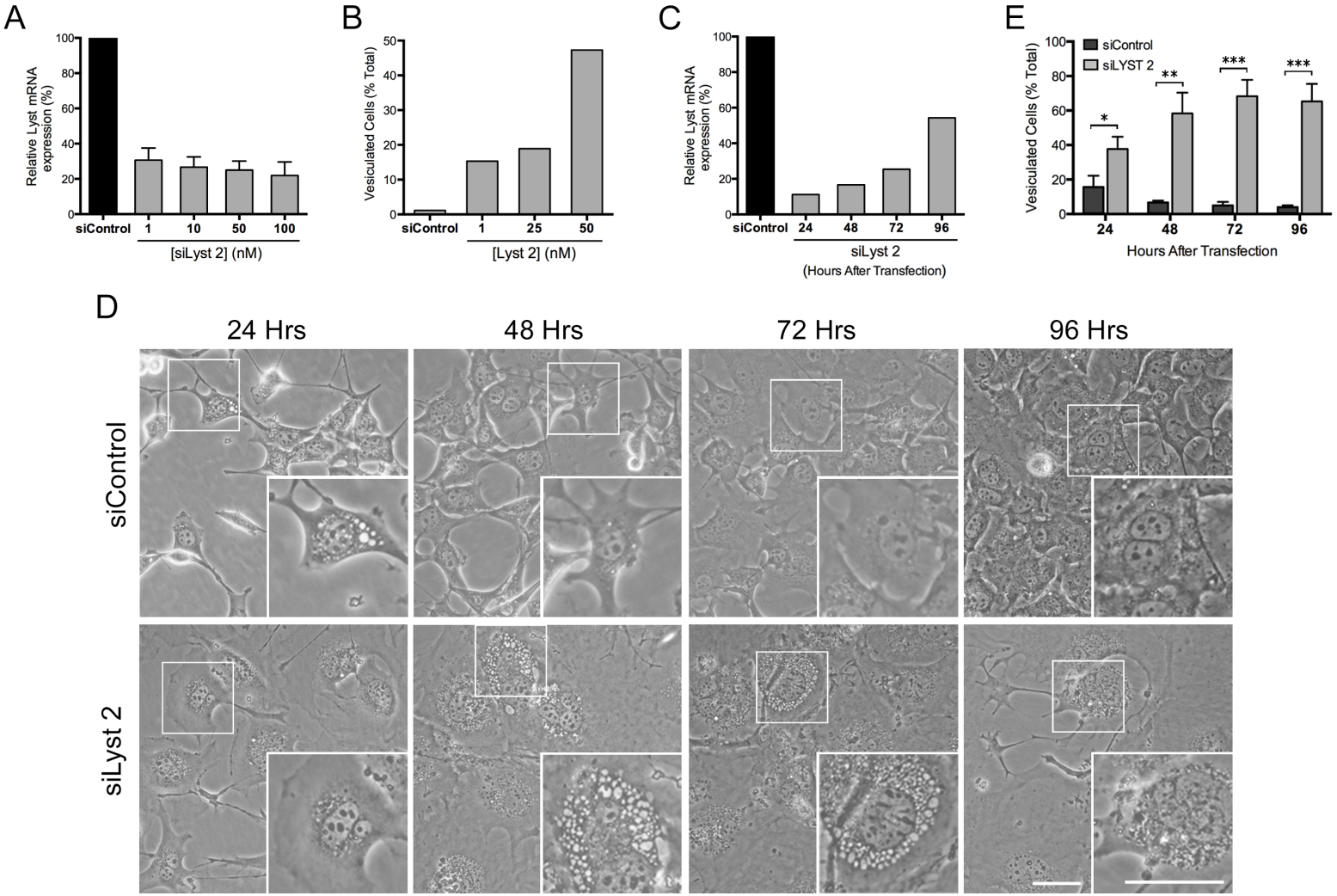
A
Relative Lyst mRNA expression (%)
100
80
60
40
20
0
siControl
1
10
50
100
[siLyst 2] (nM)
B
Vesiculated Cells (% Total)
50
40
30
20
10
0
siControl
1
25
50
[Lyst 2] (nM)
C
Relative Lyst mRNA expression (%)
100
80
60
40
20
0
siControl
24
48
72
96
siLyst 2
(Hours After Transfection)
E
Vesiculated Cells (% Total)
siControl
siLYST 2
*
**
***
***
100
80
60
40
20
0
24
48
72
96
Hours After Transfection
D
24 Hrs
48 Hrs
72 Hrs
96 Hrs
siControl
siLyst 2

Figure 4.2. Concentration- and time-dependent *Lyst* mRNA expression and vesicular phenotype in *siLyst 2*-transfected J2-3T3 fibroblasts

A) Real-time qRT-PCR measurements of the levels of *Lyst* mRNA in 3T3-J2 fibroblasts transfected with a range of concentrations of *Lyst* siRNA (1 - 100 nM) or *siControl* (100 nM), 72 hours post-transfection. Values are expressed as a percentage of the *Lyst* mRNA level in cells transfected with *siControl* and represent the means and SDs of three independent experiments. B) The percentage of cells exhibiting the vesiculated phenotype, calculated from phase contrast images of 3T3-J2 fibroblasts, 72 hours post-transfection with *siLyst* 2 (1-50 nM) or 50 nM *siControl.* C) Real-time qRT-PCR measurements of the relative *Lyst* mRNA level at different time-points after transfection with 50 nM *siLyst* 2 or *siControl*. D) Phase contrast images of cells transfected as stated in *C*. E) The percentage of cells exhibiting the vesiculated phenotype was calculated from phase contrast images of 3T3-J2 fibroblasts transfected as in *C.* Cells were deemed to be vesiculated if they contained at least four enlarged vesicles (>2 μm^2). At least 50 cells per treatment were counted in each separate experiment. The means and SDs from three independent experiments are given. * = P<0.05; ** = P<0.01; *** = P<0.001. Scale bars = 50 μm.

These data suggest the vesicular phenotype that arises in 3T3-J2 fibroblasts in response to transfection with *siLyst* 2 is maximal at 48-72 hours and is likely due to silencing of the *Lyst* gene. *Lyst* silencing gave rise to large vacuole-like vesicles, clustered around the nucleus that were very similar to the refractive vesicles in *beige* fibroblasts (Figure 3.1C, *panel iii*). However, *Lyst* silencing did not induce the formation of non-refractive granule-like vesicles observed in *beige* fibroblasts (Figure 3.1C, *panel ii*).

Next, the viability of *siLyst* 2-transfected cells was assessed using Annexin V and 7-amino-actinomycin D (7-AAD) staining to determine the proportion of healthy and apoptotic cells, as measured by flow cytometry. One of the earliest features of apoptosis is the externalisation of the phospholipid phosphatidylserine (PS) from the inner leaflet of the plasma membrane to the outer leaflet, allowing the recognition and removal of apoptotic cells by phagocytes (Fadok et al., 1998). Annexin V is a phospholipid-binding protein with high affinity for PS and is a sensitive probe for detecting cells in early apoptosis. 7-AAD is a vital dye that is excluded from intact cells but labels

the DNA in the later stages of apoptosis and necrosis, when cell membranes are fragmented and permeable. Cells stained simultaneously with these probes can be identified as healthy (double-negative), early apoptotic (Annexin V-positive/7-AAD-negative) or late apoptotic or necrotic (double-positive). The introduction of siRNA into 3T3-J2 fibroblasts caused a modest induction of early apoptosis in *siControl* cells as 14.8% of cells were Annexin V positive compared with 4.8% in the mock-transfected culture. The number of double-positive cells was comparable in *siControl* and mock populations (2.1% and 1.3% respectively (Figure 4.3). The fractions of Annexin V-positive and double-positive cells were greater in the *siLyst* population, indicating 28.1% were early apoptotic and 8.7% late apoptotic or necrotic. These results suggest that 3T3-J2 fibroblasts become apoptotic in response to *Lyst*-silencing. However, after long term culture (7-10 days) the proportion of dead cells in the *siLyst* 2 culture was only modestly greater than in the *siControl*, when viewed under a phase contrast microscope (data not shown). Phospholipid mislocalisation has been reported in CHS/*beige* fibroblasts (Ward et al., 2003). The inferred increase in surface PS could therefore be the result of altered PS trafficking in *Lyst*-silenced 3T3-J2 fibroblasts, or a heightened sensitivity of *Lyst*-silenced cells to the stresses of the experimental process. As cell death was not observed after long term culture, *Lyst*-silenced cells were therefore considered viable for further investigation.

4.3 *Lyst* Silencing by siRNA Causes Lysosomal Enlargement and Enhancement of Autophagy

Given the similarity of the vesicle phenotype of *Lyst*-silenced 3T3-J2 fibroblasts to that of *beige* fibroblasts, the identity of the enlarged vesicles was next examined. The subcellular distributions of EEA1, MPR and LAMP1 (corresponding to early endosomal, late endosomal and lysosomal compartments, respectively) and the acidotropic dye LysoTracker were analysed using immunofluorescence microscopy. There was no difference in the staining pattern of either EEA1 or MPR between *siControl*- or *siLyst* 2-transfected cells 72 hours post-transfection (Figure 4.4). However, large ring

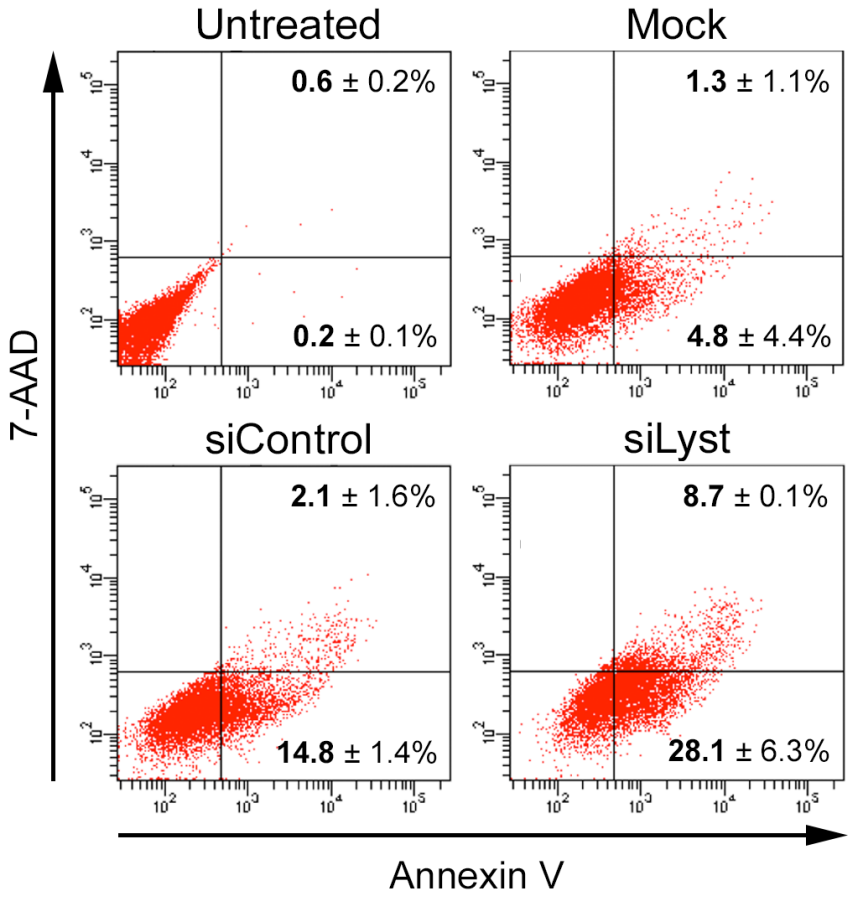

Figure 4.3. Viability assay of *siLyst 2*-transfected 3T3-J2 fibroblasts

3T3-J2 cells transfected with siRNA for 48 hours and were labelled with FITC-Annexin V and 7-AAD and the fluorescence assessed by flow cytometry. Red dots indicate intact 3T3-J2 fibroblasts. Cells in early apoptosis are positive for Annexin V only and appear in the bottom right quartile, while late-apoptotic cells double-positive for both Annexin V and 7-AAD appear in the top right quartile. Values are expressed as percentages of the intact population that fall within each gate and are given as means plus SDs from two independent experiments.

-like structures were observed with anti-LAMP1 antibody in *siLyst* 2-transfected cells but not in *siControl* cells, suggesting that the enlarged vesicles induced by *Lyst*-silencing are lysosomes. This is consistent with the *beige* phenotype in the previous chapter and previous reports (Burkhardt et al., 1993, Durchfort et al., 2012). The enlarged vesicles appeared to accumulate LysoTracker, consistent with the findings of Mohlig and colleagues (2007).

In the previous chapter, *beige* fibroblasts were found to have a higher level of constitutive autophagy (Figure 3.5). Therefore, *Lyst*-silenced 3T3-J2 fibroblasts were examined for the presence of LC3B puncta formation. 3T3-J2 fibroblasts were transfected with 50 nM *siLyst* 2 or *siControl* for 48 hours to allow sufficient time for the vesicle phenotype to be present. Cells were then treated with either DMSO or chloroquine for a further 24 hours before being immunofluorescently labelled with anti-LC3B antibody, to identify LC3B-associated autophagosomes (Figure 4.5A). The mean number of LC3B puncta in DMSO-treated cells was almost two-fold greater in the *siLyst* 2-transfected population (6.6 puncta) compared to the *siControl*-transfected population (3.5 puncta, Figure 4.5), however, there was no difference in puncta size. A similar observation was made in DMSO-treated *beige* fibroblasts, where LC3B puncta were more abundant than in DMSO-treated SCID fibroblasts, but comparable in size (Figure 3.5B). The addition of chloroquine resulted in the accumulation of large LC3B puncta in both *siControl*- and *siLyst* 2- transfected populations, but a greater fold increase in puncta was observed in *siLyst* 2 cells (8.5-fold compared to 6.7-fold in *siControl* cells). In both the *siControl* and *siLyst* 2 populations, puncta were considerably larger in the presence of chloroquine, possibly as a result of the accumulated autophagosomes fusing homotypically in the absence of lysosome-mediated degradation. However there was no difference in puncta size between *siLyst* 2- and *siControl*-transfected cells. These data suggest that constitutive autophagy is altered in *Lyst*-silenced 3T3-J2 fibroblasts, similar to *beige* fibroblasts, however, further experiments are needed to confirm this.

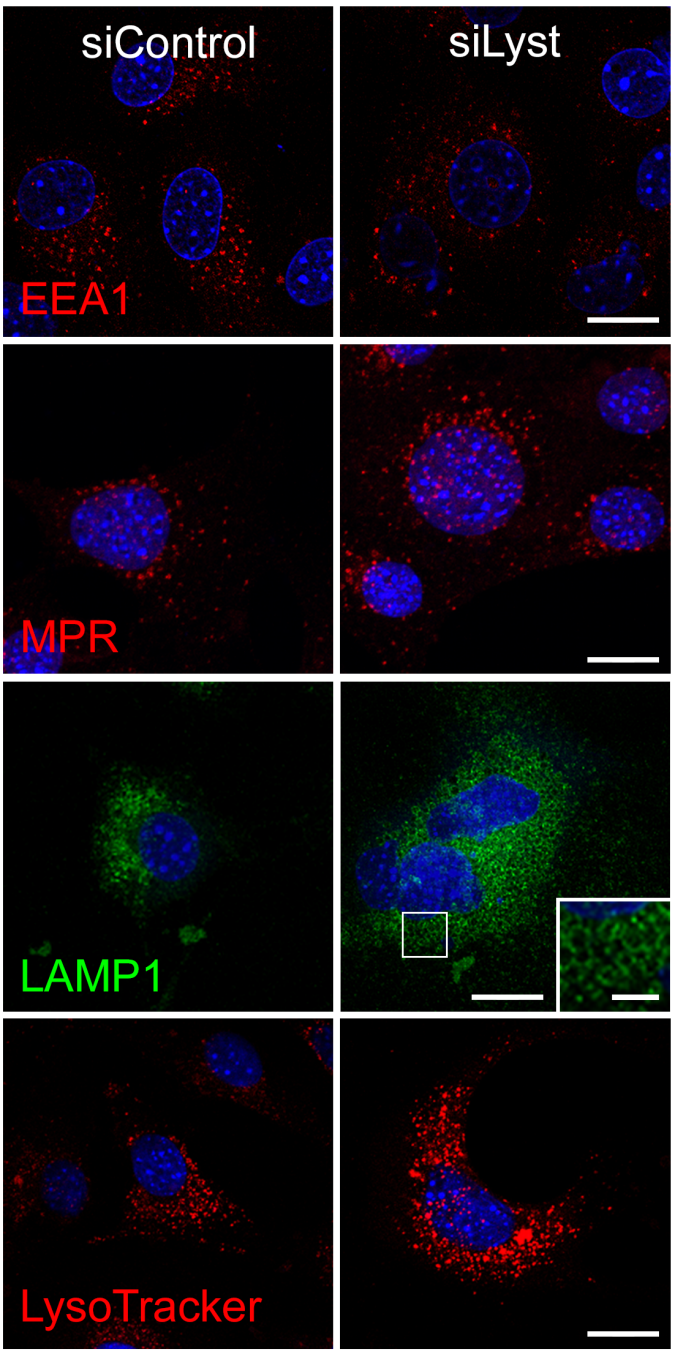

Figure 4.4. The large vesicles in *siLyst* 2-silenced 3T3-J2 fibroblasts are lysosomes

3T3-J2 fibroblasts were transfected for 72 hours with 50 nM *siControl* or *siLyst* 2. Identical staining patterns of EEA1 and CI-MPR were observed in *siLyst* 2 and *siControl* cells, however large ring-like structures were observed with anti-LAMP1 antibody in *siLyst* 2-transfected cells but not in *siControl* cells. Enlarged vesicles were LysoTracker positive, suggesting that the enlarged vesicles induced by *Lyst*-silencing are lysosomes. DAPI (*blue*) was used to visualise the nucleus. Images are maximum intensity projections of confocal z-stacks, except for the top panel which are single confocal sections. Scale bar: *main images*, 20 µm; *inset*, 5 µm

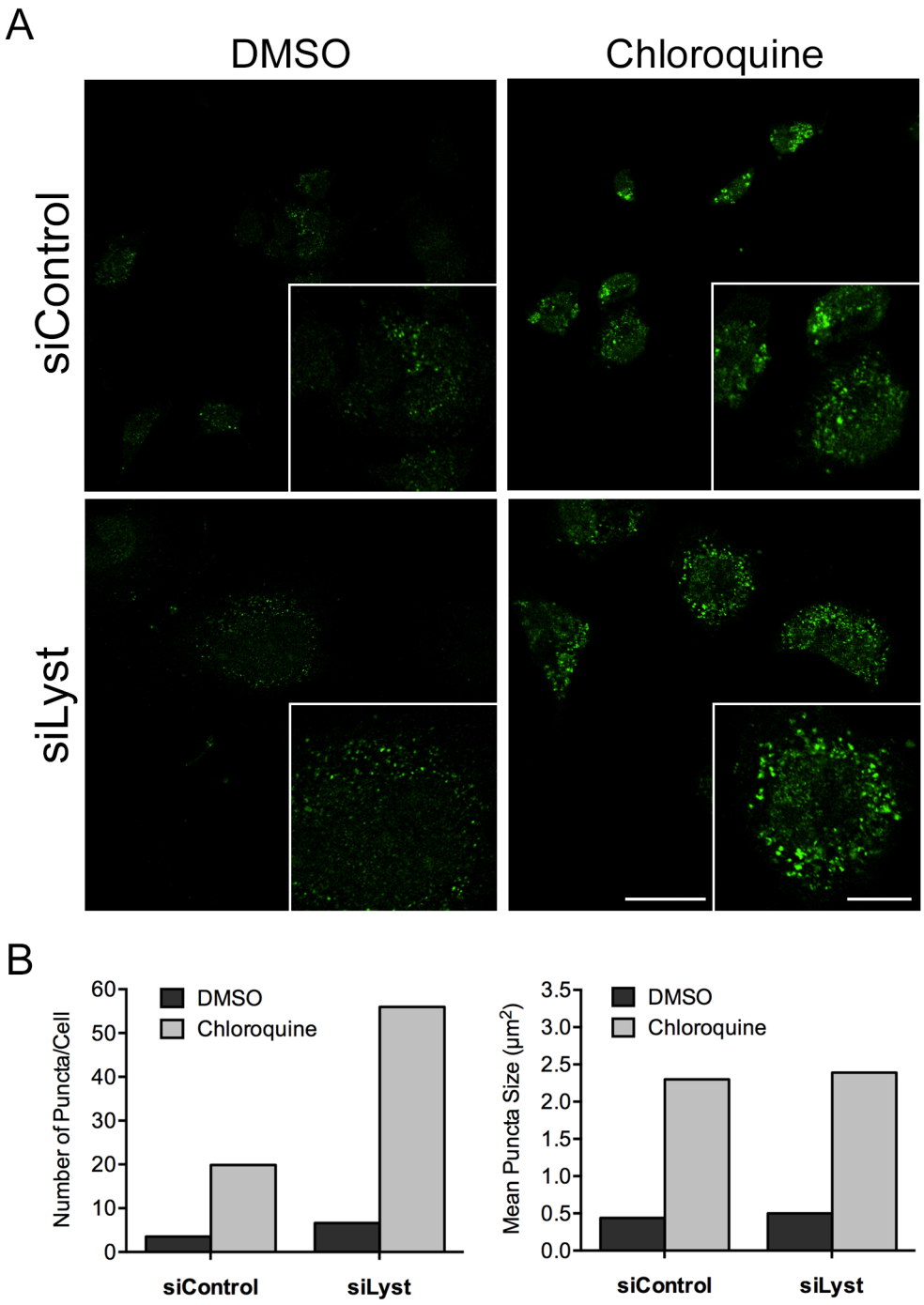

Figure 4.5. LC3B puncta formation in *siLyst* 2-silenced 3T3-J2 fibroblasts

A) Maximum intensity projections of confocal z-stacks showing LC3B-puncta in *siLyst* 2- and *siControl*-treated cells 24 hours post treatment with chloroquine (25 µM) or DMSO. 3T3-J2 were transfected with 50 nM or either *siControl* or *siLyst* 2. Insets are magnifications of the main image. B) Quantification of the mean number of puncta per cell (*left graph*) and mean puncta size (*right graph*) was performed from a single experiment. At least 50 cells per treatment were analysed. Scale bar: *main images*, 50 µm; *insets*, 20 µm.

4.4 *Lyst*-Silencing Induces Senescent-Like Changes in Fibroblasts

Another striking phenotypic change in *Lyst*-silenced cells was observed. Cells became unusually large and flattened and spread extensively across the culture vessel surface (Figure 4.2D). Cell enlargement was apparent from 24 hours post-transfection and persisted through to 96 hours, with no apparent increase in cell number after 48 hours. Total cell area was calculated from immunofluorescent images of phalloidin-stained cells using ImageJ software. *Lyst*-silenced cells were found to be almost two-fold larger than control cells (n = 60 cells, Figure 4.6). Individual cell sizes are indicated in the scatter dot plot (Figure 4.6A). The mean sizes of *siControl* and *siLyst* 2 cells were 1450 ± 1238 μm^2 and 2872 ± 1773 μm^2 respectively, with some cells in the *siLyst* 2 population reaching over 5000 μm^2. A large, flattened cell morphology is a hallmark of cellular senescence: a state of irreversible growth arrest brought about by persistent DNA damage response signalling and oncogenic and culture stresses (Rodier and Campisi, 2011). Senescent cells frequently double in size compared to non-senescent cells (Hayflick, 1965). To examine if the increased size was due to the induction of senescence, a positive control senescent 3T3-J2 cell population was created by exposing cells to *γ*-radiation. The forward and side scatter parameters of a flow cytometer are routinely used to distinguish cell populations based on their size and granularity. The low-angle forward scatter of light that occurs when a cell passes through a laser beam is roughly proportional to the diameter of the cell. The forward scatter parameter was used to quantify the percentage of cells in transfected or irradiated 3T3-J2 populations that were enlarged relative to their untransfected and non-senescent counterparts, respectively. In the *siLyst* 2 population, 48.1% of cells were enlarged, relative to untransfected cells after, 48 hours post-transfection (Figure 4.6B); significantly more than in the *siControl* population (16.6%). As expected, the radiation-induced senescent population contained the greatest number of enlarged cells (70.4%). These results confirm *Lyst* silencing stimulates a dramatic increase in cell size in nearly 50% of the population, and this increase may be associated with senescence.

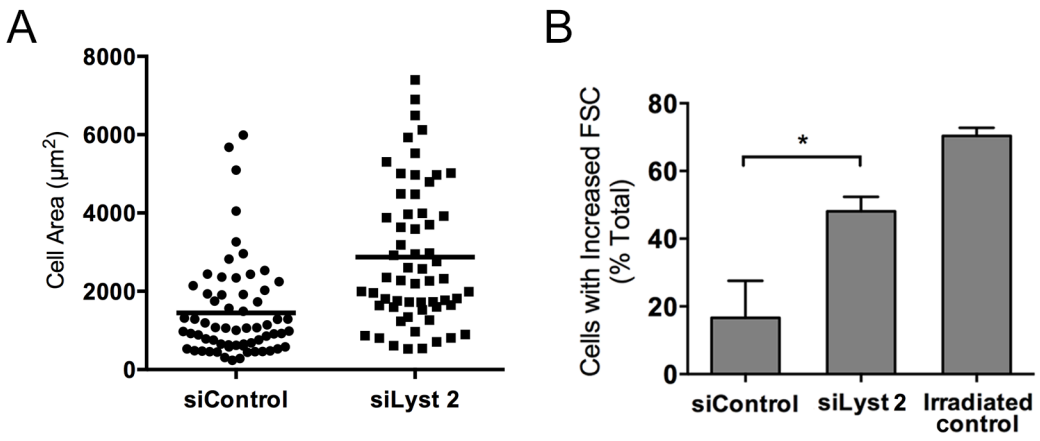

Figure 4.6. Cell size is increased in *siLyst 2*-transfected 3T3-J2 fibroblasts

A) Cell area was calculated from maximum intensity projections of confocal z-stacks of phalloidin-stained cells, 48 hours post-transfection with 50 nM *siLyst* 2 or *siControl.* Horizontal bars indicate the mean cell sizes. At least 60 cells per population were analysed. B) The forward scatter parameter of a flow cytometer was used to determine the number of enlarged cells in a population. 3T3-J2 cells exposed to *γ*-radiation or transfected with 50 nM *siLyst* 2 or *siControl* for 48 hours were analysed. The percentage of cells with increased forward scatter relative to untreated cells was calculated. The means and SDs were calculated form three independent experiments *, P=0.0097.

The senescent-like morphology of *Lyst*-silenced cells is intriguing for several reasons. Firstly, as mentioned in the previous chapter, CHS/*beige* cells contain unusually high levels of ceramide. Endogenous ceramide is elevated in senescent human endothelial cells and fibroblasts (Mouton and Venable, 2000, Venable and Yin, 2009) and treatment of cells with exogenous C_6-ceramide induces replicative senescence in fibroblasts, marked by inhibited proliferation and increased senescence-associated *β*-Galactosidase (SA-*β*-Gal) activity (Mouton and Venable, 2000). Secondly, two proteins identified as LYST-binding partners in two-hybrid assay (Tchernev et al., 2002), CK2β and 14-3-3τ, are implicated in cell cycle control (Hanna et al., 1995, Kang et al., 2009, Wang et al., 2010). On the basis of these reports, a novel role for Lyst in the regulation of cell cycle control seemed both attractive and

plausible, and prompted further characterisation of the senescent-like phenotype of *Lyst*-silenced cells.

In addition to increased size, the senescent state is characterised by permanent growth arrest, secretion of cytokines and growth factors and expression of SA-*β*-Gal and p16INK4a (Rodier and Campisi, 2011). Although not all of these markers may coexist in a senescent population. To assess proliferation, cells transfected with either 50 nM *siLyst* 2 or *siControl* were seeded at a density of $2.5x10^4$ cells/mL and then counted 48 hours later. The number of cells was markedly reduced in siLyst 2-transfected cells compared to *siControl* cells (Figure 4.7A), with no increase in cell death in *siLyst* cells (as determined by trypan blue, data not shown). This data indicates that transfection with *siLyst* 2 slows the rate of proliferation. *β*-galactosidase is an enzyme that catalyses the hydrolysis of *β*-D-galactose from molecules such as glycoproteins and glycosphingolipids and functions optimally at pH 4.5. However, substantial induction of *β*-galactosidase expression in senescent cells permits the detection of activity at suboptimal pH 6.0 (Dimri et al., 1995) and is widely used to discriminate between senescent and non-senescent cells. SA-*β*-Gal activity was detected at pH 6.0 in fixed transfected and irradiated cells by a cytochemical assay that utilises the chromogenic property of 5-bromo-4-chloro-3-indolyl-*β*-D-galactopyranoside (X-gal). Cleavage of X-gal by SA-*β*-Gal yields an insoluble blue product that is readily detectible by phase contrast microscopy. Phase contrast images were taken 12-16 hours later when the presence of the blue product was maximal. Both siRNA-transfected and irradiated cells were stained with X-gal after 48 hours, in the presence of a citric acid/sodium phosphate buffer at pH 6.0 and examined for the presence of blue product (Figure 4.7B). Low-level SA-*β*-Gal activity was detected in some *siControl* cells, but the majority of cells were negative (Figure 4.7B). In stark contrast however, almost all the large flattened cells in the *siLyst* culture were strongly positive for SA-*β*-Gal activity, whereas the smaller cells of normal morphology, presumed to be untransfected or unresponsive to siRNA, had little or no SA-*β*-Gal activity. Similarly, many large flattened cells were observed in the radiation-induced senescent population and were strongly positive for SA-*β*-Gal expression (Figure 4.7B).

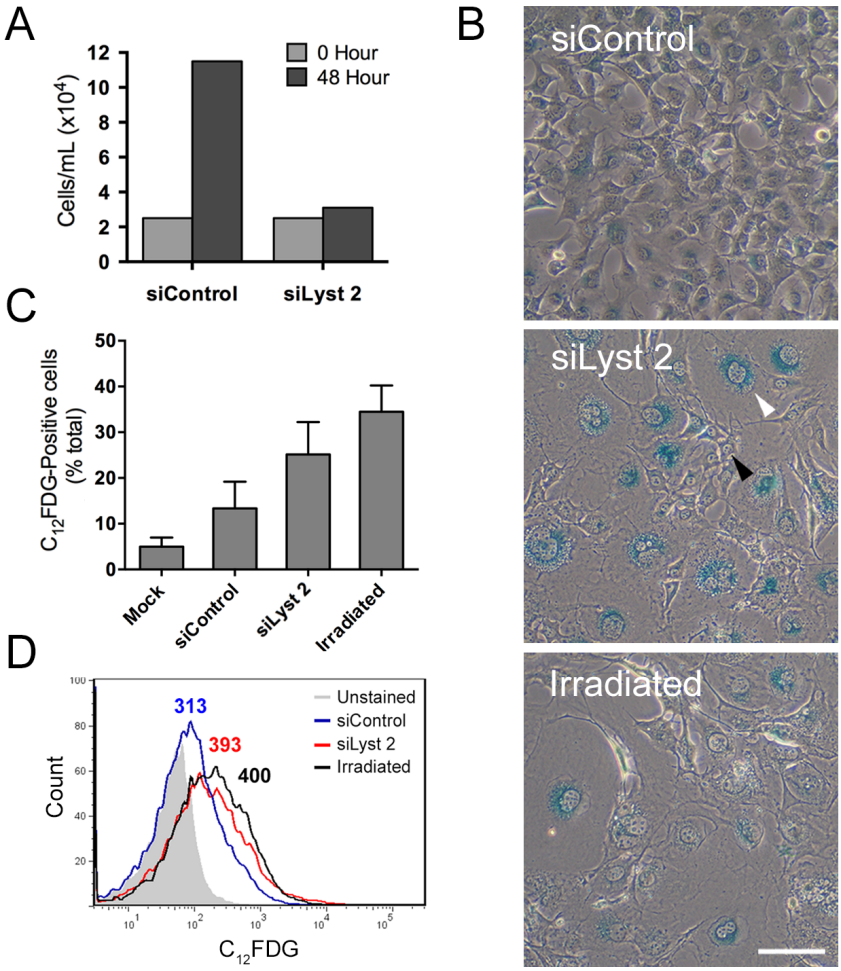

Figure 4.7. Growth arrest and SA-*β*-Gal activity in *siLyst 2*-transfected 3T3-J2 fibroblasts

3T3-J2 cells transfected with 50 nM *siControl* or *siLyst* were assessed for proliferation and SA-*β*-Gal activity after 48 hours. A) Cell counts revealed proliferation was markedly reduced in *siLyst* 2 cells compared to *siControl* cells. B) SA-*β*-Gal activity was detected using X-gal in fixed transfected and *γ*-irradiated cells. *siControl* cells (*left*) have typical morphology and low or no SA-*β*-Gal activity. In contrast, *siLyst* 2 cells (*middle*) are enlarged, flattened and have high SA-*β*-Gal activity (*white arrow*), similar to radiation-induced senescent cells (*right*). Some *siLyst* 2 cells were not enlarged and had low SA-*β*-Gal activity (*black arrow*). Scale bar = 50 µm. C) SA-*β*-Gal activity was measured in live cells using C_{12}FDG and analysed by flow cytometry. The percentage of cells positive for SA-*β*-Gal activity was greater in the *siLyst* 2 population compared to *siControl* or mock-transfected cells. The means and SDs from two independent experiments are given. D) C_{12}FDG fluorescence histograms show the relative level of SA-*β*-Gal activity. The values above the peaks represent the median fluorescence intensity of the respective populations. The grey histogram indicates the autofluorescence of a culture treated with bafilomycin A1 only.

Therefore, an alternative flow cytometric method was adopted to detect SA-*β*-Gal activity in substantially larger sample sizes. 5-dodecanoylamino-fluorescein di-*β*-D-galactopyranoside (C_{12}FDG) is a cell permeable substrate for SA-*β*-Gal that when hydrolysed, becomes membrane-impermeable and emits fluorescence upon excitation at 500-510 nm (Noppe et al., 2009). In this assay, the V-ATPase inhibitor bafilomycin A1 was used to raise pH to 6.0, prior to staining with C_{12}FDG. Both transfection reagent alone and control siRNA caused a modest induction of SA-*β*-Gal activity in 3T3-J2 fibroblasts (5.0 ± 2.0% and 13.3 ± 5.9% respectively, Figure 4.7C). SA-*β*-Gal activity was further increased in *siLyst* 2 cells (25.1 ± 7.1), but was maximal in the irradiated cells (34.5 ± 5.8%). Treatment with bafilomycin alone did not alter cell viability (data not shown). When considered together with Figure 4.4, these results suggest that *Lyst*-silencing not only induces an enlarged lysosomal phenotype consistent with CHS/*beige*, but also induces senescent-like changes in 3T3-J2 fibroblasts.

4.5 *siLyst 2* Transfection Results in a Failure to Initiate Cytokinesis, Aberrant Nuclei and Cell Enlargement

Lyst-silenced cells were found to be positive for three markers of senescence: increased size, arrested growth and expression of SA-*β*-Gal. No direct role for LYST in the regulation of cell cycle control is documented and so the underlying mechanism responsible for the senescent like changes was unclear. It was noted that the enlarged SA-*β*-Gal expressing cells frequently contained multiple or abnormal nuclei. Binucleated cells were apparent 24 hours post-transfection with *siLyst* 2 (Figure 4.2D). At later time points, gross nuclear abnormalities, similar to those seen in irradiated cells, were observed (Figure 4.8A). Some of the unusual nuclear morphologies observed are represented by confocal sections of DAPI-stained *siLyst 2*-silenced cells in Figure 4.8B. Large invaginations gave the appearance of multi-lobed nuclei and cells often contained micronuclei (Figure 4.8B, *arrowhead*) or more than one nuclei. 72 hours post-transfection, the *siLyst* 2 population contained significantly more cells with aberrant nuclei than the *siControl* population (45.6% and 5.8% respectively)

This was almost identical to the number observed in irradiated cells (45.2%; Figure 4.8C).

The finding that *Lyst*-silenced cells appeared senescent and contained abnormal nuclei in the absence of stress-inducing or DNA-damaging stimuli was puzzling and the underlying cause of these nuclear abnormalities was unclear. Kwak et al., 1999 reported that LvsA, the *Dictyostelium* BEACH protein related to LYST, is required for proper cytokinesis. They observed that LvsA mutants enter cytokinesis normally but eventually fail in their division attempt, becoming large and multinucleate. To investigate whether a similar cytokinesis failure occurred in *siLyst* 2-transfected cells, time-lapse microscopy of live fibroblasts was performed to monitor cell division. From as early as seven hours post-transfection, cells with normal oval nuclei were observed to round up and remained rounded, for between 40-60 minutes, before reattaching and spreading out (Figure 4.9A and B). Abnormal nuclear morphologies and nuclear number appeared immediately after the cells reattached. Continuous imaging of the cells that contained abnormal nuclei following a prolonged rounding event, revealed a gradual increase in cell size over many hours that eventually led to the characteristic large and flattened morphology of senescence (Figure 4.9C). In contrast, cells transfected with *siControl* rounded and initiated division within 15-30 minutes (Figure 4.9D).

Cell rounding is a common feature of cell division and apoptosis. On the basis that *siLyst 2*-transfected cells are growth arrested and did not apoptose after rounding, it was presumed that cell rounding was the result of mitotic events that failed to produce two daughter cells. Occasionally apoptosis did occur after some rounding events and probably accounts for the slight increase in 7-AAD-positive cells in the viability assay (Figure 4.3). In contrast to LvsA mutants, which formed two distinct daughter cells prior to the eventual relapse into one body (Kwak et al., 1999), *siLyst 2*-silenced cells rounded and relapsed, without the obvious initiation of cytokinesis.

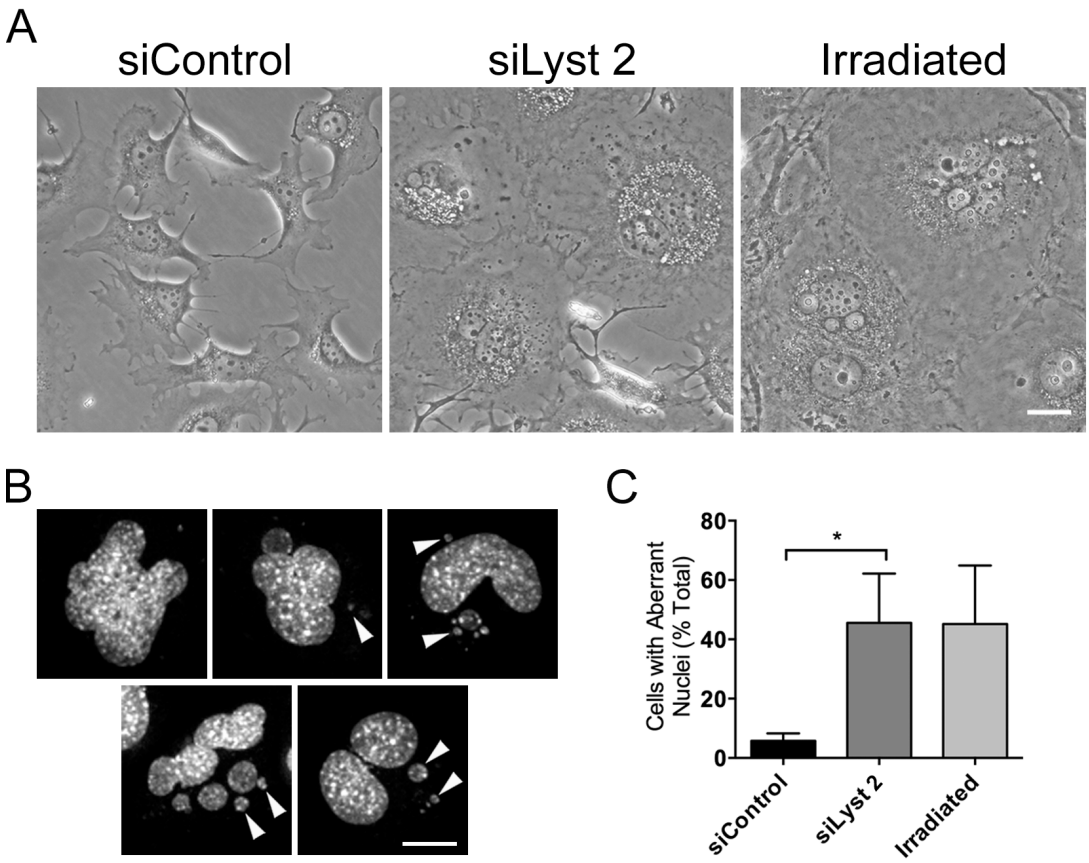

Figure 4.8. Nuclear defects in *siLyst* 2-transfected cells

A) Phase contrast images of *siControl* cells with normal oval nuclei (*left*). In contrast, the large flattened cells of the *siLyst* 2-silenced population (*middle*) had unusual nuclear morphologies and were often binucleated. Similar nuclear morphologies were present in the *γ*-irradiated senescent population (*right*). B) Representative confocal images of DAPI-stained nuclei from five *siLyst* 2-silenced cells. Several large invaginations gave a multi-lobed appearance and cells were often bi- or multi-nucleated. Micronuclei were common (*arrowheads*). C) The number of cells with aberrant nuclear morphology and number, 72 hours post-transfection was expressed as a percentage of the total number of cells. More than 450 cells per sample were scored from three independent experiments. The means and SDs are given. *: P=0.0147. Scale bars = 20 μm.

When considered together with the results in Section 4.4, these findings suggest that nuclear abnormalities formed during mitosis cause failure to initiate cytokinesis and senescence-like changes in *siLyst* 2-transfected cells.However, an alternative trigger for cell rounding in *siLyst* 2-transfected cells cannot be dismissed from these observations alone.

4.6 Off-Target Binding of *siLyst* 2 and Further siRNA Validation

One disadvantage of siRNA-mediated gene silencing is the occasional silencing of genes other than the intended target. Such off-target effects arise through sequence identity of the siRNA strands to non-target mRNA. However, such off-target effects are expected to be minimal with pre-designed sequences that have undergone rigorous validation by the manufacturer. Nonetheless, as only one out of the four siRNA sequences targeted against *Lyst* mRNA resulted in the large lysosomal- and senescent-like- combined phenotypes, it was unknown whether these were a direct consequence of *Lyst*-silencing or due to off-target effects of the siRNA. Therefore, a BLAST search (www.ncbi.nlm.nih.gov/BLAST) was performed on the *siLyst* 2 sequence using the mouse RNA sequence database, to identify potential sequence matches other than Lyst. All 19 nucleotides of the *siLyst* 2 sequence matched a region of transcription factor 7 like 1 (*Tcf7l1*) mRNA (*E* value = 0.001) and 18/19 nucleotides matched a region of *Tcf7l2* mRNA (*E* value = 0.023). qRT-PCR analysis confirmed *siLyst 2* targeted *Tcf7l1* and *Tcf7l2* mRNA for degradation (Figure 4.10). Compared to *siControl*-transfected cells, *Tcf7l1* and *Tcf7l2* mRNAs were reduced by 92.6% and 90.4% respectively, with 50 nM *siLyst 2*. Reducing the concentration of siRNA transfected into cells can reduce the likelihood of off-target effects, however even at 1 nM *siLyst 2,* mRNA expressions of *Tcf7l1* and *Tcf7l2* were reduced by at least 70% (data not shown).

TCF7L1 and TCF7L2 (also known as TCF3 and TCF4) are members of the T cell factor/enhanced lymphoid factor family of transcription factors that function downstream of *β*-catenin in the Wnt (wingless and Int) signalling pathway and are predominantly expressed in epithelial tissues (Korinek et al., 1998). TCF7L1 silencing in breast cancer epithelial cell lines reduced proliferation and induced a flattened cell morphology (Slyper et al., 2012), therefore, it is possible that the senescent-like phenotype in *siLyst* 2-transfected cells is wholly or in part due to reduced *Tcf7l1/2* expression, as a consequence of off-target binding of the siRNA.

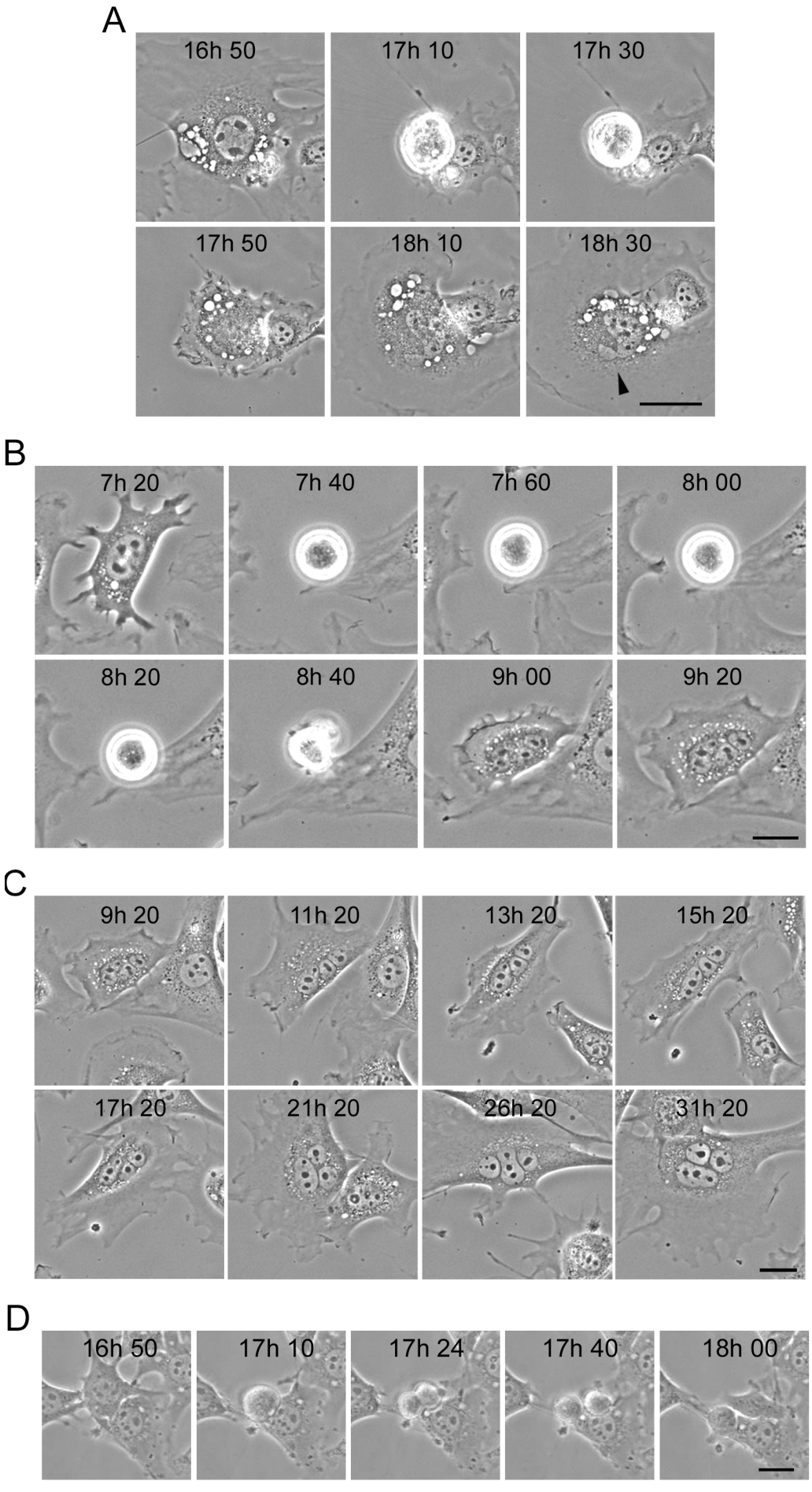
A
16h 50
17h 10
17h 30
17h 50
18h 10
18h 30
B
7h 20
7h 40
7h 60
8h 00
8h 20
8h 40
9h 00
9h 20
C
9h 20
11h 20
13h 20
15h 20
17h 20
21h 20
26h 20
31h 20
D
16h 50
17h 10
17h 24
17h 40
18h 00

Figure 4.9. Failure to initiate cytokinesis precedes formation of aberrant nuclei and cell enlargement in *siLyst* 2-transfected cells

3T3-J2 fibroblasts seeded into glass-bottomed dishes were transfected with 50 nM *siLyst* 2 (*A*-*C*) or *siControl* (*C*). Phase contrast images were acquired every 1 minute. Time after transfection accompanies each frame and is indicated in hours and minutes. A) A cell with a typical oval nucleus rounds up but fails to divide and eventually reattaches and spreads. Following this, the nucleus has become irregular and invaginated (*arrowhead*). B) A cell containing a single oval nucleus rounds up and persists in this state for over an hour without dividing. The cell contains three nuclei after eventually reattaching. C) Continuous observation of the cell featured in *B,* revealing a gradual cell enlargement to almost double the original cell size, over a 22 hour period. D) An *siControl* cell divides shortly after rounding up and produces two daughter cells. Scale bars = 20 μm.

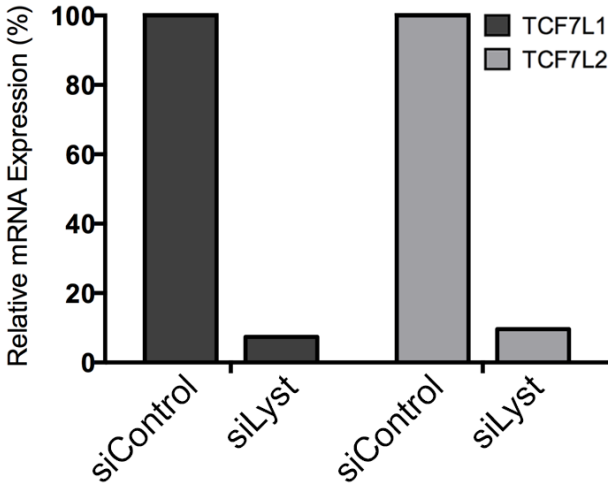

Figure 4.10. Reduced expression of *Tcf7l1* and *Tcf7l2* mRNA transcripts in *siLyst* 2-transfected cells

Real-time qRT-PCR measurements of the relative expression levels of *Tcf7l1* and *Tcf7l2* mRNA in 3T3-J2 fibroblasts transfected with 50 nM *siLyst* 2 or *siControl*, 48 hours post-transfection. Values are expressed as a percentage of the *Tcf7l1* and *Tcf7l2* mRNA levels in the *siControl*-transfected population.

Since *siLyst* 2 was the only sequence out of four to induce lysosomal enlargement and aberrant nuclei, a further four individual siRNA sequences (*siLyst* 5, -6, -7 and -8) targeted against *Lyst* were purchased from an alternative manufacturer and assessed for their ability to induce these phenotypes. mRNA transcript levels were quantified by qRT-PCR and phase contrast microscopy was used to monitor the appearance of large refractive vesicles and irregular nuclear number or morphology. All four *siLyst* sequences reduced *Lyst* mRNA transcripts by at least 60% when measured by qRT-PCR 48 hours post-transfection (Figure 4.11A). However, despite the appreciable level of silencing, the percentage of cells that displayed an enlarged vesicle phenotype was relatively low. Transfection with *siLyst* 5 and *siLyst* 8 stimulated the greatest reduction in *Lyst* mRNA (89.1% and 79.2% respectively) and the greatest induction of vesicles (Figure 4.11B). However, only ~30% of cells were vesiculated in either population after 48 hours, compared with 6.5 ± 5.8% in the control. No difference in the number of vesiculated cells was observed between *siLyst* 6 and *siControl* populations and only a 12.6% increase in vesiculated cells in *siLyst* 7-transfected cells relative to the control. The large cytoplasmic vacuole-like vesicles observed in *siLyst* 5, -7 and -8 populations were indistinguishable from those observed in *siLyst* 2-transfected cells (Figure 4.11C), suggesting they are of a similar morphology. The level of silencing by *siLyst* 5 and -8 was comparable to that generated by *siLyst* 2, yet induction of a vesicle phenotype after 48 hours was not as pronounced (comparison of Figure 4.2 with Figure 4.11).

Overall, eight individually transfected siRNA sequences were evaluated for their *Lyst* silencing capacity. All sequences reduced *Lyst* mRNA levels by varying degrees (34% - 83%) but only four out of the eight siRNAs tested induced a measureable vesicle phenotype. Only when mRNA expression was decreased by at least 70% did the population contain cells that exhibited large vesicles. The extent of mRNA reduction roughly correlated with the percentage of vesiculated cells and the sequence that gave the greatest reduction in *Lyst* mRNA (*siLyst 2*) induced the greatest number of vesiculated cells.

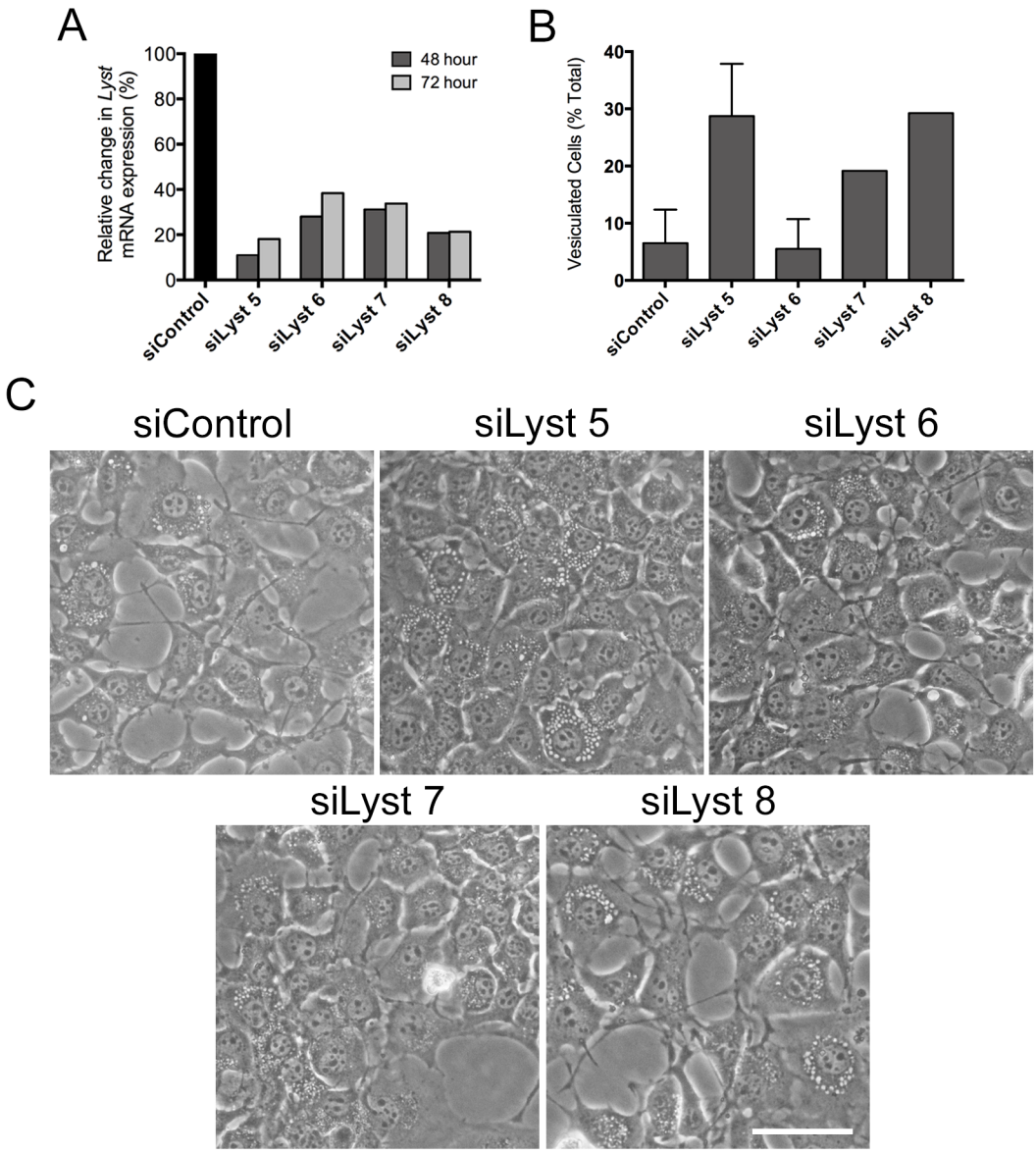

Figure 4.11. *Lyst* mRNA expression and vesiculation analysis of additional *siLyst* sequences

3T3-J2 fibroblasts were transfected with 50 nM *siControl* or *siLyst* sequences 5–8. A) Real-time qRT-PCR measurements of *Lyst* mRNA 48 and 72 hours post-transfection. Values are expressed as a percentage of mRNA level in cells transfected with *siControl*. B) The percentage of cells exhibiting the vesiculated phenotype after 48 hours was calculated from phase contrast images of cells transfected as described in *A.* Cells were deemed to be vesiculated if they contained at least four enlarged vesicles (>2 μm^2). At least 200 cells per siRNA treatment were counted in each experiment. The means and SDs from two independent experiments are given. Bars with no SD are from one experiment only. C) Phase contrast images of 3T3-J2 transfected with 50 nM *Control* or *Lyst* siRNA, 48 hours post-transfection. Original magnification: 20x.

An aberrant nuclear phenotype was not observed in vesiculated cells transfected with *siLyst* 5, -7 or -8 (data not shown), nor did they acquire a senescent morphology. From these observations it seems unlikely that *Lyst* silencing is responsible for the nuclear abnormalities in *siLyst* 2-transfected cells, and these abnormalities may be due to off-target silencing of *Tcf7l1 and Tcf7l2*. However, no other siRNAs decreased *Lyst* mRNA expression to the extent of *siLyst* 2, or induced as many vesiculated cells. Consequently, from these studies alone it cannot be concluded whether silencing of *Lyst* or *Tcf7l1* disrupts nuclear morphology during mitosis. Unfortunately, due to time constraints, further study of the siRNA sequences was not continued.

4.7 Discussion

The aim of the present study was to utilise the method of siRNA-mediated gene silencing to explore the function of Lyst. Silencing of *Lyst* has not been reported elsewhere and so carried the potential to reveal novel phenotypes associated with Lyst-deficiency and to pinpoint molecular pathways in which Lyst functions. The key finding of this chapter is that siRNA-mediated *Lyst* silencing in cultured mouse fibroblasts successfully recapitulates the major aspect of the CHS/*beige* phenotype: formation of abnormally large and clustered lysosomes.

In the absence of a Lyst antibody, effective silencing was determined from the level of *Lyst* mRNA present in cells after transfection, and the appearance of an enlarged vesicle phenotype. The ability of individual *Lyst* siRNAs to degrade target mRNA varied greatly and may depend on the intracellular stability of the molecule and duration of the siRNA-RISC-mRNA complex formed. Efficient but short-lived siRNA-RISC-mRNA complex formation might explain why some of the siRNA molecules effectively decreased mRNA but induced low or no vesiculation when quantified at the same time-point. Existing Lyst protein might outlive the duration of mRNA degradation and thus maintain normal vesicle homeostasis, even when mRNA expression is low. Cell doubling time can also affect the duration of silencing: silencing in non-dividing cells is prolonged compared to rapidly dividing ones as the siRNA becomes diluted during divisions (Bartlett and

Davis, 2006). This is noteworthy because the siRNA which induced the greatest number of vesiculated cells was also linked with reduced proliferation from mitotic failure as early as seven hours post-transfection. mRNA silencing in these non-dividing cells would therefore be prolonged compared to normally proliferating cells transfected with other *Lyst* siRNA molecules. Lysosomal enlargement might only occur when Lyst protein is reduced below a threshold, or a fraction of its pre-transfection value. The abundance or turnover of Lyst protein is not known, however observations in this study indicate that Lyst protein remains stable and functional for a period exceeding the doubling time of 3T3-J2 cells (~18-24 hours). This suggests that siRNA dilution occurring through cell division would result in an insufficient level of mRNA silencing and thus a lack of lysosomal enlargement in normally proliferating cells. Repeat transfections of the siRNAs that gave excellent knockdown, but low or no phenotype, should prolong gene silencing and may stimulate vesiculation at later time points. Further optimisation of the conditions required for maximal silencing of each individual sequence, or pooling of sequences, may enhance the phenotypic effect also.

I report for the first time that siRNA-mediated silencing of *Lyst* in a murine fibroblast cell line induces an enlarged lysosomal phenotype similar to that of CHS/*beige* fibroblasts (Burkhardt et al., 1993, Mohlig et al., 2007, Huynh et al., 2004 and observations in Chapter 3). One of the novel findings that emerged from the previous chapter was that of enhanced constitutive autophagy of *beige* fibroblasts. Evaluation of autophagy in *Lyst*-silenced 3T3-J2 fibroblasts yielded a similar result: the number of LC3B puncta in *siLyst*-transfected cells was greater than in control-transfected cells. However, these data are limited to a small number of independent experiments and cannot alone conclude the effect of *Lyst*-deficiency on the autophagic process. Nonetheless, in view of the fact that other BEACH family members are implicated in the autophagic pathway (Simonsen et al., 2004, Lopez-Herrera et al., 2012, Rahman et al., 2012), these data provide sufficient motive to carefully examine the autophagic pathway in CHS/*beige* which has previously been overlooked.

The siRNA sequence that induced the greatest number of vesiculated cells also inhibited proliferation and induced significant cell enlargement; both of which are common features of senescence, prompting further characterisation. The arrested growth of cells transfected with siRNA 2 appears to be the result of mitotic failure as early as seven hours post-transfection. Live-cell time-lapse imaging indicated that after rounding up, cells failed to ingress and the formation of two distinct daughter cells was not observed, suggesting that cytokinesis was not initiated. Following the failed division events, cells became bi-/multi-nucleated, contained multi-lobed-nuclei or micronuclei and later adopted a senescent morphology. Cells were strikingly similar in morphology to *γ*-irradiated senescent cells and positive for three hallmarks of senescence: large and flat morphology, arrested growth and expression SA-β-Gal activity. However, it was identified that the sequence of *siLyst* 2 could induce off-target effects in the Tcf7l1/2 genes and without further experiments, it cannot be ascertained whether the observations are caused by depletion of Lyst or Tcf7l1/2, as mRNA levels of both were greatly suppressed by *siLyst* 2. In the absence of specific antibodies, it is not known whether a corresponding decrease in Tcf7l1/2 protein was achieved. TCF7L1 and TCF7L2 are downstream effectors in the Wnt/β-catenin signalling pathway that regulates proliferation and differentiation. Recent reports show that siRNA-mediated depletion of *TCF7L1* induces growth arrest concurrent with flattened cell morphology in breast cancer epithelial cells (Slyper et al., 2012) and silencing of TCF7L2 induces apoptosis in colon cancer cells (Xie et al., 2012). Based on these reports it is tempting to conclude that Tcf7l1/2 deficiency is responsible for mitotic defects in *siLyst* 2-transfected cells. However, in the studies by Slyper and colleagues (2012), *TCF7L1*-silencing did not induce formation of aberrant nuclei and apoptosis was only slightly elevated in *siLyst* 2-transfected cells, suggesting an additional or alternative Lyst-mediated mechanism is at play.

It is worth noting that several proteins identified as Lyst-binding partners by Tchernev et al., 2002 are implicated in cell cycle regulation and mitosis: 14-3-3τ, centrobin and CENPJ (Wang et al., 2010, Jeffery et al., 2010, Zou et al., 2005, McIntyre et al., 2012). Furthermore, the *Dictyostelium* BEACH

protein LvsA is required for cytokinesis (Kwak et al., 1999). Therefore, the possibility that Lyst-deficiency is responsible for nuclear defects cannot be ruled out. The nuclear defects in *siLyst 2*-transfected cells were remarkably similar to those observed in *γ*-irradiated senescent cells. Abnormal nuclear morphologies of senescent cells in response to ionising radiation are well documented (Hayflick, 1965, Raj and Mahajan, 2011). In mammalian cells, duplication of centrosomes is central to the formation of bipolar spindles that enable chromosome segregation during mitosis. The unusual assembly of multipolar spindles in cells with abnormal centrosomes causes an unbalanced segregation of chromosomes and is one proposed cause for multinucleation in *γ*-irradiated tumour cell lines (Sato et al., 2000). Binding between LYST and a core centrosome protein, centrobin, was demonstrated by Tchernev and colleagues (2002). Centrobin is required for centriole duplication and proper cytokinesis during mitosis (Zou et al., 2005). Depletion of centrobin disrupts centriole duplication, causing lengthy mitoses, cytokinesis failure and formation of bi- and multi-nucleated cells (Zou et al., 2005). Centrobin is also required for the attachment of centrosomes to the mitotic spindle, as centrobin-depleted cells have unfocussed spindle poles that cause spindle assembly checkpoint activation and metaphase arrest (Jeffery et al., 2010). These cells also exhibit reduced stability in the attachment of chromosomes to kinetochores, which is known to generate lagging chromosomes during anaphase (Thompson and Compton, 2011). These become separately encapsulated by the nuclear envelope, forming micronuclei, a common feature in *siLyst* 2-transfected cells. Similarly, CENPJ plays a key structural role in maintaining normal centriole duplication during the cell cycle and depletion of human or mouse CENPJ induces centrosome and spindle abnormalities (Cho et al., 2006, McIntyre et al., 2012). Furthermore, siRNA-mediated CENPJ silencing leads to apoptosis of cells arrested in mitosis, and lagging chromosomes were frequently observed in cells with multipolar spindles (Cho et al., 2006).

siLyst 2-transfected cells failed to form daughter cells during mitosis and this may be because the cells failed to initiate cytokinesis. Early stages of cytokinesis involve positioning of the division plane and formation of an actomyosin ring. Contraction of the ring, via attachment to the plasma

membrane, results in ingression and formation of a cleavage furrow that partitions the cytoplasm between the two cells. The small GTPase RhoA is recruited to the division plane and functions as a master regulator of cytoskeletal reorganisation, mediating contraction of the actomyosin ring and ingression of the cleavage furrow (Fededa and Gerlich, 2012). The role of PtdIns(4,5)P_2 in cytokinesis is well documented and thought to mediate recruitment of RhoA, the attachment of the contractile actomyosin ring to the plasma membrane and the regulation of cytoskeletal remodelling during furrow ingression (Emoto et al., 2005). A recent study using super-resolution microscopy demonstrated that SM is required for localisation of phosphatidylinositol 4-phosphate 5-kinase beta (PIP5Kβ) and PtdIns(4,5)P_2 production at the cleavage furrow (Abe et al., 2012). Ablating SM levels by adding exogenous SMase resulted in lost accumulation of both PtdIns(4,5)P_2 and RhoA at the furrow, cytokinesis failure and formation of binucleated cells. PtdIns(4,5)P_2 is mislocalised in *beige* fibroblasts (Ward et al., 2003) and SM levels are significantly decreased compared to normal fibroblasts through enhanced SMase activity (Tanabe et al., 2000). A similarly elevated SMase activity in *siLyst* 2-transfected 3T3-J2 cells might inhibit PtdIns(4,5)P_2 accumulation at the furrow and block cytokinesis initiation. Indeed, no ingression furrow was observed in *siLyst* 2-transfected cells which entered mitosis but failed to divide. Furthermore, studies in mammals and yeast suggest both calmodulin and PKC generate a positive feedback loop for PtdIns(4,5)P_2 synthesis at the cleavage furrow. PKC activity is down-regulated in *beige* fibroblasts (Tanabe et al., 2000) and calmodulin is a binding partner of Lyst (Tchernev et al., 2002). Treatment of HeLa cells with a Ca^{2+}/calmodulin inhibitor prevents the formation and ingression of the cleavage furrow (Yu et al., 2004), while interfering with PKCβ causes microtubule disorganisation and cytokinesis failure (Chen et al., 2004). PKCβ expression is decreased in *beige* cells (Chapter 3.5), thus, mitotic failure in *Lyst*-silenced cells could be due loss of PKC and calmodulin activity.

How or why a protein whose central function lies in lysosomal trafficking should interact with key regulators of centrosome and spindle maintenance is puzzling. However, if Lyst is required for proper centrobin or Cenpj

function, the formation of multi- and micro-nuclei in Lyst-depleted cells is not surprising. One mechanism by which LYST might regulate CENPJ function is to mediate an interaction between CENPJ and its activating proteins polo-like kinase (PLK) 2 and PLK4. Phosphorylation of CENPJ by these kinases is essential for centrosome duplication during the cell cycle (Chang et al., 2010, Habedanck et al., 2005). Failure to phosphorylate CENPJ in the absence of LYST might induce centrosome and spindle abnormalities and could explain the aberrant nuclear morphologies in *siLyst 2*-silenced cells. Time-lapse studies (Figure 4.9) revealed a variety of nuclear abnormalities in *siLyst 2*-transfected cells. It is likely that *siLyst* 2 cells carry multiple defects, for example, in both mitosis and checkpoint control. This is because cells containing gross defects that would normally initiate apoptosis or mitotic catastrophe, escaped apoptosis and instead became senescent. Lyst interacts with the checkpoint protein 14-3-3τ (Tchernev et al., 2002). Wang and colleagues reported that 14-3-3τ upregulation in MCF7 breast cancer cells mediates cell survival by targeting p21 for proteasomal degradation, allowing G_1/S entry (Wang et al., 2004). Furthermore, siRNA depletion of 14-3-3τ induces G1 arrest and inhibits MCF7 proliferation. A similar growth arrest was observed in *siLyst* 2-transfected cells. This raises the intriguing possibility that Lyst scaffolds a 14-3-3τ-p21 interaction in 3T3-J2 cells, permitting proliferation even in the presence of genotoxic stresses such as gross nuclear defects. Loss of this interaction during silencing could promote p21 survival and initiate cell-cycle arrest. Determining the levels of 14-3-3τ and p21 protein in senescent cells of the *siLyst 2*-transfected population would help to determine whether this is the case.

Aberrant nuclear shape can often arise from defects in the nuclear lamina, microtubules or lipid synthesis. Lamin A and B are components of the nuclear lamina and involved in the breakdown and reformation of the nuclear envelope around the separated chromosome bundles following segregation, to form two separate nuclei (Webster et al., 2009). Mutations in lamin A that result in a constitutively lipidated (farnesylated) protein cause a variety of abnormal nuclear morphologies in the cells of patients with the premature ageing syndrome Hutchinson-Gilford progeria syndrome (Glynn and Glover, 2005). On the basis that 14-3-3τ is reported to bind both lamin A/C and lamin

B1 (Meek et al., 2004), it is conceivable that nuclear lamina defects could be the root cause of the multitude of nuclear morphologies observed in *Lyst*-silenced cells that are strikingly similar to those of Hutchinson-Gilford progeria syndrome.

The ultimate goal of this study was to measure the effect of siRNA-mediated *Lyst* silencing in cells with secretory lysosomes such as NK cells, and to identify other proteins that might function in the same secretory pathway as Lyst. Regrettably, due to the lengthy validation of the *Lyst*-silenced phenotype, the investigation did not get this far. However, *Lyst* silencing did mimic the major aspect of CHS/*beige*, and could be used as an alternative system in which to study CHS/*beige*. The growth arrest of *siLyst* 2-silenced cells may be the result of a combined effect of both a mitotic defect and checkpoint dysregulation. Pinpointing whether this is due to loss of Lyst, Tcf7l1/2 or both, could yield some very interesting information on the function of Lyst and may identify a novel and surprising role for Lyst in mitosis and cell cycle control. However, at present, it is difficult to reconcile the growth arrest of *siLyst* 2-silenced cells with the viability of CHS patients and the *beige* mouse.

For the study of NK cell secretory lysosomes, another approach was sought. NK cells are notoriously difficult to transfect, therefore inhibitors of protein function are useful for mimicking the effects of RNAi in these cells. In the absence of an inhibitor of LYST, attention was turned to the PIKfyve inhibitor YM201636 which, in fibroblasts, induces grossly enlarged vesicles, a superficially similar phenotype of CHS/*beige*.

Chapter 5
The Inositol Lipid Kinase PIKfyve is Required for the Exocytosis of Natural Killer Cell Lytic Granules

5.1 Introduction

NK cells participate in the clearance of virus-infected cells and cancer cells as part of the innate immune system. The ability to exocytose preformed lytic granules (specialised secretory lysosomes) in response to these stimuli is critical to NK cell immune function (Orange and Ballas, 2006). Granule secretion is a tightly-regulated process, the mechanisms of which are not fully understood. Mutation of genes encoding proteins involved in the granule secretory pathway impair NK cell function and underlie many rare and severe immunological diseases such as CHS, Griscelli syndrome and HPS-2. Indeed, the giant lysosome phenotype associated with CHS/*beige* was the first mutation shown to affect NK cell function (Roder and Duwe, 1979, Katz et al., 1982). Much work has focussed on the protein exocytic machinery components such as SNARE and Munc family members. In addition to these, the importance of lipids, particularly the inter-conversion of PIs, in regulated exocytosis is becoming increasingly evident. Recently, a role for PIKfyve in regulating the exocytosis of secretory vesicles was identified (Ikonomov et al., 2007, Osborne et al., 2008, Ikonomov et al., 2009b). Interestingly, inhibition of PIKfyve activity induces an enlarged vesicle phenotype that appears similar to that observed with LYST-deficiency. The hypothesis was that PIKfyve inhibition would induce a giant vesicle phenotype in NK cells and impair granule exocytosis similar to the effects of LYST mutations. The apparent similarity between the CHS/*beige* and PIKfyve phenotypes might also reveal more about the mechanism by which LYST functions. To test this hypothesis, a pharmacological inhibitor of PIKfyve, YM201636, was used.

5.2 PIKfyve Inhibition Induces Endosome Enlargement in Fibroblasts

PtdIns(3,5)P_2 regulates many intracellular processes including endosome-to-Golgi retrograde trafficking, vesicle homeostasis and glucose transport (Rutherford et al., 2006, Jefferies et al., 2008, Ikonomov et al., 2002b). PIKfyve catalyses the phosphorylation of PtdIns(3)P to PtdIns(3,5)P_2 and is the sole enzyme responsible for PtdIns(3,5)P_2 production in the brain, heart, lung, kidney, thymus and spleen (Zolov et al., 2012). PIKfyve is implicated in maintaining endosome fusion and fission events. Studies show that reduction of PtdIns(3,5)P_2 levels by siRNA-mediated PIKfyve silencing or the expression of inactive PIKfyve mutants causes the formation of enlarged cytoplasmic vesicles (Ikonomov et al., 2002a). Short-term (20 minutes to two hours) treatment of cells with the small molecule inhibitor of PIKfyve, YM201636, induces vesicle enlargement in many cell types (Jefferies et al., 2008, Osborne et al., 2008).

The activity of the inhibitor was first tested by analysing its ability to induce the giant vesicle phenotype in 3T3-J2 fibroblasts. In agreement with previous reports, YM201636 induced the formation of large refractive cytoplasmic vesicles in 3T3-J2 cells as analysed by light microscopy, whereas an equivalent volume of vehicle alone (DMSO) did not (Figure 5.1A, *bottom panel*). The vesicle phenotype induced by YM201636 was indeed similar to that of *beige* fibroblasts (Figure 5.1A, *top panel*). To quantify this phenotype, cells were scored if they contained four or more enlarged vesicles (>2 μm^2). After two hours of treatment, 39.2% of cells treated with YM201636 contained enlarged vesicles, compared to only 1.8% of cells treated with DMSO (Figure 5.1B). The effect of PIKfyve inhibition was reversible and vesicles returned to normal size upon withdrawal of YM201636, with similar kinetics to the duration of inhibition (see *Appendix*) in agreement with previous observations (Jefferies et al., 2008).

The origin of the enlarged vesicles in PIKfyve-inhibited fibroblasts was then analysed and compared to the fibroblasts derived from *beige* mice.

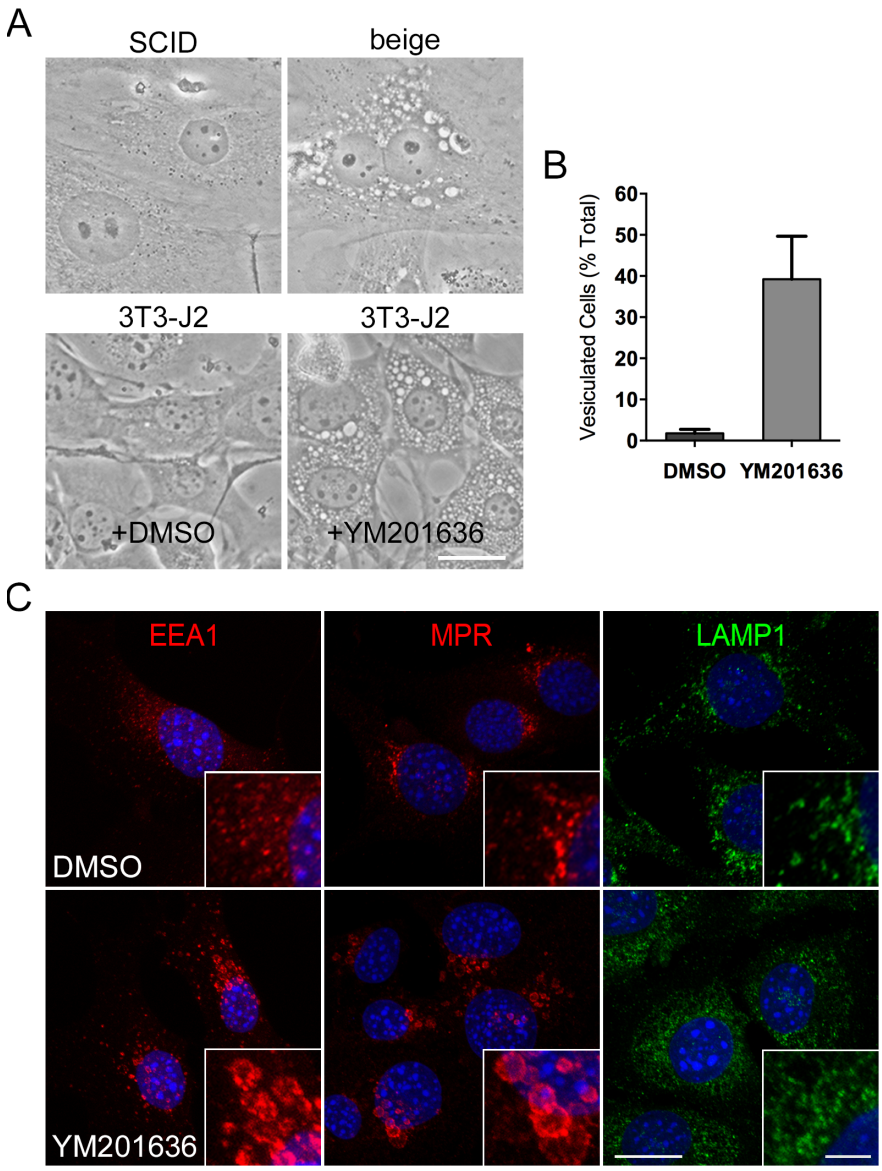

Figure 5.1. YM201636 induces enlarged endosomes in 3T3-J2 cells

A) Phase contrast images of untreated *beige* and control *SCID* fibroblasts (*top panel*) or 3T3-J2 cells treated with DMSO or 800 nM YM201636 for two hours (*bottom panel*). B) The percentage of cells with enlarged vesicles was determined from phase contrast images of DMSO- or YM201636- (800 nM) treated 3T3-J2 cells after 2 hours. Cells were scored if they contained at least four enlarged vesicles (>2 μm^2). At least 100 cells were scored per treatment, per experiment. The means and SDs from three independent experiments are shown. C) 3T3-J2 cells treated with YM201636 (800 nM) or DMSO for two hours were immunofluorescently labelled with anti-EEA1-, anti-CI-MPR- or anti-LAMP1- antibodies and analysed using a confocal microscope. Cells were counterstained with DAPI (blue) to visualise the nucleus. Images are maximum intensity projections of confocal z-stacks. Scale bar: *A*, 20 µm; *C*, *main images,* 20 µm, *insets* = 5 µm.

Immunofluorescence microscopy revealed that the lysosomal marker LAMP1 showed a typical punctate distribution in cells treated with 800 nM YM201636, that was indistinguishable from that found in cells treated with DMSO alone (Figure 5.1C). Conversely, the early endosomal marker EEA1 and the late lysosomal marker CI-MPR both revealed a distinct localisation to the enlarged vesicles after inhibitor treatment, but not with DMSO (Figure 5.1C). These results indicate that inhibition of PIKfyve activity disrupts endosomes but not lysosomes in 3T3-J2 fibroblasts. This agrees with previous findings (Ikonomov et al., 2001, Ikonomov et al., 2003a, Jefferies et al., 2008, Osborne et al., 2008). To the best of my knowledge, this is the first direct comparison between the giant vesicle phenotypes induced by LYST and PIKfyve inhibition. These results indicate that although the phenotypes are superficially similar, disruption of PIKfyve and LYST activity affects the integrity of distinct endocytic compartments, namely endosomes and lysosomes, respectively.

5.3 PIKfyve Inhibition Impairs NK Cell Lytic Granule Exocytosis But Not Cytokine Secretion

The original hypothesis was that the giant vesicles of PIKfyve inhibited cells would represent a phenocopy of the LYST mutation and as a consequence, NK cell granule exocytosis would be impaired following PIKfyve inhibition. However, the findings above indicate that PIKfyve and LYST affect different compartments and hence PIKfyve inhibition might not affect NK cell granule exocytosis. Therefore, functional studies of human NK cells treated with the PIKfyve inhibitor were performed.

Full NK cell cytotoxic potential is dependent on the prior-activation of cells with cytokines such as IL-2 and IL-15 (Meade et al., 2009). Like primary NK cells, the majority of human NK cell lines require exogenous IL-2 for prolonged culture.

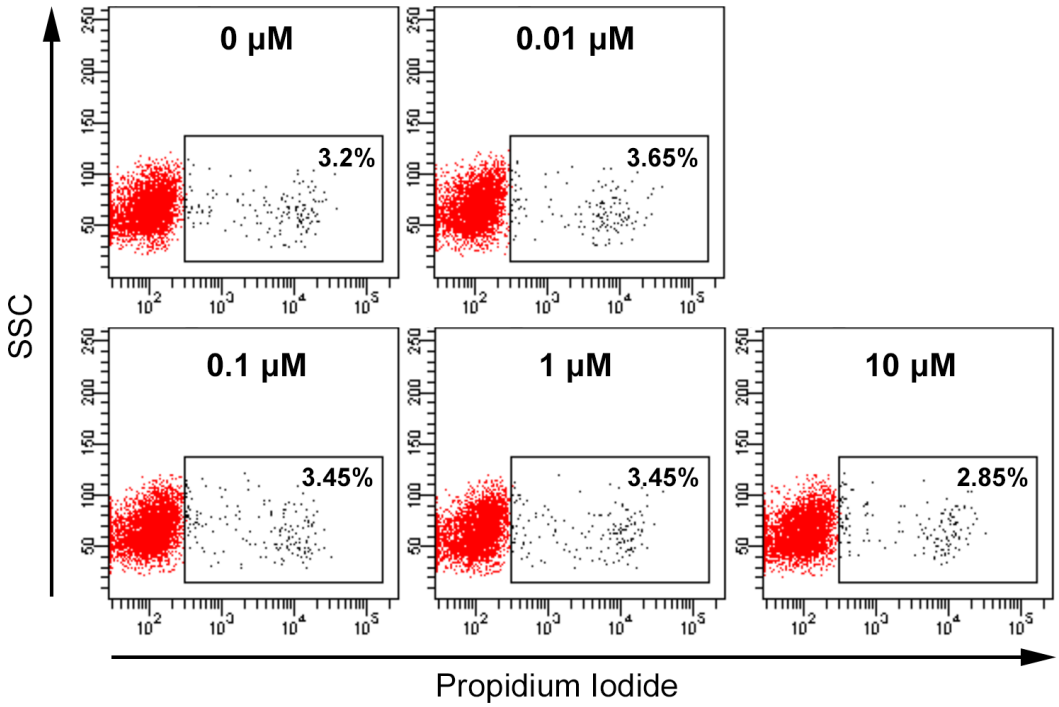

Figure 5.2. YM201636-treated NK-92 cells are viable

NK-92 cells were stained with propidium iodide to identify dead cells following treatment of NK-92 with various concentrations of YM201636 for four hours and analysed by flow cytometry. Dot plots show intact NK-92 cells (propidium iodide-negative, labelled red) together with propidium iodide-positive dead cells (labelled black and defined by the gate shown). The values show the proportion of propidium iodide-positive cells as a percentage of the total population. SSC, side scatter.

For convenience, a human NK cell line (NK-92) stably expressing human IL-2 was used in the majority of these experiments; this cell line is formally designated as NK-92MI (Tam et al., 1999) but is referred to as NK-92 in the present study. First, I investigated the affect of YM201636 on NK-92 cell viability using the membrane-impermeable dye propidium iodide to discriminate between live (impermeable, propidium iodide-negative) and dead (permeable, propidium iodide-positive) cells. No difference was observed in the frequency of dead cells in response to YM201636 treatment across a range of concentrations (0–10 µM) as measured by flow cytometry (Figure 5.2), indicating that YM201636 is not toxic to NK-92 cells at these concentrations.

I then compared the phenotypes of PIKfyve inhibition in fibroblasts (Figure 5.1C) to that found in NK-92 cells. Confocal microscopy showed that, like the situation in fibroblasts, PIKfyve inhibition did not affect the LAMP1-positive compartment (lysosomes) but did result in the generation of enlarged EEA1-positive structures (Figure 5.3). However, in fibroblasts the giant vesicles contained CI-MPR, whereas this was not evident in NK-92 cells and the distribution of CI-MPR appeared unaffected by PIKfyve inhibition in NK-92 cells. Ikonomov and colleagues have shown previously that PIKfyve depletion caused an initial enlargement of EEA1-positive early endosomes followed later by an enlargement of CI-MPR positive vesicles that they describe as late endosomes (Ikonomov et al., 2001, Ikonomov et al., 2003a). Although the duration of PIKfyve inhibition was the same in 3T3-J2 fibroblasts and NK-92 cells (two hours), the kinetics of endosome disruption may be slower in NK-92 cells and it is possible that enlargement of CI-MPR-positive vesicles may occur with prolonged PIKfyve inhibition. An alternative explanation is that the difference in endosomal disruption between 3T3-J2 and NK-92 cells may reflect localisation of PIKfyve to different endosome populations in these cells. For example, PIKfyve might associate predominantly with early endosomes in NK-92 cells and with both early- and late-endosomes in 3T3-J2 fibroblasts. Indeed, over-expressed PIKfyve was found to localise to different endosomes in COS and HeLa cells (Shisheva et al., 2001). These results suggest that PIKfyve is required for maintaining normal endosome homeostasis in NK-92 cells.

Previous studies have implicated PIKfyve in the insulin-mediated translocation of the glucose transporter GLUT4 to the plasma membrane (Berwick et al., 2004). In addition, PIKfyve negatively regulates LDCV exocytosis in neurosecretory cells (Osborne et al., 2008). To investigate whether PIKfyve plays a role in the exocytosis of NK cell lytic granules, I analysed the degranulation of PIKfyve-inhibited NK-92 cells in response to the tumour cell line K562. This cell line expresses low levels of cell surface MHC class I and high levels of ligands to several NK cell activating receptors and is the most widely used target cell to analyse human NK cell responses.

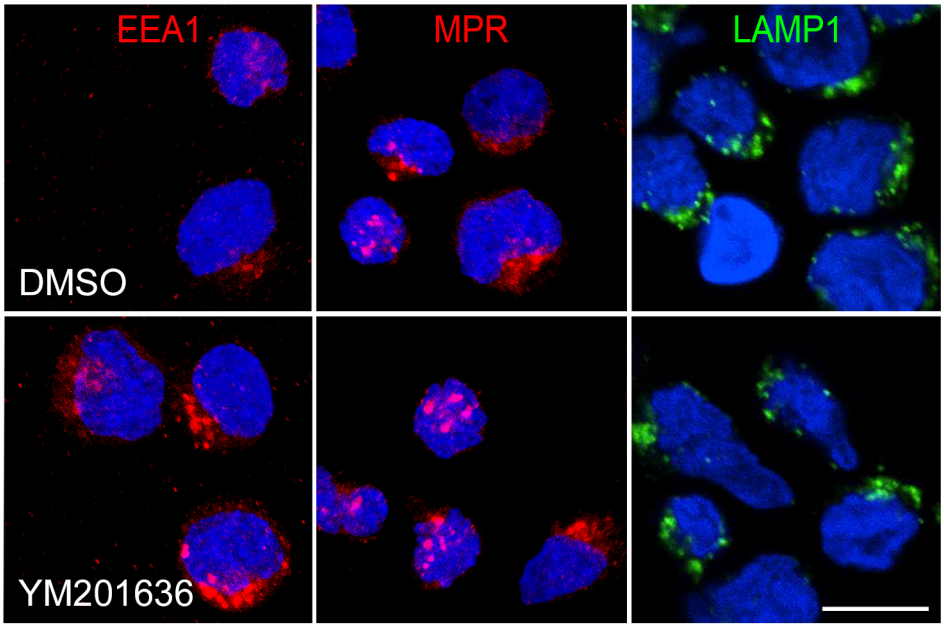

Figure 5.3. PIKfyve inhibition causes endosome enlargement in NK-92 cells

NK-92 cells treated with either DMSO or YM201636 (800 nM) for 2 hours were immunofluorescently labelled with anti-EEA1-, anti-MPR- (specific to the cation independent MPR) or anti-LAMP1- antibodies. Cells were counterstained with DAPI (*blue*) and analysed using a confocal microscope. Images are maximum intensity projections of z-stacks. Scale bar = 20 µm.

Co-culture of NK cells and K562 results in NK cell activation and induction of granule exocytosis, leading to killing of K562 by granzyme/perforin-induced apoptosis (Alter et al., 2004). The fusion of the NK cell lytic granules with the plasma membrane during degranulation results in the externalisation of LAMP1 to the cell surface which is readily detectable using flow cytometry (Alter et al., 2004). NK-92 cells had a markedly decreased capacity to degranulate in response to K562 when pre-treated with 1 µM YM201636, compared to DMSO (18% versus 32%, Figure 5.4A) and that degranulation was reduced across a range of inhibitor concentrations (0.01-10 µM; Figure 5.4B). NK cell degranulation can be potently induced in the absence of target cells using a combination of PMA (an activator of PKC) and the calcium ionophore ionomycin (Alter et al., 2004).

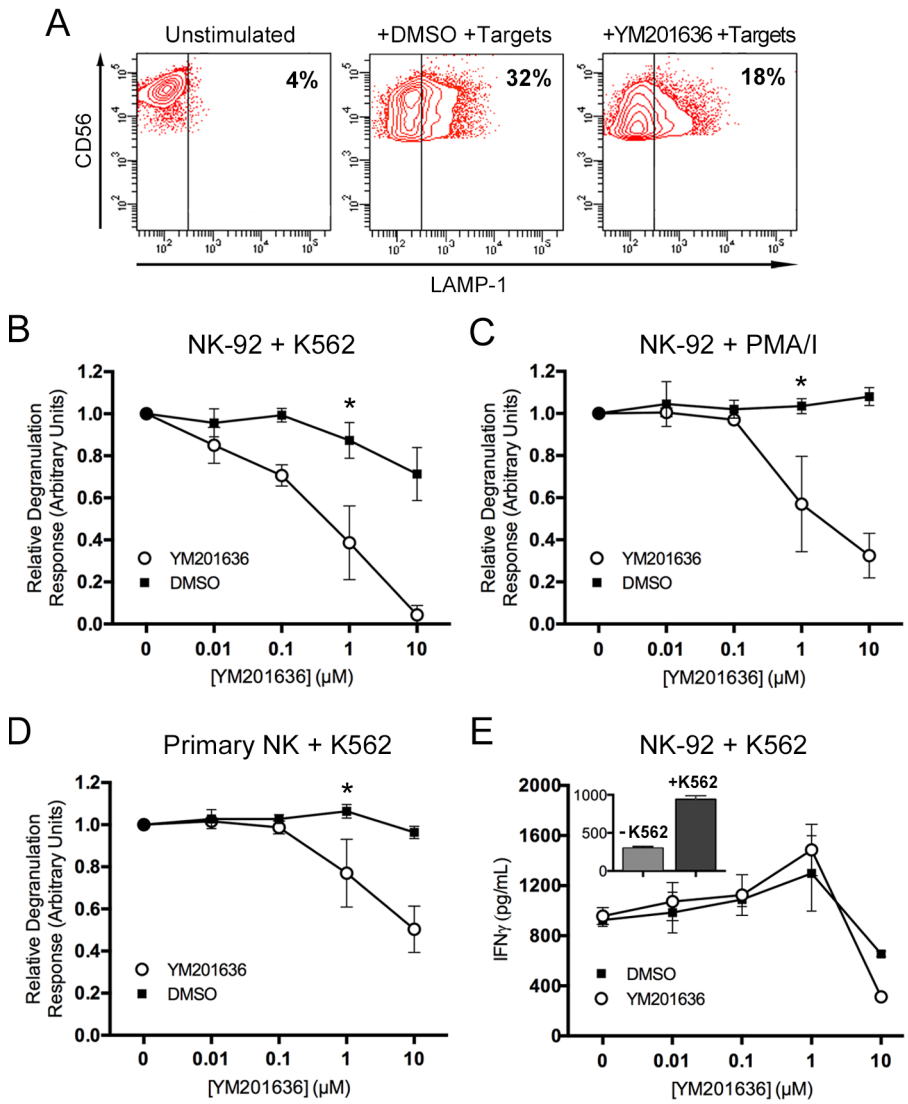

Figure 5.4. PIKfyve activity is required for NK cell degranulation but not cytokine secretion

A) NK-92 cells were pre-treated with DMSO or YM201636 (1 μM) for 20 minutes and the level of degranulation in response to K562 was measured. The proportion of degranulating CD56-positive NK-92 cells is given as a percentage of the total population and was determined by the presence of LAMP1 on the cell surface as detected by flow cytometry. NK-92 (*B, C and E*) or primary NK cells (*D*) activated with IL-2 for 7-11 days were pre-treated with various concentrations of YM201636 for 20 minutes and co-cultured with either K562 target cells for one hour (*B, D and E*) or PMA in combination with ionomycin (*PMA/I*) for 30 minutes (*C*). For *B, C* and *D*, the degranulation response is expressed relative to the degranulation induced in the absence of inhibitor (*0 μM*). E) IFNγ secretion from YM201636- or DMSO-treated NK-92 cells in response to K562 was determined by ELISA using NK-92/K562 co-culture supernatants. The inset shows that NK-92 induce IFNγ secretion in response to K562 cells. *: $P < 0.05$ ($n = 3$).

Pre-treatment of NK-92 cells with 1 μM YM201636 significantly reduced degranulation in response to stimulation with PMA and ionomycin as well as to K562 target cells (Figure 5.4C and B respectively). Furthermore, the inhibition of degranulation was not confined to the NK-92 cell line. Primary NK cells were purified from healthy donor blood samples, cultured in IL-2 for 6-10 days and pre-treated with YM201636 (or DMSO) for 20 minutes prior to co-culture with K562. This resulted in a similarly impaired degranulation response (Figure 5.4D), although this was not as pronounced as that seen with NK-92. These results indicate that NK lytic granule exocytosis is impaired in the absence of catalytically-active PIKfyve, establishing a role for this enzyme in the granule exocytosis pathway.

As well as lytic granule-mediated killing, NK cell activation also results in the production of immunomodulatory cytokines such as TNFα and IFNγ, that recruit and activate inflammatory cells and other immune cells, coordinating immunity (Vivier et al., 2011). Cytokines are transported to the cell surface and secreted in a non-polarised manner via a population of vesicles that are distinct from the lytic granules (Reefman et al., 2010). To asses whether PIKfyve inhibition impaired lytic granule exocytosis specifically or secretion in general, the secretion of IFNγ from NK-92 cells was measured in response to stimulation with K562 (Figure 5.4). Co-culture of NK-92 cells with K562 induced IFNγ secretion. However, no difference was observed in the amount of IFNγ secreted from NK-92 cells pre-treated with up to 1 μM YM201636 or DMSO, in response to K562 (Figure 5.4E). A markedly reduced secretion of IFNγ at 10 μM occurred with both YM201636- and DMSO- treatments. DMSO was not toxic to NK-92 cells at 10 μM (Figure 5.2), suggesting that DMSO inhibits secretion at this concentration by an unknown mechanism. Importantly, these data suggest that YM201636 inhibits degranulation but does not interfere with activation-induced signalling pathways that elicit downstream effector responses such as cytokine secretion. Furthermore, stimulation with K562 induced IFNγ secretion by a factor of three-fold and this induction was not affected by pre-treatment with YM201636 (Figure 5.4E). This indicates that K562-induced NK cell activation is unaffected by PIKfyve inhibition.

These data reveal that PIKfyve inhibition does not affect NK cell activation or cytokine secretion but selectively inhibits the secretion of lytic granules. Reduced K562-mediated degranulation in YM201636-treated NK-92 cells could result from a failure to form stable conjugates required for degranulation. To test this, YM201636-treated NK-92 cells were co-cultured with K562 targets, fixed, and the conjugates examined using immunofluorescence microscopy. NK-92-K562 conjugates were observed in the presence of YM201636 (Figure 5.5A, *left panel*). Furthermore, the number of conjugated cells was similar between YM201636 and DMSO treatments (Figure 5.5A, *right panel*) indicating that the decreased degranulation observed is not due to failed conjugate formation.

During degranulation, several stages precede granule fusion at the plasma membrane, such as polarisation of the MTOC toward the immunological synapse, docking of granules at the plasma membrane and priming of the granules to facilitate fusion (reviewed in Orange, 2008). LAMP1-positive granules were frequently observed clustered at the interface with K562 in YM201636-treated NK-92 cells (Figure 5.5A, *arrowhead*). The number of cells with granules clustered at the interface was higher in cells treated with YM201636 (44% versus 36% with DMSO, Figure 5.5B), although this was not statistically tested. This may be because YM201636-treated NK-92 cells are unable to elicit target cell killing and remain conjugated to K562, whereas some NK-92 cells in the DMSO treatment may have undergone a successful round of killing and reattached to new targets, but not yet polarised their granules at the time of fixation. Importantly, granule clustering at the K562 interface reveals that MTOC polarisation occurs normally in PIKfyve inhibited NK-92 cells, suggesting that PIKfyve acts downstream of MTOC polarisation.

To determine whether PIKfyve associates with NK lytic granule membranes to mediate plasma membrane docking and/or fusion events, the localisation of PIKfyve was analysed in K562-conjugated NK-92 cells by immuno-fluorescence microscopy (Figure 5.5C).

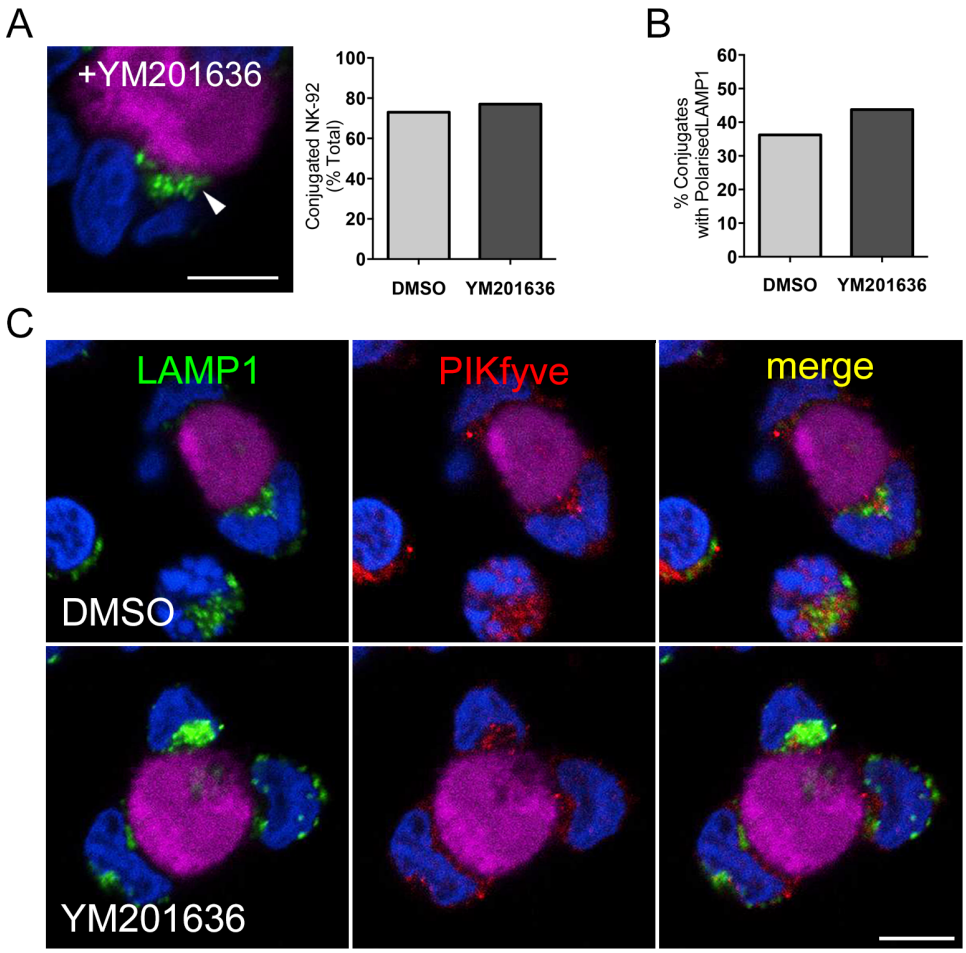

Figure 5.5. PIKfyve inhibition does not affect conjugate formation or granule polarisation

A) Maximum intensity projection of a confocal z-stack showing a DAPI-stained NK-92 cell (*blue*) conjugated to a K562 cell stained with CellTrace™ Far Red DDAO-SE (*violet*), in the presence of 1 μM YM201636 (*left panel*). Anti-LAMP1 antibody (*green*) reveals clustering of the lytic granules at the NK-92-K562 interface (*arrowhead*). Z-stacks were used to determine the number of NK-92 cells conjugated to K562 cells (*right panel*). B) The number of conjugated NK-92 cells with LAMP1 granules polarised towards K562 cells was also calculated. C) Cells were stained as in *A*, and counterstained with anti-PIKfyve antibody (*red*). An overlay of the PIKfyve and LAMP1 fluorescence is shown (*merge*) and colocalised regions appear yellow.

PIKfyve displayed both a diffuse and punctate localisation in DMSO-treated NK-92 cells, similar to that observed in chromaffin neurosecretory cells (Osborne et al., 2008). A comparable PIKfyve staining pattern was observed in YM201636-treated NK-92 cells. PIKfyve puncta were predominantly

absent of LAMP1 fluorescence in both DMSO- and YM201363-treated NK-92 cells, with only a small degree of overlap observed between the two signals. This suggests that PIKfyve is not associated with granule membranes during degranulation. Although minimal colocalisation with LAMP1 was observed, PIKfyve puncta were proximal to LAMP1-positive granules polarised at interface in conjugated NK-92 cells (Figure 5.5) and this positioning may be important during degranulation. Taken together, these data suggest that PIKfyve functions at a late stage of NK cell granule exocytosis after MTOC polarisation, but prior to granule fusion with the plasma membrane. However the exact mechanism(s) governing this process remain undetermined at this stage.

5.4 Discussion

NK cells and CTLs are central to the defence against virus-infected cells and tumour cells. Their cytolytic function requires the stimulated secretion of cytolytic effector molecules towards the target cell upon ligation of activating receptors. The effector molecules are housed within specialised secretory lysosomes (the lytic granules) that function as degradative organelles but with the added capacity to engage in regulated exocytosis in response to extracellular stimuli (reviewed in de Saint Basile et al., 2010). Granule secretion is a tightly-regulated process and the mechanisms involved are not fully understood. I have shown here that treatment with YM201636, the specific inhibitor of PIKfyve, selectively impairs NK lytic granule exocytosis, with no apparent impact on cytokine secretion or target conjugation.

The use of YM201636 as a specific inhibitor of PIKfyve is well documented (Jefferies et al., 2008, Osborne et al., 2008, de Lartigue et al., 2009). Recently, however, the specificity of YM201636 has come under question. Dual inhibition of insulin-activated class IA phosphoinositide 3-kinase (PI3K) and PIKfyve by YM201363 in adipocytes has been reported (Ikonomov et al., 2009b). NK cytotoxicity is dependent on a PI3K-mediated signalling cascade initiated by ligation of activation receptors. Pharmacological inhibition of PI3K activity supresses lytic granule polarisation towards the target, resulting in reduced target cell lysis (Jiang et al., 2000), while class IA

PI3K subunit knockout mice have normal lytic function but reduced cytokine secretion (Kim et al., 2007). However, the experiments performed here with YM201636 showed that NK lytic granules polarised normally to the NK-92-K562 immunological synapse. Furthermore, secretion of IFNγ in YM201636-inhibited NK-92 cells was unaffected, revealing that the activation-induced signalling pathway is unperturbed and showing different effects to those documented by PI3K inhibition (Ikonomov et al., 2009b). This suggests that the impaired lytic granule exocytosis observed here is most likely due to YM201636-mediated inhibition of PIKfyve, rather than inhibition of PI3K.

Lytic granule secretion is a complex process involving many stages, including the polarisation of the MTOC to the immunological synapse, docking of granules at the plasma membrane and the priming of granules to facilitate fusion. Given the similarities between NK- and CTL-mediated cytotoxicity, much of what we assume of NK lytic granule biogenesis and secretion is derived from the study of CTLs. Two molecules essential for lytic granule exocytosis are Rab27a and Munc13-4 (Ménasché et al., 2000, Feldmann et al., 2003). Rab27a mediates the docking of lytic granules at the plasma membrane, whereas Munc13-4 is implicated in a priming step that renders granules competent for fusion with the plasma membrane. Accordingly, deficiencies in Rab27a and Munc13-4 impair NK cell cytotoxicity in patients with Griscelli syndrome type 2 and FHL3, respectively (Stinchcombe et al., 2001, Marcenaro et al., 2006, Feldmann et al., 2003). In the present study, the delivery of lytic granules to the synapse of conjugated NK-92 cells was intact in PIKfyve-inhibited cells. Thus, PIKfyve appears to function downstream of MTOC polarisation but prior to granule fusion with the plasma membrane. Due to the limited resolution of the acquired images, it was not possible to determine whether the lytic granules were docked at, or just proximal to, the plasma membrane in YM201636-inhibited cells.

The localisation of PIKfyve to a sub-population of LDCVs in neurosecretory cells in response to nicotine stimulation, is important for preventing the over-secretion of a pool of PtdIns(3)P-primed granules through the depletion of PtdIns(3)P on the vesicle membrane (Osborne et al., 2008). In these cells, PIKfyve appears to function as a negative regulator of exocytosis, as

YM201636-mediated PIKfyve inhibition potentiated the nicotine-stimulated secretion of LDCVs (Osborne et al., 2008). Furthermore, the relocation of PIKfyve to the secretory vesicles from the cytoplasm upon nicotine stimulation appears to be important for its priming function. Contradictory to the role of PIKfyve as a negative regulator of exocytosis in neuroendocrine cells, PIKfyve was found to positively regulate lytic granule exocytosis in NK cells in the present study. Interestingly, PIKfyve was not found to associate with LAMP1 on lytic granule membranes in NK-92 cells, indicating that PIKfyve is unlikely to participate in a granule membrane priming step that promotes exocytosis. Instead, PIKfyve may function in a granule-independent step to mediate secretion of these organelles.

Expression of a dominant-negative kinase-deficient PIKfyve mutant inhibits the insulin-induced translocation of the GLUT4 to the cell surface in adipocytes (Ikonomov et al., 2002b, Ikonomov et al., 2007). This finding indicates a positive regulatory role for PIKfyve in the translation of GLUT4 storage vesicles to the plasma membrane during regulated exocytosis. Insulin-induced surface GLUT4 trafficking is coupled with an increase in PtdIns(3,5)P_2, yet it is unclear how the increased lipid level mediates GLUT4 translocation. One suggested mechanism is that PtdIns(3,5)P_2 on early endosomes promotes the budding of carrier vesicles containing GLUT4 that have undergone re-internalisation from the plasma membrane and routes them to newly synthesised GLUT4 storage vesicles (Shisheva, 2008). This likely serves to replenish the depleted pool of readily-releasable GLUT4 storage vesicles during insulin challenge. In NK cells, the recycling endosome was recently found to mediate the refilling of newly synthesised lytic granules with perforin (Reefman et al., 2010), suggesting that an interaction between endocytic vesicles and lytic granules is important for granule maturation. PIKfyve-mediated production of PtdIns(3,5)P_2 might be required for the trafficking of lytic granule components from early endosomes to lytic granules to facilitate granule maturation and/or secretion.

In addition to its priming function, Munc13-4 was also found to mediate a lytic granule maturation step involving recycling endosomes in CTLs. In an elegant study by Ménager et al., 2007, Munc13-4 was found to mediate the

association of Rab11-positive recycling endosomes with Rab27-positive late endosomes to form exocytic vesicles carrying secretory machinery components. Upon target recognition, these exocytic vesicles simultaneously polarised to the immunological synapse with perforin-containing lytic granules, where they fused together immediately before secretion. This fusion step confers Munc13-4 and Rab27a proteins to the membranes of lytic granules rendering them competent to dock and fuse with the plasma membrane (Ménager et al., 2007). For a summary of lytic granule maturation steps, see Figure 1.4. PIKfyve is unlikely to form part of the exocytic machinery, as we would expect a degree of colocalisation between PIKfyve and LAMP1 at the NK-92-K562 immunological synapse, though this was not the case (Figure 5.5). The role of PIKfyve in maintaining endosome integrity and endosome-linked pathways is well documented (Jefferies et al., 2008, Ikonomov et al., 2003a, de Lartigue et al., 2009). Thus, PIKfyve may instead function in one of the lytic granule maturation steps involving endocytic vesicles. Indeed, PIKfyve puncta polarised simultaneously with LAMP1-positive granules at the NK-92-K562 interface and this positioning may be important during degranulation. Simultaneous polarisation with lytic granules has been demonstrated for Rab27a- and Munc13-4-containing vesicles that do not colocalise with lytic granule proteins until immediately prior to secretion (Capuano et al., 2012, Ménager et al., 2007).

PIKfyve is directed to endocytic membranes by its PtdIns(3)P-binding FYVE domain where it generates PtdIns(3,5)P_2 and PtdIns(5)P (Jefferies et al., 2008, Ikonomov et al., 2011). The disrupted endosomal morphology observed during suppressed PIKfyve activity is mediated solely through the loss of PtdIns(3,5)P_2, as micro-injection of PtdIns(3,5)P_2, but not PtdIns(5)P, into vacuolated cells reversed the phenotype (Ikonomov et al., 2002a). Furthermore, lysosomal degradation of the internalised epidermal growth factor (EGF) receptor was blocked by PIKfyve inhibition and is thought to result from inhibited PtdIns(3,5)P_2-mediated fusion between EGF receptor-containing endosomes and lysosomes (de Lartigue et al., 2009).

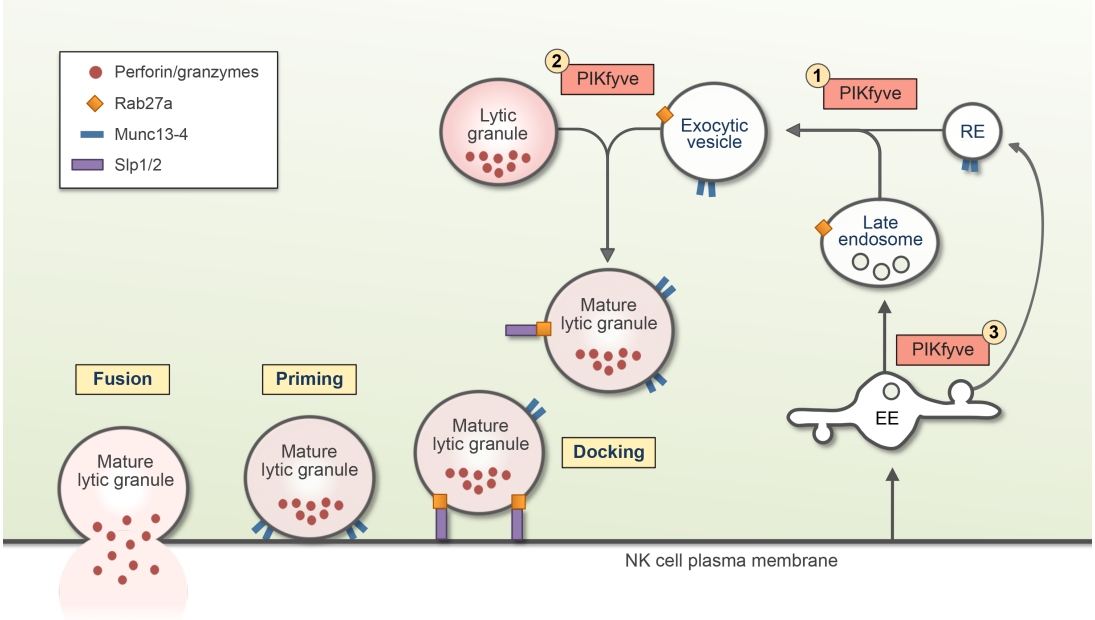

Figure 5.6. The proposed function of PIKfyve in the NK lytic granule maturation pathway

A schematic diagram (based on Figure 1.4), representing the stages of lytic granule exocytosis and including the possible steps in which PIKfyve may function. Through the generation of PtdIns(3,5)P_2 on late endosomal membranes, PIKfyve could mediate the fusion of this compartment with recycling endosomes, to form the exocytic vesicle (*1*), or the formation of mature lytic granules upon target conjugation, in the final maturation stage immediately preceding exocytosis (*2*). Alternatively, following degranulation and the re-internalisation of secretory machinery components into the early endosome, PIKfyve could mediate their sorting into their respective endocytic compartments. This function would ensure the correct protein machinery is ultimately delivered to the lytic granule during the maturation process, and enable the replenishment of vesicles necessary for further rounds of exocytosis (*3*). Furthermore, PIKfyve may promote normal endosome maturation, ensuring a continuous supply of endosome vesicles available for granule maturation events. Adapted from de Saint Basile et al., 2010. RE, recycling endosome; EE, early endosome.

In NK cells, PIKfyve-mediated production of PtdIns(3,5)P_2 on the membranes of late endosomes might prime them for fusion with recycling endosomes to form exocytic vesicles, or promote the fusion of exocytic vesicles with lytic granules upon target recognition (Figure 5.6, *steps 1* and *2*). Alternatively, PtdIns(3,5)P_2 might promote the trafficking of granule

components from early endosomes directly to newly synthesised lytic granules, replenishing the pool of granules ready for maturation and/or fusion, similar to the mechanism proposed by Shisheva and colleagues (2008). This hypothesis is strengthened by observations in the present study that PIKfyve inhibition causes early endosome enlargement in NK cells, which may reflect inhibited trafficking out of early endosomes. Thus, PIKfyve inhibition would impede interaction between endosomes and lytic granules, rendering these compartments refractory to fusion and impairing lytic granule maturation. Alternatively, PIKfyve may promote endosome maturation in NK cells, as has been shown in other cell types (Ikonomov et al., 2003a). Late endosomes can form from the gradual maturation of early endosomes that accumulate ILVs and become increasingly multivesicular (Futter et al., 1996, Huotari and Helenius, 2011). Catalytically-inactive mutant PIKfyve results in the formation of enlarged late endosomes with relatively few ILVs (Ikonomov et al., 2003a), suggesting that ILV formation requires the production of PtdIns(3,5)P_2. Although the enlarged organelles in YM201636-treated NK-92 cells in the present study were found to be early endosomes positive for EEA1 (Figure 5.3), this may reflect a similar failure in ILV formation that inhibits normal early-to-late endosome maturation. A reduced number of mature late endosomes may affect the pool of exocytic vesicles available for fusion during degranulation (Figure 5.6, *step 3*).

NK cells are able achieve multiple rounds of killing within a short time period (Bhat and Watzl, 2007). The recycling of cytolytic machinery components from the plasma membrane after degranulation is thought to be a rate-limiting step of subsequent rounds of target lysis. The mechanisms governing the recycling process in either NK and CTLs is unknown. A recent study found that Munc13-4 internalisation from the plasma membrane following an initial degranulation event was required for subsequent rounds of killing by the same NK cell (Capuano et al., 2012). Recycling was dependent on the formation of PtdIns(4,5)P_2-rich raft domains and is proposed to replenish the pool of endocytic vesicles available for further rounds of fusion. It is possible that PIKfyve is involved in the membrane retrieval of other secretory components, such as Rab27a for example, back to endocytic vesicles, though PIKfyve-mediated membrane retrieval is not

documented. Alternatively, PIKfyve might function at the early endosome to correctly sort re-internalised secretory components back to their respective compartments following degranulation (Figure 5.6, *step 3*). Reports documenting perturbed endosome-to-Golgi trafficking in cells expressing kinase-inactive PIKfyve, as well as reduced degradative sorting of EGF receptor with addition of YM201636, would seem to support this function, though the exact mechanism is disputed (de Lartigue et al., 2009, Rutherford et al., 2006). In both cases, PIKfyve inhibition in NK cells would permit an initial degranulation event, but limit subsequent rounds of degranulation with multiple targets.

PIKfyve is also a major source of PtdIns(5)P synthesis through the phosphorylation of PtdIns (Ikonomov et al., 2011, Zolov et al., 2012). Although perturbed endosomal homeostasis is mediated by loss of PtdIns(3,5)P_2 rather than PtdIns(5)P (Ikonomov et al., 2002a), the inhibition of degranulation in YM201636-treated NK cells might be uncoupled from endosome enlargement. Instead, it is possible that changes in PtdIns(5)P levels during PIKfyve inhibition might contribute to the loss of NK cell cytotoxicity observed in the present study. Remodelling of the F-actin stress fibre network in response to insulin in adipocytes was shown to be important for GLUT4 translocation and appears to be modulated by PtdIns(5)P levels (Sbrissa et al., 2004). Overexpression of wild type PIKfyve or microinjection of PtdIns(5)P, but not other PIs, enhances F-actin disassembly and promotes GLUT4 translocation. Conversely, ectopic expression of a peptide containing multiple PHD (plant homeodomains) domains that selectively bind and sequester PtdIns(5)P, block insulin-induced F-actin disassembly (Sbrissa et al., 2004). The physiological relevance of PtdIns(5)P in NK cells is unknown. It may be important for regulating F-actin reorganisation at the immunological synapse required for lytic granule secretion in response to conjugate formation (Rak et al., 2011). Thus, depletion of PtdIns(5)P through PIKfyve inhibition might impair lytic granule exocytosis by blocking actin reorganisation at the plasma membrane.

The function of PtdIns(3,5)P_2 or PtdIns(5)P has not been studied in NK cells. My results suggest that PIKfyve-mediated production of PtdIns(3,5)P_2, and

possibly PtdIns(5)P, is important for NK lytic granule secretion and may highlight a function of PIKfyve in secretory lysosome exocytosis in other cell types. PIKfyve regulates PI levels and may be involved in fine-tuning vesicle priming during the lytic granule maturation pathway. It is important to note that PIKfyve heterozygous mice (Ikonomov et al., 2011) or patients suffering from the autosomal dominant syndrome Francois-Neetens corneal fleck dystrophy (caused by mutations in PIKfyve; Li et al., 2005), do not suffer from any obvious immune dysfunction. Lytic granule exocytosis in primary NK cells is decreased, but not abolished, upon PIKfyve inhibition. This could suggest that PIKfyve is not required for NK cell cytotoxicity, or may reflect a functional redundancy of PIKfyve, indicating PIKfyve is important but not absolutely required for NK cell cytotoxicity (Figure 5.4D). In addition to its lipid kinase activity, PIKfyve also phosphorylates a number of proteins involved in endocytic trafficking (Ikonomov et al., 2003b). It is possible that NK cell degranulation requires PIKfyve protein kinase activity and that YM201636 somehow interferes with this function. In the present study, only the short-term effect of PIKfyve inhibition was examined. It is possible that the effect of reduced PIKfyve activity on degranulation may be overcome after prolonged stimulation of NK cells. Nonetheless, the lack of immune dysfunction in patients carrying PIKfyve mutations is difficult to explain given the observations made in the present study. The apparent reduction in NK cytotoxicity may indeed be independent of reduced PIKfyve lipid kinase activity, instead reflecting the YM201636-mediated inhibition of other proteins required for NK cell lytic granule exocytosis. Further examination of the role of PtdIns(3,5)P_2 and PtdIns(5)P in NK cells is needed before the contribution of these PIs to NK granule exocytosis can be determined. In particular, the effects of siRNA-mediated PIKfyve silencing and the expression of kinase-inactive PIKfyve mutants are needed to confirm a role for PIKfyve in lytic granule exocytosis. Close inspection of the vesicle compartment to which PIKfyve is localised, through staining with various endocytic markers such as Rab proteins, may help pin-point which step in the granule maturation pathway that PIKfyve might function.

Chapter 6
Conclusion and Future Work

6.1 Key Findings

The objective of this work was to define the mechanisms that contribute to NK cell lytic granule biogenesis and exocytosis. An additional aim was to investigate the giant lysosome phenotype seen in CHS/*beige* using RNA interference and the contribution of PtdIns(4,5)P_2 and autophagy to the cellular defect of *beige.*

The major findings of the present study are:

- siRNA-mediated silencing of *Lyst* in mouse fibroblasts successfully recapitulates the major aspect of the CHS/*beige* phenotype, namely the generation of giant lysosomes.
- The phosphatidylinositol 3-phosphate 5-kinase PIKfyve is required for the exocytosis of NK cell cytotoxic granules.

6.2 Conclusion and Future Work

At the time of this study, many questions still remained unanswered regarding the mechanistic pathways underlying the biogenesis and exocytosis of secretory lysosomes in cells of the immune system. Several proteins involved in the exocytosis of granules from cytotoxic lymphocytes (NK cells and CTLs) are well defined, such as Rab27a and Munc13-4. Yet many proteins remain unidentified, or their function uncharacterised, such is the case for LYST. Clear evidence is emerging that lytic granules undergo a series of maturation steps involving endocytic vesicles and that these steps occur rapidly after cellular stimulation, but prior to secretion (Ménager et al., 2007, Wood et al., 2009, Capuano et al., 2012). However, our knowledge of the molecular machinery involved in these pathways is limited. Furthermore, the role of PIs in granule exocytosis downstream of stimulation is reported in relatively few studies. The present study provides evidence that PIKfyve is involved in the NK cell lytic granule exocytosis pathway, as pharmacological

inhibition of PIKfyve impaired degranulation in response to stimulation with tumour cells in the NK cell line NK-92 and in primary NK cells isolated from the blood. PIKfyve did not colocalise with LAMP1-positive puncta in NK cells; however, upon conjugation with a target cell, PIKfyve-positive puncta simultaneously trafficked to the immunological synapse with LAMP1-positive granules. Similar redistribution of the fusion machinery components Rab27a and Munc13-4 (located on endocytic vesicles distinct from lytic granules) occurs in response to target conjugation in both NK cells and CTLs (Ménager et al., 2007, Wood et al., 2009). Defects in these proteins result in lytic granules that polarise normally but are unable to fuse with the plasma membrane (Ménasché et al., 2000, Feldmann et al., 2003). Fusion events between lytic granules and endocytic vesicles containing Rab27a and Munc13-4 are a prerequisite for exocytosis. Previous studies support a role for PIKfyve in endocytic trafficking, fusion/fission events and exocytosis of storage vesicles (Jefferies et al., 2008, Ikonomov et al., 2003a, de Lartigue et al., 2009, Ikonomov et al., 2007, Ikonomov et al., 2009b). Based on these published reports and the data presented here, it seems likely that PIKfyve functions in a fusion or trafficking step involving endosomes and that this activity facilitates the maturation of fusion-competent granules in NK cells. It remains to be determined whether the impaired degranulation observed in PIKfyve inhibitor-treated NK cells is due to reduced PtdIns(3,5)P_2 or PtdIns(5)P or both. Examining the changes in levels of these PIs in NK cells in response to stimulation may provide further insight, but this is difficult to determine in the absence of a functional PtdIns(3,5)P_2 probe. Altered levels of PtdIns(3,5)P_2 are linked with Francois-Neetons corneal fleck dystrophy (caused by mutations in PIKfyve; Li et al., 2005) and peripheral neuropathy in patients with Charcot-Marie-Tooth disease type 4 (caused by mutations in Sac3; Chow et al., 2007). Immunological impairment is not reported in these patients and this is difficult to reconcile with the defective NK cell function observed in PIKfyve inhibited cells. Patients with Charcot-Marie-Tooth disease type 2 (caused by mutations in Dynamin 2; Zuchner et al., 2005), suffer from peripheral neuropathy yet do not exhibit immunological defects, despite the recent finding that depletion of Dynamin 2 impairs NK cell cytotoxicity (Arneson et al., 2008). Dynamin 2 is thought to function in a

terminal stage of lytic granule exocytosis and like PIKfyve, traffics independently but polarises simultaneously with lytic granules at the immunological synapse upon target conjugation (Arneson et al., 2008). Furthermore, depletion of Dynamin 2 reduces but does not completely block NK lytic granule exocytosis, similar to PIKfyve inhibition.

In the present study, the effect of suppressed PIKfyve activity on NK cell cytotoxicity was tested through a single means; YM201636-mediated PIKfyve inhibition, therefore, impaired granule exocytosis as a result of non-specific YM201636-mediated inhibition of other proteins cannot be ruled out. Inhibition of PIKfyve activity through alternative means, i.e., expression of kinase-deficient PIKfyve mutants and RNAi, is needed to validate the theory that PIKfyve is required for NK cell cytotoxicity. Careful colocalisation analysis of PIKfyve with endocytic markers such as Rab5, Rab27a and Rab11 during stimulation is required to ascertain whether PIKfyve associates with early, late or recycling endosomes, respectively. Such analyses will help determine whether PIKfyve co-ordinates an endocytic fusion or trafficking event which contributes to granule maturation.

If potentiation of granule exocytosis occurs alongside an increase in intracellular PtdIns(3,5)P_2, this would confirm a requirement for PtdIns(3,5)P_2 in granule secretion. Such an increase could be generated experimentally through the overexpression of wild type PIKfyve, or inhibition of the Sac3 phosphatase that depletes PtdIns(3,5)P_2. Indeed, siRNA-mediated depletion of Sac3 in adipocytes causes a slight but significant elevation in PtdIns(3,5)P_2 that potentiates insulin-stimulated GLUT4 vesicle exocytosis (Ikonomov et al., 2009a). The present study is the first to examine the role of PIKfyve in the regulated secretion of NK lytic granules and the data suggest a role for this protein and its products, PtdIns(3,5)P_2 and PtdIns(5)P, in the exocytosis of secretory lysosomes.

This study reports that siRNA-mediated *Lyst* silencing in cultured mouse fibroblasts successfully recapitulates the major aspect of the CHS/*beige* phenotype of abnormally large and clustered lysosomes. Knockdown at the level of *Lyst* mRNA was confirmed but in the absence of a working Lyst antibody, the level of Lyst protein knockdown could not be determined.

Nonetheless, this is the first study that uses RNAi to examine the function of Lyst and demonstrates that siRNA-mediated *Lyst* silencing could be used as a model system to study Lyst function and CHS/*beige*. Future studies could involve using siRNA to screen the LYST-interacting proteins identified by Tchernev and colleagues (2002) for a similar induction of lysosomal enlargement, which might establish them as functioning in the same pathway of lysosome regulation as LYST.

A gene network regulating lysosomal biogenesis and autophagy was recently discovered to be controlled by the transcription factor EB (TFEB) (Settembre et al., 2013). Lysosomal dysfunction (that occurs with lysosomal storage diseases, for example) was found to trigger TFEB nuclear translocation where it upregulated the expression of genes associated with the lysosomal-autophagy pathway (Sardiello et al., 2009). The increase in basal autophagy and abundance of the lysosomal membrane protein LAMP1 observed in *beige* cells here could be the result of nuclear TFEB signalling in response to lysosomal dysfunction and is a potential area for investigation.

Severe immunologic dysfunction in CHS patients and the *beige* mouse is caused by the defective exocytosis of enlarged secretory lysosomes in many immune cell types. Despite extensive analysis of the biogenesis and morphology of the enlarged lysosomes, several aspects of the CHS/*beige* phenotype remain relatively unexplored. In particular, the role of LYST in the regulation of PtdIns(4,5)P_2 metabolism is unknown. The subcellular localisation of PtdIns(4,5)P_2 was discovered to be significantly altered in CHS/*beige* fibroblasts (Ward et al., 2003), but the contribution of altered PtdIns(4,5)P_2 levels to the CHS/*beige* phenotype has not been examined. My results suggest that an increase in plasma membrane PtdIns(4,5)P_2 is coupled with a decreased abundance of two PtdIns(4,5)P_2 hydrolysing isoenzymes, PLCγ1 and PLCγ2 in *beige* fibroblasts.

PLCγ and the products of its enzymatic activity, Ins(1,4,5)P_3 and DAG, have indispensible roles in the stimulated exocytosis of secretory lysosomes from mast cells and NK cells (Hammond et al., 2006, Caraux et al., 2006). Thus, reduced PLCγ activity in these cells might contribute to the degranulation defect of CHS/*beige*. The concomitant hydrolysis of PtdIns(4,5)P_2 and

production of DAG by PLC is required for the exocytosis of mast cell granules (Hammond et al., 2006). Both PLCγ1 and PLCγ2 are expressed by NK cells (Upshaw et al., 2005) and PLCγ2 is a key component in the degranulation pathway of NK cells (Caraux et al., 2006). NK cells from PLCγ2-/- mice failed to secrete their lytic granules, despite conjugate formation and polarisation of granules to the immunological synapse (Caraux et al., 2006). The secretory defect was specific to lytic granules, as secretion of IFNγ was unaffected (Caraux et al., 2006). Similarly, CHS/*beige* NK cells and CTLs have normal cytokine secretion, but fail to secrete cytotoxic granules despite normal polarisation (Baetz et al., 1995, Targan and Oseas, 1983, Shiflett et al., 2002).

No definitive pathway has been identified in which Lyst functions to regulate lysosome morphology or exocytosis of secretory lysosomes. The defective lytic granule exocytosis in CHS/*beige* NK cells has previously been attributed to enhanced PKC proteolysis (Ito et al., 1988, Ito et al., 1989, Tanabe et al., 1998, Tanabe et al., 2009), but a link between LYST deficiency and enhanced PKC proteolysis has not been established. My study documents for the first time that the abundance of PLCγ, which lies upstream of PKC in the same pathway, is reduced in *beige* fibroblasts and implicates LYST in the PtdIns(4,5)P_2 signal transduction pathway. Thus, these findings identify an area for further research. If immunoblot analysis reveals a similar depletion of PLCγ protein in CHS/*beige* NK cells, it is likely that perturbations in this signalling pathway will contribute to the defective exocytosis of lytic granules in LYST-deficient NK cells, and indeed other cell types whose secretory function is abolished in CHS/*beige*. As mentioned previously, depletion of plasma membrane PtdIns(4,5)P_2 by PLCγ is essential for mast cell degranulation (Hammond et al., 2006). A similar scenario might exist in NK cells, but was not examined in the present study. To test this, immunofluorescence analysis could be used to monitor PtdIns(4,5)P_2 levels at the plasma membrane at fixed time points following stimulation in both normal and CHS/*beige* NK cells.

The notion that the PH and BEACH domains function as a single unit (Jogl et al., 2002, Gebauer et al., 2004), coupled with the finding that the PH

domain of FAN is PtdIns(4,5)P_2-binding (Haubert et al., 2007) is a significant development in establishing BEACH domain function. HEAT and Armadillo-like domains have recently been confirmed to be PtdIns(4,5)P_2-binding modules (Catimel et al., 2008), further supporting a PtdIns(4,5)P_2-binding capacity for LYST that may be important for its localisation and/or function. PtdIns(4,5)P_2-rich lipid rafts are found at the NK cell immunological synapse and are important for lytic granule exocytosis (Capuano et al., 2012). An interesting hypothesis is that specific extracellular stimuli, such as NK cell receptor activation, induces binding of LYST to target proteins which in turn triggers a conformational change in the PH-BEACH domain that, opens up the lipid-binding pocket of the PH domain. This could target LYST to PtdIns(4,5)P_2-rich sites at the synapse where it might function to recruit and scaffold protein complexes involving PLCγ or PKC and co-ordinate signalling events that facilitate granule exocytosis. Indeed, several other BEACH proteins act as scaffolds for protein interactions (Newlon et al., 1999, Filimonenko et al., 2010).

The PH domains of several protein-tyrosine kinases mediate high affinity interactions with PKC (Yao et al., 1997). LYST might interact with PKC through its PH domain, scaffolding it to substrates and protecting it from proteolysis. In the absence of a LYST scaffold, PKC may become vulnerable to degradation, thus resulting in the reduced level of PKC observed in the present study and by others (Tanabe et al., 2000, Tanabe et al., 2009). PKC and PLC are potent signalling transducers and restricting their subcellular localisations through scaffolding, coupled with enhanced degradation when not scaffolded, may be an important mechanism for restricting unwarranted ectopic signalling. Clearly the need for a working antibody is crucial, as this will answer many questions pertaining to the function and localisation of LYST.

PI conversion is tightly regulated; perturbed levels of one species will likely affect the overall metabolism of many others and the cellular pathways in which they function. This might go some way to explain the enhanced basal autophagy observed in *beige* cells of the present study, as autophagy is intrinsically linked to PtdIns(3)P and Ins(1,4,5)P_3 levels (Mizushima and

Komatsu, 2011, Decuypere et al., 2011). Several lines of evidence exist to support a role for LYST in maintaining correct lipid signalling and/or metabolism. These include reduced levels of PKC, elevated ceramide and PtdIns(4,5)P_2 mislocalisation in CHS/*beige* cells (Tanabe et al., 1998, Tanabe et al., 2000, Ward et al., 2003). The present study also documents an altered abundance of the PtdIns(4,5)P_2-binding protein PLCγ which generates the lipid second messengers DAG and Ins(1,4,5)P_3. PIs are essential for a plethora of cellular processes, including cytoskeletal reorganisation, cell signalling and vesicle transport (Roth, 2004). Thus, perturbed PI trafficking or altered enrichment or depletion of specific lipids at membranes in LYST-deficient cells may account for the impaired lysosome homeostasis and defective exocytosis of these cells. Furthermore, the function of LYST as master regulator of vesicle and membrane fusion events is an attractive hypothesis. LYST function may be differentially regulated according to cell type, the organelle to which it associates and the specific stimuli, such as NK cell activation and lytic granule secretion. Secretion is tightly regulated and even a slight disturbance in lipid signalling or metabolism might disrupt this mechanism. This is supported by my finding that inhibition of PIKfyve activity reduces NK cell granule exocytosis.

The regulated exocytosis of secretory lysosomes is critical to the function of many immune cell types that contain them. Future studies which examine the contribution of specific PIs and their regulatory proteins to exocytosis of these specialised organelles will undoubtedly emphasise the importance of these lipids in coordinating immune responses.

References

ABE, K., ARASHIMA, S. & HONMA, M. 1982. Distribution pattern of lysosomal granules in fibroblasts of the Chediak-Higashi syndrome. *Journal of Clinical Pathology,* 35**,** 496-501.

ABE, M., MAKINO, A., HULLIN-MATSUDA, F., KAMIJO, K., OHNO-IWASHITA, Y., HANADA, K., MIZUNO, H., MIYAWAKI, A. & KOBAYASHI, T. 2012. A Role for Sphingomyelin-Rich Lipid Domains in the Accumulation of Phosphatidylinositol-4,5-Bisphosphate to the Cleavage Furrow during Cytokinesis. *Molecular and Cellular Biology,* 32**,** 1396-407.

ADAM-KLAGES, S., ADAM, D., WIEGMANN, K., STRUVE, S., KOLANUS, W., SCHNEIDER-MERGENER, J. & KRONKE, M. 1996. FAN, a novel WD-repeat protein, couples the p55 TNF-receptor to neutral sphingomyelinase. *Cell,* 86**,** 937-47.

ALI, S. H. & DECAPRIO, J. A. 2001. Cellular transformation by SV40 large T antigen: interaction with host proteins. *Seminars in Cancer Biology,* 11**,** 15-23.

ALTER, G., MALENFANT, J. M. & ALTFELD, M. 2004. CD107a as a functional marker for the identification of natural killer cell activity. *Journal of Immunological Methods,* 294**,** 15-22.

ANDRADE, M. A., PETOSA, C., O'DONOGHUE, S. I., MULLER, C. W. & BORK, P. 2001. Comparison of ARM and HEAT protein repeats. *Journal of Molecular Biology,* 309**,** 1-18.

ARNESON, L. N., SEGOVIS, C. M., GOMEZ, T. S., SCHOON, R. A., DICK, C. J., LOU, Z., BILLADEAU, D. D. & LEIBSON, P. J. 2008. Dynamin 2 regulates granule exocytosis during NK cell-mediated cytotoxicity. *Journal of Immunology,* 181**,** 6995-7001.

BAETZ, K., ISAAZ, S. & GRIFFITHS, G. M. 1995. Loss of cytotoxic T lymphocyte function in Chediak-Higashi syndrome arises from a secretory defect that prevents lytic granule exocytosis. *Journal of Immunology,* 154**,** 6122-31.

BARBOSA, M. D., NGUYEN, Q. A., TCHERNEV, V. T., ASHLEY, J. A., DETTER, J. C., BLAYDES, S. M., BRANDT, S. J., CHOTAI, D., HODGMAN, C., SOLARI, R. C., LOVETT, M. & KINGSMORE, S. F. 1996. Identification of the homologous beige and Chediak-Higashi syndrome genes. [Erratum appears in Nature 1997 Jan 2;385(6611):97]. *Nature,* 382**,** 262-5.

BARRAT, F. J., AULOGE, L., PASTURAL, E., LAGELOUSE, R. D., VILMER, E., CANT, A. J., WEISSENBACH, J., LE PASLIER, D., FISCHER, A. & DE SAINT BASILE, G. 1996. Genetic and physical mapping of the Chediak-Higashi syndrome on chromosome 1q42-43. *Am J Hum Genet,* 59**,** 625-32.

BARRAT, F. J., LE DEIST, F., BENKERROU, M., BOUSSO, P., FELDMANN, J., FISCHER, A. & DE SAINT BASILE, G. 1999. Defective CTLA-4 cycling pathway in Chediak-Higashi syndrome: a possible mechanism for deregulation of T lymphocyte activation.

Proceedings of the National Academy of Sciences of the United States of America, 96**,** 8645-50.

BARTLETT, D. W. & DAVIS, M. E. 2006. Insights into the kinetics of siRNA-mediated gene silencing from live-cell and live-animal bioluminescent imaging. *Nucleic Acids Res,* 34**,** 322-33.

BERWICK, D. C., DELL, G. C., WELSH, G. I., HEESOM, K. J., HERS, I., FLETCHER, L. M., COOKE, F. T. & TAVARE, J. M. 2004. Protein kinase B phosphorylation of PIKfyve regulates the trafficking of GLUT4 vesicles. *Journal of Cell Science,* 117**,** 5985-93.

BEYENBACH, K. W. & WIECZOREK, H. 2006. The V-type H+ ATPase: molecular structure and function, physiological roles and regulation. *Journal of Experimental Biology,* 209**,** 577-589.

BHAT, R. & WATZL, C. 2007. Serial killing of tumor cells by human natural killer cells--enhancement by therapeutic antibodies. *PLoS One,* 2**,** e326.

BLOTT, E. J. & GRIFFITHS, G. M. 2002. Secretory lysosomes. *Nat Rev Mol Cell Biol,* 3**,** 122-31.

BONIFACINO, J. S. & TRAUB, L. M. 2003. Signals for sorting of transmembrane proteins to endosomes and lysosomes. *Annual Review of Biochemistry,* 72**,** 395-447.

BOTS, M. & MEDEMA, J. P. 2006. Granzymes at a glance. *Journal of Cell Science,* 119**,** 5011-4.

BRAULKE, T. & BONIFACINO, J. S. 2009. Sorting of lysosomal proteins. *Biochimica et Biophysica Acta,* 1793**,** 605-14.

BRIGHT, N. A., REAVES, B. J., MULLOCK, B. M. & LUZIO, J. P. 1997. Dense core lysosomes can fuse with late endosomes and are re-formed from the resultant hybrid organelles. *Journal of Cell Science,* 110**,** 2027-40.

BRIGHT, N. A., GRATIAN, M. J. & LUZIO, J. P. 2005. Endocytic delivery to lysosomes mediated by concurrent fusion and kissing events in living cells. *Current Biology,* 15**,** 360-5.

BRYCESON, Y. T., MARCH, M. E., LJUNGGREN, H. G. & LONG, E. O. 2006. Activation, coactivation, and costimulation of resting human natural killer cells. *Immunological Reviews,* 214**,** 73-91.

BRYCESON, Y. T., RUDD, E., ZHENG, C., EDNER, J., MA, D., WOOD, S. M., BECHENSTEEN, A. G., BOELENS, J. J., CELKAN, T., FARAH, R. A., HULTENBY, K., WINIARSKI, J., ROCHE, P. A., NORDENSKJOLD, M., HENTER, J. I., LONG, E. O. & LJUNGGREN, H. G. 2007. Defective cytotoxic lymphocyte degranulation in syntaxin-11 deficient familial hemophagocytic lymphohistiocytosis 4 (FHL4) patients. *Blood,* 110**,** 1906-15.

BURGESS, A., MORNON, J.-P., DE SAINT-BASILE, G. & CALLEBAUT, I. 2009. A concanavalin A-like lectin domain in the CHS1/LYST protein, shared by members of the BEACH family. *Bioinformatics,* 25**,** 1219-22.

BURKHARDT, J. K., HESTER, S., LAPHAM, C. K. & ARGON, Y. 1990. The lytic granules of natural killer cells are dual-function organelles combining secretory and pre-lysosomal compartments. *Journal of Cell Biology,* 111**,** 2327-40.

BURKHARDT, J. K., WIEBEL, F. A., HESTER, S. & ARGON, Y. 1993. The giant organelles in beige and Chediak-Higashi fibroblasts are derived

from late endosomes and mature lysosomes. *Journal of Experimental Medicine,* 178**,** 1845-56.

CAPUANO, C., PAOLINI, R., MOLFETTA, R., FRATI, L., SANTONI, A. & GALANDRINI, R. 2012. PIP2-dependent regulation of Munc13-4 endocytic recycling: impact on the cytolytic secretory pathway. *Blood*.

CARAUX, A., KIM, N., BELL, S. E., ZOMPI, S., RANSON, T., LESJEAN-POTTIER, S., GARCIA-OJEDA, M. E., TURNER, M. & COLUCCI, F. 2006. Phospholipase C-gamma2 is essential for NK cell cytotoxicity and innate immunity to malignant and virally infected cells. *Blood,* 107**,** 994-1002.

CARPENTER, G. & JI, Q. 1999. Phospholipase C-gamma as a signal-transducing element. *Experimental Cell Research,* 253**,** 15-24.

CATIMEL, B., SCHIEBER, C., CONDRON, M., PATSIOURAS, H., CONNOLLY, L., CATIMEL, J., NICE, E. C., BURGESS, A. W. & HOLMES, A. B. 2008. The PI(3,5)P2 and PI(4,5)P2 interactomes. *J Proteome Res,* 7**,** 5295-313.

CHANG, J., CIZMECIOGLU, O., HOFFMANN, I. & RHEE, K. 2010. PLK2 phosphorylation is critical for CPAP function in procentriole formation during the centrosome cycle. *EMBO Journal,* 29**,** 2395-406.

CHARETTE, S. J. & COSSON, P. 2007. A LYST/beige homolog is involved in biogenesis of Dictyostelium secretory lysosomes. *Journal of Cell Science,* 120**,** 2338-2343.

CHEN, D., PUROHIT, A., HALILOVIC, E., DOXSEY, S. J. & NEWTON, A. C. 2004. Centrosomal anchoring of protein kinase C betaII by pericentrin controls microtubule organization, spindle function, and cytokinesis. *Journal of Biological Chemistry,* 279**,** 4829-39.

CHERRA, S. J., KULICH, S. M., UECHI, G., BALASUBRAMANI, M., MOUNTZOURIS, J., DAY, B. W. & CHU, C. T. 2010. Regulation of the autophagy protein LC3 by phosphorylation. *Journal of Cell Biology,* 190**,** 533-539.

CHI, E. Y. & LAGUNOFF, D. 1975. Abnormal mast cell granules in the beige (Chediak-Higashi syndrome) mouse. *Journal of Histochemistry and Cytochemistry,* 23**,** 117-22.

CHO, J. H., CHANG, C. J., CHEN, C. Y. & TANG, T. K. 2006. Depletion of CPAP by RNAi disrupts centrosome integrity and induces multipolar spindles. *Biochemical and Biophysical Research Communications,* 339**,** 742-7.

CHOW, C. Y., ZHANG, Y., DOWLING, J. J., JIN, N., ADAMSKA, M., SHIGA, K., SZIGETI, K., SHY, M. E., LI, J., ZHANG, X., LUPSKI, J. R., WEISMAN, L. S. & MEISLER, M. H. 2007. Mutation of FIG4 causes neurodegeneration in the pale tremor mouse and patients with CMT4J. *Nature,* 448**,** 68-72.

CLARK, R. & GRIFFITHS, G. M. 2003. Lytic granules, secretory lysosomes and disease. *Current Opinion in Immunology,* 15**,** 516-21.

CLARK, R. H., STINCHCOMBE, J. C., DAY, A., BLOTT, E., BOOTH, S., BOSSI, G., HAMBLIN, T., DAVIES, E. G. & GRIFFITHS, G. M. 2003. Adaptor protein 3-dependent microtubule-mediated movement of lytic granules to the immunological synapse. *Nat Immunol,* 4**,** 1111-20.

COTE, M., MÉNAGER, M. M., BURGESS, A., MAHLAOUI, N., PICARD, C., SCHAFFNER, C., AL-MANJOMI, F., AL-HARBI, M., ALANGARI, A., LE DEIST, F., GENNERY, A. R., PRINCE, N., CARIOU, A.,

NITSCHKE, P., BLANK, U., EL-GHAZALI, G., MÉNASCHÉ, G., LATOUR, S., FISCHER, A. & DE SAINT BASILE, G. 2009. Munc18-2 deficiency causes familial hemophagocytic lymphohistiocytosis type 5 and impairs cytotoxic granule exocytosis in patient NK cells. *Journal of Clinical Investigation,* 119**,** 3765-73.

CUI, S. H., TANABE, F., TERUNUMA, H., IWATANI, Y., NUNOI, H., AGEMATSU, K., KOMIYAMA, A., NOMURA, A., HARA, T., ONODERA, T., IWATA, T. & ITO, M. 2001. A thiol proteinase inhibitor, E-64-d, corrects the abnormalities in concanavalin A cap formation and the lysosomal enzyme activity in leucocytes from patients with Chediak-Higashi syndrome by reversing the down-regulated protein kinase C activity. *Clinical and Experimental Immunology,* 125**,** 283-90.

DE LARTIGUE, J., POLSON, H., FELDMAN, M., SHOKAT, K., TOOZE, S. A., URBE, S. & CLAGUE, M. J. 2009. PIKfyve regulation of endosome-linked pathways. *Traffic,* 10**,** 883-93.

DE SAINT BASILE, G., MÉNASCHÉ, G. & FISCHER, A. 2010. Molecular mechanisms of biogenesis and exocytosis of cytotoxic granules. *Nature Reviews Immunology,* 10**,** 568-79.

DE SOUZA, N., VALLIER, L. G., FARES, H. & GREENWALD, I. 2007. SEL-2, the C. elegans neurobeachin/LRBA homolog, is a negative regulator of lin-12/Notch activity and affects endosomal traffic in polarized epithelial cells. *Development,* 134**,** 691-702.

DECUYPERE, J. P., WELKENHUYZEN, K., LUYTEN, T., PONSAERTS, R., DEWAELE, M., MOLGO, J., AGOSTINIS, P., MISSIAEN, L., DE SMEDT, H., PARYS, J. B. & BULTYNCK, G. 2011. Ins(1,4,5)P3 receptor-mediated Ca2+ signaling and autophagy induction are interrelated. *Autophagy,* 7**,** 1472-89.

DELL'ANGELICA, E. C., SHOTELERSUK, V., AGUILAR, R. C., GAHL, W. A. & BONIFACINO, J. S. 1999. Altered trafficking of lysosomal proteins in Hermansky-Pudlak syndrome due to mutations in the beta 3A subunit of the AP-3 adaptor. *Molecular Cell,* 3**,** 11-21.

DERETIC, V. 2010. A master conductor for aggregate clearance by autophagy. *Dev Cell,* 18**,** 694-6.

DIMRI, G. P., LEE, X. H., BASILE, G., ACOSTA, M., SCOTT, C., ROSKELLEY, C., MEDRANO, E. E., LINSKENS, M., RUBELJ, I., PEREIRASMITH, O., PEACOCKE, M. & CAMPISI, J. 1995. A Biomarker That Identifies Senescent Human-Cells in Culture and in Aging Skin in-Vivo. *Proceedings of the National Academy of Sciences of the United States of America,* 92**,** 9363-9367.

DURCHFORT, N., VERHOEF, S., VAUGHN, M. B., SHRESTHA, R., ADAM, D., KAPLAN, J. & WARD, D. M. 2012. The enlarged lysosomes in beige j cells result from decreased lysosome fission and not increased lysosome fusion. *Traffic,* 13**,** 108-19.

DUVE, C. D., PRESSMAN, B. C., GIANETTO, R., WATTIAUX, R. & APPELMANS, F. 1955. Tissue Fractionation Studies .6. Intracellular Distribution Patterns of Enzymes in Rat-Liver Tissue. *Biochemical Journal,* 60**,** 604-617.

EAPEN, M., DELAAT, C. A., BAKER, K. S., CAIRO, M. S., COWAN, M. J., KURTZBERG, J., STEWARD, C. G., VEYS, P. A. & FILIPOVICH, A.

H. 2007. Hematopoietic cell transplantation for Chediak-Higashi syndrome. *Bone Marrow Transplantation,* 39**,** 411-5.

ELBASHIR, S. M., HARBORTH, J., LENDECKEL, W., YALCIN, A., WEBER, K. & TUSCHL, T. 2001. Duplexes of 21-nucleotide RNAs mediate RNA interference in cultured mammalian cells. *Nature,* 411**,** 494-8.

EMOTO, K., INADOME, H., KANAHO, Y., NARUMIYA, S. & UMEDA, M. 2005. Local change in phospholipid composition at the cleavage furrow is essential for completion of cytokinesis. *Journal of Biological Chemistry,* 280**,** 37901-7.

FADOK, V. A., BRATTON, D. L., FRASCH, S. C., WARNER, M. L. & HENSON, P. M. 1998. The role of phosphatidylserine in recognition of apoptotic cells by phagocytes. *Cell Death and Differentiation,* 5**,** 551-62.

FAIGLE, W., RAPOSO, G., TENZA, D., PINET, V., VOGT, A., KROPSHOFER, H., FISCHER, A., DE SAINT-BASILE, G. & AMIGORENA, S. 1998. Deficient peptide loading and MHC class II endosomal sorting in a human genetic immunodeficiency disease: the Chediak-Higashi syndrome. *Journal of Cell Biology,* 141**,** 1121.

FEDEDA, J. P. & GERLICH, D. W. 2012. Molecular control of animal cell cytokinesis. *Nat Cell Biol,* 14**,** 440-7.

FELDMANN, J., CALLEBAUT, I., RAPOSO, G., CERTAIN, S., BACQ, D., DUMONT, C., LAMBERT, N., OUACHEE-CHARDIN, M., CHEDEVILLE, G., TAMARY, H., MINARD-COLIN, V., VILMER, E., BLANCHE, S., LE DEIST, F., FISCHER, A. & DE SAINT BASILE, G. 2003. Munc13-4 is essential for cytolytic granules fusion and is mutated in a form of familial hemophagocytic lymphohistiocytosis (FHL3). *Cell,* 115**,** 461-73.

FILIMONENKO, M., ISAKSON, P., FINLEY, K. D., ANDERSON, M., JEONG, H., MELIA, T. J., BARTLETT, B. J., MYERS, K. M., BIRKELAND, H. C., LAMARK, T., KRAINC, D., BRECH, A., STENMARK, H., SIMONSEN, A. & YAMAMOTO, A. 2010. The selective macroautophagic degradation of aggregated proteins requires the PI3P-binding protein Alfy. *Molecular Cell,* 38**,** 265-79.

FUTTER, C. E., PEARSE, A., HEWLETT, L. J. & HOPKINS, C. R. 1996. Multivesicular endosomes containing internalized EGF-EGF receptor complexes mature and then fuse directly with lysosomes. *Journal of Cell Biology,* 132**,** 1011-23.

GEBAUER, D., LI, J., JOGL, G., SHEN, Y., MYSZKA, D. G. & TONG, L. 2004. Crystal structure of the PH-BEACH domains of human LRBA/BGL. *Biochemistry,* 43**,** 14873-80.

GEUZE, H. J., STOORVOGEL, W., STROUS, G. J., SLOT, J. W., BLEEKEMOLEN, J. E. & MELLMAN, I. 1988. Sorting of mannose 6-phosphate receptors and lysosomal membrane proteins in endocytic vesicles. *J Cell Biol,* 107**,** 2491-501.

GILLOOLY, D. J., RAIBORG, C. & STENMARK, H. 2003. Phosphatidylinositol 3-phosphate is found in microdomains of early endosomes. *Histochemistry and Cell Biology,* 120**,** 445-453.

GIURISATO, E., CELLA, M., TAKAI, T., KUROSAKI, T., FENG, Y., LONGMORE, G. D., COLONNA, M. & SHAW, A. S. 2007. Phosphatidylinositol 3-kinase activation is required to form the

NKG2D immunological synapse. *Molecular and Cellular Biology,* 27**,** 8583-99.

GLYNN, M. W. & GLOVER, T. W. 2005. Incomplete processing of mutant lamin A in Hutchinson-Gilford progeria leads to nuclear abnormalities, which are reversed by farnesyltransferase inhibition. *Human Molecular Genetics,* 14**,** 2959-69.

GOW, J. B., LAINWALA, S. & LYERLA, T. A. 1993. Cellular expression of the beige mouse mutation and its correction in hybrids with control human fibroblasts. *In Vitro Cellular and Developmental Biology. Animal,* 29A**,** 884-91.

GRIFFITHS, G., MATTEONI, R., BACK, R. & HOFLACK, B. 1990. Characterization of the cation-independent mannose 6-phosphate receptor-enriched prelysosomal compartment in NRK cells. *Journal of Cell Science,* 95 (Pt 3)**,** 441-61.

HABEDANCK, R., STIERHOF, Y. D., WILKINSON, C. J. & NIGG, E. A. 2005. The Polo kinase Plk4 functions in centriole duplication. *Nat Cell Biol,* 7**,** 1140-6.

HAMMOND, G. R., DOVE, S. K., NICOL, A., PINXTEREN, J. A., ZICHA, D. & SCHIAVO, G. 2006. Elimination of plasma membrane phosphatidylinositol (4,5)-bisphosphate is required for exocytosis from mast cells. *Journal of Cell Science,* 119**,** 2084-94.

HAMMOND, G. R., SCHIAVO, G. & IRVINE, R. F. 2009. Immunocytochemical techniques reveal multiple, distinct cellular pools of PtdIns4P and PtdIns(4,5)P(2). *Biochemical Journal,* 422**,** 23-35.

HAN, J. D., BAKER, N. E. & RUBIN, C. S. 1997. Molecular characterization of a novel A kinase anchor protein from Drosophila melanogaster. *Journal of Biological Chemistry,* 272**,** 26611-9.

HANNA, D. E., RETHINASWAMY, A. & GLOVER, C. V. 1995. Casein kinase II is required for cell cycle progression during G1 and G2/M in Saccharomyces cerevisiae. *Journal of Biological Chemistry,* 270**,** 25905-14.

HARDING, C. V. 1995. Intracellular organelles involved in antigen processing and the binding of peptides to class II MHC molecules. *Seminars in Immunology,* 7**,** 355-60.

HAUBERT, D., GHARIB, N., RIVERO, F., WIEGMANN, K., HOSEL, M., KRONKE, M. & KASHKAR, H. 2007. PtdIns(4,5) P-restricted plasma membrane localization of FAN is involved in TNF-induced actin reorganization. *EMBO Journal,* 26**,** 3308-3321.

HAYFLICK, L. 1965. The Limited in Vitro Lifetime of Human Diploid Cell Strains. *Experimental Cell Research,* 37**,** 614-36.

HIRST, J., BARLOW, L. D., FRANCISCO, G. C., SAHLENDER, D. A., SEAMAN, M. N., DACKS, J. B. & ROBINSON, M. S. 2011. The fifth adaptor protein complex. *PLoS Biol,* 9**,** e1001170.

HOLT, O., KANNO, E., BOSSI, G., BOOTH, S., DANIELE, T., SANTORO, A., ARICO, M., SAEGUSA, C., FUKUDA, M. & GRIFFITHS, G. M. 2008. Slp1 and Slp2-a localize to the plasma membrane of CTL and contribute to secretion from the immunological synapse. *Traffic,* 9**,** 446-57.

HUME, A. N., COLLINSON, L. M., RAPAK, A., GOMES, A. Q., HOPKINS, C. R. & SEABRA, M. C. 2001. Rab27a regulates the peripheral

distribution of melanosomes in melanocytes. *Journal of Cell Biology,* 152**,** 795-808.

HUOTARI, J. & HELENIUS, A. 2011. Endosome maturation. *EMBO Journal,* 30**,** 3481-500.

HURLEY, J. H. 2010. The ESCRT complexes. *Critical Reviews in Biochemistry and Molecular Biology,* 45**,** 463-87.

HUYNH, C., ROTH, D., WARD, D. M., KAPLAN, J. & ANDREWS, N. W. 2004. Defective lysosomal exocytosis and plasma membrane repair in Chediak-Higashi/beige cells. *Proceedings of the National Academy of Sciences of the United States of America,* 101**,** 16795-800.

HUYNH, K. K., ESKELINEN, E. L., SCOTT, C. C., MALEVANETS, A., SAFTIG, P. & GRINSTEIN, S. 2007. LAMP proteins are required for fusion of lysosomes with phagosomes. *EMBO Journal,* 26**,** 313-24.

IHRKE, G., KYTTALA, A., RUSSELL, M. R. G., ROUS, B. A. & LUZIO, J. P. 2004. Differential use of two AP-3-mediated pathways by lysosomal membrane proteins. *Traffic,* 5**,** 946-962.

IKONOMOV, O. C., SBRISSA, D. & SHISHEVA, A. 2001. Mammalian cell morphology and endocytic membrane homeostasis require enzymatically active phosphoinositide 5-kinase PIKfyve. *Journal of Biological Chemistry,* 276**,** 26141-7.

IKONOMOV, O. C., SBRISSA, D., MLAK, K., KANZAKI, M., PESSIN, J. & SHISHEVA, A. 2002a. Functional dissection of lipid and protein kinase signals of PIKfyve reveals the role of PtdIns 3,5-P2 production for endomembrane integrity. *Journal of Biological Chemistry,* 277**,** 9206-11.

IKONOMOV, O. C., SBRISSA, D., MLAK, K. & SHISHEVA, A. 2002b. Requirement for PIKfyve enzymatic activity in acute and long-term insulin cellular effects. *Endocrinology,* 143**,** 4742-54.

IKONOMOV, O. C., SBRISSA, D., FOTI, M., CARPENTIER, J. L. & SHISHEVA, A. 2003a. PIKfyve controls fluid phase endocytosis but not recycling/degradation of endocytosed receptors or sorting of procathepsin D by regulating multivesicular body morphogenesis. *Molecular Biology of the Cell,* 14**,** 4581-91.

IKONOMOV, O. C., SBRISSA, D., MLAK, K., DEEB, R., FLIGGER, J., SOANS, A., FINLEY, R. L., JR. & SHISHEVA, A. 2003b. Active PIKfyve associates with and promotes the membrane attachment of the late endosome-to-trans-Golgi network transport factor Rab9 effector p40. *Journal of Biological Chemistry,* 278**,** 50863-71.

IKONOMOV, O. C., SBRISSA, D. & SHISHEVA, A. 2006. Localized PtdIns 3,5-P2 synthesis to regulate early endosome dynamics and fusion. *Am J Physiol Cell Physiol,* 291**,** C393-404.

IKONOMOV, O. C., SBRISSA, D., DONDAPATI, R. & SHISHEVA, A. 2007. ArPIKfyve-PIKfyve interaction and role in insulin-regulated GLUT4 translocation and glucose transport in 3T3-L1 adipocytes. *Experimental Cell Research,* 313**,** 2404-16.

IKONOMOV, O. C., SBRISSA, D., IJUIN, T., TAKENAWA, T. & SHISHEVA, A. 2009a. Sac3 is an insulin-regulated phosphatidylinositol 3,5-bisphosphate phosphatase: gain in insulin responsiveness through Sac3 down-regulation in adipocytes. *Journal of Biological Chemistry,* 284**,** 23961-71.

IKONOMOV, O. C., SBRISSA, D. & SHISHEVA, A. 2009b. YM201636, an inhibitor of retroviral budding and PIKfyve-catalyzed PtdIns(3,5)P2 synthesis, halts glucose entry by insulin in adipocytes. *Biochemical and Biophysical Research Communications,* 382**,** 566-70.

IKONOMOV, O. C., SBRISSA, D., DELVECCHIO, K., XIE, Y., JIN, J. P., RAPPOLEE, D. & SHISHEVA, A. 2011. The phosphoinositide kinase PIKfyve is vital in early embryonic development: preimplantation lethality of PIKfyve-/- embryos but normality of PIKfyve+/- mice. *Journal of Biological Chemistry,* 286**,** 13404-13.

INTRONE, W., BOISSY, R. E. & GAHL, W. A. 1999. Clinical, molecular, and cell biological aspects of Chediak-Higashi syndrome. *Molecular Genetics and Metabolism,* 68**,** 283-303.

ITO, M., TANABE, F., SATO, A., TAKAMI, Y. & SHIGETA, S. 1988a. A potent inhibitor of protein kinase C inhibits natural killer activity. *International Journal of Immunopharmacology,* 10**,** 211-6.

ITO, M., TANABE, F., TAKAMI, Y., SATO, A. & SHIGETA, S. 1988b. Rapid down-regulation of protein kinase C in (Chediak-Higashi syndrome) beige mouse by phorbol ester. *Biochemical and Biophysical Research Communications,* 153**,** 648-56.

ITO, M., SATO, A., TANABE, F., ISHIDA, E., TAKAMI, Y. & SHIGETA, S. 1989. The thiol proteinase inhibitors improve the abnormal rapid down-regulation of protein kinase C and the impaired natural killer cell activity in (Chediak-Higashi syndrome) beige mouse. *Biochemical and Biophysical Research Communications,* 160**,** 433-40.

JEFFERIES, H. B., COOKE, F. T., JAT, P., BOUCHERON, C., KOIZUMI, T., HAYAKAWA, M., KAIZAWA, H., OHISHI, T., WORKMAN, P., WATERFIELD, M. D. & PARKER, P. J. 2008. A selective PIKfyve inhibitor blocks PtdIns(3,5)P(2) production and disrupts endomembrane transport and retroviral budding. *EMBO Rep,* 9**,** 164-70.

JEFFERY, J. M., URQUHART, A. J., SUBRAMANIAM, V. N., PARTON, R. G. & KHANNA, K. K. 2010. Centrobin regulates the assembly of functional mitotic spindles. *Oncogene,* 29**,** 2649-58.

JESSEN, B., MAUL-PAVICIC, A., UFHEIL, H., VRAETZ, T., ENDERS, A., LEHMBERG, K., LANGLER, A., GROSS-WIELTSCH, U., BAY, A., KAYA, Z., BRYCESON, Y. T., KOSCIELNIAK, E., BADAWY, S., DAVIES, G., HUFNAGEL, M., SCHMITT-GRAEFF, A., AICHELE, P., ZUR STADT, U., SCHWARZ, K. & EHL, S. 2011. Subtle differences in CTL cytotoxicity determine susceptibility to hemophagocytic lymphohistiocytosis in mice and humans with Chediak-Higashi syndrome. *Blood,* 118**,** 4620-9.

JIANG, K., ZHONG, B., GILVARY, D. L., CORLISS, B. C., HONG-GELLER, E., WEI, S. & DJEU, J. Y. 2000. Pivotal role of phosphoinositide-3 kinase in regulation of cytotoxicity in natural killer cells. *Nat Immunol,* 1**,** 419-25.

JOGL, G., SHEN, Y., GEBAUER, D., LI, J., WIEGMANN, K., KASHKAR, H., KRONKE, M. & TONG, L. 2002. Crystal structure of the BEACH domain reveals an unusual fold and extensive association with a novel PH domain. *EMBO Journal,* 21**,** 4785-95.

JOHNSON, E. E., OVERMEYER, J. H., GUNNING, W. T. & MALTESE, W. A. 2006. Gene silencing reveals a specific function of hVps34

phosphatidylinositol 3-kinase in late versus early endosomes. *Journal of Cell Science,* 119**,** 1219-32.

JORDAN, M. B., HILDEMAN, D., KAPPLER, J. & MARRACK, P. 2004. An animal model of hemophagocytic lymphohistiocytosis (HLH): CD8+ T cells and interferon gamma are essential for the disorder. *Blood,* 104**,** 735-43.

JUSTICE, M. J., SILAN, C. M., CECI, J. D., BUCHBERG, A. M., COPELAND, N. G. & JENKINS, N. A. 1990. A molecular genetic linkage map of mouse chromosome 13 anchored by the beige (bg) and satin (sa) loci. *Genomics,* 6**,** 341-51.

KABEYA, Y., MIZUSHIMA, N., UENO, T., YAMAMOTO, A., KIRISAKO, T., NODA, T., KOMINAMI, E., OHSUMI, Y. & YOSHIMORI, T. 2000. LC3, a mammalian homologue of yeast Apg8p, is localized in autophagosome membranes after processing. *EMBO Journal,* 19**,** 5720-8.

KANG, J. Y., KIM, J. J., JANG, S. Y. & BAE, Y. S. 2009. The p53-p21(Cip1/WAF1) pathway is necessary for cellular senescence induced by the inhibition of protein kinase CKII in human colon cancer cells. *Molecules and Cells,* 28**,** 489-94.

KAPLAN, J., DE DOMENICO, I. & WARD, D. M. 2008. Chediak-Higashi syndrome. *Current Opinion in Hematology,* 15**,** 22-9.

KARIM, M. A., SUZUKI, K., FUKAI, K., OH, J., NAGLE, D. L., MOORE, K. J., BARBOSA, E., FALIK-BORENSTEIN, T., FILIPOVICH, A., ISHIDA, Y., KIVRIKKO, S., KLEIN, C., KREUZ, F., LEVIN, A., MIYAJIMA, H., REGUEIRO, J., RUSSO, C., UYAMA, E., VIERIMAA, O. & SPRITZ, R. A. 2002. Apparent genotype-phenotype correlation in childhood, adolescent, and adult Chediak-Higashi syndrome. *American Journal of Medical Genetics,* 108**,** 16-22.

KATZ, P., ZAYTOUN, A. M. & FAUCI, A. S. 1982. Deficiency of active natural killer cells in the Chediak-Higashi syndrome. Localization of the defect using a single cell cytotoxicity assay. *Journal of Clinical Investigation,* 69**,** 1231-8.

KAWAI, A., UCHIYAMA, H., TAKANO, S., NAKAMURA, N. & OHKUMA, S. 2007. Autophagosome-lysosome fusion depends on the pH in acidic compartments in CHO cells. *Autophagy,* 3**,** 154-7.

KIESSLING, R., KLEIN, E., PROSS, H. & WIGZELL, H. 1975. "Natural" killer cells in the mouse. II. Cytotoxic cells with specificity for mouse Moloney leukemia cells. Characteristics of the killer cell. *European Journal of Immunology,* 5**,** 117-21.

KIM, N., SAUDEMONT, A., WEBB, L., CAMPS, M., RUCKLE, T., HIRSCH, E., TURNER, M. & COLUCCI, F. 2007. The p110delta catalytic isoform of PI3K is a key player in NK-cell development and cytokine secretion. *Blood,* 110**,** 3202-8.

KIMURA, S., FUJITA, N., NODA, T. & YOSHIMORI, T. 2009. Monitoring autophagy in mammalian cultured cells through the dynamics of LC3. *Autophagy in mammalian systems***,** 1.

KJELDSEN, L., CALAFAT, J. & BORREGAARD, N. 1998. Giant granules of neutrophils in Chediak-Higashi syndrome are derived from azurophil granules but not from specific and gelatinase granules. *Journal of Leukocyte Biology,* 64**,** 72.

KOCH, M. & HOLT, M. 2012. Coupling exo- and endocytosis: an essential role for PIP(2) at the synapse. *Biochimica et Biophysica Acta,* 1821**,** 1114-32.

KORINEK, V., BARKER, N., WILLERT, K., MOLENAAR, M., ROOSE, J., WAGENAAR, G., MARKMAN, M., LAMERS, W., DESTREE, O. & CLEVERS, H. 1998. Two members of the Tcf family implicated in Wnt/beta-catenin signaling during embryogenesis in the mouse. *Molecular and Cellular Biology,* 18**,** 1248-56.

KORNFELD, S. & MELLMAN, I. 1989. The biogenesis of lysosomes. *Annual Review of Cell Biology,* 5**,** 483-525.

KUNDRA, R. & KORNFELD, S. 1999. Asparagine-linked oligosaccharides protect Lamp-1 and Lamp-2 from intracellular proteolysis. *Journal of Biological Chemistry,* 274**,** 31039-46.

KWAK, E., GERALD, N., LAROCHELLE, D. A., VITHALANI, K. K., NISWONGER, M. L., MAREADY, M. & DE LOZANNE, A. 1999. LvsA, a protein related to the mouse beige protein, is required for cytokinesis in Dictyostelium. *Molecular Biology of the Cell,* 10**,** 4429-39.

KWONG, J., ROUNDABUSH, F. L., HUTTON MOORE, P., MONTAGUE, M., OLDHAM, W., LI, Y., CHIN, L. S. & LI, L. 2000. Hrs interacts with SNAP-25 and regulates Ca(2+)-dependent exocytosis. *Journal of Cell Science,* 113 (Pt 12)**,** 2273-84.

LANE, P. W. & MURPHY, E. D. 1972. Susceptibility to spontaneous pneumonitis in an inbred strain of beige and satin mice. *Genetics,* 72**,** 451-60.

LEWIS, V., GREEN, S. A., MARSH, M., VIHKO, P., HELENIUS, A. & MELLMAN, I. 1985. Glycoproteins of the lysosomal membrane. *Journal of Cell Biology,* 100**,** 1839-47.

LI, D. & ROBERTS, R. 2001. WD-repeat proteins: structure characteristics, biological function, and their involvement in human diseases. *Cellular and Molecular Life Sciences,* 58**,** 2085-2097.

LI, S., TIAB, L., JIAO, X., MUNIER, F. L., ZOGRAFOS, L., FRUEH, B. E., SERGEEV, Y., SMITH, J., RUBIN, B., MEALLET, M. A., FORSTER, R. K., HEJTMANCIK, J. F. & SCHORDERET, D. F. 2005. Mutations in PIP5K3 are associated with Francois-Neetens mouchetee fleck corneal dystrophy. *Am J Hum Genet,* 77**,** 54-63.

LOPEZ, J. A., BRENNAN, A. J., WHISSTOCK, J. C., VOSKOBOINIK, I. & TRAPANI, J. A. 2012. Protecting a serial killer: pathways for perforin trafficking and self-defence ensure sequential target cell death. *Trends Immunol,* 33**,** 406-12.

LOPEZ-HERRERA, G., TAMPELLA, G., PAN-HAMMARSTROM, Q., HERHOLZ, P., TRUJILLO-VARGAS, C. M., PHADWAL, K., SIMON, A. K., MOUTSCHEN, M., ETZIONI, A., MORY, A., SRUGO, I., MELAMED, D., HULTENBY, K., LIU, C., BARONIO, M., VITALI, M., PHILIPPET, P., DIDEBERG, V., AGHAMOHAMMADI, A., REZAEI, N., ENRIGHT, V., DU, L., SALZER, U., EIBEL, H., PFEIFER, D., VEELKEN, H., STAUSS, H., LOUGARIS, V., PLEBANI, A., GERTZ, E. M., SCHAFFER, A. A., HAMMARSTROM, L. & GRIMBACHER, B. 2012. Deleterious mutations in LRBA are associated with a syndrome of immune deficiency and autoimmunity. *Am J Hum Genet,* 90**,** 986-1001.

LUZIO, J. P., PRYOR, P. R. & BRIGHT, N. A. 2007. Lysosomes: fusion and function. *Nat Rev Mol Cell Biol,* 8**,** 622-32.

MARCENARO, S., GALLO, F., MARTINI, S., SANTORO, A., GRIFFITHS, G. M., ARICO, M., MORETTA, L. & PENDE, D. 2006. Analysis of natural killer-cell function in familial hemophagocytic lymphohistiocytosis (FHL): defective CD107a surface expression heralds Munc13-4 defect and discriminates between genetic subtypes of the disease. *Blood,* 108**,** 2316-23.

MARCET-PALACIOS, M., ODEMUYIWA, S. O., COUGHLIN, J. J., GAROFOLI, D., EWEN, C., DAVIDSON, C. E., GHAFFARI, M., KANE, K. P., LACY, P., LOGAN, M. R., BEFUS, A. D., BLEACKLEY, R. C. & MOQBEL, R. 2008. Vesicle-associated membrane protein 7 (VAMP-7) is essential for target cell killing in a natural killer cell line. *Biochemical and Biophysical Research Communications,* 366**,** 617-623.

MARONE, G., CASOLARO, V., PATELLA, V., FLORIO, G. & TRIGGIANI, M. 1997. Molecular and cellular biology of mast cells and basophils. *International Archives of Allergy and Immunology,* 114**,** 207-17.

MATTEONI, R. & KREIS, T. E. 1987. Translocation and Clustering of Endosomes and Lysosomes Depends on Microtubules. *Journal of Cell Biology,* 105**,** 1253-1265.

MCINTYRE, R. E., LAKSHMINARASIMHAN CHAVALI, P., ISMAIL, O., CARRAGHER, D. M., SANCHEZ-ANDRADE, G., FORMENT, J. V., FU, B., DEL CASTILLO VELASCO-HERRERA, M., EDWARDS, A., VAN DER WEYDEN, L., YANG, F., RAMIREZ-SOLIS, R., ESTABEL, J., GALLAGHER, F. A., LOGAN, D. W., ARENDS, M. J., TSANG, S. H., MAHAJAN, V. B., SCUDAMORE, C. L., WHITE, J. K., JACKSON, S. P., GERGELY, F. & ADAMS, D. J. 2012. Disruption of mouse Cenpj, a regulator of centriole biogenesis, phenocopies Seckel syndrome. *PLoS Genet,* 8**,** e1003022.

MCNICOL, A. & ISRAELS, S. J. 1999. Platelet dense granules: structure, function and implications for haemostasis. *Thrombosis Research,* 95**,** 1-18.

MEADE, J. L., WILSON, E. B., HOLMES, T. D., DE WYNTER, E. A., BRETT, P., STRASZYNSKI, L., BALLARD, P. A., TRAPANI, J. A., MCDERMOTT, M. F. & COOK, G. P. 2009. Proteolytic activation of the cytotoxic phenotype during human NK cell development. *Journal of Immunology,* 183**,** 803-13.

MEEK, S. E., LANE, W. S. & PIWNICA-WORMS, H. 2004. Comprehensive proteomic analysis of interphase and mitotic 14-3-3-binding proteins. *Journal of Biological Chemistry,* 279**,** 32046-54.

MEISTER, G. & TUSCHL, T. 2004. Mechanisms of gene silencing by double-stranded RNA. *Nature,* 431**,** 343-9.

MÉNAGER, M. M., MENASCHE, G., ROMAO, M., KNAPNOUGEL, P., HO, C. H., GARFA, M., RAPOSO, G., FELDMANN, J., FISCHER, A. & DE SAINT BASILE, G. 2007. Secretory cytotoxic granule maturation and exocytosis require the effector protein hMunc13-4. *Nat Immunol,* 8**,** 257-67.

MÉNASCHÉ, G., PASTURAL, E., FELDMANN, J., CERTAIN, S., ERSOY, F., DUPUIS, S., WULFFRAAT, N., BIANCHI, D., FISCHER, A., LE DEIST, F. & DE SAINT BASILE, G. 2000. Mutations in RAB27A

cause Griscelli syndrome associated with haemophagocytic syndrome. *Nature Genetics,* 25**,** 173-6.

MÉNASCHÉ, G., MÉNAGÉR, M. M., LEFEBVRE, J. M., DEUTSCH, E., ATHMAN, R., LAMBERT, N., MAHLAOUI, N., COURT, M., GARIN, J., FISCHER, A. & DE SAINT BASILE, G. 2008. A newly identified isoform of Slp2a associates with Rab27a in cytotoxic T cells and participates to cytotoxic granule secretion. *Blood,* 112**,** 5052-62.

MENTLIK, A. N., SANBORN, K. B., HOLZBAUR, E. L. & ORANGE, J. S. 2010. Rapid lytic granule convergence to the MTOC in natural killer cells is dependent on dynein but not cytolytic commitment. *Molecular Biology of the Cell,* 21**,** 2241-56.

MESAKI, K., TANABE, K., OBAYASHI, M., OE, N. & TAKEI, K. 2011. Fission of tubular endosomes triggers endosomal acidification and movement. *PLoS One,* 6**,** e19764.

MIZUSHIMA, N. & KOMATSU, M. 2011. Autophagy: renovation of cells and tissues. *Cell,* 147**,** 728-41.

MOHLIG, H., MATHIEU, S., THON, L., FREDERIKSEN, M. C., WARD, D. M., KAPLAN, J., SCHUTZE, S., KABELITZ, D. & ADAM, D. 2007. The WD repeat protein FAN regulates lysosome size independent from abnormal downregulation/membrane recruitment of protein kinase C. *Experimental Cell Research,* 313**,** 2703-18.

MONTFORT, A., MARTIN, P. G., LEVADE, T., BENOIST, H. & SEGUI, B. 2010. FAN (factor associated with neutral sphingomyelinase activation), a moonlighting protein in TNF-R1 signaling. *Journal of Leukocyte Biology,* 88**,** 897-903.

MORGAN, A., BURGOYNE, R. D., BARCLAY, J. W., CRAIG, T. J., PRESCOTT, G. R., CIUFO, L. F., EVANS, G. J. & GRAHAM, M. E. 2005. Regulation of exocytosis by protein kinase C. *Biochemical Society Transactions,* 33**,** 1341-4.

MOUTON, R. E. & VENABLE, M. E. 2000. Ceramide induces expression of the senescence histochemical marker, beta-galactosidase, in human fibroblasts. *Mechanisms of Ageing and Development,* 113**,** 169-81.

MU, F. T., CALLAGHAN, J. M., STEELE-MORTIMER, O., STENMARK, H., PARTON, R. G., CAMPBELL, P. L., MCCLUSKEY, J., YEO, J. P., TOCK, E. P. & TOH, B. H. 1995. EEA1, an early endosome-associated protein. EEA1 is a conserved alpha-helical peripheral membrane protein flanked by cysteine "fingers" and contains a calmodulin-binding IQ motif. *Journal of Biological Chemistry,* 270**,** 13503-11.

MULLOCK, B. M., BRIGHT, N. A., FEARON, C. W., GRAY, S. R. & LUZIO, J. P. 1998. Fusion of lysosomes with late endosomes produces a hybrid organelle of intermediate density and is NSF dependent. *Journal of Cell Biology,* 140**,** 591-601.

NAGLE, D. L., KARIM, M. A., WOOLF, E. A., HOLMGREN, L., BORK, P., MISUMI, D. J., MCGRAIL, S. H., DUSSAULT, B. J., JR., PEROU, C. M., BOISSY, R. E., DUYK, G. M., SPRITZ, R. A. & MOORE, K. J. 1996. Identification and mutation analysis of the complete gene for Chediak-Higashi syndrome. *Nature Genetics,* 14**,** 307-11.

NAIR, R., LAUKS, J., JUNG, S., COOKE, N. E., DE WIT, H., BROSE, N., KILIMANN, M. W., VERHAGE, M. & RHEE, J. 2013. Neurobeachin

regulates neurotransmitter receptor trafficking to synapses. *Journal of Cell Biology,* 200**,** 61-80.

NEEFT, M., WIEFFER, M., DE JONG, A. S., NEGROIU, G., METZ, C. H., VAN LOON, A., GRIFFITH, J., KRIJGSVELD, J., WULFFRAAT, N., KOCH, H., HECK, A. J., BROSE, N., KLEIJMEER, M. & VAN DER SLUIJS, P. 2005. Munc13-4 is an effector of rab27a and controls secretion of lysosomes in hematopoietic cells. *Molecular Biology of the Cell,* 16**,** 731-41.

NEWLON, M. G., ROY, M., MORIKIS, D., HAUSKEN, Z. E., COGHLAN, V., SCOTT, J. D. & JENNINGS, P. A. 1999. The molecular basis for protein kinase A anchoring revealed by solution NMR. *Nature Structural Biology,* 6**,** 222-7.

NOPPE, G., DEKKER, P., DE KONING-TREURNIET, C., BLOM, J., VAN HEEMST, D., DIRKS, R. W., TANKE, H. J., WESTENDORP, R. G. & MAIER, A. B. 2009. Rapid flow cytometric method for measuring senescence associated beta-galactosidase activity in human fibroblasts. *Cytometry A,* 75**,** 910-6.

ORANGE, J. S., RAMESH, N., REMOLD-O'DONNELL, E., SASAHARA, Y., KOOPMAN, L., BYRNE, M., BONILLA, F. A., ROSEN, F. S., GEHA, R. S. & STROMINGER, J. L. 2002. Wiskott-Aldrich syndrome protein is required for NK cell cytotoxicity and colocalizes with actin to NK cell-activating immunologic synapses. *Proceedings of the National Academy of Sciences of the United States of America,* 99**,** 11351-6.

ORANGE, J. S. & BALLAS, Z. K. 2006. Natural killer cells in human health and disease. *Clinical Immunology,* 118**,** 1-10.

ORANGE, J. S. 2008. Formation and function of the lytic NK-cell immunological synapse. *Nature Reviews Immunology,* 8**,** 713-725.

OSBORNE, S. L., WEN, P. J., BOUCHERON, C., NGUYEN, H. N., HAYAKAWA, M., KAIZAWA, H., PARKER, P. J., VITALE, N. & MEUNIER, F. A. 2008. PIKfyve negatively regulates exocytosis in neurosecretory cells. *Journal of Biological Chemistry,* 283**,** 2804-13.

OZER, H. L., BANGA, S. S., DASGUPTA, T., HOUGHTON, J., HUBBARD, K., JHA, K. K., KIM, S. H., LENAHAN, M., PANG, Z., PARDINAS, J. R. & PATSALIS, P. C. 1996. SV40-mediated immortalization of human fibroblasts. *Experimental Gerontology,* 31**,** 303-10.

PEROU, C. M. & KAPLAN, J. 1993a. Complementation analysis of Chediak-Higashi syndrome: the same gene may be responsible for the defect in all patients and species. *Somatic Cell and Molecular Genetics,* 19**,** 459-68.

PEROU, C. M. & KAPLAN, J. 1993b. Chediak-Higashi syndrome is not due to a defect in microtubule-based lysosomal mobility. *Journal of Cell Science,* 106**,** 99-107.

PEROU, C. M., MOORE, K. J., NAGLE, D. L., MISUMI, D. J., WOOLF, E. A., MCGRAIL, S. H., HOLMGREN, L., BRODY, T. H., DUSSAULT, B. J., JR., MONROE, C. A., DUYK, G. M., PRYOR, R. J., LI, L., JUSTICE, M. J. & KAPLAN, J. 1996. Identification of the murine beige gene by YAC complementation and positional cloning. *Nature Genetics,* 13**,** 303-8.

PEROU, C. M., LESLIE, J. D., GREEN, W., LI, L., WARD, D. M. & KAPLAN, J. 1997a. The Beige/Chediak-Higashi syndrome gene encodes a

widely expressed cytosolic protein. *Journal of Biological Chemistry,* 272**,** 29790-4.

PEROU, C. M., PRYOR, R. J., NAAS, T. P. & KAPLAN, J. 1997b. The bg allele mutation is due to a LINE1 element retrotransposition. *Genomics,* 42**,** 366-8.

PETERS, P. J., BORST, J., OORSCHOT, V., FUKUDA, M., KRAHENBUHL, O., TSCHOPP, J., SLOT, J. W. & GEUZE, H. J. 1991. Cytotoxic T lymphocyte granules are secretory lysosomes, containing both perforin and granzymes. *Journal of Experimental Medicine,* 173**,** 1099-109.

PLEBANI, A., CIRAVEGNA, B., PONTE, M., MINGARI, M. C. & MORETTA, L. 2000. Interleukin-2 mediated restoration of natural killer cell function in a patient with Griscelli syndrome. *European Journal of Pediatrics,* 159**,** 713-4.

POTERYAEV, D., DATTA, S., ACKEMA, K., ZERIAL, M. & SPANG, A. 2010. Identification of the Switch in Early-to-Late Endosome Transition. *Cell,* 141**,** 497-508.

PROIKAS-CEZANNE, T., RUCKERBAUER, S., STIERHOF, Y. D., BERG, C. & NORDHEIM, A. 2007. Human WIPI-1 puncta-formation: a novel assay to assess mammalian autophagy. *FEBS Letters,* 581**,** 3396-404.

PRYOR, P. R. & LUZIO, J. P. 2009. Delivery of endocytosed membrane proteins to the lysosome. *Biochimica et Biophysica Acta,* 1793**,** 615-24.

RAHMAN, M., HABERMAN, A., TRACY, C., RAY, S. & KRAMER, H. 2012. Drosophila mauve Mutants Reveal a Role of LYST Homologs Late in the Maturation of Phagosomes and Autophagosomes. *Traffic*.

RAJ, V. & MAHAJAN, S. 2011. Dose Response Relationship of Nuclear Changes with Fractionated Radiotherapy in Assessing Radiosensitivity of Oral Squamous Cell Carcinoma. *Journal of Clinical and Experimental Dentistry,* 3**,** 193-200.

RAK, G. D., MACE, E. M., BANERJEE, P. P., SVITKINA, T. & ORANGE, J. S. 2011. Natural killer cell lytic granule secretion occurs through a pervasive actin network at the immune synapse. *PLoS Biol,* 9**,** e1001151.

RAPOSO, G., TENZA, D., MURPHY, D. M., BERSON, J. F. & MARKS, M. S. 2001. Distinct protein sorting and localization to premelanosomes, melanosomes, and lysosomes in pigmented melanocytic cells. *Journal of Cell Biology,* 152**,** 809-24.

REDDY, A., CALER, E. V. & ANDREWS, N. W. 2001. Plasma membrane repair is mediated by Ca2+-regulated exocytosis of lysosomes. *Cell,* 106**,** 157-69.

REEFMAN, E., KAY, J. G., WOOD, S. M., OFFENHAUSER, C., BROWN, D. L., ROY, S., STANLEY, A. C., LOW, P. C., MANDERSON, A. P. & STOW, J. L. 2010. Cytokine secretion is distinct from secretion of cytotoxic granules in NK cells. *Journal of Immunology,* 184**,** 4852-62.

RODER, J. & DUWE, A. 1979. Beige Mutation in the Mouse Selectively Impairs Natural Killer Cell-Function. *Nature,* 278**,** 451-453.

RODIER, F. & CAMPISI, J. 2011. Four faces of cellular senescence. *Journal of Cell Biology,* 192**,** 547-56.

ROTH, M. G. 2004. Phosphoinositides in constitutive membrane traffic. *Physiological Reviews,* 84**,** 699-730.

RUTHERFORD, A. C., TRAER, C., WASSMER, T., PATTNI, K., BUJNY, M. V., CARLTON, J. G., STENMARK, H. & CULLEN, P. J. 2006. The mammalian phosphatidylinositol 3-phosphate 5-kinase (PIKfyve) regulates endosome-to-TGN retrograde transport. *Journal of Cell Science,* 119**,** 3944-3957.

SAFTIG, P. & KLUMPERMAN, J. 2009. Lysosome biogenesis and lysosomal membrane proteins: trafficking meets function. *Nat Rev Mol Cell Biol,* 10**,** 623-35.

SANBORN, K. B., RAK, G. D., MARU, S. Y., DEMERS, K., DIFEO, A., MARTIGNETTI, J. A., BETTS, M. R., FAVIER, R., BANERJEE, P. P. & ORANGE, J. S. 2009. Myosin IIA associates with NK cell lytic granules to enable their interaction with F-actin and function at the immunological synapse. *Journal of Immunology,* 182**,** 6969-84.

SARDIELLO, M., PALMIERI, M., DI RONZA, A., MEDINA, D. L., VALENZA, M., GENNARINO, V. A., DI MALTA, C., DONAUDY, F., EMBRIONE, V., POLISHCHUK, R. S., BANFI, S., PARENTI, G., CATTANEO, E. & BALLABIO, A. 2009. A gene network regulating lysosomal biogenesis and function. *Science,* 325**,** 473-7.

SATO, N., MIZUMOTO, K., NAKAMURA, M., UENO, H., MINAMISHIMA, Y. A., FARBER, J. L. & TANAKA, M. 2000. A possible role for centrosome overduplication in radiation-induced cell death. *Oncogene,* 19**,** 5281-90.

SBRISSA, D., IKONOMOV, O. C. & SHISHEVA, A. 1999. PIKfyve, a mammalian ortholog of yeast Fab1p lipid kinase, synthesizes 5-phosphoinositides. Effect of insulin. *Journal of Biological Chemistry,* 274**,** 21589-97.

SBRISSA, D., IKONOMOV, O. C., STRAKOVA, J. & SHISHEVA, A. 2004. Role for a novel signaling intermediate, phosphatidylinositol 5-phosphate, in insulin-regulated F-actin stress fiber breakdown and GLUT4 translocation. *Endocrinology,* 145**,** 4853-65.

SBRISSA, D., IKONOMOV, O. C., FENNER, H. & SHISHEVA, A. 2008. ArPIKfyve homomeric and heteromeric interactions scaffold PIKfyve and Sac3 in a complex to promote PIKfyve activity and functionality. *Journal of Molecular Biology,* 384**,** 766-79.

SCHU, P. V., TAKEGAWA, K., FRY, M. J., STACK, J. H., WATERFIELD, M. D. & EMR, S. D. 1993. Phosphatidylinositol 3-kinase encoded by yeast VPS34 gene essential for protein sorting. *Science,* 260**,** 88-91.

SCOTT, G. B., MEADE, J. L. & COOK, G. P. 2008. Profiling killers; unravelling the pathways of human natural killer cell function. *Brief Funct Genomic Proteomic,* 7**,** 8-16.

SETTEMBRE, C., FRALDI, A., MEDINA, D. L. & BALLABIO, A. 2013. Signals from the lysosome: a control centre for cellular clearance and energy metabolism. *Nat Rev Mol Cell Biol,* 14**,** 283-96.

SHIFLETT, S. L., KAPLAN, J. & WARD, D. M. 2002. Chediak-Higashi Syndrome: a rare disorder of lysosomes and lysosome related organelles. *Pigment Cell Research,* 15**,** 251-7.

SHIRAISHI, M., KAWASHIMA, S., MOROI, M., SHIN, Y., MORITA, T., HORII, Y., IKEDA, M. & ITO, K. 2002a. A defect in collagen receptor-

Ca2+ signaling system in platelets from cattle with Chediak-Higashi syndrome. *Thrombosis and Haemostasis,* 87**,** 334-41.

SHIRAISHI, M., OGAWA, H., IKEDA, M., KAWASHIMA, S. & ITO, K. 2002b. Platelet dysfunction in Chediak-Higashi syndrome-affected cattle. *Journal of Veterinary Medical Science,* 64**,** 751-760.

SHISHEVA, A., RUSIN, B., IKONOMOV, O. C., DEMARCO, C. & SBRISSA, D. 2001. Localization and insulin-regulated relocation of phosphoinositide 5-kinase PIKfyve in 3T3-L1 adipocytes. *Journal of Biological Chemistry,* 276**,** 11859-69.

SHISHEVA, A. 2008. PIKfyve: Partners, significance, debates and paradoxes. *Cell Biology International,* 32**,** 591-604.

SIMONSEN, A., BIRKELAND, H. C., GILLOOLY, D. J., MIZUSHIMA, N., KUMA, A., YOSHIMORI, T., SLAGSVOLD, T., BRECH, A. & STENMARK, H. 2004. Alfy, a novel FYVE-domain-containing protein associated with protein granules and autophagic membranes. *Journal of Cell Science,* 117**,** 4239-51.

SLYPER, M., SHAHAR, A., BAR-ZIV, A., GRANIT, R. Z., HAMBURGER, T., MALY, B., PERETZ, T. & BEN-PORATH, I. 2012. Control of breast cancer growth and initiation by the stem cell-associated transcription factor TCF3. *Cancer Research,* 72**,** 5613-24.

STENBECK, G. 2002. Formation and function of the ruffled border in osteoclasts. *Seminars in Cell and Developmental Biology,* 13**,** 285-92.

STINCHCOMBE, J. C., PAGE, L. J. & GRIFFITHS, G. M. 2000. Secretory lysosome biogenesis in cytotoxic T lymphocytes from normal and Chediak Higashi syndrome patients. *Traffic,* 1**,** 435-44.

STINCHCOMBE, J. C., BARRAL, D. C., MULES, E. H., BOOTH, S., HUME, A. N., MACHESKY, L. M., SEABRA, M. C. & GRIFFITHS, G. M. 2001. Rab27a is required for regulated secretion in cytotoxic T lymphocytes. *Journal of Cell Biology,* 152**,** 825-34.

STINCHCOMBE, J. C. & GRIFFITHS, G. M. 2007. Secretory mechanisms in cell-mediated cytotoxicity. *Annual Review of Cell and Developmental Biology,* 23**,** 495-517.

STRUTZ, F., OKADA, H., LO, C. W., DANOFF, T., CARONE, R. L., TOMASZEWSKI, J. E. & NEILSON, E. G. 1995. Identification and characterization of a fibroblast marker: FSP1. *Journal of Cell Biology,* 130**,** 393-405.

TAM, Y. K., MAKI, G., MIYAGAWA, B., HENNEMANN, B., TONN, T. & KLINGEMANN, H. G. 1999. Characterization of genetically altered, interleukin 2-independent natural killer cell lines suitable for adoptive cellular immunotherapy. *Human Gene Therapy,* 10**,** 1359-73.

TANABE, F., CUI, S. H. & ITO, M. 1998. Ceramide promotes calpain-mediated proteolysis of protein kinase C beta in murine polymorphonuclear leukocytes. *Biochemical and Biophysical Research Communications,* 242**,** 129-33.

TANABE, F., CUI, S. H. & ITO, M. 2000. Abnormal down-regulation of PKC is responsible for giant granule formation in fibroblasts from CHS (beige) mice--a thiol proteinase inhibitor, E-64-d, prevents giant granule formation in beige fibroblasts. *Journal of Leukocyte Biology,* 67**,** 749-55.

TANABE, F., KASAI, H., HE, L., KIN, T., FUJIKADO, T., KUMAMOTO, T., HARA, T., IWATA, T. & ITO, M. 2009. Improvement of deficient

natural killer activity and delayed bactericidal activity by a thiol proteinase inhibitor, E-64-d, in leukocytes from Chediak-Higashi syndrome patients in vitro. *International Immunopharmacology,* 9**,** 366-70.

TARDIEU, M., LACROIX, C., NEVEN, B., BORDIGONI, P., DE SAINT BASILE, G., BLANCHE, S. & FISCHER, A. 2005. Progressive neurologic dysfunctions 20 years after allogeneic bone marrow transplantation for Chediak-Higashi syndrome. *Blood,* 106**,** 40-2.

TARGAN, S. R. & OSEAS, R. 1983. The "lazy" NK cells of Chediak-Higashi syndrome. *Journal of Immunology,* 130**,** 2671-4.

TCHERNEV, V., MANSFIELD, T., GIOT, L., KUMAR, A., NANDABALAN, K., LI, Y., MISHRA, V., DETTER, J., ROTHBERG, J. & WALLACE, M. 2002. The Chediak-Higashi protein interacts with SNARE complex and signal transduction proteins. *Molecular Medicine,* 8**,** 56.

THOMAS, C. L., STEEL, J., PRESTWICH, G. D. & SCHIAVO, G. 1999. Generation of phosphatidylinositol-specific antibodies and their characterization. *Biochemical Society Transactions,* 27**,** 648-52.

THOMPSON, S. L. & COMPTON, D. A. 2011. Chromosome missegregation in human cells arises through specific types of kinetochore-microtubule attachment errors. *Proceedings of the National Academy of Sciences of the United States of America,* 108**,** 17974-8.

TOMINAGA, M., KITAGAWA, Y., TANAKA, S. & KISHIMOTO, A. 1991. Phosphorylation of type II (beta) protein kinase C by casein kinase II. *J Biochem,* 110**,** 655-60.

TOOZE, J. & HOLLINSHEAD, M. 1991. Tubular early endosomal networks in AtT20 and other cells. *Journal of Cell Biology,* 115**,** 635-53.

TRANTOW, C. M. 2009. *Genetic pathways of Lyst and exfoliation syndrome.* PhD Thesis, University of Iowa. http://ir.uiowa.edu/etd/896.

TRANTOW, C. M., MAO, M., PETERSEN, G. E., ALWARD, E. M., ALWARD, W. L., FINGERT, J. H. & ANDERSON, M. G. 2009. Lyst mutation in mice recapitulates iris defects of human exfoliation syndrome. *Investigative Ophthalmology and Visual Science,* 50**,** 1205-14.

TRANTOW, C. M., HEDBERG-BUENZ, A., IWASHITA, S., MOORE, S. A. & ANDERSON, M. G. 2010. Elevated oxidative membrane damage associated with genetic modifiers of Lyst-mutant phenotypes. *PLoS Genet,* 6**,** e1001008.

UPSHAW, J. L., SCHOON, R. A., DICK, C. J., BILLADEAU, D. D. & LEIBSON, P. J. 2005. The isoforms of phospholipase C-gamma are differentially used by distinct human NK activating receptors. *Journal of Immunology,* 175**,** 213-8.

VENABLE, M. E. & YIN, X. 2009. Ceramide induces endothelial cell senescence. *Cell Biochemistry and Function,* 27**,** 547-51.

VIVIER, E., RAULET, D. H., MORETTA, A., CALIGIURI, M. A., ZITVOGEL, L., LANIER, L. L., YOKOYAMA, W. M. & UGOLINI, S. 2011. Innate or adaptive immunity? The example of natural killer cells. *Science,* 331**,** 44-9.

VONDERHEIT, A. & HELENIUS, A. 2005. Rab7 associates with early endosomes to mediate sorting and transport of Semliki forest virus to late endosomes. *PLoS Biol,* 3**,** e233.

WAGURI, S., DEWITTE, F., LE BORGNE, R., ROUILLE, Y., UCHIYAMA, Y., DUBREMETZ, J. F. & HOFLACK, B. 2003. Visualization of TGN to endosome trafficking through fluorescently labeled MPR and AP-1 in living cells. *Molecular Biology of the Cell,* 14**,** 142-155.

WANG, B., LIU, K., LIN, F. T. & LIN, W. C. 2004. A role for 14-3-3 tau in E2F1 stabilization and DNA damage-induced apoptosis. *Journal of Biological Chemistry,* 279**,** 54140-52.

WANG, B., LIU, K., LIN, H. Y., BELLAM, N., LING, S. & LIN, W. C. 2010. 14-3-3Tau regulates ubiquitin-independent proteasomal degradation of p21, a novel mechanism of p21 downregulation in breast cancer. *Molecular and Cellular Biology,* 30**,** 1508-27.

WANG, J. W., HOWSON, J., HALLER, E. & KERR, W. G. 2001. Identification of a novel lipopolysaccharide-inducible gene with key features of both A kinase anchor proteins and chs1/beige proteins. *Journal of Immunology,* 166**,** 4586-95.

WANG, X., HERBERG, F. W., LAUE, M. M., WULLNER, C., HU, B., PETRASCH-PARWEZ, E. & KILIMANN, M. W. 2000. Neurobeachin: A protein kinase A-anchoring, beige/Chediak-higashi protein homolog implicated in neuronal membrane traffic. *Journal of Neuroscience,* 20**,** 8551-65.

WARD, D., SHIFLETT, S., HUYNH, D., VAUGHN, M., PRESTWICH, G. & KAPLAN, J. 2003. Use of expression constructs to dissect the functional domains of the CHS/beige protein: identification of multiple phenotypes. *Traffic,* 4**,** 403-415.

WARD, D. M., GRIFFITHS, G. M., STINCHCOMBE, J. C. & KAPLAN, J. 2000. Analysis of the lysosomal storage disease Chediak-Higashi syndrome. *Traffic,* 1**,** 816-22.

WARD, D. M., SHIFLETT, S. L. & KAPLAN, J. 2002. Chediak-Higashi syndrome: a clinical and molecular view of a rare lysosomal storage disorder. *Current Molecular Medicine,* 2**,** 469-77.

WATT, S. A., KULAR, G., FLEMING, I. N., DOWNES, C. P. & LUCOCQ, J. M. 2002. Subcellular localization of phosphatidylinositol 4,5-bisphosphate using the pleckstrin homology domain of phospholipase C delta1. *Biochem J,* 363**,** 657-66.

WEBSTER, M., WITKIN, K. L. & COHEN-FIX, O. 2009. Sizing up the nucleus: nuclear shape, size and nuclear-envelope assembly. *Journal of Cell Science,* 122**,** 1477-86.

WEI, M. L. 2006. Hermansky-Pudlak syndrome: a disease of protein trafficking and organelle function. *Pigment Cell Research,* 19**,** 19-42.

WHITE, J. G. & CLAWSON, C. C. 1980. The Chediak-Higashi syndrome; the nature of the giant neutrophil granules and their interactions with cytoplasm and foreign particulates. I. Progressive enlargement of the massive inclusions in mature neutrophils. II. Manifestations of cytoplasmic injury and sequestration. III. Interactions between giant organelles and foreign particulates. *American Journal of Pathology,* 98**,** 151-96.

WILLINGHAM, M. C., SPICER, S. S. & VINCENT, R. A., JR. 1981. The origin and fate of large dense bodies in beige mouse fibroblasts. Lysosomal fusion and exocytosis. *Experimental Cell Research,* 136**,** 157-68.

WILSON, J., HUYNH, C., KENNEDY, K. A., WARD, D. M., KAPLAN, J., ADEREM, A. & ANDREWS, N. W. 2008. Control of parasitophorous vacuole expansion by LYST/Beige restricts the intracellular growth of Leishmania amazonensis. *PLoS Pathog,* 4**,** e1000179.

WOOD, S. M., MEETHS, M., CHIANG, S. C., BECHENSTEEN, A. G., BOELENS, J. J., HEILMANN, C., HORIUCHI, H., ROSTHOJ, S., RUTYNOWSKA, O., WINIARSKI, J., STOW, J. L., NORDENSKJOLD, M., HENTER, J. I., LJUNGGREN, H. G. & BRYCESON, Y. T. 2009. Different NK cell-activating receptors preferentially recruit Rab27a or Munc13-4 to perforin-containing granules for cytotoxicity. *Blood,* 114**,** 4117-27.

WU, H., YANG, J. M., JIN, S., ZHANG, H. & HAIT, W. N. 2006. Elongation factor-2 kinase regulates autophagy in human glioblastoma cells. *Cancer Research,* 66**,** 3015-23.

WU, W. I., YAJNIK, J., SIANO, M. & DE LOZANNE, A. 2004. Structure-function analysis of the BEACH protein LvsA. *Traffic,* 5**,** 346-55.

XIE, J., XIANG, D. B., WANG, H., ZHAO, C., CHEN, J., XIONG, F., LI, T. Y. & WANG, X. L. 2012. Inhibition of Tcf-4 induces apoptosis and enhances chemosensitivity of colon cancer cells. *PLoS One,* 7**,** e45617.

YAO, L., KAWAKAMI, Y. & KAWAKAMI, T. 1994. The pleckstrin homology domain of Bruton tyrosine kinase interacts with protein kinase C. *Proceedings of the National Academy of Sciences of the United States of America,* 91**,** 9175-9.

YAO, L., SUZUKI, H., OZAWA, K., DENG, J., LEHEL, C., FUKAMACHI, H., ANDERSON, W. B., KAWAKAMI, Y. & KAWAKAMI, T. 1997. Interactions between protein kinase C and pleckstrin homology domains. Inhibition by phosphatidylinositol 4,5-bisphosphate and phorbol 12-myristate 13-acetate. *Journal of Biological Chemistry,* 272**,** 13033-9.

YU, Y. Y., CHEN, Y., DAI, G., CHEN, J., SUN, X. M., WEN, C. J., ZHAO, D. H., CHANG, D. C. & LI, C. J. 2004. The association of calmodulin with central spindle regulates the initiation of cytokinesis in HeLa cells. *International Journal of Biochemistry and Cell Biology,* 36**,** 1562-72.

ZHANG, H., FAN, X., BAGSHAW, R. D., ZHANG, L., MAHURAN, D. J. & CALLAHAN, J. W. 2007a. Lysosomal membranes from beige mice contain higher than normal levels of endoplasmic reticulum proteins. *Journal of Proteome Research,* 6**,** 240-9.

ZHANG, H., MAHURAN, D. J. & CALLAHAN, J. W. 2010. Identification of proteins in the ceroid-like autofluorescent aggregates from liver lysosomes of Beige, a mouse model for human Chediak-Higashi syndrome. *Molecular Genetics and Metabolism,* 99**,** 389-95.

ZHANG, Y., ZOLOV, S. N., CHOW, C. Y., SLUTSKY, S. G., RICHARDSON, S. C., PIPER, R. C., YANG, B., NAU, J. J., WESTRICK, R. J., MORRISON, S. J., MEISLER, M. H. & WEISMAN, L. S. 2007b. Loss of Vac14, a regulator of the signaling lipid phosphatidylinositol 3,5-bisphosphate, results in neurodegeneration in mice. *Proceedings of the National Academy of Sciences of the United States of America,* 104**,** 17518-23.

ZOLOV, S. N., BRIDGES, D., ZHANG, Y., LEE, W. W., RIEHLE, E., VERMA, R., LENK, G. M., CONVERSO-BARAN, K., WEIDE, T.,

ALBIN, R. L., SALTIEL, A. R., MEISLER, M. H., RUSSELL, M. W. & WEISMAN, L. S. 2012. In vivo, Pikfyve generates PI(3,5)P2, which serves as both a signaling lipid and the major precursor for PI5P. *Proceedings of the National Academy of Sciences of the United States of America,* 109**,** 17472-7.

ZOU, C., LI, J., BAI, Y., GUNNING, W. T., WAZER, D. E., BAND, V. & GAO, Q. 2005. Centrobin: a novel daughter centriole-associated protein that is required for centriole duplication. *The Journal of cell biology,* 171**,** 437-45.

ZUCHNER, S., NOUREDDINE, M., KENNERSON, M., VERHOEVEN, K., CLAEYS, K., DE JONGHE, P., MERORY, J., OLIVEIRA, S. A., SPEER, M. C., STENGER, J. E., WALIZADA, G., ZHU, D., PERICAK-VANCE, M. A., NICHOLSON, G., TIMMERMAN, V. & VANCE, J. M. 2005. Mutations in the pleckstrin homology domain of dynamin 2 cause dominant intermediate Charcot-Marie-Tooth disease. *Nature Genetics,* 37**,** 289-94.

Appendix

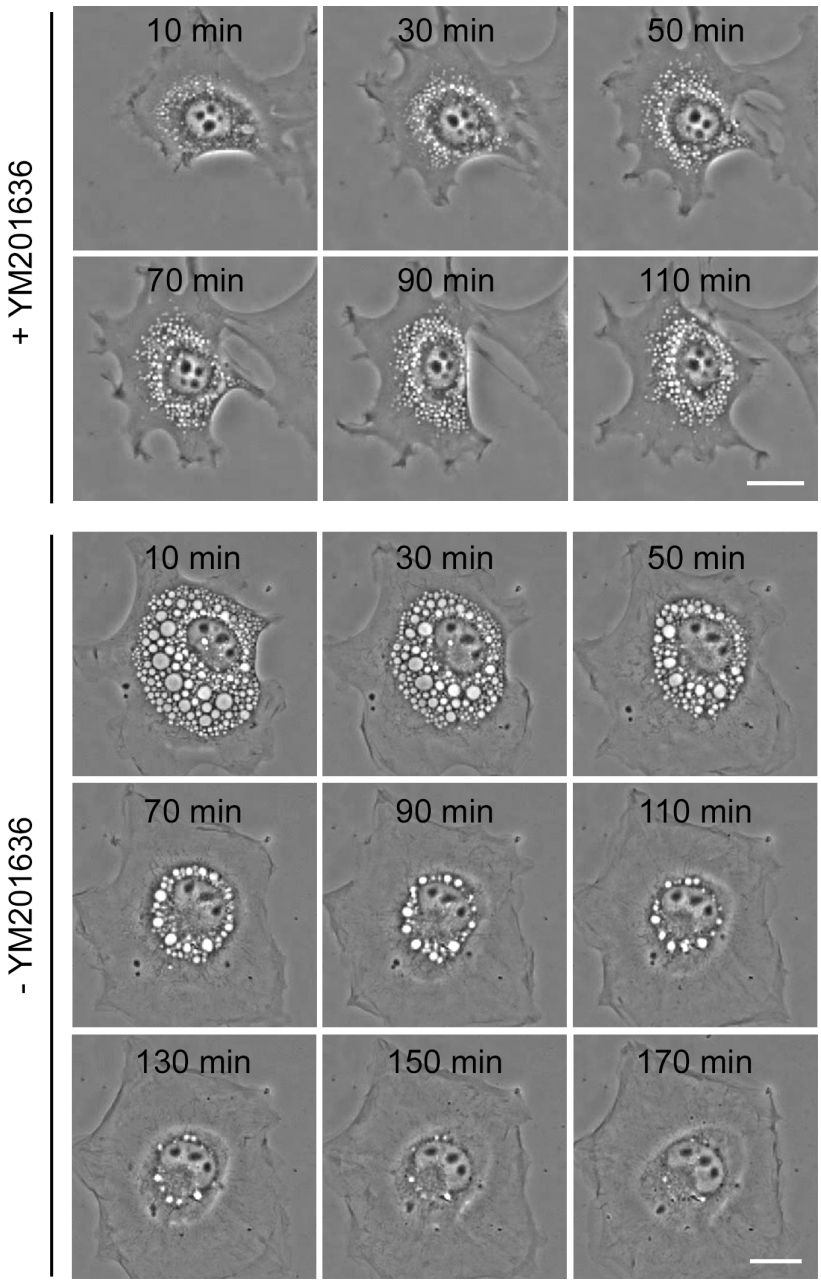

Time-lapse analysis of the swollen vesicles induced by YM201636

Frames are taken from a film of 3T3-J2 cells treated with 800 nM YM201636 (+YM201636). The time above each image indicates the time elapsed after the addition of YM201636. In a separate experiment, cells which had been treated with YM201636 for four hours were washed free of YM201636 and then imaged (–YM201636). The time above each image indicates the time elapsed after the removal of YM201636. The enlarged vesicles return to normal size after withdrawal of YM201636. Scale bar = 20 μm.